Control of Heat Conduction in Manufacturing Processes: A Distributed Parameter Systems Approach

by

Upendra V. Ummethala

Bachelor of Technology in Mechanical Engineering
Indian Institute of Technology, Madras (1990)

Master of Science in Mechanical Engineering
University of California, Los Angeles (1992)

SUBMITTED TO THE DEPARTMENT OF MECHANICAL ENGINEERING
IN PARTIAL FULFILLMENT OF
THE REQUIREMENTS FOR THE DEGREE OF

DOCTOR OF PHILOSOPHY

at the

MASSACHUSETTS INSTITUTE OF TECHNOLOGY

June, 1997

© Massachusetts Institute of Technology 1997

Signature of Author _____
Department of Mechanical Engineering
June 1997

Certified by _____
David E. Hardt
Thesis Supervisor

Accepted by _____
Ain A. Sonin
Department of Mechanical Engineering
Chairman, Department Graduate Committee

LIBRARIES

Control of Heat Conduction in Manufacturing Processes: A Distributed Parameter Systems Approach

by

Upendra V. Ummethala

Submitted to the Department of Mechanical Engineering
on May 8th, 1997 in partial fulfillment of the requirements
for the Degree of Doctor of Philosophy in Mechanical Engineering.

Abstract

There are several manufacturing processes where heat conduction is one of the key physical phenomena that influence the process performance. Such processes include molding operations, heat treatment, welding, flame bending etc. Typical temperature control implemented in these processes, at best involves independent multi-zone type regulation. (For example: barrel heaters in injection molding.) This thesis has addressed the problem of controlling entire temperature distributions in such processes. Several techniques developed in the theoretical literature on the control of distributed parameter systems (DPS) have been investigated for their applicability to manufacturing processes.

An experiment has been setup using a scanned TIG torch to heat a rectangular specimen with several thermocouples embedded within it. A detailed simulation study was performed on a model of this experimental setup, to study the closed loop behavior of the model under different scenarios. The simulations used a linear quadratic gaussian (LQG) controller. The conclusion from this study was that the distribution of inputs and sensors in the controlled object had a significant impact on the performance of the controller in rejecting disturbances. However, there are no available techniques in the theoretical literature to adequately address the issue of optimally distributing inputs.

This motivated the development of a technique for optimally distributing inputs across a controlled object. The technique comprises separating the space and time part of the governing partial differential equation, which results in the steady-state equation for heat conduction within the controlled object. The steady-state Green's function corresponding to this steady state heat conduction equation is determined. A quadratic performance index comprising a heat flux term and a temperature error term is defined over the spatial domain. A general form of a higher order cost functional is used along with the Green's function to set up the optimization problem. Variational calculus is used to determine the optimal heat flux distribution in steady state. This optimal heat flux distribution is in a linear proportional feedback form wherein the heat flux needed in steady state depends on the steady-state temperature error. Therefore such an approach can better adapt to model errors and external disturbances.

Simulations have been performed on a rectangular solid to illustrate the optimal distribution technique based on the steady-state optimization. The constraints on the locations of the inputs and the types of disturbances considered were selected based on typical requirements in a resin transfer molding (RTM) or a compression molding application. The Green's functions were derived using a finite difference formulation for the heat conduction in the solid. The design of the heating was separated into two parts: In the first part, the heat flux locations and strengths were selected to satisfy the requirements on the steady-state performance. In the second part, additional heaters were introduced to improve the transient performance. In the first part of the design, the high gain (MIMO) obtained as a part of the steady-state analysis was rolled off using a first order frequency blending function. The MIMO Nyquist criterion was then used to determine if the closed loop system was stable. The break frequency for the frequency blending function is used as a controller design parameter and a suitable value is selected. The predictions of the MIMO Nyquist criterion have been verified by simulating the closed loop system. Additional heaters placed closed to the surface have been incorporated into the design using a cross-over network type design. The improvement in the transient performance has been demonstrated.

The problem of accelerated cooling of hot-rolled steel has been addressed as a transient temperature distribution control problem. The major source of disturbance in this process is a variation in the initial temperature of steel. There are no measurements possible once the cooling process begins. The anomalous nature of the cooling process amplifies the variations in the initial temperature distribution, if not compensated for. To compensate for the variations in the initial conditions, a finite horizon quadratic performance index is setup. The resulting feedback form for the optimal solution is simulated on the model for the process, with the initial condition varied from the nominal initial condition. The simulated input is then used as an open-loop input to the process to compensate for the variations in the initial condition.

Thesis Supervisor: Prof. David E. Hardt.
Title: Professor of Mechanical Engineering, Massachusetts Institute of Technology.

Committee:

Prof. David E. Hardt (Chairman)	Department of Mechanical Engineering MIT.
Prof. Jung Hoon Chun	Department of Mechanical Engineering MIT.
Prof. Harris Doumanidis	Department of Mechanical Engineering Tufts University.
Dr. Kenneth W. Kaiser	Charles Stark Draper Laboratory.
Dr. Herschell B. Smartt	Idaho National Engineering Laboratory.

Acknowledgements

I would like to thank my advisor Prof. David Hardt for his guidance and support throughout my thesis, working with Dave has been an invaluable learning experience. I would also like to thank the other members of my committee: Prof. Jung Hoon Chun, Prof. Harris Doumanidis, Dr. Kenneth Kaiser and Dr. Herschell Smartt for their invaluable comments and criticism. I would especially like to thank Dr. Kaiser for spending many hours discussing and verifying the work on optimal input distribution. Also, I would like to say a special thanks to Prof. Doumanidis for letting me use his laboratory facilities. I would also like to thank the U.S. Department of Energy for supporting this research.

Fred Cote in the machine shop has helped me with the machining for the experimental setups and I would like to thank him for his patience and help. I would also like to acknowledge the help that Nikos provided.

My parents and my wife have been extremely supportive during my thesis and I would like to thank them for their support. I would also like to thank all my friends who have made my stay at MIT rich with fond memories.

Upendra Ummethala
June 1997.

This thesis is dedicated to my parents and my wife

Table of Contents

Chapter 1

MOTIVATION AND BACKGROUND FOR TEMPERATURE CONTROL IN MANUFACTURING PROCESSES

1.1. Introduction:

In many manufacturing processes, temperature fields and heat fluxes are the primary determinants of the process output and product quality. Such processes include all solidification processes (casting, molding, welding) as well as solid phase processes where thermal cycles are used to change properties or shape (e.g. heat treating and line heating). A few such processes are discussed in section 1.2.

Influencing the process outputs such as material, geometric and mechanical properties in all such processes, involves controlling the temperatures and heat fluxes. The processes considered in this thesis involve situations where heat conduction is the dominant physical phenomenon in determining the temperature distributions. This means that the temperature distributions and heat fluxes are governed by the heat diffusion equation. Equation 1.1.1., shows the heat diffusion equation:

$$\begin{aligned} &\rho C_p \frac{\partial T}{\partial t}(\bar{x},t) = \nabla(k(\bar{x})\nabla)T(\bar{x},t) + \phi(\bar{x},t); \\ &Bo(T(\bar{x},t)) = 0; \qquad Boundary \quad Condition \end{aligned} \tag{1.1.1}$$

Where:

ρ: *is the density*
C_p: *is the specificheat*
$k(\bar{x})$: *is the conductivity of the material*
$\bar{x}$: *is the vector spatial coordinates*
t : *is time*

$$\nabla = \frac{\partial}{\partial x} + \frac{\partial}{\partial y} + \frac{\partial}{\partial z}$$

Bo: *Boundary conditions* 1.1.2

$T(\bar{x},t)$: *temperature distribution*
$\phi(\bar{x},t)$: *distribution of the heat flux*

The heat flux $\phi(\bar{x},t)$, which is incident on the solid within which the temperature is being controlled, comprises of two components (see equation 1.2.3.). The first component is the heat flux that can be actively manipulated and it will be referred to as the controller heat flux $\phi_C(\bar{x},t)$. The second component of the total heat flux, which cannot be actively manipulated, is referred to as the disturbance heat flux $\phi_D(\bar{x},t)$.

$$\phi(\bar{x},t) = \phi_C(\bar{x},t) + \phi_D(\bar{x},t) \qquad 1.2.3.$$

For example, consider the problem of controlling the temperature distribution in an injection mold, using cartridge heaters and cooling oil, when ambient temperature changes during operation. The heat flux generated by cartridge heaters and cooling passages can be actively controlled and hence any heat flux input due to these devices will be considered to be the controller heat flux. However, the heat flux experienced by the mold due to changes in the ambient temperature would be a part of the disturbance heat flux.

Section 1.2 discusses some example processes where temperature control is of importance. These are the processes that have motivated this thesis.

1.2 Processes with heat conduction:

Manufacturing processes are characterized by phenomena that have a spatial and temporal variation. In the processes being studied here, heat conduction which is a spatially distributed phenomenon, determines the process outputs. In some such processes, simple lumped parameter models that do not capture the distributed nature of the heat conduction phenomenon are used. These may be adequate in the manufacture of components where the requirements on the process are not demanding. However, with more stringent quality, productivity and energy consumption requirements on the processes, one needs to fully consider the spatially distributed nature of the heat conduction in these processes. This will lead to techniques that better aid in designing systems for heating and cooling and thereby improving process quality, productivity and energy consumption.

1.2.1. Heat treatment.

Several products are manufactured by varying the temperature trajectory through which the material of the product is taken through. Most steel products such as sheet steel, beams for construction, steel slabs for bridges and pressure vessels are subjected to different types of heat treatment. The specific temperature trajectory for each product is dependent on the microstructure desired at different locations in the product. See Kalpakjian(1995) for some examples of heat-treatment operations and corresponding desired temperature trajectories.

Figure 1.2.1. shows a schematic of a steel slab being cooled using jets of water. The edges have to be warmed with induction heaters to ensure the uniformity of temperature across the slab.

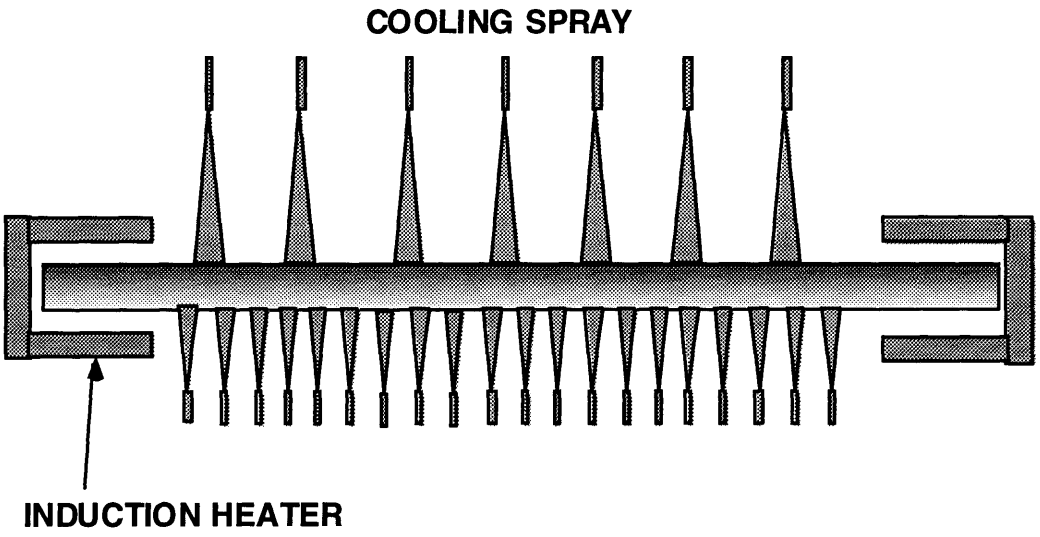

Figure 1.2.1. A cross-sectional schematic of the heat treatment operation for steel slabs.

The goal in this process is to take the material through a desired temperature trajectory T(x,y,z,t). The temperatures experienced at different locations determine the material properties at different locations within the slab being produced. By modulating the cooling sprays and the induction heaters at different locations, the temperature distribution throughout the slab can be manipulated.

This control has to be implemented such that the total amount of water consumed is within acceptable limits. Simultaneously one has to ensure that the temperature distribution trajectory achieved should be within acceptable limits in the presence of process disturbances. The benefits of using such controlled cooling will be discussed in

detail in Chapter 5., which details the specifics of the method for controlling transient temperature distributions.

1.2.2. Injection Molding:

The mold temperature is one of the determining factors in the quality and consistency of a product produced using injection molding. There are several disturbances on the process that include: change in the ambient temperature, change in the temperature of the plastic, changes in the performance of the cartridge heaters or cooling oil of the mold, gradual heating and cooling of the mold due to coming in contact with the plastic etc.

Sometimes it is desirable to impose gradients across the mold. (See Jansen(1993) for example). The residual stress state in the part being produced using injection molding, is dependent on the coupling between the pressure and the temperature profiles of the cooling plastic. By carefully controlling the temperature profile, one can ensure that parts with desirable residual stress states are produced. Jansen(1993) and Sha(1995) have done some preliminary studies on the effect of temperature variations on the stress-state and distortions on a part produced by injection molding. These studies have shown qualitatively, that changes in mold temperature distributions do effect the residual stress state and the optical properties of objects being produced. However, in order to conduct better experimental studies, efficient mold temperature control is needed.

The temperature distribution within the mold is dependent on the locations of the heating and cooling. Similarly, locations of the thermocouples determine the efficiency with which disturbances are detected. The ability of any controller to efficiently compensate

for the disturbances occurring is also dependent on the locations of heating and cooling. Chapter 4., shows a technique for designing locations of heating and cooling in order to accurately control the temperatures in a mold.

1.2.3. Compression Molding and Resin Transfer Molding (RTM):

Compression molding and RTM are processes used for manufacturing composite parts for different applications. Both these processes are matched die processes, which involve taking the composite part through a specified temperature trajectory. Typically the part is heated so that the temperature everywhere is uniform. The heating causes an exothermic reaction in the resin within the part and causes it to cure. The disturbances in this process include all of the disturbances one would deal with in the case of injection molding and in addition, the uncertainty in the exothermic reaction manifests itself as an additional disturbance. Figure 1.2.2. shows a schematic of a typical mold with heating and cooling in it.

The controller design needs to be performed so that the steady-state temperature error is minimized while ensuring a stable operation for the closed loop system. At the same time one needs to minimize the number of heaters and cooling passages that one uses to control the process. The best location for a given set of heaters and coolers needs to be found.

In Chapter 4., presents an approach for designing the distribution of heating and cooling in such a mold so as to maintain a desired temperature distribution on the mold surface.

1.2.4. Welding:

In a welding process, an intense heat source such as an electric arc or a laser is moved over the surface of the component being welded. Filler material is sometimes added. The nature of heat transfer in a traditional welding process, causes a heat effected zone (HAZ) around the weld. In addition, the geometric attributes of the weld such as the width W of the weld and the depth D of the weld are dependent on the temperature trajectory that the base material goes through. See Doumanidis (1988) and Masmoudi (1993). The process outputs such as the depth of weld, HAZ etc. are highly coupled and it is very difficult to independently control these attributes The welding process could be better controlled using a flexible heat source got by scanning a heat source such as a welding torch. Doumanidis (1996) has recently implemented such a control for a scan welding process. The goal of the controller in this process is to be able to achieve a certain specified characteristics for the weld. However, approaching this problem via distributed parameter systems could yield insight into the best achievable performance given the constraints on the process.

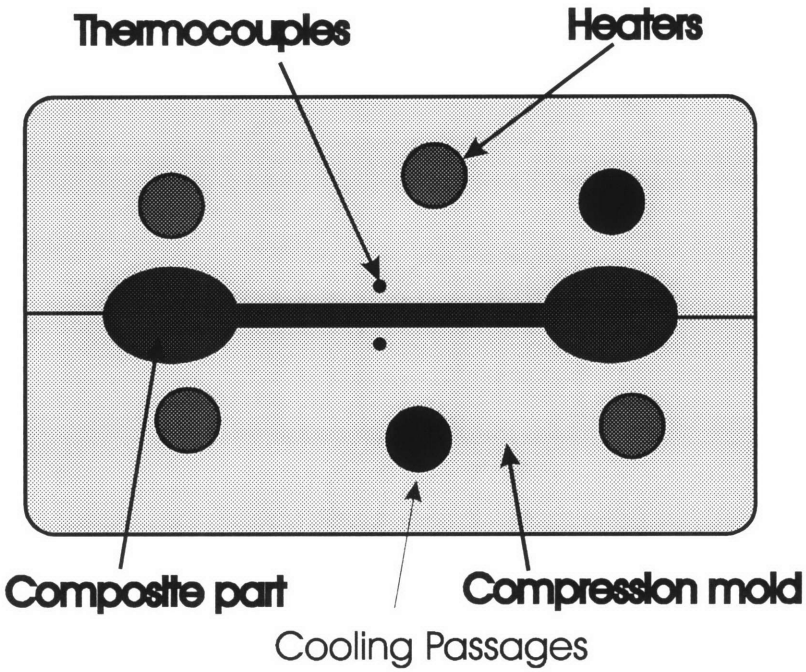

Figure 1.2.2 A schematic of a mold with heating and cooling.

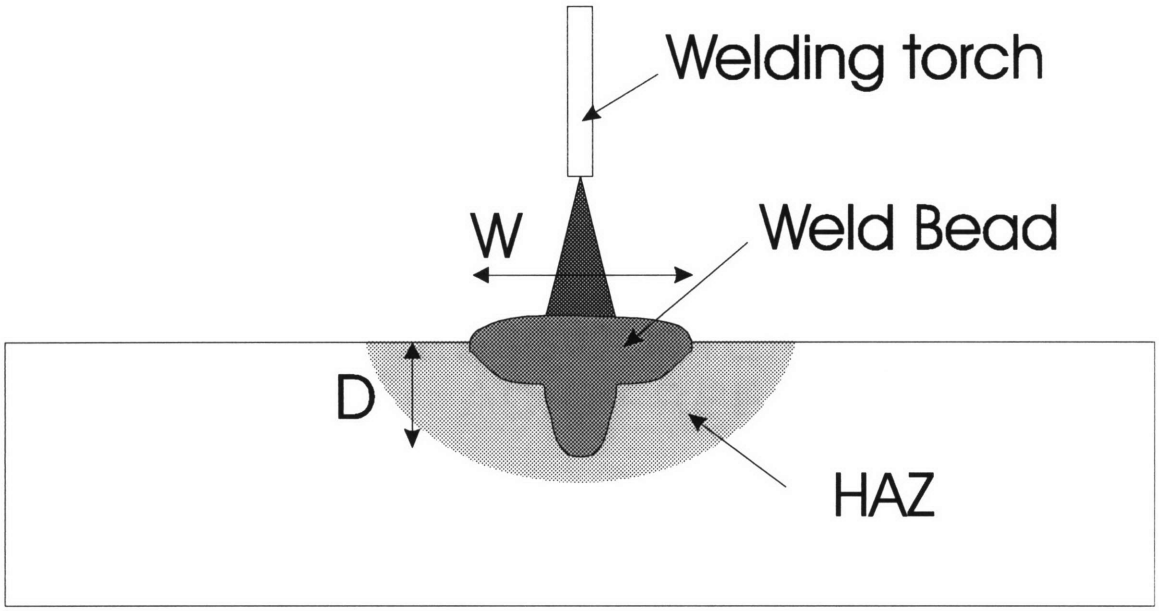

Figure 1.2.3. Geometry of the weld in a typical welding process.

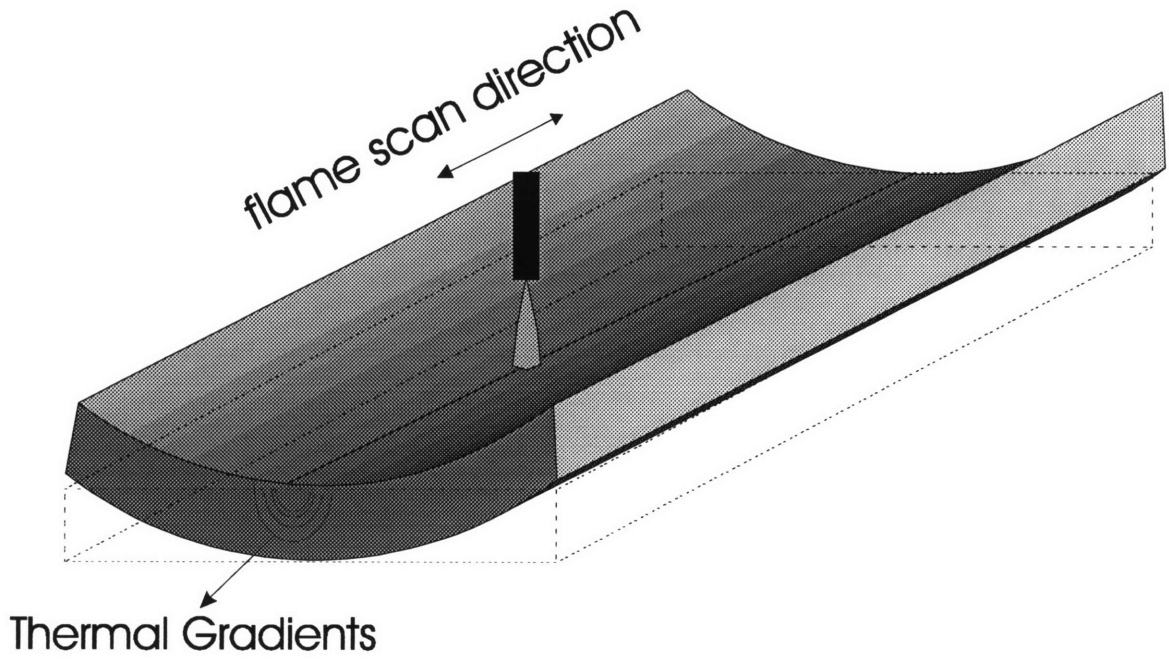

Figure 1.2.4. Flame bending or tool-less forming

1.2.5. Flame bending:

Flame bending is a process used to manufacture one of a kind plates with specific curvature. Flame bending is also termed as tool-less forming. A heat source such as a flame or a plasma torch is scanned along specific lines in the component to induce thermal stresses in the component. The thermal stresses cause permanent distortions in the plate being deformed.

This process is employed to bend large and thick components in very low volume production. The components produced by this method are typically used in ship building and the manufacture of pressure vessels. Additionally, this approach could be used to rectify the errors induced by other methods of forming.

The current industrial practice of flame bending involves bending the parts using a trial and error method where incremental amount of bending is induced at each pass of the flame. However, by better controlling the temperature distribution in this process better control over the distortions could be obtained.

1.2.6. The requirements on the processes:

In all of the processes discussed in this section, there is a need for controlling temperature distributions. The specific requirements may vary from process to process. In some instances, one is interested in controlling the steady-state temperature distribution. (Example: Mold temperature control). In other instances one needs to control a time trajectory of the temperature distribution. (Example: Heat treatment). In examples such as distortion control and length control one needs to control either the gradient of the

temperature or an integral of the temperature. One of the common requirements among all the processes is that one needs to minimize the amount of hardware (e.g., heaters, torches, thermocouples etc.) and the amount of energy used. This has to be done while guaranteeing the performance of the process. The control theory that is of relevance to present applications is in the field of distributed parameter systems (DPS) theory. The DPS theory is concerned with controlling phenomena that are distributed in space and vary with time. The problem of controlling heat conduction/ diffusion equations has been widely studied in the distributed parameter systems literature. In the following sections a review of the literature in the control of Distributed Parameter Systems (DPS) is presented.

1.3. Distributed Parameter Systems (DPS) Literature:

There is a good deal of published research on the topic of controlling distributed parameter systems. The theoretical aspects of controlling such systems have been addressed, among others, by: Lions, (1971,1980), Balakrishnan, (1965,1976), Butkovskii, (1969,1987), Delfour (1972,1982), Fattorini (1967,1985), Mitter (1969), Russell (1973), Wang, (1964) Vidyasagar (1973). Several books and collections of papers have been published on this topic: Butkovskii (1969,1987), Omatu and Sienfeld(1983), Ray and Lainiotis (1978), Aziz, Wingate and Balas (1977), El Jai and Pritchard (1988), Tzafestas (1982) etc.

1.3.1. Publications on controllability, observability and stability:

There is a plethora of publications dealing with system theoretic concepts such as controllability, observability and stability of distributed parameter systems.

Controllability of the heat conduction system has been studied by several authors, for example: Omatu and Seinfeld (1989), Tzafestas (1978), Amouroux (1975,78), Goodson and Klein (1970), Sakawa (1974), Butkovskii (1969), Russell (1973), Fattorini (1967), Seidman (1973) , Kamen (1976), Lions (1980), Triggiani (1975), etc. The range of publications is varied. While Omatu and Seinfeld (1989), Tzafestas (1978) etc. have studied the controllability problem using eigen function expansions, authors such as Lions (1980), Triggiani (1975), etc. have addressed the problem using function theoretic concepts.

Observability for DPS was defined by Wang(1964). Goodson and Klien (1970) have derived observability results using an eigen-function expansion and this approach for checking for observability can be found in a wide variety of publications. See: Omatu and Seinfeld (1989) for a detailed derivation of several observability results.

Publications dealing with stability issues are far fewer and are very situation specific. Wang, (1964b, 1971) show a couple of publications with stability results for specific diffusion systems with delays.

1.3.2. Publications on optimal control and optimal sensor and actuator location:

For manufacturing applications, optimal control and optimal sensor and actuator location are by far the most important issues to be considered. Butkovskii (1969), Goldwyn, Sriram and Graham (1967) present a technique for time optimal control of heat conduction systems. Amouroux and Babary (1978) discuss optimal control with point actuators. Butkovskii (1987) addresses several issues dealing with optimally controlling

systems with mobile actuators. Ahmed and Teo (1981) has a collection of papers dealing with Optimal control of DPS. Bellman (1957) and Lions (1971) treat the theoretical aspects of the problem of optimal control of DPS. Lausterer (1977) discusses an example of optimal control of a steel billet using LQG techniques. Kaiser (1968) discusses an optimal control approach that addresses the problem of steady-state optimal control of temperatures.

The problem of optimal location of actuators and sensors is unique to distributed parameter systems. The performance of any controller depends critically on the location of the sensors and actuators. This problem has been widely studied in the literature. El Jai and Pritchard (1988) and Kubrusly and Malebranche (1985) have exhaustive surveys on this topic. Sensor location literature primarily deals with locating point sensors, however there are no guidelines for locating sensors that might have a distribution to them. For example: if one could scan a pyrometer along specific lines to estimate temperatures, there are no guidelines on how to select the lines along which the pyrometer measurements should be scanned on. Kaiser (1971) illustrates one way of optimally distributing sensing for a steady-state one-dimensional length control problem. Most of the sensor location publications deal with minimizing some measure of steady-state error covariance of an optimal estimator such as a Kalman Filter. Some algorithms involve, sequentially locating the sensors, minimizing the error covariance at each step. Other algorithms attempt to simultaneously locate N sensors so as to minimize the error covariance of the optimal estimate. Bensoussan (1972) showed the existence of solution for the optimal location problem using the covariance of the optimal estimate. Yu and

Seinfeld (1973) first developed a sub-optimal method of sequentially locating sensors. Most algorithms used to evaluate the optimal locations involve some form of numerical optimization and are very numerically intensive, even for problems with simple geometries.

Amouroux and Babary (1975,78) discuss optimal location of actuators where the locations of the actuators are selected so that a quadratic performance index similar to the cost in a linear quadratic regulator problem is minimized. Omatu and Seinfeld (1983) illustrate a technique for optimal location of both point actuators and point sensors, simultaneously. This technique involves minimizing the performance criterion on the LQG problem. Kaiser (1971) illustrates a technique for determining optimal sensor-actuator location and distribution for controlling steady-state temperature distributions.

El Jai and Pritchard (1988) , Amouroux and Babary (1979) have addressed the problem of determining optimal shapes or domain of action (regions within the controlled solid where the input acts) for inputs. These publications deal with extremely simple geometries and simple shapes for domains of action. The problems are numerically solved after posing a parametric optimization problem. The applicability of these techniques is in doubt due to the several simplifying assumptions made. A technique developed by Kaiser (1969) which uses a 'Greens function' based description for the heat conduction process, can be efficiently applied to problems dealing with steady-state temperature control. The approach presented by Kaiser, involves minimizing a quadratic performance index defined in the spatial domain to obtain a optimal distribution of heat

flux. The optimal heat flux distribution thus obtained is in a feed-back form wherein the heat flux depends on the temperature error. This implies that the heat flux distribution is dependent on the disturbances and model errors and therefore a better scheme from an application point of view. This thesis builds on the techniques developed by Kaiser (1969).

1.3.3. Applications of DPS techniques:

The applications and experimental implementations to the DPS theory have been very few. Lausterer (1977), Morari and O'Dowd (1980), Mader(1976), Kaiser (1968) have performed experiments on controlling temperature distributions. All of these experiments involved control of steady state temperature distributions. In Lausterer and Ray (1977) the heaters and thermocouples were placed at arbitrary locations in the solid and a sub-optimal state estimator has been implemented. The purpose of the experiment was to verify the performance of the theoretical results in DPS estimation rather than to facilitate better control in any specific process. Kaiser (1968) demonstrated temperature control in a rod for controlling the length in the presence of thermal disturbances. All the other applications involve experimental setups used to verify theoretical results as opposed to real applications.

1.3.4. Conclusions from literature survey:

In spite of the vast amount of theoretical and experimental research on the control of distributed parameter systems (DPS), there are virtually no real industrial applications of DPS theory to manufacturing processes. The reasons for this could be many. One of the reasons for this could be that implementing optimal estimation and control algorithms

require a large amount of computing power. With computing power becoming cheaper, these methods will be more attractive to implement. Additionally, quality, productivity and flexibility issues in manufacturing processes are becoming increasingly important. Environmental requirements on processes have put energy conservation requirements on the processes. Hence, the investigation of more advanced control methodologies, which might yield better performance of the manufacturing processes, has to be performed.

In the following section, model forms used in implementing DPS controllers will be discussed.

1.4. Model forms:

Equations 1.1.1. and 1.1.2. show the governing equation for linear conduction of heat. For control and analysis purposes, this equation needs to be modified into forms that are more suited to applying different control techniques. There are three major approaches for performing this:

1. The first approach involves the use of the eigen function expansion of the partial differential equation (PDE) in equation 1.1.1. and 1.1.2. The PDE can be equivalently represented using an infinite set of ordinary differential equations that are derived using the orthogonality property of the eigen functions. The infinite set of equations is then truncated to get a finite dimensional approximation to the PDE. This approach is by far the most common approach seen in most of the distributed parameter systems literature.

2. The second approach uses some form of spatial discretization such as a finite difference equations (FDE) based scheme. This involves spatially lumping the geometry and deriving governing ordinary differential equations by performing energy balance between neighboring nodes. Finite element and boundary element approaches are also based on spatially discretizing the solid, similar to FDE. These methods are widely employed in the analysis of thermal systems.
3. The third approach utilizes an integral equation representation for the temperature distribution using Green's functions. The Green's function can be experimentally determined, hence this is a useful technique.

These three approaches have been used in this thesis for different problems. In this section a brief description of each of the techniques is presented along with the pros and cons of each approach.

1.4.1. Eigen function expansion based models

The eigen-function expansion based approach involves computing the eigen values and eigen functions associated with equation 1.1.1. Say the eigen functions and eigen values associated with equation 1.1.1. are:

$$\begin{aligned} \Phi_i(\bar{x}) &: \textit{Eigen functions} \qquad i = 1,2,\ldots,\infty \\ \lambda_i &: \textit{Eigen values} \end{aligned} \tag{1.4.1.}$$

Where $\bar{x}$ is a vector of spatial coordinates used in the problem. For the heat conduction system, the eigen values are all negative and decreasing and the eigen functions form a complete set. This implies that any piece-wise continuous function can be represented as a weighted infinite sum of the eigen functions. (See Courant and Hilbert (1962)). The

temperature within a solid is a continuous function, hence the temperature can be written as an infinite sum of the eigen functions as:

$$T(\bar{x},t) = \sum_{i=1}^{\infty} a_i(t)\Phi_i(\bar{x}) \qquad 1.4.2.$$

Where:

$\bar{x}$: Vector of coordinates
t : time
$T(\bar{x},t)$: Time varying temperature distribution in the solid
$a_i(t)$: Fourier coefficients corresponding to the i^{th} eigen function $\Phi_i(\bar{x})$

Based on this eigen-function expansion a state-space representation can be derived by substituting equation 1.4.2 in 1.1.1. (See Kubrusly and Malebrance (1985) for a detailed derivation of the state-space equations). Additionally, chapter 2., presents a detailed example of using an eigen-function expansion to derive a state-space description to the heat conduction problem. In the eigen function expansion based model, the Fourier coefficients $a_i(t)$'s are the states and the corresponding state-space model is given in equations 1.4.3-1.4.8.

$$\begin{aligned} \dot{\mathbf{X}} &= \mathbf{AX} + \mathbf{BU} \\ \mathbf{Y} &= \mathbf{CX} \end{aligned} \qquad 1.4.3.$$

Where the state vector and the initial value of the state are given by:

$$\begin{aligned} \mathbf{X}(t) &= [a_1(t), a_2(t), \cdots]^T \\ \mathbf{X}(0) &= [a_1(0), a_2(0), \ldots]^T \end{aligned} \qquad 1.4.4.$$

The **A** matrix of this infinite dimensional system is given by:

$$\mathbf{A}_{\infty x\infty} = diag\{-\gamma\lambda_n\},\ \ n = 1,2,3,\cdots\infty \qquad 1.4.5.$$

where $\gamma = \dfrac{k}{\rho C_p}$ is the diffusivity.

If the heat flux distribution can be separated into its space and time parts, it can be written as shown in equation 1.4.6.:

$$\phi(\bar{x},t) = \mathbf{Q}(\bar{x})^T\,\mathbf{U}(t) \qquad 1.4.6.$$

Where $\mathbf{Q}(\bar{x})$ is the vector of functions describing the distribution of the inputs and **U**(t) is the vector of intensities of each of the inputs. This separation is only possible in situations where the locations where heat flux is applied is fixed in time, for example: heaters and cooling passages whose locations do not change with time. The length of the $\mathbf{Q}(\bar{x})$ vector is dependent on the number of independent inputs that are available in the process. The time varying amplitude of each of the inputs is governed by the values of each entry in **U**(t). This decoupling is not possible in situations where the heat input devices are moving, for example: heating with moving torches etc.

In situations where the space and time parts can be decoupled, the **B** matrix of equation 1.4.3. is given by: (See Kubrusly and Malebrance (1985))

$$B_{ij} = \iiint_D \Phi_i(\bar{x})\mathbf{Q}_j(\bar{x})dV \quad i = 1,2,\cdots\infty;\quad j = 1,2,\cdots p$$
$$p : Number\ of\ inputs \qquad 1.4.7.$$
$$D : Whole\ spatial\ domain\ spanning\ the\ solid$$

Similarly, if thermocouples in fixed locations are used to measure temperatures, the **C** matrix can be computed as:

$$C_{ij} = \iiint_D \Phi_j(\bar{x})\delta(\bar{x} - \bar{x}_i)dV \qquad i = 1,2,\ldots q \quad j = 1,2,\ldots \infty \qquad 1.4.8.$$

Where $\delta(\bar{x} - \bar{x}_i)$ is Kroneker delta with $\bar{x}_i$'s the locations of the q thermocouples.

This eigen function based model is truncated at a suitable dimension to give a finite dimensional approximation to the infinite-dimensional system. In most applications the physical input devices (heaters and coolers) do not have a high spatial frequency content, hence it is very difficult to "excite" the higher spatial harmonics. The eigen function based models are, therefore, tend to be of a lower order.

The main disadvantages of using eigen function based models are:

1. The eigen functions are very sensitive to parameter variations and changes in boundary conditions.
2. For complicated geometries they are more difficult to evaluate. Most standard Finite Difference Equations (FDE) and Finite Element Analysis (FEA) packages do not have the ability to extract eigen functions and eigen values for the heat diffusion problem.
3. They cannot be experimentally computed.
4. The effects of non-linearities and model uncertainties cannot be easily studied.

1.4.2. Models Based on Spatial discretization:

Modeling techniques such as finite differences and finite elements, involve discretizing the domain into smaller parts and applying energy conservation to each element to determine the interaction between successive elements. For example the rectangular solid shown in 1.4.1. is discretized into a finite difference grid. The notation for the

temperatures at different nodes, in this finite difference grid is shown in figure 1.4.2. Using this discretization, the governing equation for the temperature at the ij^{th} node can be written by performing energy balance at that node. Equation 1.4.9., shows the resulting equation:

$$\rho C_p \frac{dT_{i,j}}{dt} = k\left\{\frac{1}{(\Delta x)^2}\left[T_{i+1,j} + T_{i-1,j} - 2T_{i,j}\right]\right\} + k\left\{\frac{1}{(\Delta y)^2}\left[T_{i,j+1} + T_{i,j-1} - 2T_{i,j}\right]\right\} + q_{i,j} \qquad 1.4.9.$$

In equation 1.4.9., q_{ij} is the external heat input or the internal heat generated at the ij^{th} node, ρ is the density of the solid, C_p is the specific heat of the solid and k is the thermal conductivity. Δx *and* Δy are the dimensions of the finite difference grid as shown in figure 1.4.2.

Equations similar to 1.4.9. can be written for all the nodes in the solid and arranged in a vector to create the matrix differential equation:

$$\begin{aligned} &\dot{\mathbf{X}} = \mathbf{AX} + \mathbf{BU}; \\ &\mathbf{X} = [T_1, T_2, \cdots, T_{mn}]^T; \\ &\mathbf{U} = [q_1, q_2, \cdots q_{mn}]^T; \\ &m : \textit{number of nodes along thickness} \\ &n : \textit{number of nodes along width} \end{aligned} \qquad 1.4.10.$$

X is the vector of temperature at each of the nodes and **U** is the vector of the heat flux generated/input at each of the nodes. The above equation is a finite dimensional approximation to state space representation for the heat conduction problem, obtained by spatial discretization.

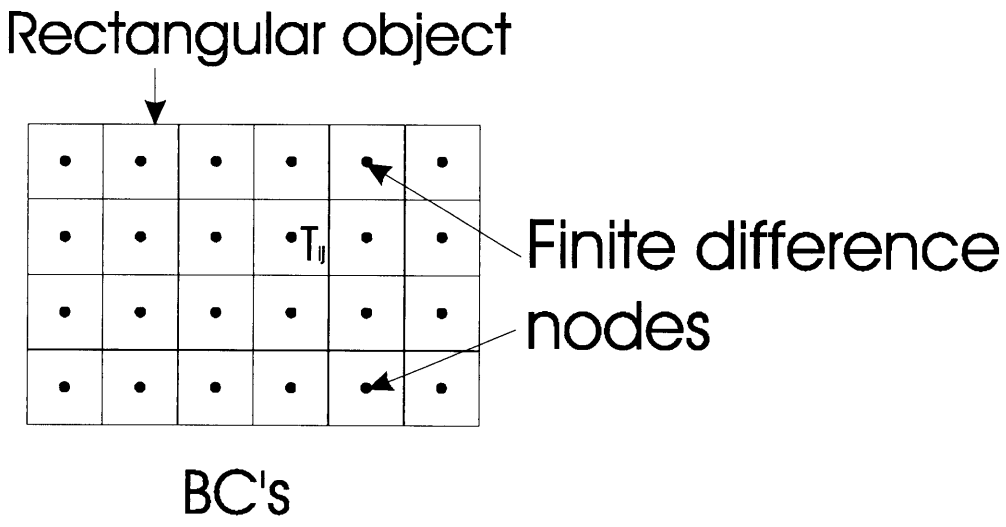

Figure 1.4.1. Spatial discretization of the rectangular domain into finite differences.

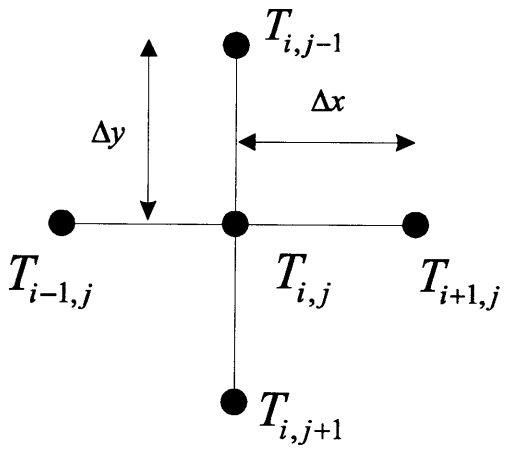

Figure 1.4.2. Temperatures at the different nodes in a finite difference scheme.

The advantages of using this representation are:

1. Finite differences are widely used in the analysis of heat conduction problems and there are many commercially available packages that could be used to simulate the models.
2. Non-linearities can be easily incorporated in the models.
3. The state of the system has a direct physical interpretation and therefore could aid in developing better intuition in the process and thereby be able to design better compensators.

The chief disadvantage of using a finite difference scheme is that the dimension of the state space grows rapidly with the increased accuracy needed in the computation. This makes it unattractive for real-time applications. However, with increased availability of inexpensive computational power this may not be a problem. Another disadvantage of the finite difference formulation is that the model cannot be experimentally derived.

1.4.3 Green's Function based models:

Green's function models use an integral equation representation for the PDE in 1.1.1. The Green's function corresponding to equation 1.1.1., $G(\bar{x},\bar{\xi},t)$ is defined as the temperature response at a location $\bar{x}$ (vector of coordinates) and at a time instant t caused by a unit impulse of heat flux at a location $\bar{\xi}$ (vector of coordinates). Equation 1.4.11. illustrates the definition of the Green's function.

$$\begin{aligned} &\rho C_p \frac{\partial G}{\partial t}(\bar{x},\bar{\xi},t) = \nabla(k(\bar{x})\nabla)G(\bar{x},\bar{\xi},t) + \delta(\bar{x}-\bar{\xi},t); \\ &Bo(G(\bar{x},\bar{\xi},t)) = 0; \qquad \textit{Boundary Condition} \end{aligned} \tag{1.4.11.}$$

Where:

ρ : *Density of solid*
C_p : *Specific heat of solid*
∇ : *The Laplacian operator*
$\bar{x}, \bar{\xi}$: *Vectors of coordinates describing the solid*
$\delta(\bar{x} - \bar{\xi}, t)$: *unit impulse at* $\bar{x} = \bar{\xi}$, *at* $t = 0$
$G(\bar{x}, \bar{\xi}, t)$: *The Green's Function*

The temperature within the solid due to arbitrary heat input $\phi(\bar{x}, t)$ can then be computed by the principle of linear superposition as shown in equation 1.4.12.

$$T(\bar{x}, t) = \int_D G(\bar{x}, \bar{\xi}, t)\phi(\bar{\xi}, t)d\xi; \qquad \text{1.4.12.}$$
$$D\text{: The entire domain}$$

Similarly, a steady-state Green's function can be defined as the steady state temperature distribution obtained at a location $\bar{x}$ caused by a unit heat input at a location $\bar{\xi}$. Equation 1.4.13 shows the definition of a steady state Green's function.

$$\nabla\big(k(\bar{x})\nabla\big)G(\bar{x}, \bar{\xi}) = -\delta(\bar{x} - \bar{\xi})$$
$$Bo_s(G(\bar{x}, \bar{\xi})) = 0;\ \textit{Boundary condition} \qquad \text{1.4.13.}$$

Where, $\delta(\bar{x} - \bar{\xi})$ is a unit (steady state) input at a location $\bar{x} = \bar{\xi}$ and $k(\bar{x})$ is the conductivity and $G(\bar{x}, \bar{\xi})$ is the steady-state Green's function. The steady state temperature $T(\bar{x})$ can then be written by linear superposition as:

$$T(\bar{x}) = \int_D G(\bar{x}, \bar{\xi})\phi(\bar{\xi})d\xi; \qquad \text{1.4.14.}$$
$$D\text{ :The entire domain}$$

One of the chief advantages in using a Green's function based model is that the model could be experimentally derived. From the definition of the Green's function we have seen that it is the temperature response due to a unit input at $\bar{x} = \bar{\xi}$. We could spatially

discretize the controlled solid into several smaller regions and apply input to one of these regions and measure the temperature everywhere. By repeating this process for all the discrete regions we could experimentally determine the Green's function. See Wilkinson (1965) for a detailed explanation of this technique. The dimensionality of the problem is dependent on the accuracy needed in the temperature distribution. As will be seen in Chapter 4, the size of the problem can, however, be reduced considerably, after the heating and cooling locations have been selected.

1.5 Cost functionals:

In manufacturing processes the energy and hardware available is limited and where possible these should be conserved. However, in all applications, using less energy and lesser amount of hardware manifests itself as degradation in the accuracy and speed of response to which the temperature can be controlled. There is, therefore, a trade off between the amount of energy used and the accuracy in the achieved temperature. This trade off can be accomplished by implementing controllers that are optimal in some sense. The quantity being optimized is termed as the cost functional. In this thesis, all the cost-functionals considered are quadratic because of the availability of suitable theory and the ease of implementation of the solutions obtained for such a formulation.

There are three classes of quadratic performance indices that are considered in this thesis:

1. An infinite horizon quadratic cost functional as shown in equation 1.5.1.

$$J = \int_0^\infty (\bar{x}^T \mathbf{P} \bar{x} + \bar{u}^T \mathbf{Q} \bar{u}) dt \qquad 1.5.1.$$

where, $\bar{x}$ is the state vector and $\bar{u}$ is the input vector as derived in any of the state-space models discussed in section 1.4. **P** is the weighting matrix for the error in the state and **Q** is the weighting matrix for the input. This cost functional is used in situations where steady-state temperatures are being controlled. In situations where the measurements and the states are not corrupted by noise, the problem of optimizing the cost function in 1.5.1. reduces to the standard Linear Quadratic Regulator (LQR) problem (See Anderson and Moore, (1989) pp. 35-55).

In the situation where the states and the outputs are corrupted with noise (assumed Gaussian), the expected value of 1.5.1. is to be minimized. This leads to a Linear Quadratic Gaussian (LQG) compensator. (See Kwakernaak and Sivan (1972) for details). The controllers designed this way need an estimate of all the states. In situations where model uncertainties are high and measurements are too few, these full state estimates may not be adequately accurate and this technique is not suitable in such situations. However, in situations where the models are better known and full state estimates can be constructed, the structure of the compensator has several desirable characteristics.

2. A finite horizon quadratic cost functional with penalty on the final value of the state:

$$J(\mathbf{U}) = \left(\mathbf{X}(T_f) - \mathbf{X}_D(T_f)\right)^T \mathbf{P}\left(\mathbf{X}(T_f) - \mathbf{X}_D(T_f)\right) + \int_0^{T_f} \left\{\left(\mathbf{X}(t) - \mathbf{X}_D(t)\right)^T \mathbf{Q}\left(\mathbf{X}(t) - \mathbf{X}_D(t)\right) + \mathbf{U}^T \mathbf{R}\mathbf{U}\right\} dt \qquad 1.5.2.$$

t : *time during cooling*
T_f : *The final time at the end of cooling*
$\mathbf{X}(t)$: *Vector of temperatures at all nodes*
$\mathbf{X}_D(t)$: *Vector of desired temperature trajectories*
$\mathbf{U}(t)$: *input vector*
$\mathbf{P} \geq 0; \mathbf{Q} \geq 0; \mathbf{R} > 0$; *weighting matrices*

This cost functional is useful in situations where a temperature trajectory has to be achieved during a specific duration of time. Heat treatment operations have such requirements on the temperature trajectory. By picking values for **P**, **Q** and **R,** different weights can be placed on the final value of temperature, the error in the temperature trajectory and the amount of control effort used, respectively. This gives a tool for trading off these three, often competing requirements. Chapter 5., deals with this problem and its solution in some detail.

3. The third type of cost functional deals with spatial rather than time optimization. Equation 1.5.3., shows a general form of such a cost functional.

$$J = \int_S L_1(T(\bar{x}), T_i'(\bar{x}), \phi_c(\bar{x}), \bar{x}) d\bar{x} + \iint_S L_2(T(\bar{x}), T_i'(\bar{x}), \phi_c(\bar{x}), \bar{x}, T(\bar{\xi}), T_i'(\bar{\xi}), \phi_c(\bar{\xi}), \bar{\xi}) d\bar{x} d\bar{\xi} \qquad 1.5.3.$$

L_1 and L_2 are quadratic functions of the first and second order respectively. $\bar{x}$ and $\bar{\xi}$ are vectors of coordinates describing the geometry of the solid in which the temperature is being controlled. S is the region of space occupied by the solid of interest and the integrations are performed over this space. $T(\bar{x})$ *and* $T(\bar{\xi})$ are the temperature distributions in steady state at locations $\bar{x}$ and $\bar{\xi}$ respectively. $T_i'(\bar{x})$ is

the gradient of temperature in the i^{th} direction at a location $\bar{x}$. $\phi_c(\bar{x})$ is the control heat flux input applied at a location $\bar{x}$.

Such cost functionals are used in determining steady state distribution of heat fluxes that achieve a desired steady state temperature distribution, therefore, this cost functional does not involve time. The integrations are carried out over the space variables, in both the terms of equation 1.5.3. This is in contrast to the two cost-functionals discussed previously, where the integration was performed with respect to time. L_1 and L_2 are two quadratic kernels, which could be functions of the temperature, temperature gradient and controller heat flux. One of the advantages of this cost functional over the cost functional considered in equation 1.5.1. is that the compensators designed this way do not need full state estimates and lower order compensators could be constructed with relative ease. The draw back here is that the transient design has to be performed separately on a case by case basis. Chapters 3., and 4., discuss the use of such cost-functionals in great detail.

1.6. Structure of the thesis:

Figure 1.6.1. shows a schematic detailing the different aspects of controlling heat conduction systems. Temperatures need to be controlled in a solid of an arbitrary shape. The solid may have actuators such as heaters and cooling passages embedded within it and may have actuators such as cooling sprays and plasma torches providing heat fluxes at the surface. Similarly there could be measurement devices such as thermocouples embedded within the solid or could have measurement devices such as pyrometers that

measure surface temperatures. The process requirements can be translated into a desired temperature distribution trajectory $T_D(x,y,z,t)$ for the solid, whereas the actual temperature achieved in the sold could be $T(x,y,z,t)$. External disturbances such as changes in the ambient temperature effect the temperature distribution in the solid.

Typically there is a maximum error in temperature that could be tolerated in a process and external disturbances and model uncertainties exist and should be compensated for by the controller. Based on these requirements designer then needs to select the following:

1. The types of models that are the most appropriate for the specific application.
2. The number, locations and intensities of the inputs (heaters and coolers) needed.
3. The locations of measurements.
4. The type of optimal control algorithms that best satisfy the process requirements.

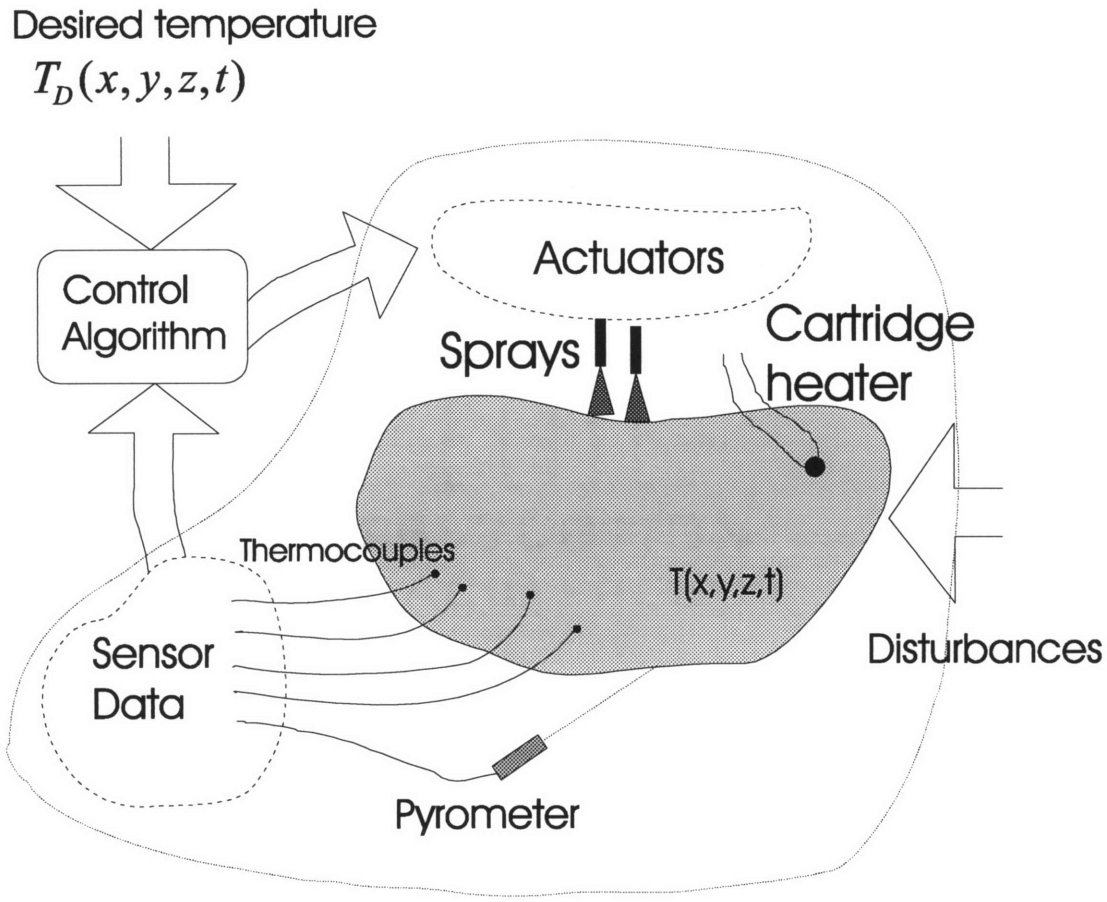

Figure 1.6.1. Schematic of a typical closed-loop temperature distribution control problem.

The models for the heat conduction process are well developed, however, selecting the appropriate model for each application is of great importance since it determines whether real-time control can be applied or not. Sometimes picking the right kind of model can reduce redundancy in hardware used (See, Wilkinson (1965)). This thesis shows the use of an eigen-function expansion based model in Chapter 2., a Green's function based model in Chapter 4., and a finite difference equation based model in Chapter 5.

The problem of arranging thermocouples and other point measurement devices is well understood (see El Jai and Pritchard (1988)) and could be used directly in any application. However, the problem of designing the locations and distribution for actuation is not well understood. This is one area this thesis has explored in some detail and a method for determining heater/cooler locations for steady-state temperature control has been developed.

Chapter 2., discusses an example of steady-state temperature distribution control in a steel specimen. A scanning type heat source is used as a heat input device. Several restrictions posed by hardware limitations are examined here. An experiment was built using a welding apparatus and a scanning mechanism with the purpose of exploring the hardware issues that one would face in such a control problem. A detailed simulation study was performed on a model of the experimental specimen. The use of an eigen-function expansion based model is demonstrated in this study and a linear quadratic gaussian (LQG) compensator based optimal control approach was used as for control. This approach is the most commonly used approach in DPS literature and the purpose of the

experiment and simulation study that accompanied it was to explore the limitations of the current state of the art in DPS control.

Chapters 3 and 4 form the central contributions of this thesis. Chapter 3., develops the theory needed for determining the optimal spatial distribution of inputs for performing steady state temperature control. A variational calculus approach is used to derive the conditions of optimality. Cost functionals defined on a space (as opposed to time) are used here (see equation 1.5.3.). Chapter 4., builds on this technique to illustrate an application to designing a temperature controller for a molding application. The use of a Green's function based model is illustrated in these two chapters. A technique for designing stable controllers that satisfy the steady-state requirements on the process is presented in Chapter 4.

A transient temperature control problem is presented in Chapter 5. A finite horizon optimal tracker is implemented on a model of a steel slab. This problem is motivated by the accelerated cooling process used in the manufacture of hot rolled steel slabs. A finite-difference based model is used along with a finite horizon linear quadratic cost-functional (see equation 1.5.2.) in this application.

Chapter 2

STEADY STATE OPTIMAL CONTROL OF TEMPERATURE IN TWO DIMENSIONS

2.1 Prior experiments

In section 1.2. we have studied several possible applications of distributed parameter systems control to manufacturing processes. As was mentioned in the previous chapter, very few experimental implementations of distributed control for temperature have been performed. Ray (1978) has a detailed survey of all the applications of distributed parameter systems theory, till that date and there have been very few applications or experiments since that review paper (See, Miho et. al.(1992)). In this section some of these past experiments are discussed

Ray (1978), Lausterer (1977) and Morari and O'Dowd (1980) use an experimental setup which has a cylindrical specimen in which temperature distributions are controlled. The specimen is an annular cylinder in which the outer surface is insulated and the inner surface is cooled with water. There are three sets of heaters embedded in the specimen at different axial locations with a set of thermocouples embedded at different axial and radial locations. Ray (1978) and Lausterer (1977) have implemented a sub-optimal temperature estimator on the cylindrical specimen while Morari and O'Dowd (1980) have used the same specimen to study the effect of non-stationary noise in heat conduction systems. In this experiment the locations for heaters and sensors and their numbers were selected arbitrarily. The purpose of this experiment is to verify the performance of

theoretical results in DPS theory rather than to facilitate better control of any process in particular. In all the experiments performed by this group, an eigen-function expansion based model was used.

The second experiment was performed by Ball and Hewitt (1974). This experiment involved a copper bar with heating on one end of the bar. The copper bar was modeled as a one-dimensional solid and the controller was designed to achieve a desired final temperature distribution in the shortest amount of time. The model that was used here was based on a Green's function for the transient problem, which was experimentally evaluated. Again, the purpose of this experiment was to demonstrate a theoretical result in time optimal control of the final value of the temperature and was not motivated by any particular application.

The third experimental set up was built at the MIT instrumentation laboratory. Gould and Murray-Lasso (1966) and Kaiser (1971) have used this experimental set up to verify several theoretical techniques developed by them. The experiment comprised of an insulated metallic bar in which temperatures were controlled. The bar was modelled as a one-dimensional solid in these experiments. Gould and Murray-Lasso (1966) have used this experimental set up to demonstrate modal control methods to control temperature distributions, while Kaiser(1971) has performed experiments that involved steady state temperature control involving a Green's function based approach. No optimal estimator was utilized in these experiments and the temperatures were estimated by interpolating

the measured temperatures at specific locations. These experiments were motivated by temperature control in precision instrumentation for aerospace applications.
One common thread to all the experiments performed is that they use some form of optimal control to achieve the desired temperatures. This is also a suitable approach for most processes because in all real processes there is a trade-off to be made between the accuracy achieved and the amount of heating/cooling used. An optimal control approach to the temperature control problem lends itself to making this trade off in an efficient manner.

This chapter discusses an experiment that was set up, as a part of this thesis, to explore the hardware limitations that limit the applicability of current distributed parameter systems approaches to manufacturing processes. Several simulations were performed on a model of the experimental specimen used in this experiment that highlight some of the shortcomings of the present state-of-the-art.

2.1.1. The need for a detailed study to identify deficiencies in the state-of-the-art:

As can be seen from the prior section, the amount of experimental and application oriented research work in the DPS area is very meager when compared to the vast amount of literature on the theory. The lack of enough experimentation and applications of distributed parameter systems control theory suggests that there are limitations in both the theory and hardware available for designing controllers for processes with heat conduction. There is therefore a need for more specific studies to investigate the obstacles for implementing DPS control. The limitations could be caused by:

1. The availability and short comings of suitable actuators or sensors.
2. The deficiencies in the models used.
3. Computing requirements in implementing several types of control.
4. Suitability of different control approaches for different problems

Hence, there is a need to perform detailed studies to evaluate the short-comings in the current state of the art. The experiment discussed in this chapter was set up with this in mind. In all the experimental investigations discussed earlier in this section, the inputs were limited in terms of their spatial manipulability. This is because, they were fixed in space at arbitrary locations within the controlled solids. In manufacturing applications, there are several input devices such as scanning torches, lasers, cooling jets etc. that can be scanned on the surfaces of solids being heated/cooled. This gives a greater manipulability for the input heat flux distribution. The experiment discussed in this chapter uses a scanned Tungsten Inert Gas (TIG) welding torch. This provides a highly flexible input device that is better suited for studying DPS control. The experiment aims to control steady state temperatures in a steel specimen and is very similar to the control problems that one deals with in welding, furnace temperature control, mold temperature control etc.

As a part of this study, detailed simulations have been performed on a model of the experimental setup. The key areas that need further investigation have been identified as a part of this simulation study using the model. Some preliminary experiments were

conducted on the experimental setup, however in the interest of time, detailed implementation of the controllers studied in simulation has not been performed.

2.2 Description of the experimental setup:

The experiment comprises of a mild steel rectangular specimen which is 1cm x 10cm x 0.4cm. The two rectangular faces of the specimen were insulated with strips of Maycor (sheets of Alumina), which is a ceramic insulating material. There are fourteen thermocouples embedded within the specimen for temperature measurements. Figure 2.2.1 shows the specimen and the thermocouple locations. The thermocouples are laid down in two rows, each with seven thermocouples evenly spaced, with a spacing of 12.5mm between them. The holes for the thermocouples are drilled to the mid point of the steel specimen in its thickness direction (into the plane of the paper). The upper row of thermocouples is 3mm from the surface and the lower row of thermocouples is 7mm from the surface of the specimen.

The steel specimen and the Maycor strips are assembled on to a water cooled copper jacket. Three sides of the rectangular block are in contact with the copper block and the fourth side lies exposed to the top. A paste of thermally conductive grease is applied to the interface of the copper block and the steel specimen. This ensures a good thermal contact between the copper block and the steel specimen. The Maycor strips and the water cooled copper jacket allow us to model the specimen as a two-dimensional rectangular solid with a constant temperature boundary condition on the three surfaces in contact with the copper block and a free convection boundary condition on the fourth surface. (This will be discussed in detail in Section 2.3.) A cross-sectional schematic of

the copper block is shown in figure 2.2.2. Figure 2.2.3. shows the assembly of the steel specimen and the copper block.

The specimen and the copper block are placed under a TIG torch. The TIG torch is reciprocating rapidly over the top surface of the steel specimen. The arc voltage, which is a function of the arc height, is kept constant while the torch is moving. This is accomplished by a servo on to which the torch is fitted in which the arc voltage is measured and is fed back to the servo. This is indicated as the high bandwidth servo in figure 2.2.4. The servo along with the torch is mounted on to a set of horizontal guide ways and a lead screw. A DC motor actuates the lead screw and there is an encoder to measure the rotational displacement of the motor. This DC motor along with the encoder is used to control the horizontal motion of the torch parallel to the surface of the specimen.

2.2.1. Idea behind the experiment:

If the scanning of the torch along the top surface is much faster than the dominant time constant of the thermal system, the distribution of the heat flux will "look" to be continuously distributed over the upper surface of the specimen. This means that the temperature responses of the thermocouples will be very similar in the two cases: one in which the heat flux is distributed everywhere and the other where this high speed scanning is used.

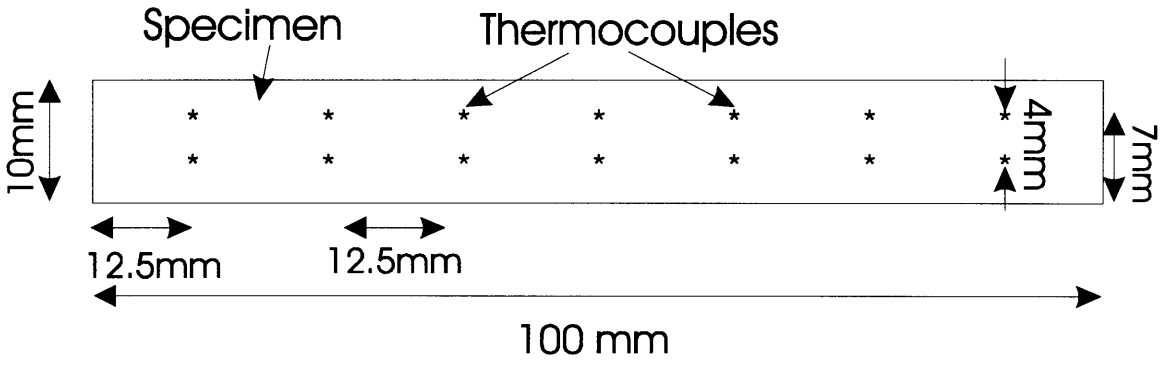

Figure 2.2.1 The dimensions of the steel slab with locations of the thermocouples.

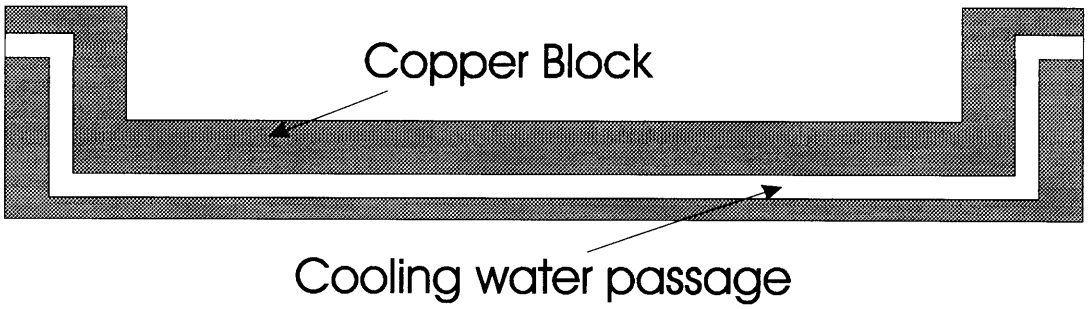

Figure 2.2.2. Cross section of the copper block.

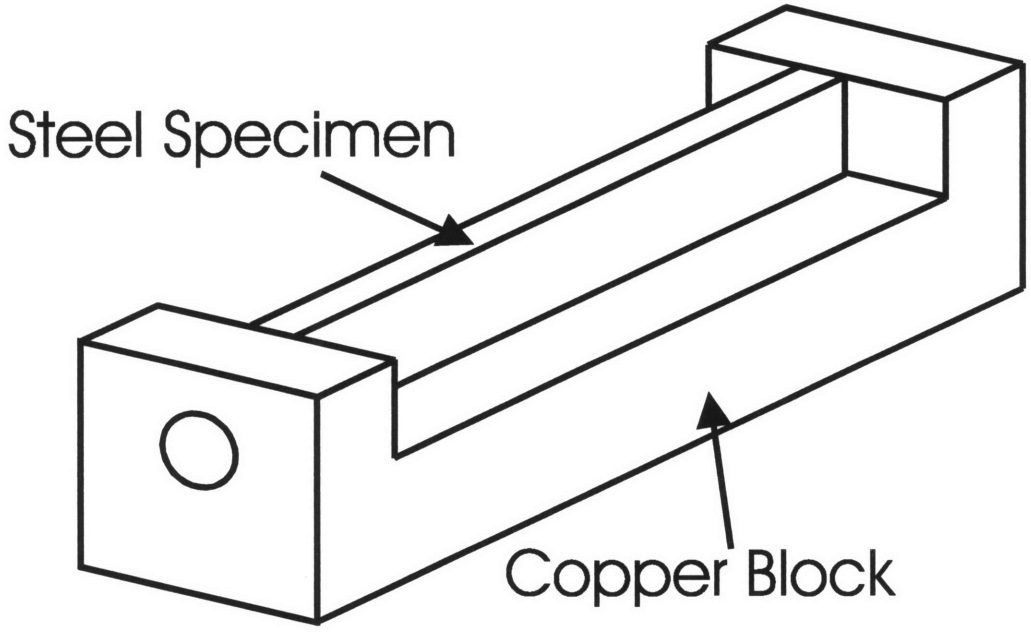

Figure 2.2.3. The steel specimen assembled on to the copper block.

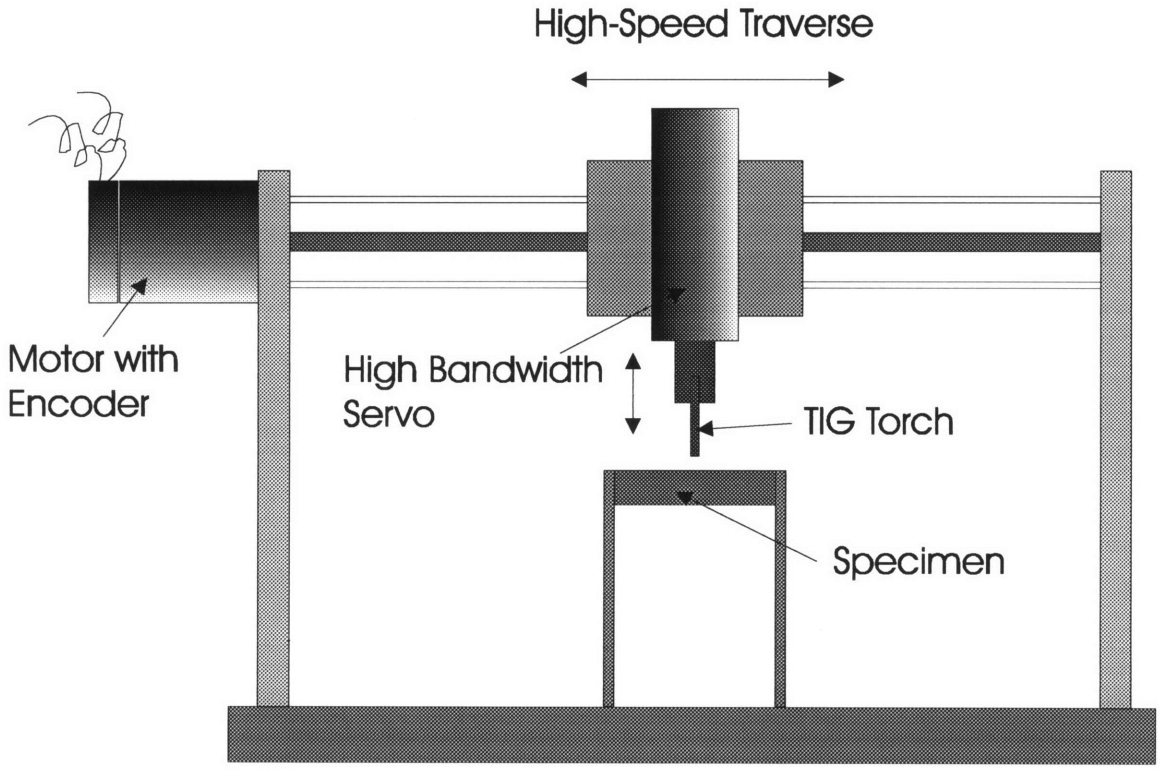

Figure 2.2.4. The arc-scanning mechanism.

The position of the torch can be sensed using the encoder data and the current through the torch can be varied with position. The high bandwidth servo is used to maintain the voltage across the torch constant by controlling the arc length. The heat flux incident on the surface at any location, $\phi(x,t)$ is then given by:

$$\phi(x,t) = \eta_{eff} I(x,t) V(x,t) \qquad 2.2.1$$

Where η_{eff} is an efficiency factor, *I(x,t)* is the value of the current through the welding torch which is varied along the length of the specimen and with time. The voltage of the arc *V(x,t)* can similarly be varying, but during the experiment it is held constant. Hence, changing the current through the torch, the heat flux that is incident on the surface of the specimen is varied. Figure 2.2.5 shows this effect.

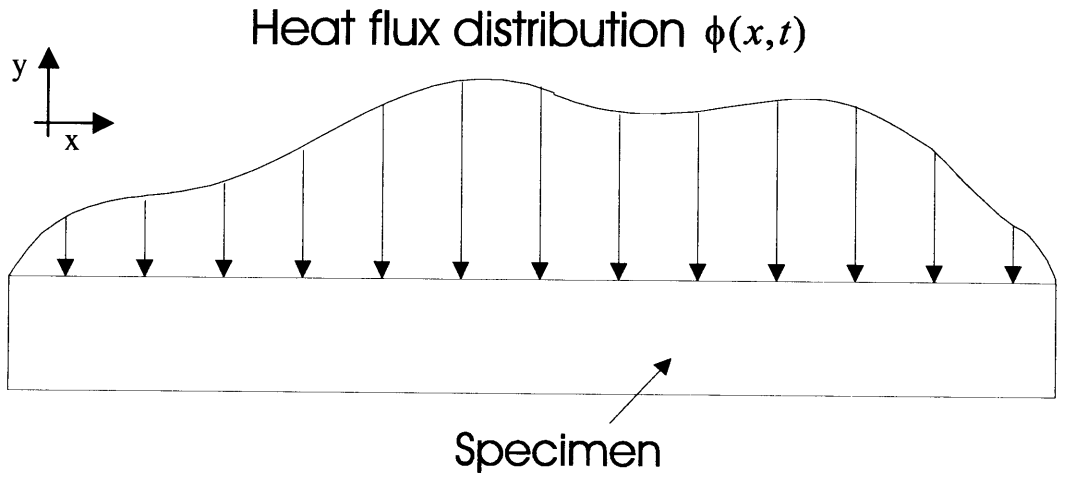

Figure 2.2.5. Continuously distributed heat flux due to scanning.

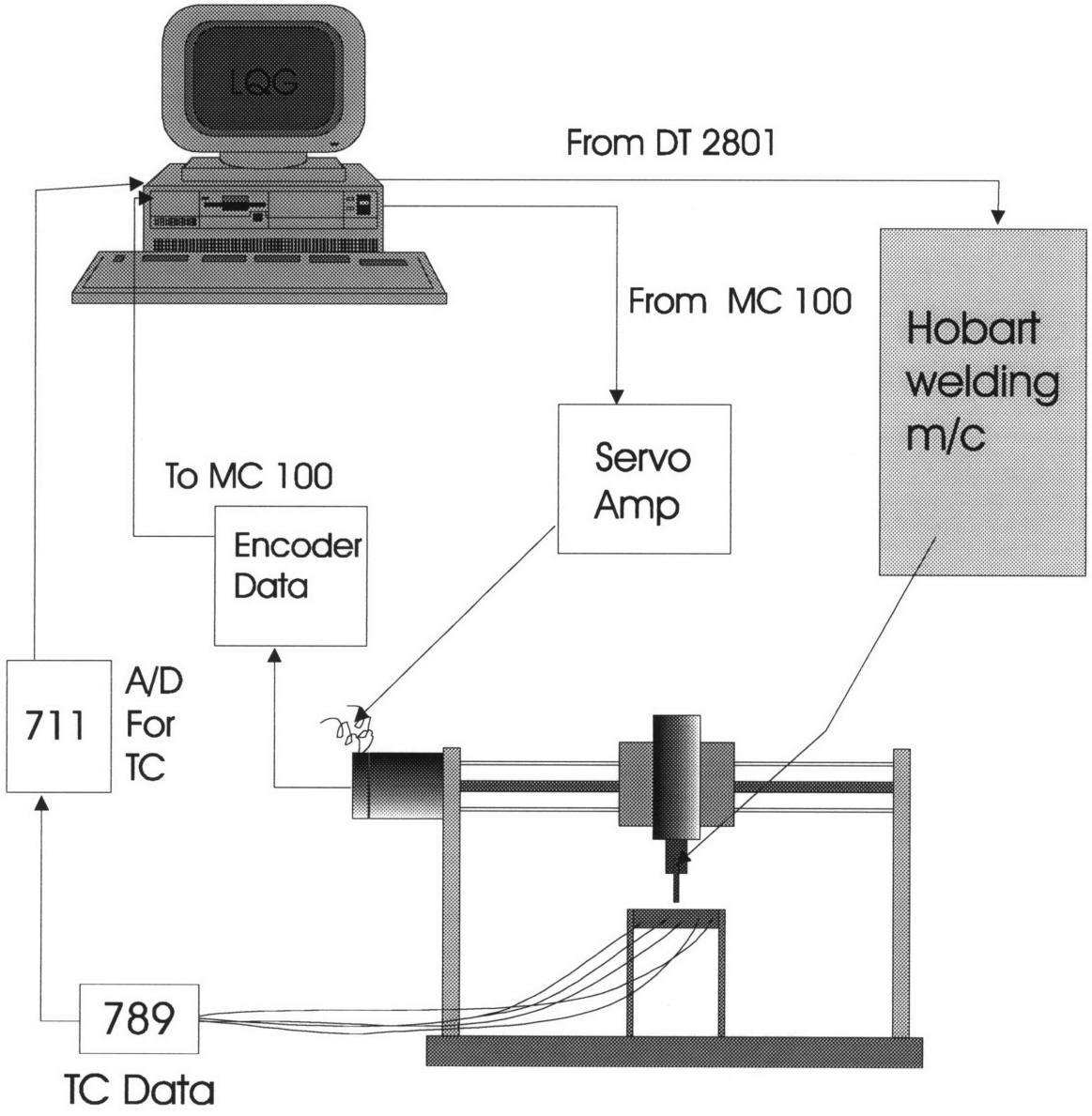

Figure 2.2.6. The layout of the experiment.

2.2.2. Description of the hardware used for experiment:

A Hobart Cyber-TIG III welding power supply is used to power the TIG torch used in the experiment. The power supply is a voltage driven current amplifier. A D/A (Data Translation 2801 board) is used for the voltage input. The temperature data is acquired using two boards: Omega 711 and Omega 789. The boards support 16 channels of which 14 are used for the experiment. An MC 100 single axis motion control card is used to achieve the rapid traverse of the torch assembly across the specimen. The encoder data is also read in by the MC 100 motion control card and an EG&G servo amplifier is used to power the motor. Figure 2.2.6 shows a schematic of how the hardware is connected.

2.3. Model for control:

The two lateral sides of the rectangle are insulated with Maycor (ceramic) sheets. If we can assume that the insulation is perfect, the heat transfer within the steel specimen can be simplified to a two dimensional problem. This is because, the Maycor strips ensure that there is no significant heat transfer in the direction perpendicular to the plane of the page in figure 2.2.1. The three sides of the rectangle are in contact with the water-cooled copper block. Copper has a significantly higher thermal conductivity than steel and if the temperature of the water is constant, this boundary condition can be modeled as a constant temperature boundary condition on three sides of the rectangle. The fourth side facing up, is exposed to the ambient. Hence, this can be modeled as a free convection boundary condition. Equation 2.3.1., shows the governing Partial Differential Equation.

$$\rho C_p \frac{\partial}{\partial t} T(x,y,t) = K \frac{\partial^2}{\partial x^2} T(x,y,t) + K \frac{\partial^2}{\partial y^2} T(x,y,t); \qquad 2.3.1.$$
$$0 < x < b;\ 0 < y < a;$$

Where, the dimensions of the rectangular solid are "*a*" by "*b*". It is assumed here that the different material properties remain constant with space and temperature. The boundary conditions are then given by:

$$B.C.'s:$$

$$\left.\begin{aligned} &T(x,0,t)=0;\\ &T(x,a,t)=0;\\ &T(b,y,t)=0; \end{aligned}\right\} \cdots \left|\begin{aligned} &Cooling\ on\ three\ sides\\ &modelled\ as\ constant\\ &temperature \end{aligned}\right. \qquad 2.3.2.$$

$$-\alpha\frac{\partial T}{\partial x}+\beta T\Big|_{x=0}=\phi(0,y,t);\ \cdots \left|\begin{aligned} &Top\ surface\ with\ heat\ flux\ from\\ &torch\ and\ convection \end{aligned}\right.$$

With the initial condition:

$$T(x,y,0)=0; \qquad 2.3.3.$$

Figure 2.3.1. shows the setup of the model (notice the change in axes from figure 2.2.5.). Equations 2.3.1., 2.3.2. and 2.3.3. give us the equations for the heat conduction within the specimen. These should be modified into a form that is more suitable for control. As was seen in Chapter 1., there are several ways of representing this system of partial differential equations. Here an eigen function expansion based model will be used. The geometry is simple and the boundary conditions are well controlled and so we can derive the eigen functions analytically. These eigen values and eigen functions are used for deriving a state space system of equations, as will be discussed in what follows.

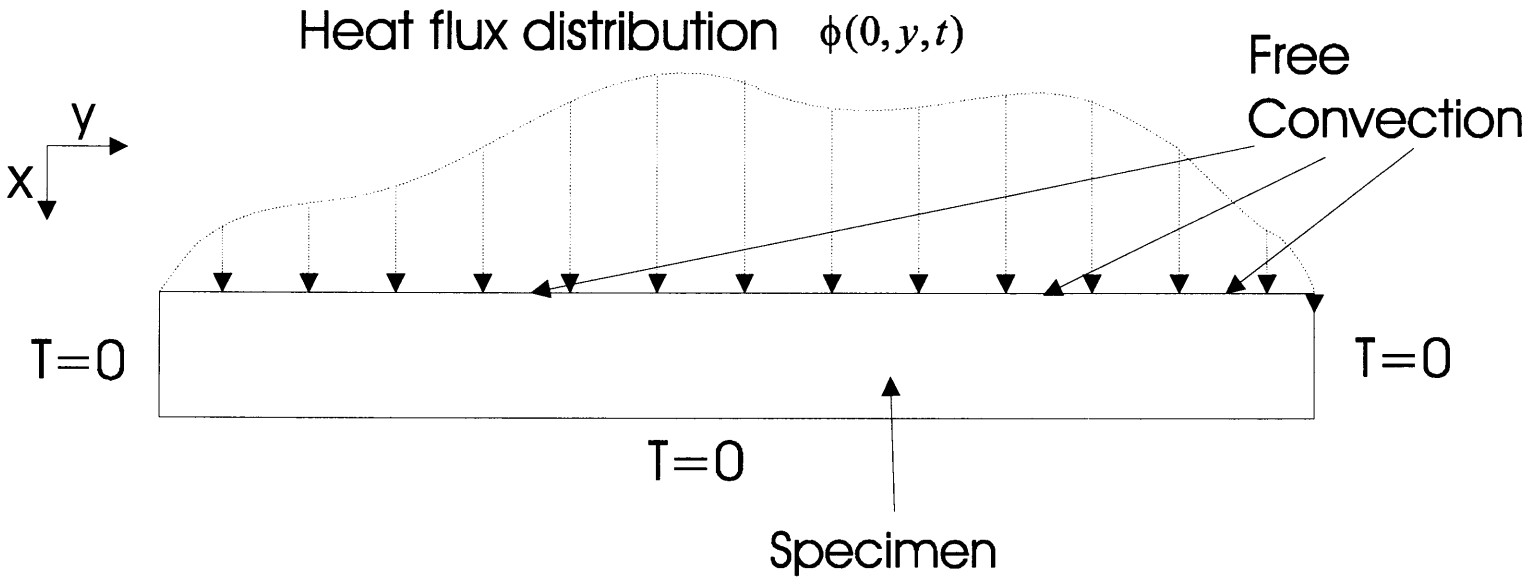

Figure 2.3.1. The model for the heat conduction within the specimen

2.3.1. Computation of the eigen functions and the eigen values:

The homogenous part of the PDE in 2.3.1.-2.3.3. is considered for deriving the eigen values and eigen functions. The homogenous part of the equations is obtained by dropping the heat flux term from the boundary conditions:

$$\begin{aligned} &B.C.'s: \\ &T(0,y,t)=0;\ \ T(a,y,t)=0; \\ &T(x,b,t)=0; \\ &-\alpha\frac{\partial T}{\partial x}+\beta T\Big|_{x=0}=0; \end{aligned} \qquad 2.3.4.$$

Writing the temperature for the homogenous problem in a separated form as:

$$T(x,y,t)=G(t)F(x)H(y) \qquad 2.3.5.$$

Substituting equation 2.3.5. in equations 2.3.1. and 2.3.4., and finally dividing throughout by $G(t)F(x)H(y)$, the following equation is obtained:

$$\frac{1}{kG(t)}\frac{dG(t)}{dt}=\frac{1}{F(x)}\frac{d^2F(x)}{dx^2}+\frac{1}{H(y)}\frac{d^2H(y)}{dy^2} \qquad 2.3.6.$$

Where $k=\dfrac{K}{\rho C_p}$ the thermal diffusivity.

The boundary conditions can be reduced to the following:

$$\begin{aligned} &H(0)=0;\ \ H(a)=0; \\ &-\alpha\frac{dF}{dx}+\beta F\Big|_{x=0}=0; \\ &F(b)=0; \end{aligned} \qquad 2.3.7.$$

To derive the eigen values and the eigen functions, both sides of equation 2.3.6. are equated to the eigen values of the problem. The eigen values are expressed as a sum of

two different terms $\lambda^2{}_{1m}$ *and* $\lambda^2{}_{1n}$ as can be seen in equation 2.3.8. It will be seen in what follows that this is a convenient form to express the eigen values of the problem.

$$\begin{aligned}\frac{1}{kG(t)}\frac{dG(t)}{dt} &= \frac{1}{F(x)}\frac{d^2F(x)}{dx^2}+\frac{1}{H(y)}\frac{d^2H(y)}{dy^2}\\ &= -\left(\lambda^2{}_{1m}+\lambda^2{}_{1n}\right)\end{aligned} \qquad 2.3.8.$$

The right hand and left hand side equations give rise to the following three equations:

$$\begin{aligned}\frac{1}{kG(t)}\frac{dG(t)}{dt} &= -\left(\lambda^2{}_{1m}+\lambda^2{}_{1n}\right)\\ \frac{1}{F(x)}\frac{d^2F(x)}{dx^2} &= -\left(\lambda^2{}_{1m}\right)\\ \frac{1}{H(y)}\frac{d^2H(y)}{dy^2} &= -\left(\lambda^2{}_{1n}\right)\end{aligned} \qquad 2.3.9.$$

Boundary conditions in 2.3.7. are applied to the last two equations in 2.3.9. and solved. This gives all the possible solutions for F(x) as $\theta(x)$ and all possible solutions for H(y) as $\vartheta(y)$:

$$\begin{aligned}\theta_m(x) &= \frac{1}{Nr}\left[\beta\sin\left(\lambda_{2m}x\right)+\alpha\lambda_{2m}\cos x\right]\\ \vartheta_n(y) &= \sqrt{\frac{2}{a}}\sin\left(\lambda_{1n}y\right)\end{aligned} \qquad 2.3.10.$$

Where,

$$\begin{aligned}&\lambda_{1n} = \frac{n\pi}{a};\ n = 1,2,\ldots,\infty\\ &\lambda_{2m}\ \textit{is positive solutions of}\\ &\beta\sin\left(\lambda_{2m}b\right) = -\alpha\lambda_{2m}\cos\left(\lambda_{2m}b\right);\ m = 1,2,\ldots,\infty\end{aligned} \qquad 2.3.11.$$

(*Nr* is picked so that the norm of the eigen function is unity). The eigen functions and eigen values of the two dimensional problem are then given by:

Eigen functions:

$$\Phi_i(x,y) = \frac{1}{Nr}\left[\beta \sin\left(\lambda_{2m} x\right) + \alpha\lambda_{2m} \cos\left(\lambda_{2m} x\right)\right]\sqrt{\frac{2}{a}} \sin\left(\lambda_{1n} y\right) \qquad 2.3.12.$$

Eigen values:

$$\lambda_i = \left(\lambda^2_{1n} + \lambda^2_{2m}\right)$$

These eigen values and eigen functions can be used to compute the state-space representation for the PDE.

2.3.2. Derivation of the State-Space model:

The state space model of the heat-conduction system is now derived, utilizing the eigen functions and eigen values derived in equation 2.3.12. The eigen function expansion of the temperature can be written as:

$$T(x,y,t) = \sum_{i=1}^{\infty} a_i(t)\Phi_i(x,y) \qquad 2.3.13.$$

Where $a_i(t)$*'s* are the Fourier coefficients for the temperature. The state-space system of equations can now be written with the Fourier coefficients as the states.

$$\begin{aligned} \dot{\mathbf{X}} &= \mathbf{AX} + \mathbf{BU} \\ \mathbf{Y} &= \mathbf{CX} \end{aligned} \qquad 2.3.14.$$

$$\mathbf{A}_{\infty x \infty} = diag\{-k\lambda_n\}, n = 1,2,3,\cdots\infty \qquad 2.3.15.$$

The states and initial condition are given by:

$$\begin{aligned} \mathbf{X}(t) &= [a_1(t), a_2(t), \cdots]^T \\ \mathbf{X}(0) &= [a_1(0), a_2(0), \ldots]^T \end{aligned} \qquad 2.3.16.$$

The matrices **B** and **C** are dependent on the distribution of the inputs and the measurements.

If the distribution of the inputs can be rewritten as:

$$\phi(x, y, t) = \mathbf{I}(x, y)^T \mathbf{U}(t) \qquad 2.3.17.$$

where the size of the vector $\mathbf{I}(x,y)$ is equal to the number of independently controlled inputs, each entry in the vector $\mathbf{I}(x,y)$ is the distribution of each of the inputs. Each entry in the vector $\mathbf{U}(t)$ is the time varying intensity of each of the inputs.

Similarly, the measurements are assumed to be distributed as $\mathbf{M}(x,y,t)$. In the present case, the measurements are point measurements using thermocouples. Therefore, $\mathbf{M}(x,y,t)$ will comprise of Kroneker δ's. The **B** and **C** matrices are then computed as:

$$B_{ij} = \int_0^a \int_0^b \Phi_i(x, y) I_j(x, y) dxdy \quad i = 1,2,\cdots\infty; \quad j = 1,2,\cdots p \qquad 2.3.18.$$

p: *Number of inputs*

$$C_{ij} = \int_0^b \int_0^a \Phi_j(x, y) \delta(x - x_i, y - y_i) dxdy \quad i = 1,2,\ldots q \quad j = 1,2,\ldots\infty \qquad 2.3.19.$$

Where p is the number of inputs and q is the number of measurements. (x_i, y_i) are the coordinates of the measurements (thermocouples).

Equations 2.3.14-2.3.19, detail the derivation of the eigen-function based state-space system of equations for the problem in equation 2.3.1. This size of the state space can be seen to be infinite. By truncating the eigen function expansion at a sufficient number, a finite dimensional approximation to the PDE is obtained. This finite dimensional model is used for control.

2.4. The controller design:

The welding supply has limited power supply (of about 2KWatts). This is typical of many processes where the power that we could use is limited. Hence a good way of trading off the amount of energy used to the accuracy of the closed loop temperature, is needed. A suitable way of achieving this is to use a quadratic performance index and Linear Quadratic Regulator (LQR) theory is used here to achieve this.

The LQR theory assumes the availability of the full state, hence an observer or an estimator that can evaluate the full-state from the partial measurements needs to be constructed. Since the measurements from the thermocouples are corrupted by noise, a Kalman Filter is used to perform this construction. This implementation of the LQR along with a Kalman Filter is the Linear Quadratic Gaussian (LQG) problem.

The equations in 2.3.14., can be rewritten to include the noise terms as:

$$\begin{aligned} \dot{\mathbf{X}} &= \mathbf{AX} + \mathbf{BU} + \Gamma w \\ \mathbf{Y} &= \mathbf{CX} + v \end{aligned} \qquad 2.4.1.$$

Where *"w" and "v"* are assumed to be zero mean Gaussian stochastic processes, with covariances:

$$E\{ww^T\} = \mathbf{W} \geq 0, \qquad E\{vv^T\} = \mathbf{V} > 0 \qquad 2.4.2.$$

Here $E\{..\}$ is the expectation operator. Hence the optimization problem that we are trying to solve is to minimize the cost-functional:

$$J = \lim_{T\to\infty} E\left\{\int_0^T (x^T\mathbf{Q}x + u^T\mathbf{R}u)dt\right\} \qquad 2.4.3.$$

Where, the weighting matrices are such that:

$$\mathbf{Q} = \mathbf{Q}^T \geq 0 \quad and \quad \mathbf{R} = \mathbf{R}^T > 0 \tag{2.4.4.}$$

By using the stochastic separation principle, this can be split up into two steps: First an optimal estimate $\hat{x}$ of the state x is obtained, by minimizing the error covariance:

$$E\{(x-\hat{x})^T(x-\hat{x})\} \tag{2.4.5.}$$

This estimate is then used in the deterministic problem of minimizing:

$$J = \int_0^\infty (x^T\mathbf{Q}x + u^T\mathbf{R}u)dt \tag{2.4.6.}$$

The optimal input with this cost function is given by:

$$u = -\mathbf{K}_c x \tag{2.4.7.}$$

Where, the matrix $\mathbf{K}_c$ is computed via the Algebraic Riccati Equation as follows:

$$\mathbf{K}_c = -\mathbf{R}^{-1}\mathbf{B}^T\mathbf{P}_c \tag{2.4.8.}$$

Where $\mathbf{P}_c$ is a symmetric positive-semi-definite solution of:

$$\mathbf{A}^T\mathbf{P}_c + \mathbf{P}_c\mathbf{A} - \mathbf{P}_c\mathbf{B}\mathbf{R}^{-1}\mathbf{B}^T\mathbf{P}_c + \mathbf{Q} = 0 \tag{2.4.9.}$$

Figure 2.4.1. shows the block diagram for the closed loop system. The discussion about the location of the disturbance in the block diagram will be presented in the next section. In the block diagram, the filter matrix $\mathbf{K}_f$ is given by another Algebraic Riccati Equation.

$$\mathbf{K}_f = \mathbf{P}_f\mathbf{C}^T\mathbf{V}^{-1} \tag{2.4.10.}$$

Where $\mathbf{P}_f$ is the symmetric-positive-semidefinite solution of:

$$\mathbf{A}^T\mathbf{P}_f + \mathbf{P}_f\mathbf{A} - \mathbf{P}_f\mathbf{C}^T\mathbf{V}^{-1}\mathbf{C}\mathbf{P}_f + \Gamma\mathbf{W}\Gamma = 0 \tag{2.4.11.}$$

If the corresponding stabilizability and detectability conditions are satisfied, (see Kwakernaak and Sivan (1972)), then the two matrices $\mathbf{K}_c$ and $\mathbf{K}_f$ exist and the implementation of the optimal compensator shown in figure 2.4.1., can be carried out.

Equations 2.4.7-2.4.11. along with figure 2.4.1. show the structure of the optimal solution and its implementation. In figure 2.4.1., **A,B,C** denote the model used for control purposes and *G(s)* is the actual plant, i.e. the dynamics within the specimen. The input of heat flux that the specimen experiences, is given by the sum of the disturbance and the controller heat flux. The disturbance heat flux is implemented by adding a known disturbance to the out-put of the controller as shown in figure 2.4.1.

As we have seen from the description of the experiment, the torch is scanned on the upper surface of the specimen. For the ease of implementation, the upper surface is divided into different zones where the input stays constant across the zone. The magnitude of the input can however change with time. The position data from the encoder (see figure 2.2.6.) is used to determine when the torch crosses from one zone to the next. Once the torch crosses over to the next zone the voltage value corresponding to the next zone is output to the Hobart welding power supply, which outputs a suitable current. Figure 2.4.2. illustrates the implementation of the heat-flux input. In the simulation study to be presented next, the same assumption is made on the distribution of the heat flux.

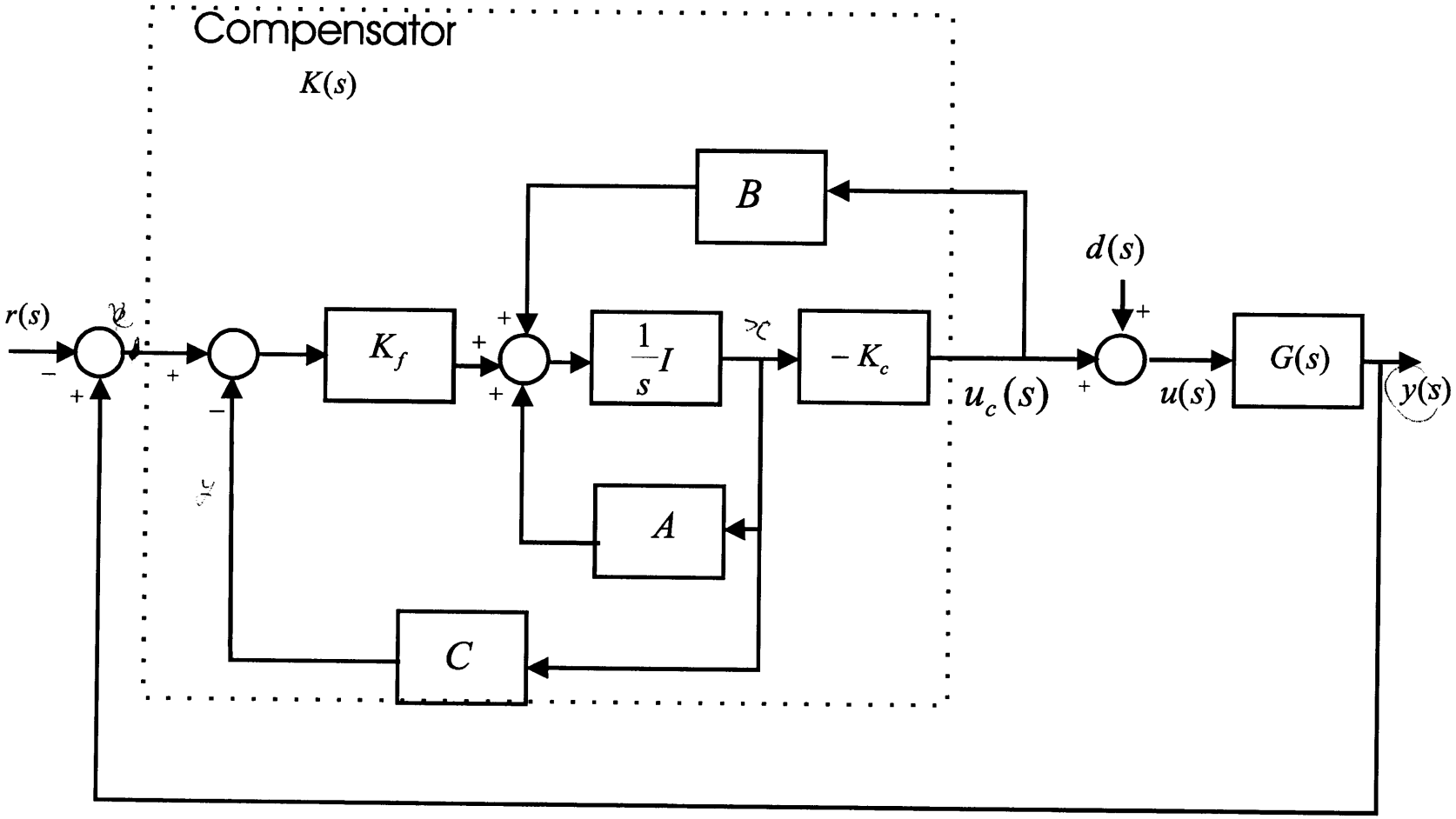

Figure 2.4.1. The LQG compensator structure used in study

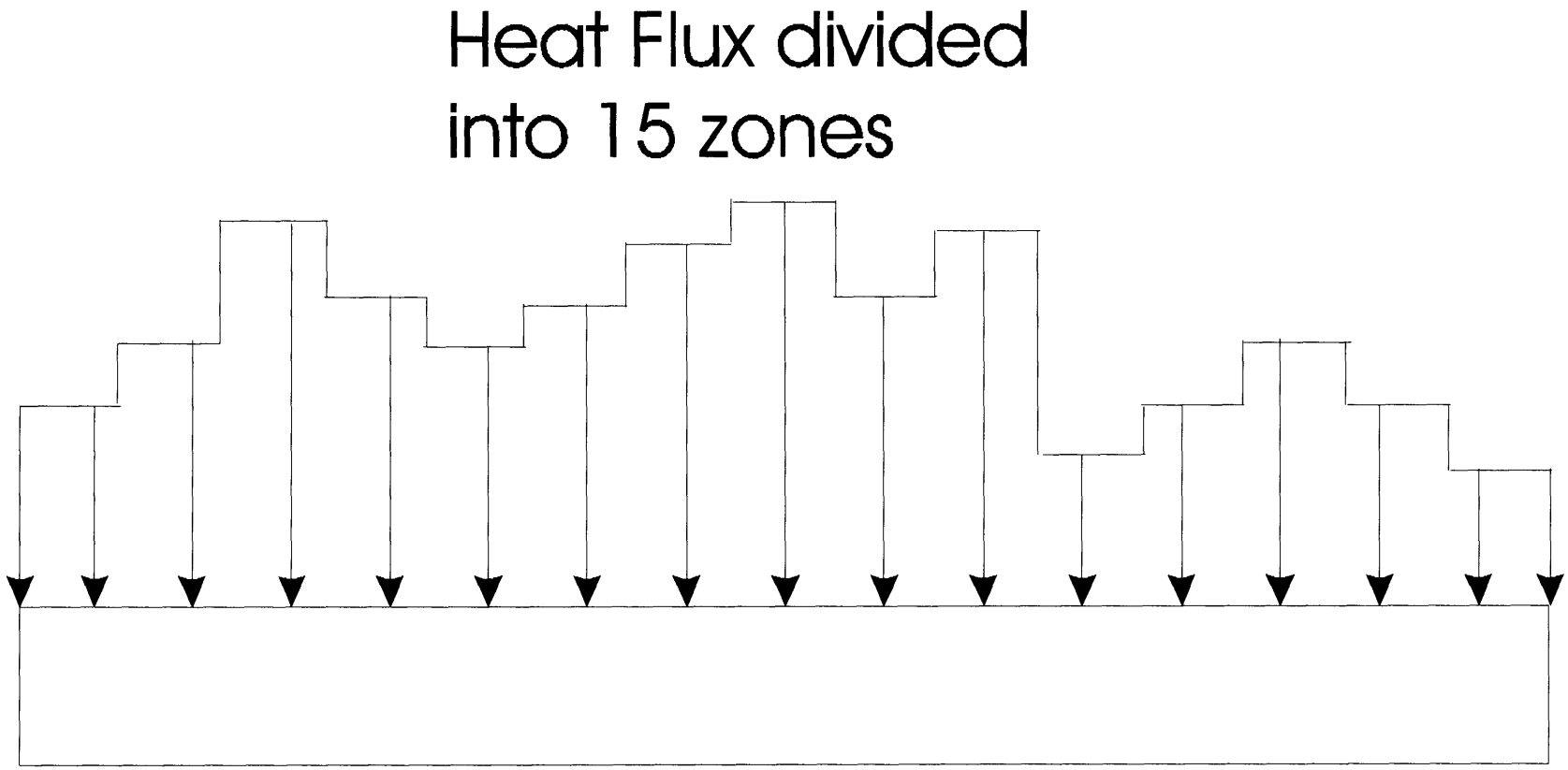

Figure 2.4.2. The spatial distribution of heat flux is divided into fifteen zones of constant heat flux.

In this case the **I**(x,y) (see equation 2.3.17.) vector has 15 entries where each entry is a function, similar to the ones shown in equation 2.4.12.

$$\begin{aligned} I_1(x,y) &= 0 \quad x > 0 \\ &= 1 \quad x = 0,\ 0 \le y \le \frac{a}{15} \\ I_2(x,y) &= 0 \quad x > 0 \\ &= 1 \quad x = 0,\ \frac{a}{15} < y \le \frac{2a}{15} \end{aligned} \qquad 2.4.12.$$

These values can be substituted in 2.3.18. to derive the **B** matrix. Similarly, knowing the coordinates of the thermocouples, the **C** matrix can be computed using equation 2.3.19.

Selecting the matrices **Q** and **R** in equation 2.4.3. is the most important step in the design of the compensator. This was done using Bryson's technique. This is a heuristic technique which has been used as a starting point for the design. (See Bryson and Ho (1975) for further details). The first step in the method is to specify the maximum allowable deviation in the values of the state and the input. Say these are x_m and u_m. Now, the matrices **Q** and **R** are selected to be diagonal of the form $q\mathbf{I}$ and $r\mathbf{I}$ where q and r are scalar variables and **I** is the identity matrix of the proper dimension. Bryson's technique then says that a general thumb rule for picking the values of q and r is:

$$\begin{aligned} q &\approx \frac{1}{x_m^2} \\ r &\approx \frac{1}{u_m^2} \end{aligned} \qquad 2.4.13.$$

These parameters could then be "tweaked" until desirable performance is obtained.

The next section details simulations that were performed for temperature control on the steel specimen and the conclusions from this study.

2.5. Simulation results.

Several simulations to study the effects of the optimal regulator under different scenarios have been performed. The model used for the simulations is based on the eigen function expansion as discussed in section 2.3. The numerical values that were selected to here, are:

1. The dimension of the block is 0.1m x 0.01m
2. The physical constants for convection boundary condition are: α = 60.2768 W/m.K, β = 10 W/m^{2}K.
3. The diffusivity $K / \rho C_p$ =1.754e-5 m^2/s.

The eigen functions and eigen values have been computed by solving the equation 2.3.11, numerically, using Newton-Raphson technique, since closed form solutions do not exist for this problem. The covariance matrix "**V**" in equation 2.4.2., has been computed by measuring the temperatures of the different thermocouples and calculating the variances of the measured temperature. The structure of the matrix was diagonal, since the thermocouple responses were not correlated to each other, with each diagonal entry to be approximately 0.0625, which corresponds to a standard deviation in the measured temperatures of 0.25 °C. The state-noise matrix **W** was chosen to be diagonal with the diagonal entries to be 0.01. The state noise is difficult to estimate using an experiment and a small value was selected arbitrarily.

Several classes of disturbances have been studied in the simulation study. For example, consider the disturbance heat flux shown in figure 2.5.1. This is the distribution of the disturbance heat flux along the top surface of the specimen. If no compensation were present, i.e. $u_c(s)=0$, in figure 2.4.1. The disturbance then results in an error temperature in the uncompensated system as shown in figure 2.5.2. The LQG compensator is then implemented on the system with the disturbance in figure 2.5.1., acting on the specimen. The effect of the compensation on the error temperature and the controller heat flux are shown in figures 2.5.2. and 2.5.3. It can be seen that when compensation is applied the error temperatures are significantly small (as shown in figure 2.5.4.).

2.5.1. Effect of sensor location on controller performance:

The following set of simulations demonstrates the importance of sensor location in disturbance rejection. To study the effect of sensor location, the thermocouple pairs 1 through 4 in figure 2.5.5. were not used for control but were still measuring temperatures to indicate the temperature error. The optimal estimator was then implemented using the measurements of thermocouple pairs indicated in figure 2.5.5. by numbers 5,6 and 7. This implies that in the controller presented in figure 2.4.1., the filter gain $\mathbf{K}_f$ was recalculated for the case when measurements are available only at thermocouple pairs indicated by 5,6 and 7.

The linear quadratic regulator (LQR) controller gain $\mathbf{K}_c$ in figure 2.4.1., is the same as in the previous study. The performance of the closed loop system with the fewer number of

sensors was studied. Figures 2.5.6. and 2.5.7. indicate the steady-state heat flux distribution and the corresponding temperature errors measured at the different thermocouples. It can be noticed that the temperature error in steady state, when the disturbance is acting on the specimen is far larger at locations where there are no measurements available for control. This demonstrates the importance of selecting suitable sensor locations for control of distributed parameter systems.

2.5.2. Effect of input location on controller performance:

To study the influence of input location on the controller performance, the controller heat flux is assumed to be available in regions shown in figure 2.5.7. The heat flux is available at all the zones across the upper surface of the specimen, except for five zones at the center. The optimal compensator gain K_c is recalculated for this input and all the thermocouples are available for control.

The steady-state controller heat flux and the steady-state error temperatures at the different thermocouples are calculated with the input restricted to the above mentioned zones. Figure 2.5.8. shows the distribution of the optimal heat flux distribution and figure 2.5.9. shows the corresponding error temperatures. It can be seen that the performance is considerably degraded for regions where there is no input available. These results demonstrate the importance of the availability of controller heat flux at the different locations in the controlled specimen.

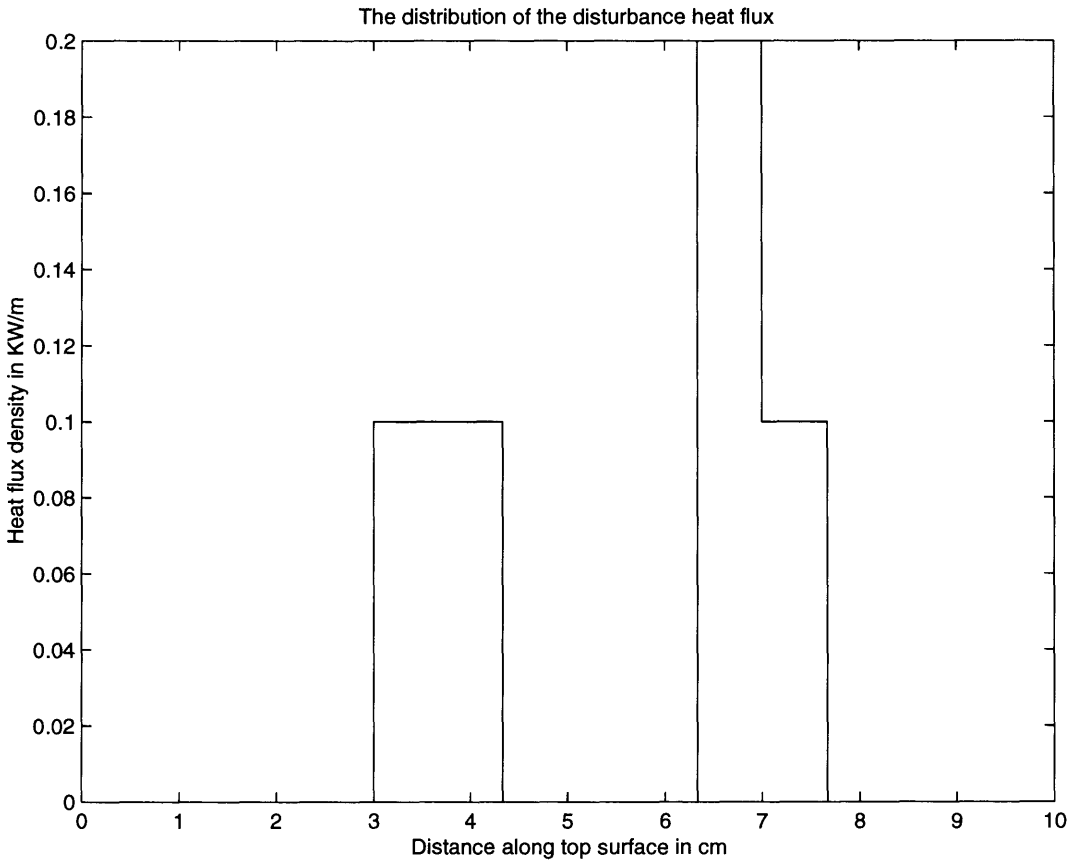

Figure 2.5.1. The distribution of disturbance heat flux along the upper surface of the specimen.

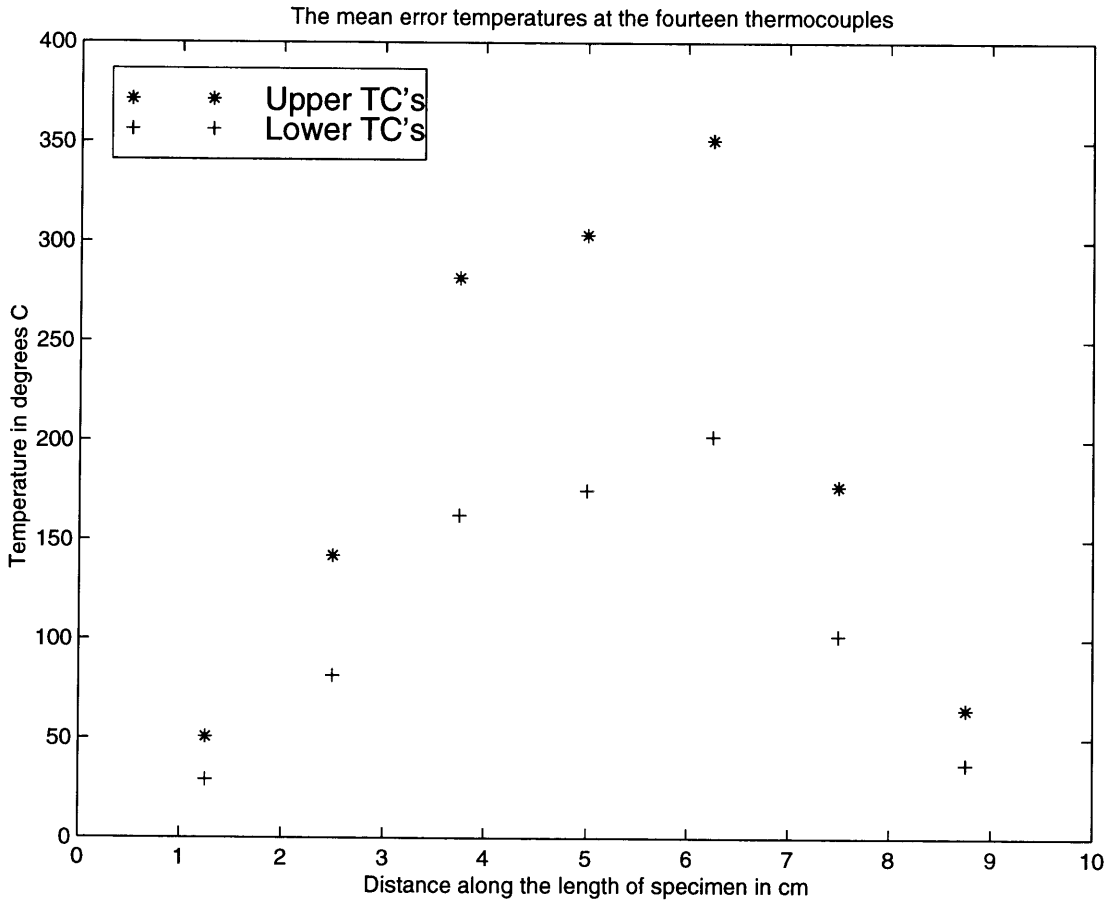

Figure 2.5.2. Error temperatures at the different thermocouples due to disturbance when no compensation is present.

MIT Libraries
Document Services

Room 14-0551
77 Massachusetts Avenue
Cambridge, MA 02139
Ph: 617.253.5668 Fax: 617.253.1690
Email: docs@mit.edu
http://libraries.mit.edu/docs

DISCLAIMER OF QUALITY

Due to the condition of the original material, there are unavoidable flaws in this reproduction. We have made every effort possible to provide you with the best copy available. If you are dissatisfied with this product and find it unusable, please contact Document Services as soon as possible.

Thank you.

The author miss-numbered some pages
and there is no page 70.

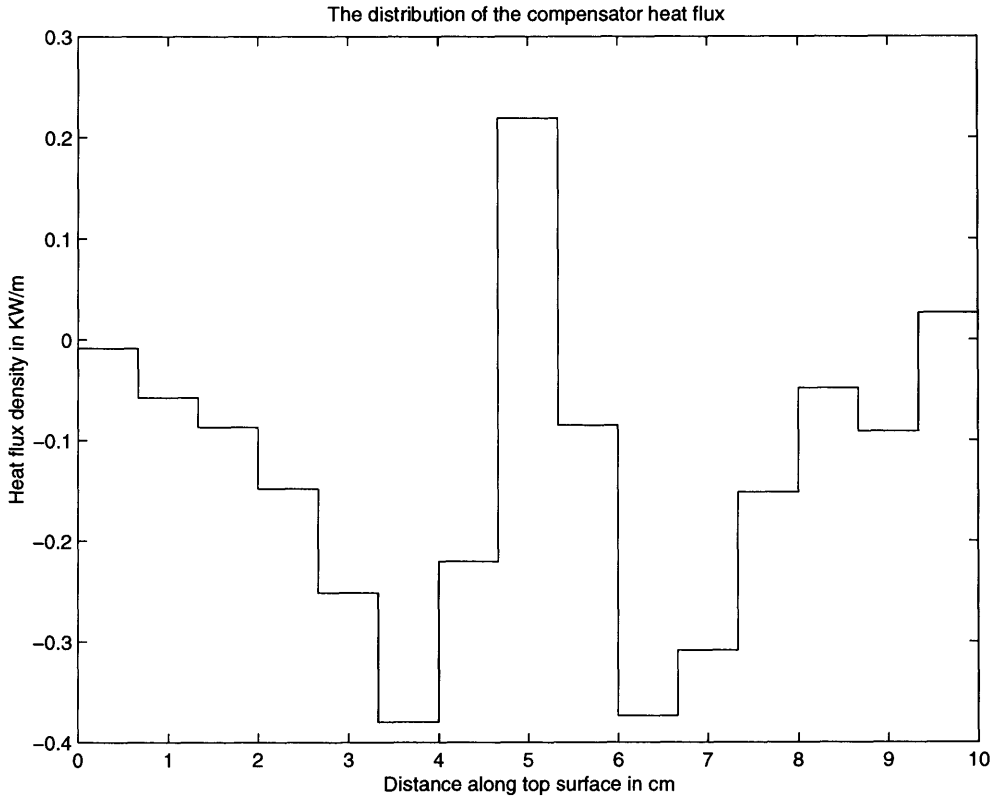

Figure 2.5.3. Heat flux output by the compensator when the disturbance is present.

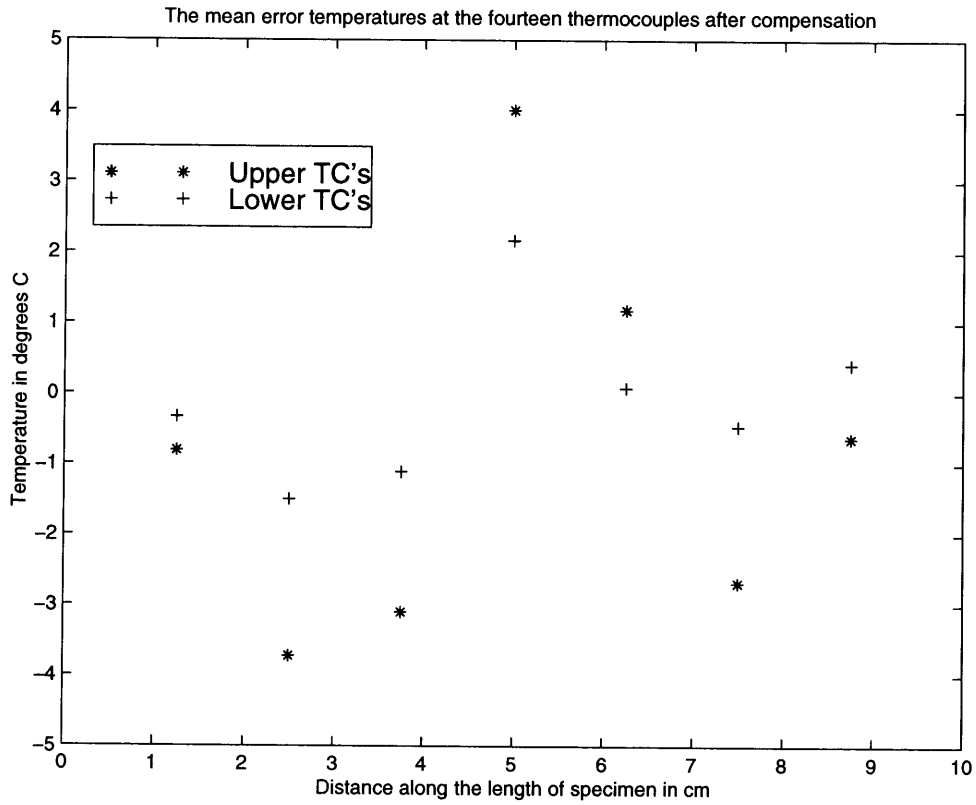

Figure 2.5.4. Error temperatures when compensation is applied.

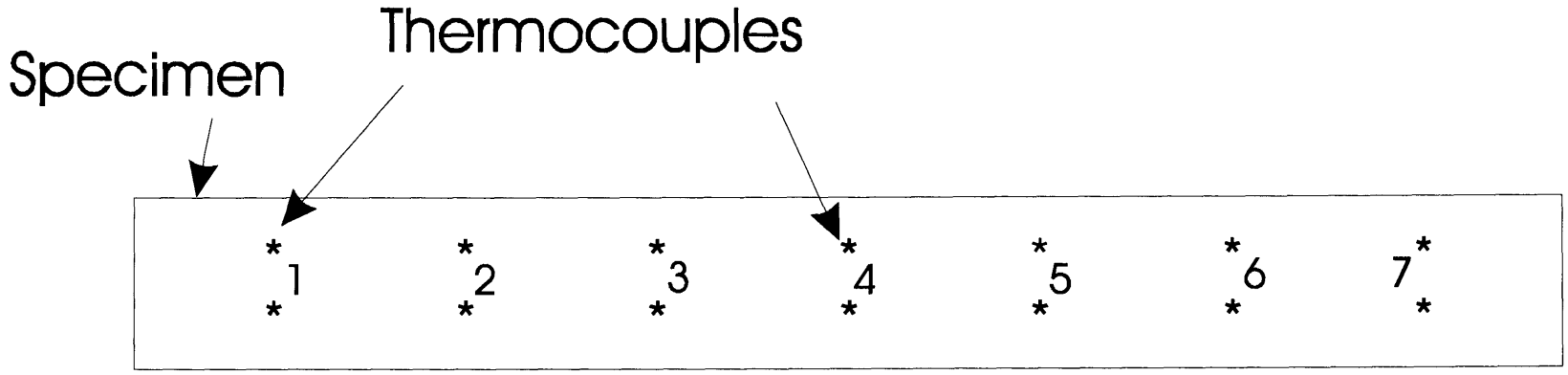

Figure 2.5.5. Numbering for thermocouple pairs embedded in the specimen.

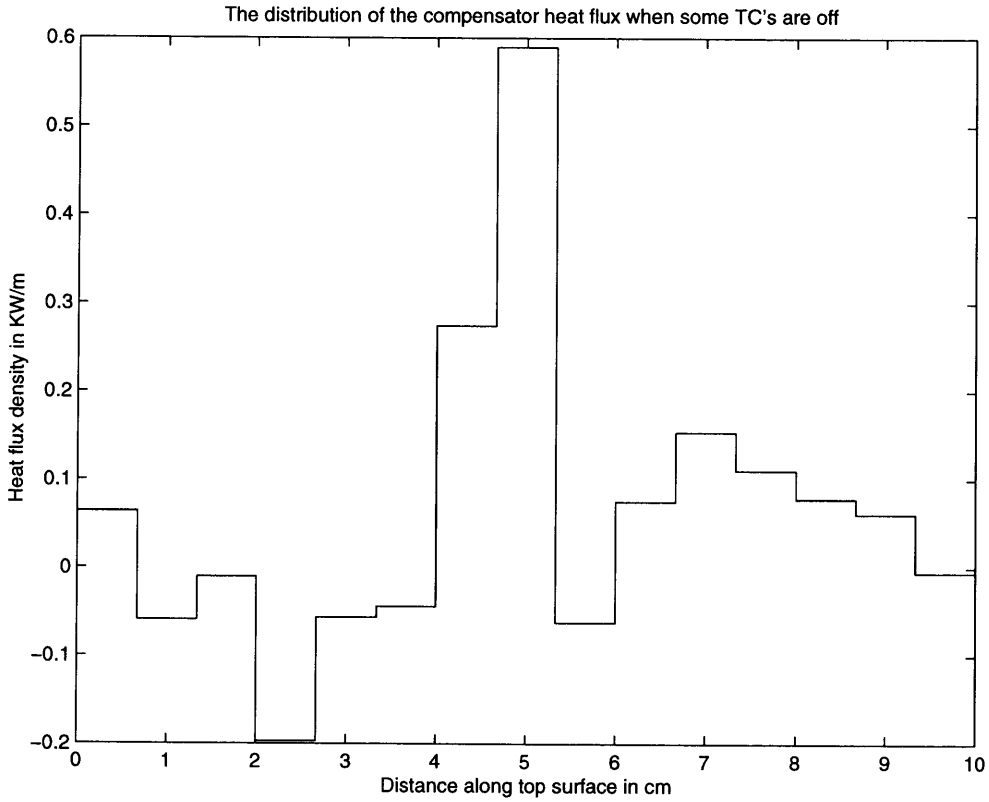

Figure 2.5.6. The compensator heat flux when some of the thermocouple readings are not used for control.

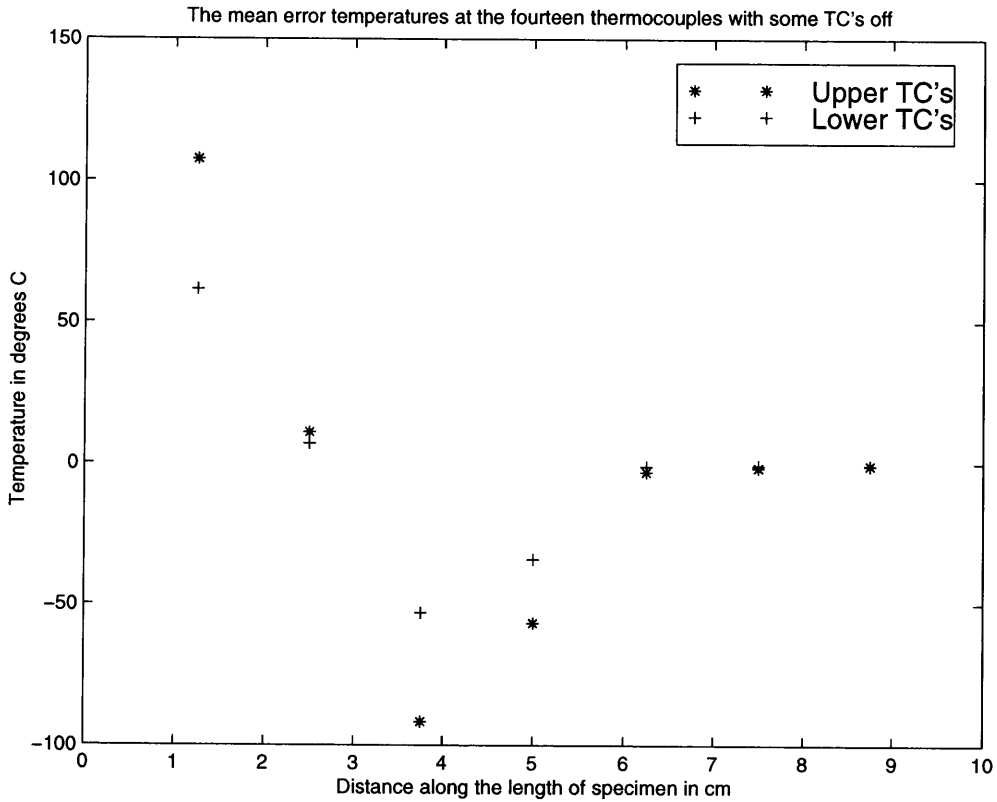

Figure 2.5.7. The error temperatures at the different thermocouples when only a few thermocouples are used for control.

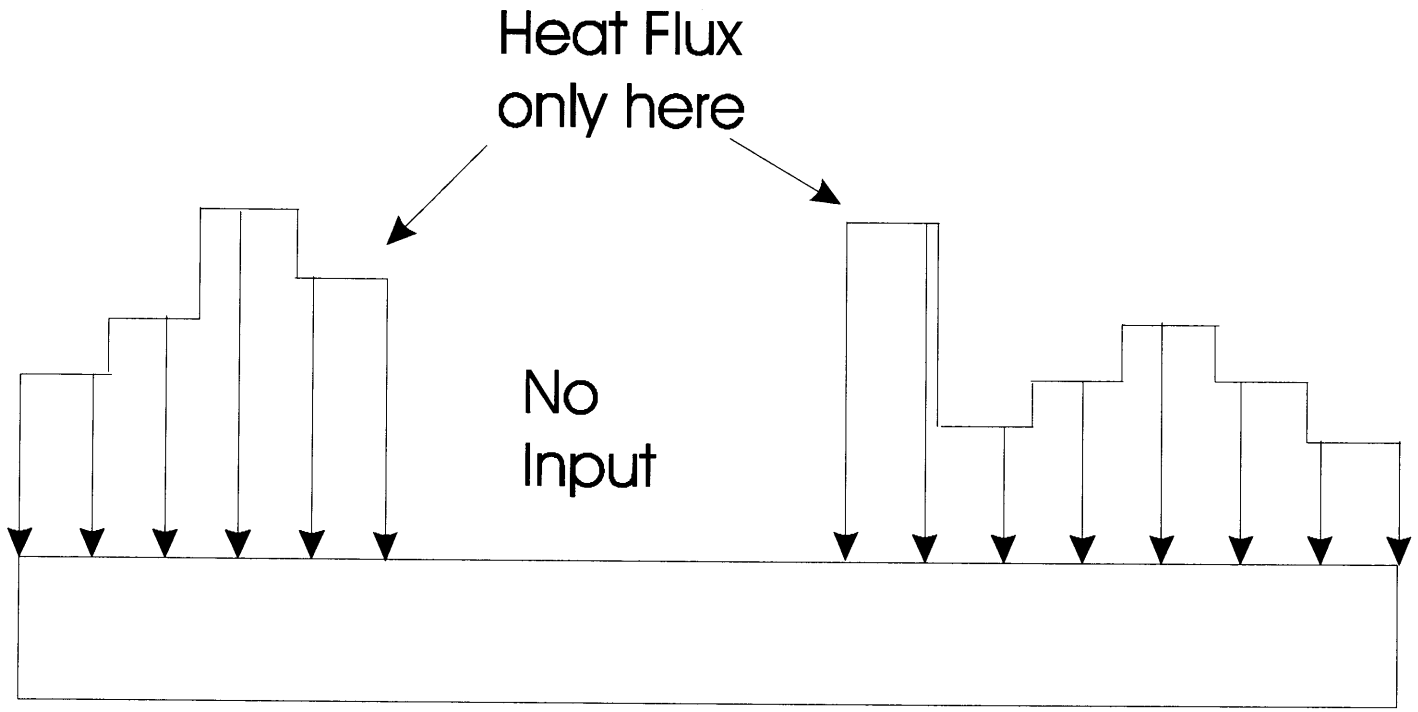

Figure 2.5.8. Controller heat flux not present in the central region of the specimen.

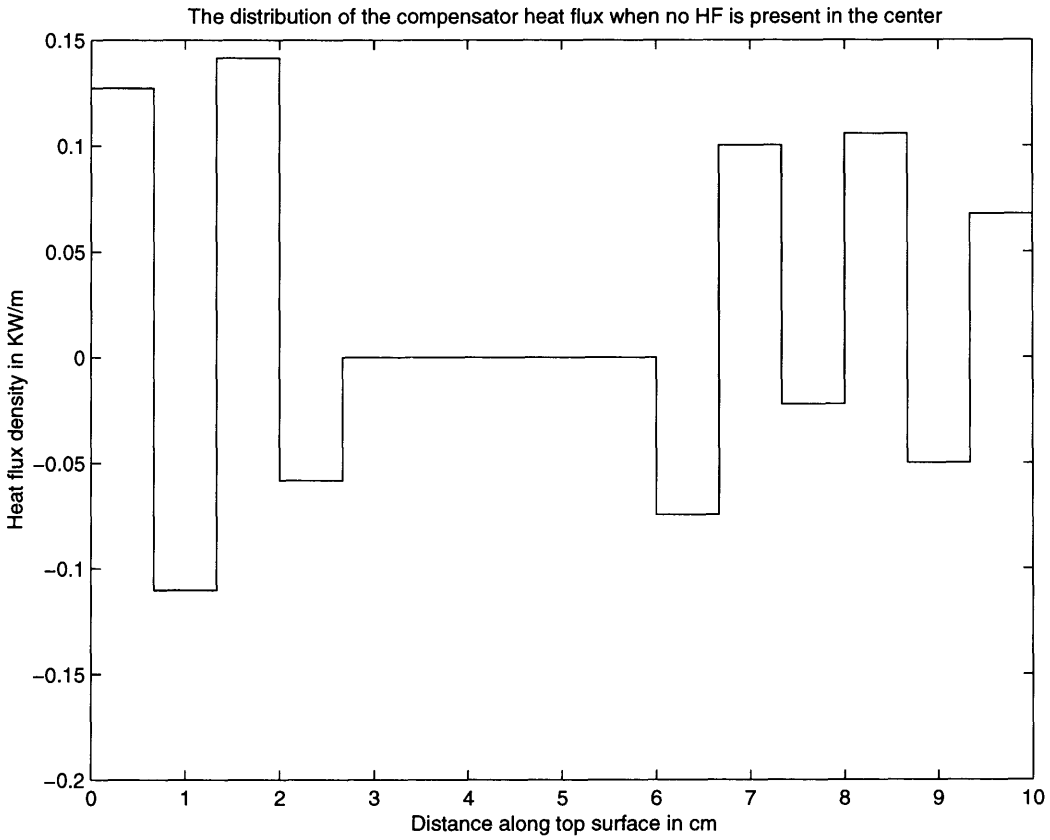

Figure 2.5.9. The distribution of the compensator heat flux if no heat flux is permitted in the central region.

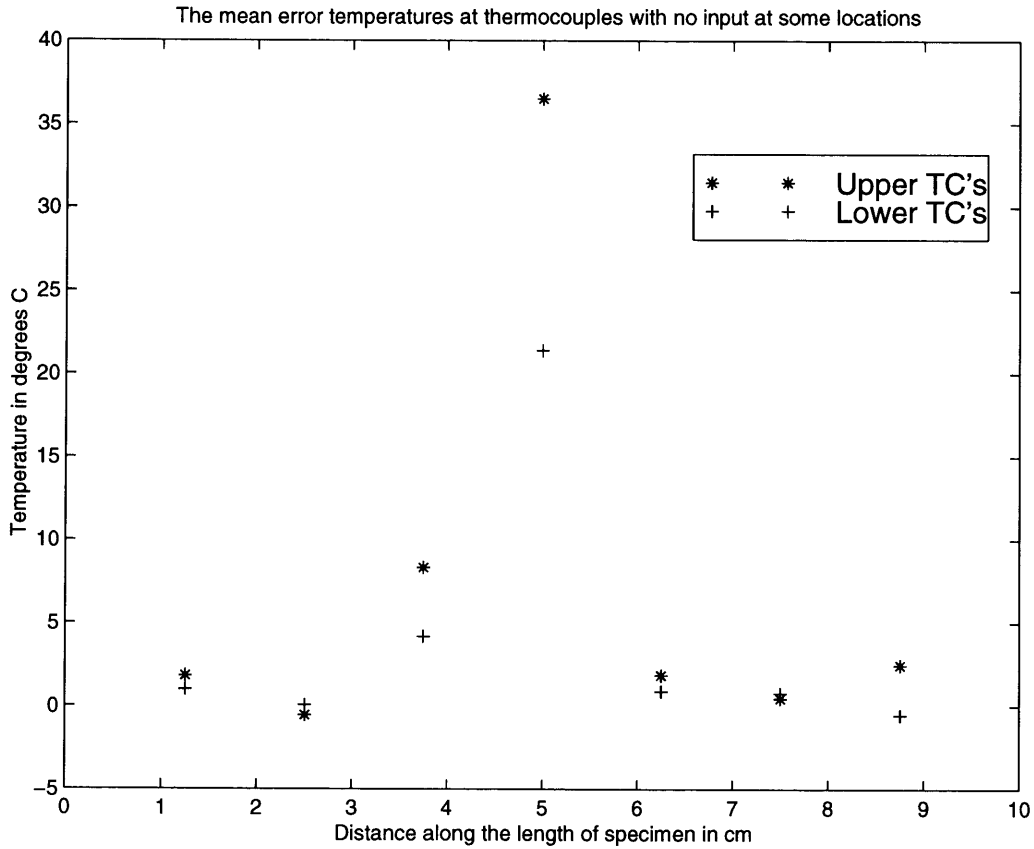

Figure 2.5.10. The error temperatures resulting due to compensator heat flux not being present over the center.

2.6. Conclusions:

The simulation study discussed in the previous section has lead to several conclusions which have motivated several topics of this thesis. These conclusions are discussed in this section.

The obvious conclusion is that an LQG compensator works satisfactorily in rejecting disturbances that were introduced when actuation and well distributed measurements were available to compensate for it. The advantages of having a flexible heat source has been demonstrated. It was seen that one could efficiently counter disturbances distributed over the controlled specimen by being able to better manipulate in space and time, the controller input distribution.

The example considered in this study is similar to the problem of furnace temperature control that occurs in many applications from steel to semiconductor manufacture. The disturbance similar to figure 2.5.1. in a furnace could be due to the malfunctioning of a heater used in the furnace. It is seen that if a distributed controller is used the rest of the heaters could take up the slack caused by the malfunction.

Apart from the obvious conclusions above, there are several problem areas that need work. In the example considered in this chapter as well as other investigations like Lausterer (1977) there is very little discussion on how to attain reference temperatures that might be needed, even when no disturbances are present. In reality, in most processes, one is required to meet a pre-specified temperature distribution across the

controlled specimen. In figure 2.6.1., if a hot spot ant cold spot are desired at locations shown, this temperature distribution is clearly not possible to achieve with the location and distribution of heat flux input used in the experiment. If such a distribution is desired, other locations for heating and cooling within the specimen or on its boundary should be found. Techniques that help process design engineers design heating and cooling so that a desired temperature distribution is achieved should be developed. The literature in the DPS community does not address this very important issue. Chapters 3., and 4., address this issue by presenting a novel method for designing heating and cooling for achieving a desired temperature distribution in steady-state along with a achieving adequate performance in the presence of process disturbances and model uncertainties. This is also an optimal control approach that does not require full state estimates and thus helps in the necessary trade off between control effort used and temperature errors tolerated, while according an implementable solution.

Similarly, if the input is constrained to lie in a specific part of the specimen and the disturbance activity is at a different part of the specimen, efficacy of the controller in rejecting external disturbances is limited. Figure 2.6.2. illustrates such a situation. Therefore, the control designer should thoroughly understand the several worst case disturbances that are possible in any specific process and carefully design the controller heat-flux distribution.

In a similar way, if the sensors are situated away from the disturbance activity, the ability of detecting and responding to the disturbance is limited. Figure 2.5.3. illustrates this

situation. The sensors should be located in a way that the disturbances are detected and eliminated efficiently.

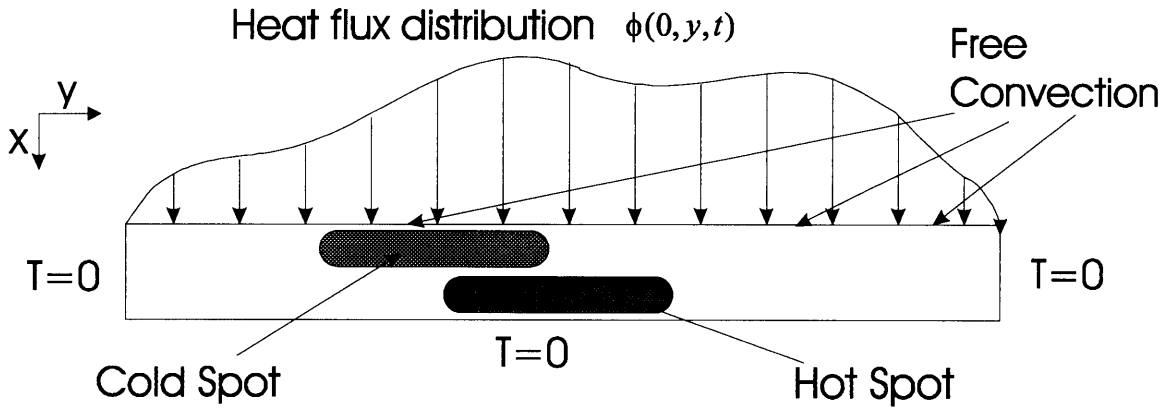

Figure 2.6.1. Unachievable desired steady state temperature distribution in the specimen.

Hence control techniques that address control heat flux distribution and sensor location while taking into account the possible worst case disturbance distributions , should be developed. Chapter 3 and 4 present techniques for designing heating and cooling so that set-points, disturbance locations and model imperfections can be incorporated into the controller design. Chapter 6. motivates the problem of picking proper sensor locations and describes an experiment that has been set up to study sensor location problems but an analytical approach to the sensor location problem has not been addressed in this thesis and should be a part of future work.

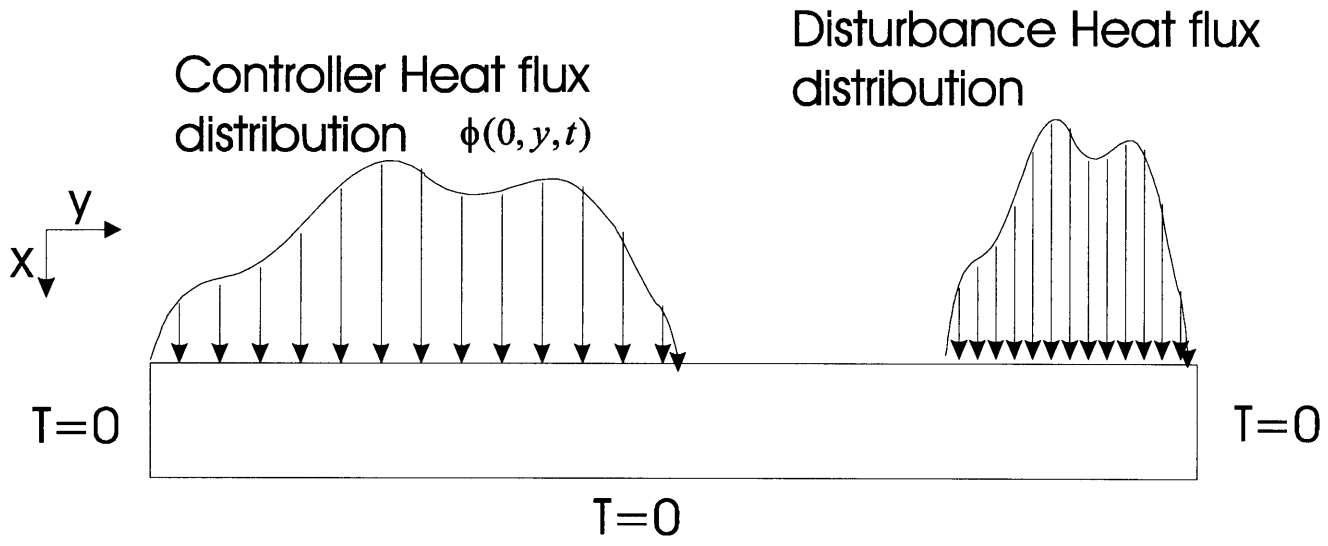

Figure 2.5.2. Disturbance occurring away from control input not easily compensated.

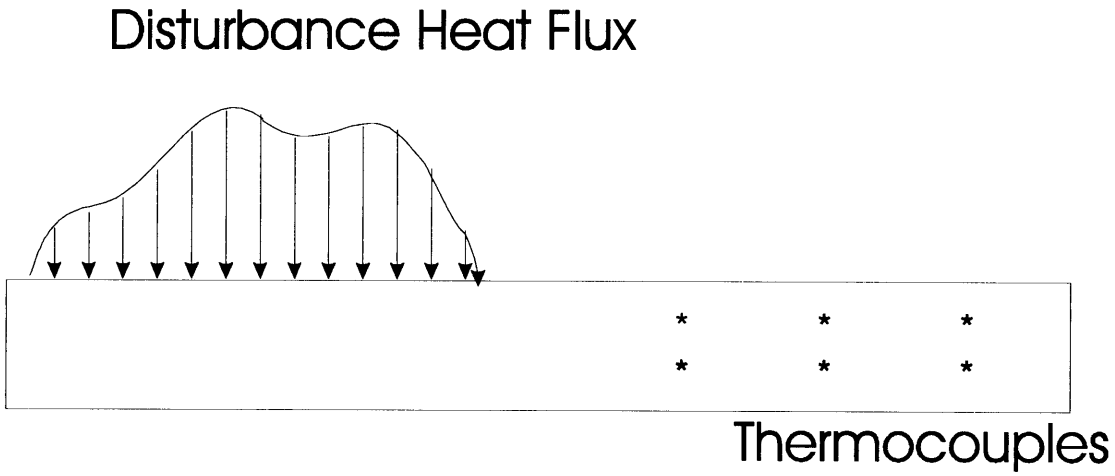

Figure 2.5.3. Sensors farther from disturbance, limits detection of disturbances.

Chapter 3

OPTIMAL INPUT DISTRIBUTION

3.1 Motivation for the distribution problem

This chapter revisits the different manufacturing processes described in Chapter 1., and explores in detail the temperature control requirements in these processes and defines an optimal control problem that addresses the requirements in these processes. It was observed in Chapter 2., that the distribution of the inputs determine:

1. The range of temperature distributions that one can achieve
2. The efficiency with which any controller could reject spatially distributed disturbances.

If infinitely manipulable heaters/coolers and temperature measurements can present everywhere in the solid being controlled, then, one could theoretically create and hold any arbitrary temperature distribution. This could be done for any possible disturbance distribution. However, this is not possible to accomplish in most real applications. In all real applications, there is always a trade-off between the amount of hardware used and the cost incurred, which results in a trade-off between the performance of the process and the cost of instrumenting a compensator. Sometimes, there are geometric constraints where by, one cannot instrument more than a certain number heaters/coolers or instrument heaters/coolers in certain locations.

Due to this trade off between the number and amount of heating/cooling used and the performance of the temperature distribution controller, any method for the designing of heating/cooling should be based on an optimal control approach. This allows the designer to arrive an the design with the least amount of hardware such as heaters/coolers. In Chapter 2., a Linear Quadratic Gaussian (LQG) controller was implemented in simulation on a model of a steel specimen, where it was seen that LQG controller functioned adequately in rejecting the disturbance applied to the specimen, when adequate input was available at the right location. However, the shortcomings of the current sate of the art in efficiently determining the distribution of inputs was detailed in Section 2.5. A method of optimal control should be therefore be able to accommodate the requirements on the desired steady-state temperatures while addressing disturbance rejection.

Additionally, optimal control techniques such as LQG are based on calculating a full state estimate. This requires a large array of sensors within the solid being controlled. Also, control approaches that require full state estimation are sensitive to model uncertainties. Therefore, this technique may not be very suitable for application in a wide variety of processes where detailed modeling efforts may not be possible. Any control methodology developed should be robust to the types of model uncertainty that could be expected.

The technique presented in this and the next chapters addresses all the considerations raised above. The method involves separating the space and time parts of the problem and applying optimal control over the space part. This gives a method for trading off

steady-state performance directly with the amount of energy used in steady-state. As will be seen in the example presented in Chapter 4, the optimal solution thus obtained can be used as a guideline for deciding on the location and distribution of inputs. In addition, this technique offers an approach for implementing feed back compensators that do not need full state estimates. This Chapter details the space part of the design which helps in guaranteeing the steady-state performance. However, the problem of designing compensators for stable operation will be posed by reintroducing time into the problem after the design for steady-state performance is performed. An example showing the details of designing such compensation is presented in Chapter 4.

In the next section, some of the processes discussed in section 1.2., are re-explored to precisely define optimization problems, that address the needs of each of the processes.

3.2 Specific temperature control requirements on different processes:

Different manufacturing processes have been studied in section 1.2. and the temperature control issues that are of importance to them have been briefly mentioned there. In this section we revisit these manufacturing processes. The different requirements on the temperature distributions in each of these processes are examined to a greater degree of detail, so as to help us precisely formulate the distribution optimization problem. These requirements can be categorized into the following three types:

1. Control of temperature distributions: either steady state temperature distributions or transient temperature distributions.
2. Control of gradients of temperature distributions.

3. Control of a functional of the temperature (typically the integral of temperature), usually to control dimensions of components exposed to thermal drifts.

3.2.1 Molding Applications:

In molding operations, we need to control the temperature of the component being manufactured. In compression molding and resin transfer molding, the process times are long enough to attain a steady state temperature distribution. This means that controlling the steady state surface temperatures in the mold can be effectively used to control the temperatures in the component being manufactured. In injection molding the mold surface temperature needs to be held mostly constant, with a pulse of heat flux to be given, at the mold surface, just at the moment of injection of the plastic (See Jansen, (1993)). The heating/cooling that one can use in this application typically, comprises of using cartridge heaters, passages of heating/cooling oil and ribbon heaters for surface heating. See figure 3.2.1., which shows a schematic of a mold with heating and cooling in it.

The problem here is then to control the temperature T(x,y,z,t) across the mold-part surface, which can be simplified to the problem of maintaining a specified steady-state temperature distribution T(x,y,z), on the mold surface.

Until recently (see Upadhyay, (1988)) this problem of optimally designing the locations of heating/cooling in molds received virtually no attention. Upadhyay, discusses a technique for locating cartridge heaters in a mold to ensure uniform temperature on the mold surface of a compression mold. However, this method does not consider model

errors, disturbances, sensor locations or stability during closed loop operation thus can be very unreliable in implementation.

Recently, rapid tooling technology that can be used to include arbitrary heating and cooling passages within molds, has been developed. These techniques include powder based processes such as 3Dimensional printing and laminate based techniques such as Profiled Edge Laminate (PEL) technology (ref. Wylonis (1995)and Walczyk (1996)). These technologies have demonstrated the possibility of incorporating conformal cooling/heating passages for tooling applications. To exploit these new innovations, techniques for designing shapes for heating and cooling, need to be developed. An optimal input distribution technique could help in determining the best shapes for the conformal cooling passages and the best locations for any cartridge heaters being used.

3.2.2 Heat treatment:

In heat-treatment operations, the object being heat treated should be put through a temperature transient. The cooling rates and the final temperatures attained at the different locations on the steel part being heat-treated determine the material properties of the steel at different locations. Cooling rates could vary from point to point in the object being heat-treated. If uniform properties are desired, the distribution of cooling heat flux has to be manipulated in a controlled manner. The manipulability of the input is dependent on the locations of the various heating and cooling elements. Cooling jets and induction heaters have a certain distribution of heat fluxes due to the physics associated with them.

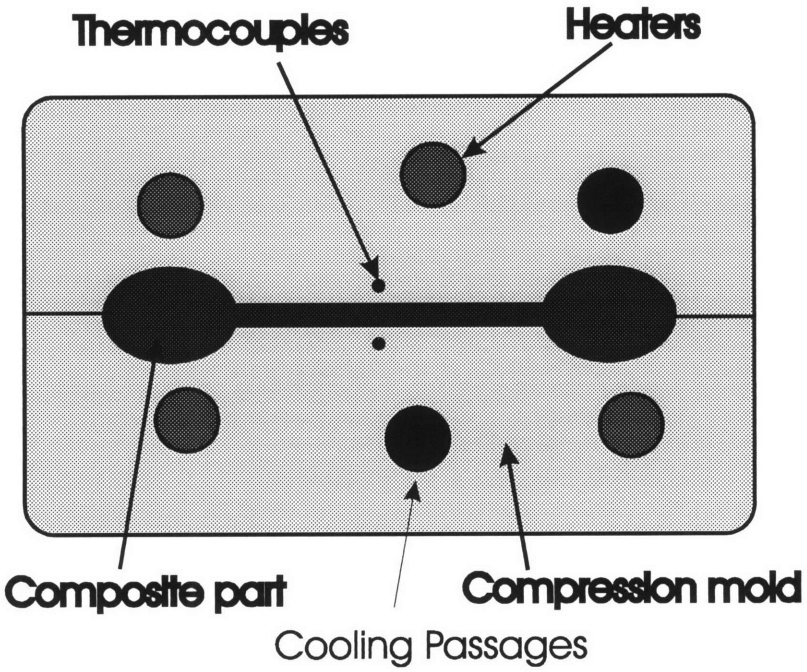

Figure 3.2.1 A schematic of a mold with heating and cooling.

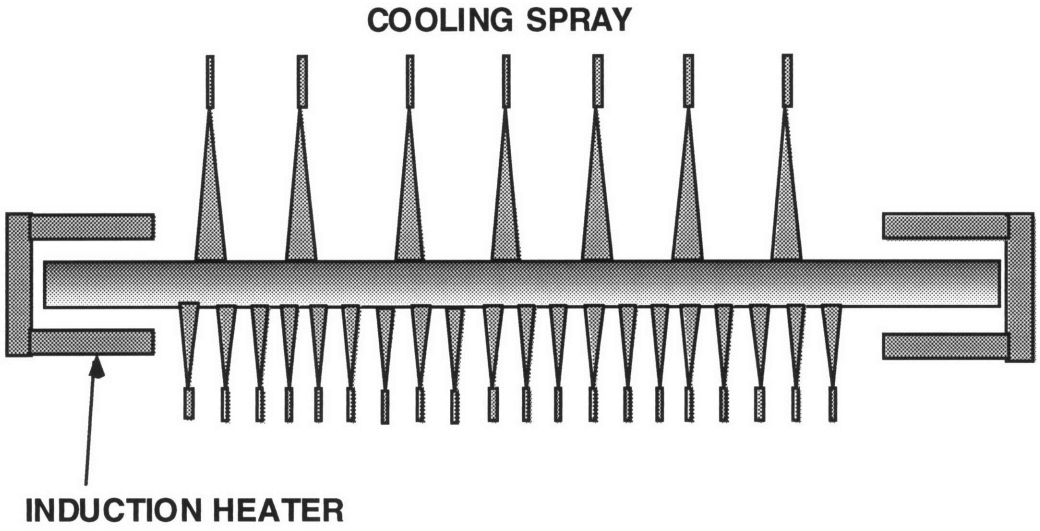

Figure 3.2.2 Cross sectional schematic of a heat treatment unit.

This constrains the range of input distributions that can be achieved. The sprays and the induction heaters should be suitably located so that the temperatures across the slab are uniform and they should be modulated so that the temperature trajectories are what is desired. Figure 3.2.2 shows a cross-sectional schematic of a cooling unit used to perform the heat-treatment.

Unlike the mold temperature control problem, this cannot be reduced into a problem of steady-state temperature distribution control. Chapter 5., details an approach for controlling such transient problems. The discussion in Chapter 3 and Chapter 4 is not relevant to this problem.

3.2.3. Flame bending:

Processes such as flame-bending involve imparting distortions to objects by inducing thermal stresses. These thermal stresses are induced by creating temperature gradients. Scanning a heat source such as a flame or a plasma torch along a predetermined path sets up these thermal gradients. In order to control the distortion in the components being produced, one has to precisely control the thermal gradients in the component. This process is similar to a welding process, without the melting of material. If the scanning is "slow" then on a reference frame moving with the flame the temperature field will look static (without any disturbances) and hence this problem can be reduced to one of controlling a steady state temperature gradient distribution.

3.2.4 Dimension control:

Controlling dimensions in the presence of thermal disturbances is of importance in many applications. Active temperature control could be used in precision machine tools, measurement equipment etc. to improve the dimensional accuracy by actively compensating for thermal drifts. This typically means that one needs to control a functional of the temperature. (Typically an integral over space). For example the change in length of a bar with a coefficient of thermal expansion α, caused by a thermal drift of T(x,t) is given by:

$$\Delta L(t) = \int_0^l \alpha T(\bar{x}, t) dx \qquad 3.2.1$$

Controlling length implies that the above functional is controlled as opposed to the temperature itself. Figure 4.2.4 shows a schematic of a controlled object which is a bar of uniform cross section with a heater that has a heat flux that is distributed all along the length of the bar. If the heat flux input along the bar can be manipulated arbitrarily, the control problem is then to determine the distribution of the heat flux output by the heater in order to achieve the control objective of controlling the length of the bar.

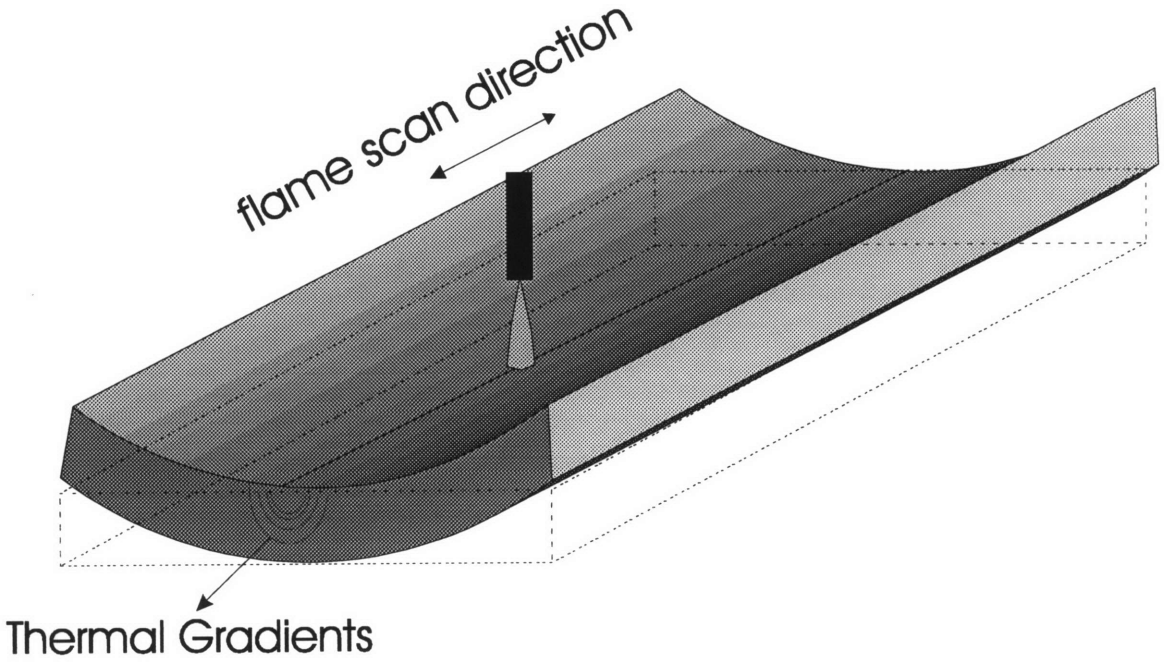

Figure 3.2.3. Flame bending or tool-less forming

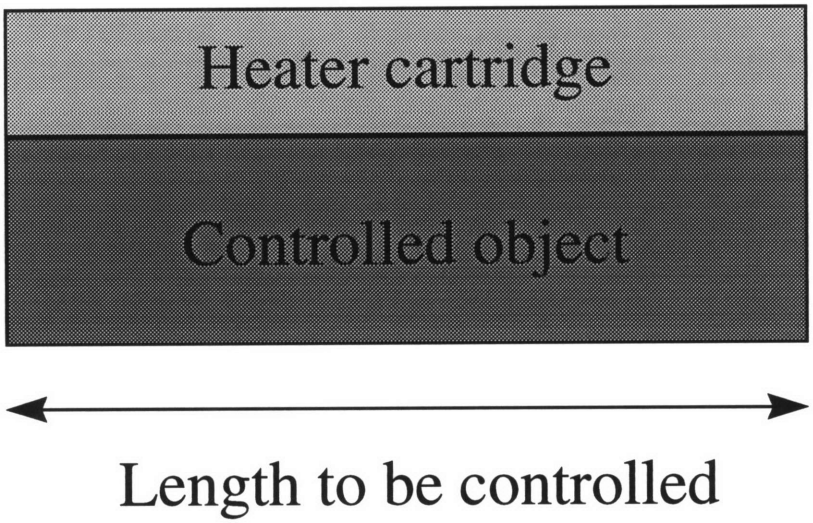

Figure 3.2.4. Schematic of length control in a bar.

3.3 Summary of requirements for input distribution:

To summarize the observations from the prior section, the temperature control requirements can be expressed in terms of quantities such as

$$\begin{aligned} &T(\bar{x},t): \textit{ Control Temperature Trajectory} \\ &\nabla_i T(\bar{x},t): \textit{ Control Temperature Gradient} \\ &\int_0^l \alpha T(\bar{x},t)dx: \textit{ Control of length} \end{aligned} \qquad 3.3.1$$

Where α is the coefficient of thermal expansion. We should control these quantities while satisfying several requirements on the processes. As was mentioned before, from a practical point of view, the most important constraint or requirement on any process is to use the least amount of energy and hardware.

3.4 Defining an approach for the problem:

In the theoretical distributed parameter systems literature, the problem of designing control inputs has received some attention. Many publications : El Jai and Pritchard (1988), Amouroux and Babary (1975, 1978,1979) etc. address this topic. However most of these publications deal with extremely simple geometries (usually one dimensional cases with Dirichlet boundary conditions) with severe restrictions on the classes of distribution of inputs that could be used. Some form of parametric optimization is then used to design the optimal shape of the input. In addition, the effect of process disturbances and model uncertainties are not considered in these formulations. Hence, the applicability of these techniques is in doubt.

A technique for designing heating for compensating thermal drifts in gyros has been developed at the MIT Instrumentation Laboratory. (Ref: Gould (1966), Wilkinson(1965),

Kaiser(1968)) This technique uses the steady-state theory for designing the shape of the distribution of the input for maintaining steady-state temperatures in the presence of disturbances. The advantage of this approach is that it provides a feed-back form of solution for the shape of the input. This is useful in studying the effect of disturbances, modelling uncertainties etc. Additionally, these techniques were tested experimentally and were later implemented on controlling thermal drifts in floated gyros. We will build on the techniques developed in the work at the MIT Instrumentation Laboratory and develop results that could be used to design heating and cooling in manufacturing processes.

The method that will be developed here must satisfy the following stipulations:

1. Model errors exist in all processes. The technique that will be developed should be able to compensate for these, or in the least one should be able to predict the effects of worst case model uncertainties with known structures.
2. External disturbances will always be present. These should be compensated for and the technique developed should be amenable to studying the effects of disturbances with different spatial variations.
3. Arbitrary temperature distributions cannot be achieved with a given distribution of heaters and coolers. Hence the best achievable temperature with the given distribution of actuators needs to be determined.
4. Estimating the full state to the desired level of accuracy may not be possible, with the number of sensors that could be used. Hence the method should be applicable in

situations where full state estimates are not available. However, if good full state estimates are available, this technique should exploit this situation.

3.4.1. The method for input distribution and controller design:

The design is performed in two steps. In the first step the space and time parts of the problem are separated and the input distribution is performed using the space part of the problem by using a quadratic cost function in space. The conditions of optimality are derived for this cost function, resulting in a feed-back form for the heat flux distribution. The corresponding closed loop solution is used to perform a detailed study of the effects of disturbances, set points and model uncertainties. If adequate performance is not obtained, the cost-functional is altered in an iterative manner until desired performance is obtained. At the end of this process, a good understanding of the steady state distribution of heat input is obtained under different "worst-case" scenarios. After the input distribution in steady-state is determined, the dynamics are reintroduced into the problem. MIMO frequency domain techniques are then used to design the controller with a stable and acceptable transient.

One of the key advantages of the technique developed here is that, if a detailed characterization of the worst case model uncertainties and disturbances can be performed over a wide range of frequencies, robust control techniques such as H-infinity and Mu-synthesis could be implemented.

3.5 Model Development:

We have seen that the governing PDE is given by:

$$\rho C_p \frac{\partial T}{\partial t}(\bar{x},t) = \nabla(k(\bar{x})\nabla)T(\bar{x},t) + \phi(\bar{x},t);$$
$$Bo(T(\bar{x},t)) = 0; \quad Boundary \quad Condition \tag{3.5.1}$$

In the above equation the different terms are:

$$\rho \ : is\, the\, density$$
$$C_p : is\, the\, specific\, heat$$
$$k(\bar{x}) : is\, the\, conductivity\, of\, the\, material$$
$$\nabla = \frac{\partial}{\partial x} + \frac{\partial}{\partial y} + \frac{\partial}{\partial z} \tag{3.5.2}$$
$$Bo : Boundary\, conditions$$
$$T(\bar{x},t) \ : temperature\, distribution$$
$$\phi(\bar{x},t) \ : distribution\, of\, the\, heat\, flux$$

This is the linear heat conduction equation. By setting $t \to \infty$, equation 3.5.1 can be reduced to its steady-state counterpart. This step has the effect of separating the space and time parts of equation 3.5.1. Applying $t \to \infty$ to the different entries of equation 3.5.1, we have:

$$\lim_{t\to\infty}\left(\frac{\partial T(\bar{x},t)}{\partial t}\right) = 0;$$
$$\lim_{t\to\infty}\left(T(\bar{x},t)\right) = T(\bar{x});$$
$$\lim_{t\to\infty}\left(\phi(\bar{x},t)\right) = \phi(\bar{x}); \tag{3.5.3}$$
$$\lim_{t\to\infty}\left(Bo(\bullet)\right) = Bo_s(\bullet);$$

Equation 3.5.1 then simplifies to the steady-state heat conduction equation:

$$\nabla(k(\bar{x})\nabla)T(\bar{x}) = -\phi(\bar{x});$$
$$Bo_s T(\bar{x}) = 0; \quad Steady - state\ b.c. \tag{3.5.4}$$

For special cases involving simple geometries and boundary conditions, equation 3.5.4 can be solved analytically. However, for more complicated situations, numerical techniques such as finite differences and finite elements can be used to solve this

equation. The question here is however to determine the heat flux input distribution $\phi(\bar{x})$ that gives a desired temperature $T(\bar{x})$. Before proceeding to answer this question, equation 3.5.4., should be represented in a more convenient form suitable for the spatial optimization to be performed. The technique that is used in this chapter is to use a Green's function description to the problem, which is a convenient representation of the heat conduction system for the purpose of deriving conditions of optimality (this is in addition to the advantages listed in Chapter 1). This is because, the Green's function implicitly captures the steady-state heat conduction equation and the associated boundary conditions in a single integral equation. This facilitates better book-keeping when calculus of variations are used to derive conditions of optimality and eliminates the need for solving a complex partial differential equation after the conditions of optimality are derived. The Green's function description for equation 3.5.4. can be written as:

$$T(\bar{x}) = \int_D G(\bar{x},\bar{\xi})\phi(\bar{\xi})d\xi; \qquad D\text{: The entire domain} \tag{3.5.5}$$

Where $G(\bar{x},\bar{\xi})$ is the Green's function of the steady state problem, D is the spatial region occupied by the controlled solid, $T(\bar{x})$ is the temperature distribution in the solid and $\phi(\bar{x})$ is the distribution of heat flux. Green's function physically has the interpretation of being the temperature that results from a point heat source at a specific location $\bar{x} = \bar{\xi}$, i.e.:

$$\nabla\big(k(\bar{x})\nabla\big)G(\bar{x},\bar{\xi}) = -\delta(\bar{x}-\bar{\xi})$$
$$Bo_s(G(\bar{x},\bar{\xi})) = 0;\ \textit{Boundary condition} \tag{3.5.6}$$

Where, $k(\bar{x})$ is the conductivity, $\delta(\bar{x}-\bar{\xi})$ is a unit heat input at $\bar{x}=\bar{\xi}$ (the steady-state spatial equivalent of an impulse function in the time domain). Hence, by linear superposition the resulting temperature distribution $T(\bar{x})$ due to an arbitrary heat flux input $\phi(\bar{x})$ can be written as shown in equation 3.5.5. This is similar to using the impulse response function to evaluate the response to arbitrary inputs in the time domain.

Just as the impulse response function could be determined experimentally and used for control, the advantage of using the Green's function representation is that, $G(\bar{x},\bar{\xi})$ can be experimentally computed. If there is access to the region within the object where inputs could be applied, the Green's function can be calculated by performing an experiment (see Wilkinson (1965)). Alternatively, if we have access to detailed higher order models such as a finite element based model, we could determine $G(\bar{x},\bar{\xi})$ via a simulation. This is done by dividing the region of the input into discrete regions and a steady state heat flux pulse is applied over each region and the response temperature is computed. Figure 3.5.1. indicates how this can be done. For example we can apply a unit pulse at a location $\bar{\xi}$ and measure the temperature distribution for all locations $\bar{x}$. By computing this for heat input at each of the nodes, we can tabulate the approximate Greens function, $G(\bar{x},\bar{\xi})$. If the Green's function is needed to be more accurate, the spatial resolution could be increased.

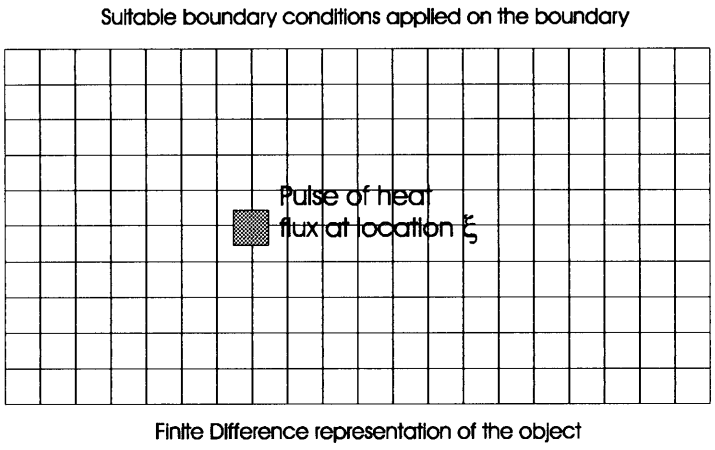

Figure 3.5.1 Numerical computation of Green's function.

In equation 3.5.5 the total heat input $\phi(\bar{x})$ that the object experiences has two components. The heat flux that the controller output $\phi_c(\bar{x})$ and the disturbance heat flux $\phi_d(\bar{x})$.

$$\phi(\bar{x}) = \phi_c(\bar{x}) + \phi_d(\bar{x}) \tag{3.5.7}$$

Similarly, the Green's function that we have computed has some uncertainty associated with it. The actual Green's function $\tilde{G}(\bar{x},\bar{\xi})$ can then be represented as the nominal Green's function with some additive uncertainty with a certain structure:

$$\tilde{G}(\bar{x},\bar{\xi}) = G(\bar{x},\bar{\xi}) + \Delta G(\bar{x},\bar{\xi}) \tag{3.5.8}$$

Where $\Delta G(\bar{x},\bar{\xi})$ is the uncertainty in the Green's function $G(\bar{x},\bar{\xi})$. The actual temperature achieved due to the controller heat flux is then given by:

$$T(\bar{x}) = \int_D \tilde{G}(\bar{x},\bar{\xi})\left(\phi_c(\bar{\xi}) + \phi_d(\bar{\xi})\right)d\xi \tag{3.5.9}$$

D: The entire domain

The compensator has to be designed so that the controller heat flux will be present at the right places in the right amounts so that the worst case disturbances could be effectively rejected. Similarly, if the structure of the worst case model uncertainty is known, the controller should be designed so that satisfactory steady-state performance could be obtained in the presence of worst case disturbance.

3.6 Cost functionals

In section 3.2, the requirements for different processes were identified. The quantities that need to be controlled have been summarized in equation 3.3.1. These quantities should be controlled while minimizing the amount of controller energy used. This is similar to the situation encountered in optimal control in the time domain for linear systems. In time domain optimal control we try to minimize the error between the desired and actual values of the state while minimizing the amount of control energy used. This is accomplished by formulating quadratic performance indices that are minimized (see Anderson and Moore (1985)). It is well known that such an approach gives a feed-back solution to the optimal input trajectory and thus giving the system an ability to operate satisfactorily in the presence of disturbances. Similarly, quadratic performance indices could be used for the steady state problem. It will shown that such an approach gives a feed-back solution to the steady-state heat flux distribution in terms of the steady-state temperature error distribution and thus has the ability to compensate for constant (or slow moving) disturbances and model uncertainties concentrated at low frequencies.

3.6.1. Example cost functionals:

Some cost functionals are presented here for a simple analytical problem, to illustrate the structure of cost-functionals in the space domain. Consider a rod whose ends are maintained at some arbitrary boundary conditions and assume that heat flux distribution can be manipulated all along the length of the bar (see figure 3.6.1.). For the examples presented here it assumed that the rod can be modeled as a one-dimensional solid. For such a one-dimensional solid, quadratic cost functionals will be defined for deriving optimal heat flux distributions for controlling quantities in equation 3.3.1.

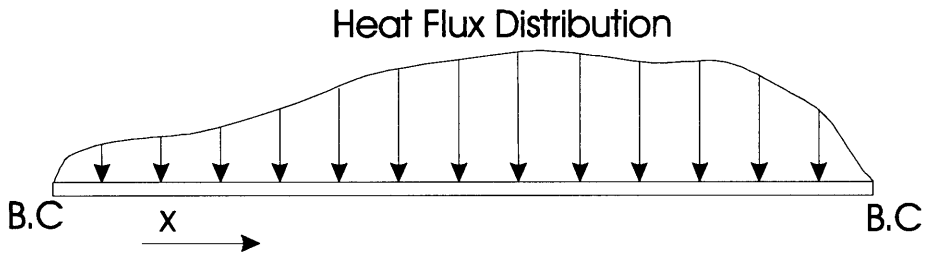

Figure 3.6.1. A rod that can be modeled as a one-dimensional solid.

Table 3.6.1 shows examples of some quadratic cost functionals that can be defined for this simple example. The first cost functional is a quadratic functional which weighs the control effort used against the temperature error. (The assumption here is that a zero temperature needs to be achieved everywhere along the rod). The second cost functional weighs the error in the gradient of the temperature with the amount of control effort used. The third cost-functional weighs the error in the length of the rod with the amount of control effort used.

$J = \int_0^1 \phi_c{}^2(x) + \lambda_1 T^2(x)dx$	This is a cost functional for attaining the zero temperature distribution while minimizing the amount of control effort used. λ_1 is a scalar multiplier that we pick later to satisfy the specs. on the process.
$J = \int_0^1 \phi_c{}^2(x) + \lambda_1 \left(\frac{\partial T(x)}{\partial x}\right)^2 dx$	This is a cost functional that could be used for controlling the temperature gradient. The temperature gradients have a direct bearing on the thermal stresses and distortions introduced in the object being controlled.
$J = \left(\int_0^1 T(x)dx\right)^2 + \frac{1}{\lambda}\int_0^1 \phi^2(x)dx$	Here we are trying to control the intergral of the temperature i.e. the length change due to temperature errors.

Table 3.6.1. The cost functionals for a one-D situation.

The second and third cost functionals in table 3.6.1. are not encountered in time domain cost functionals used in optimal cntrol. These two functionals involve derivative and integral of temperatures being weighed against the control effort used. In addition, the third cost functional can be rewritten as:

$$J = \int_0^1 \frac{1}{\lambda}\phi^2(x)dx + \int_0^1\int_0^1 T(x)T(\xi)dxd\xi \qquad 3.6.1$$

This is a higher order cost functional. In the second term of the above cost functional the integration is performed twice with respect to the space variable and thus this is a second order cost functional. In case of a problem in higher dimensions, the integration will be performed twice with respect to each of the space variables. The next section defines a generalized form for cost functionals that could be constructed in any application.

3.6.2. Generalized form of cost functionals:

Cost functionals similar to those in table 3.6.1., can be constructed for other more complex problems, depending on the requirements on the process. Any cost functional for optimal control of temperature distribution, temperature gradient distribution or length control can be represented in the general form shown in equation 3.6.2. A most generalized structure is presented here so that the conditions of optimality can be derived only once and every other cost functional can then be treated as a special case of this generalized cost functional.

The first term, $L_1(T(\bar{x}),T_i'(\bar{x}),\phi_c(\bar{x}),\bar{x})$ is a cost functional of the first order, i.e. the integration is performed only once with respect to the space variable, over this function.

This can, in general, be selected as a quadratic function of the temperature distribution $T(\bar{x})$, the temperature gradient distribution $T_i'(\bar{x})$, the controller heat flux distribution $\phi_c(\bar{x})$ and the spatial coordinates $\bar{x}$.

The second term $L_2(T(\bar{x}),T_i'(\bar{x}),\phi_c(\bar{x}),\bar{x},T(\bar{\xi}),T_i'(\bar{\xi}),\phi_c(\bar{\xi}),\bar{\xi})$ is a cost functional of the second order. It can be seen in equation 3.6.2., that the integration is being performed twice with respect to the space variable. $\bar{x}$ *and* $\bar{\xi}$ are the variables of integration representing the coordinates of all the points in the controlled object.

$$J = \int_S L_1(T(\bar{x}),T_i'(\bar{x}),\phi_c(\bar{x}),\bar{x})d\bar{x} + \iint_S L_2(T(\bar{x}),T_i'(\bar{x}),\phi_c(\bar{x}),\bar{x},T(\bar{\xi}),T_i'(\bar{\xi}),\phi_c(\bar{\xi}),\bar{\xi})d\bar{x}d\bar{\xi} \qquad 3.6.2$$

For equation 3.6.1, we can deduce that:

$$L_1 = \frac{1}{\lambda}\phi^2(x) \text{ and } L_2 = T(x)T(\xi); \qquad 3.6.3$$

The second order cost functional usually occurs only in problems involving dimensional control in the presence of heat flux disturbances distributed on the controlled object.

The following section shows the derivation of the conditions of optimality with the generalized cost functional of 3.6.2., using calculus of variations.

3.7 Derivation of the condition of optimality:

The conditions of optimality need to be derived for the generalized cost function defined in the section 3.6.2. This cost functional is rewritten below:

$$J = \int_S L_1(T(\bar{x}), T_i'(\bar{x}), \phi_c(\bar{x}), \bar{x}) d\bar{x} + \iint_S L_2(T(\bar{x}), T_i'(\bar{x}), \phi_c(\bar{x}), \bar{x}, T(\bar{\xi}), T_i'(\bar{\xi}), \phi_c(\bar{\xi}), \bar{\xi}) d\bar{x} d\bar{\xi} \quad 3.7.1.$$

The governing equation for the steady-state heat conduction is given by equation 3.5.5., which is rewritten below:

$$T(\bar{x}) = \int_D G(\bar{x}, \bar{\xi}) \phi(\bar{\xi}) d\xi; \quad 3.7.2.$$
$$D: \textit{The entire domain}$$

Let $\phi_0(\bar{x})$ be the optimal input around which small variations are considered and let the corresponding temperature and temperature gradient due to this input are $T_0(\bar{x}) \textit{ and } T_0'(\bar{x})$. Now consider small variations about this optimal value of the input and the corresponding variations in the temperature and the temperature gradient:

$$\begin{aligned} \phi_c(\bar{x}) &= \phi_0(\bar{x}) + \varepsilon \delta\phi_c(\bar{x}) \\ T(\bar{x}) &= T_0(\bar{x}) + \varepsilon \delta T(\bar{x}) \\ T'(\bar{x}) &= T_0'(\bar{x}) + \varepsilon \delta T'(\bar{x}) \end{aligned} \quad 3.7.3$$

In equation 3.7.3, $\delta\phi_c(\bar{x})$ belongs to a set of permissible variations and ε is a small number. $\delta T(\bar{x})$ and $\delta T'(\bar{x})$ are the variations that correspond to $\delta\phi_c(\bar{x})$.

The cost functional in equation 3.7.1., is expanded in a Taylor's series as:

$$J = J_0 + I_1\varepsilon + I_2\varepsilon^2 + O(\varepsilon^3) \quad 3.7.4$$

Where I_1 and I_2 are the first and second variations of J. By taking the first variation of the both sides of equation 3.7.1, we obtain:

$$I_1 = \delta J = \int_S \left(\frac{\partial L_1(\bar{x})}{\partial T} \delta T(\bar{x}) + \sum_i \frac{\partial L_1(\bar{x})}{\partial T_i'} \delta T_i'(\bar{x}) + \frac{\partial L_1(\bar{x})}{\partial \phi_c} \delta \phi_c(\bar{x}) \right) d\bar{x} +$$
$$\int_S \int_S \left(\frac{\partial L_2(\bar{x},\bar{\xi})}{\partial T(\bar{x})} \delta T(\bar{x}) + \sum_i \frac{\partial L_2(\bar{x},\bar{\xi})}{\partial T_i'(\bar{x})} \delta T_i'(\bar{x}) + \frac{\partial L_2(\bar{x},\bar{\xi})}{\partial \phi_c(\bar{x})} \delta \phi_c(\bar{x}) \right) d\bar{x} d\bar{\xi} \qquad 3.7.5$$
$$+ \int_S \int_S \left(\frac{\partial L_2(\bar{x},\bar{\xi})}{\partial T(\bar{\xi})} \delta T(\bar{\xi}) + \sum_i \frac{\partial L_2(\bar{x},\bar{\xi})}{\partial T_i'(\bar{\xi})} \delta T_i'(\bar{\xi}) + \frac{\partial L_2(\bar{x},\bar{\xi})}{\partial \phi_c(\bar{\xi})} \delta \phi_c(\bar{\xi}) \right) d\bar{x} d\bar{\xi}$$

All the first variations in the right hand side of equation 3.7.5, need to be expressed in terms of $\delta\phi_c(\bar{x})$. To achieve this, the first variation of equation 3.5.5 and the variation of the derivative of equation 3.5.5 are computed as follows:

$$\delta T(\bar{x}) = \int_S G(\bar{x},\bar{\xi}) \delta \phi_c(\bar{\xi}) d\bar{\xi}$$
$$\delta T_i'(x) = \int_S \frac{\partial G(\bar{x},\bar{\xi})}{\partial x_i} \delta \phi_c(\bar{\xi}) d\bar{\xi} \qquad 3.7.6$$

Substituting equation 3.7.6. in equation 3.7.5. and writing all the variations in terms of $\delta\phi_c(\bar{x})$ and rearranging, we obtain:

$$\int_S \left\{ \frac{dL_1(\bar{x})}{\partial \phi_c(\bar{x})} + \int_S \left(\frac{\partial L_1(\bar{x})}{\partial T(\bar{x})} G(\bar{\xi},\bar{x}) + \sum_i \frac{\partial L_1(\bar{x})}{\partial T_i'(\bar{x})} \frac{\partial G(\bar{\xi},\bar{x})}{\partial \bar{\xi}} + 2 \frac{\partial L_2(\bar{x},\bar{\xi})}{\partial \phi_c(\bar{x})} \right) d\bar{\xi} \right.$$
$$\left. + 2 \int_S \int_S \left(\frac{dL_2(\bar{\sigma},\bar{\xi})}{\partial T(\bar{\sigma})} G(\bar{\sigma},\bar{x}) + \sum_i \frac{\partial L_2(\bar{\sigma},\bar{\xi})}{\partial T_i'(\bar{\sigma})} \frac{\partial G(\bar{\sigma},\bar{x})}{\partial \bar{\sigma}} \right) d\bar{\sigma} d\bar{\xi} \right\} \delta \phi_c(\bar{x}) d\bar{x} \qquad 3.7.7$$

This is of the form:

$$\delta J = \int_S \frac{\partial H}{\partial \phi_c(\bar{x})} \delta \phi_c(\bar{x}) d\bar{x} \qquad 3.7.8$$

For a minimum of the cost functional *J*, we need to minimize δJ. For an unconstrained input case, $\delta\phi_c(\bar{x})$ can take on any arbitrary value. Hence a necessary condition for the optimum is then:

$$\frac{\partial H}{\partial \phi_c(\bar{x})} = 0 \qquad 3.7.9$$

i.e.

$$\frac{dL_1(\bar{x})}{\partial \phi_c(\bar{x})} + \int_S \left(\frac{dL_1(\bar{x})}{\partial T(\bar{x})} G(\bar{\xi}, \bar{x}) + \sum_i \frac{\partial L_1(\bar{x})}{\partial T_i'(\bar{x})} \frac{\partial G(\bar{\xi}, \bar{x})}{\partial \bar{\xi}} + 2 \frac{\partial L_2(\bar{x}, \bar{\xi})}{\partial \phi_c(\bar{x})} \right) d\bar{\xi}$$
$$+ 2 \int_S \int_S \left(\frac{\partial L_2(\bar{\sigma}, \bar{\xi})}{\partial T(\bar{\sigma})} G(\bar{\sigma}, \bar{x}) + \sum_i \frac{\partial L_2(\bar{\sigma}, \bar{\xi})}{\partial T_i'(\bar{\sigma})} \frac{\partial G(\bar{\sigma}, \bar{x})}{\partial \bar{\sigma}} \right) d\bar{\sigma} d\bar{\xi} = 0 \qquad 3.7.10$$

This is the necessary condition for an optimum for the distribution control problem. The sufficient conditions for optimality can be derived using the second variation. This is beyond the scope of this thesis and is therefore omitted.

Section 3.8 details a few simple examples illustrating the application of this optimality condition for designing the distribution of heating on simple controlled objects in order to optimally control the temperature distributions in them.

3.8 Example problems:

There are three example problems presented in this section to illustrate the use of the optimality condition derived in the previous section. All the three examples are constructed for the solid described in section 3.6.1. The first example demonstrates the usage of the optimality condition for the control of temperature and temperature gradient simultaneously, for a rod of unit length with zero temperature boundary conditions. Example 2., illustrates the solution for length control and example 3., illustrates how the information on the disturbance distribution can be used for selecting cost-functionals that yield optimal solutions for better disturbance rejection.

3.8.1. Example 1:

Consider a rod of unit length and unit conductivity with both ends of the rod maintained at zero temperature. The requirement of the heat flux is to optimally control the distribution of temperature and temperature gradient. The governing equation for the steady state temperatures in such a rod is given by:

$$\frac{\partial^2}{\partial x^2}T(x) = -\phi(x);\ for\ 0 < x < 1; \qquad T(x) = 0;\ for\ .x = 0\ and\ 1 \tag{3.8.1}$$

A cost functional shown in equation 3.8.2., is constructed for this problem. This is a first order cost functional which trades off the amount of control effort used (heating and cooling) with the accuracy achieved in both the temperature and the temperature gradient.

$$J = \int_0^1 \phi_c{}^2(x) + \lambda_1 T^2(x) + \lambda_2 \left(\frac{\partial T}{\partial x}\right)^2 dx \tag{3.8.2}$$

Equation 3.8.2 is a cost functional that only has a first order functional in it but has a penalty on the error in the temperature and the gradient of the temperature. The objective of this cost functional is to attain zero temperature and gradient of temperature along the bar. The first order kernel of the cost functional is then:

$$L_1 = \phi_c{}^2(x) + \lambda_1 T^2(x) + \lambda_2 \left(\frac{\partial T}{\partial x}\right)^2 \tag{3.8.3}$$

The second order kernel is zero. We can then calculate the following first derivatives:

$$\frac{\partial L_1}{\partial \phi_c} = 2\phi_c$$
$$\frac{\partial L_1}{\partial T} = 2\lambda_1 T \qquad 3.8.4$$
$$\frac{\partial L_1}{\partial T'} = 2\lambda_2\left(\frac{\partial T}{\partial x}\right)$$

Substituting these in the optimality condition equation 3.7.10, we obtain:

$$\phi_c(x) + \lambda_1 \int_0^1 G(\xi, x)T(\xi)d\xi + \lambda_2 \int_0^1 \frac{dT}{d\xi}\frac{\partial G(\xi, x)}{\partial \xi}d\xi = 0 \qquad 3.8.5$$

This equation shows the structure of the optimal input heat flux distribution in terms of the actual temperature and the temperature gradient. The effect of optimizing over the temperature versus the temperature gradient can be studied by setting either λ_1 or λ_2 to zero. If in the cost function in 3.8.2 we set λ_2 to be zero, the optimal heat flux is given by:

$$\phi_c(x) = -\lambda_1 \int_0^1 G(\xi, x)T(\xi)d\xi \qquad 3.8.5a$$

It can be seen that the heat flux depends on the temperature in a linear fashion. This is therefore a linear feed back form for the input heat flux. Similarly if λ_1 is set to zero, equation 3.8.5. reduces to equation 3.8.5b:

$$\phi_c(x) = -\lambda_2 \int_0^1 \frac{dT}{d\xi}\frac{\partial G(\xi, x)}{\partial \xi}d\xi \qquad 3.8.5b$$

We can see again that this is a linear feed back form for the heat flux in terms of the gradient of the temperature. Integrating the right hand side of the above equation, we have:

$$\phi_c(x) = -\lambda_2 T(x) - \lambda_2 T(\xi)\frac{\partial G(\xi,x)}{\partial \xi}\Big|_0^1 \qquad 3.8.6$$

If we had zero boundary conditions on the object the above equation reduces to:

$$\phi_c(x) = -\lambda_2 T(x) \qquad 3.8.6a$$

This equation shows that if we are interested in controlling the temperature gradient, the resultant heat flux distribution is proportional to the error temperature distribution.

To study the effect of a disturbance heat flux on the closed loop temperature distribution, 3.8.5a is substituted into equation 3.5.9. The closed loop temperature distribution is given by:

$$T_{CL}(x) = \int_0^1 G(x,\sigma)\left(-\lambda_1 \int_0^1 G(\xi,\sigma)T_{CL}(\xi)d\xi + \phi_D(\sigma)\right)d\sigma \qquad 3.8.7$$

That is,

$$T_{CL}(x) + \lambda_1 \int_0^1\int_0^1 G(\xi,\sigma)G(x,\sigma)T_{CL}(\xi)d\xi d\sigma = \int_0^1 G(x,\sigma)\phi_D(\sigma)d\sigma \qquad 3.8.8$$

Equation 3.8.7 can be used to compute the closed loop temperature that results due to a disturbance heat flux. Increasing λ_1 has the effect of reducing the closed loop error temperature, therefore if the worst case disturbance distribution is known, λ_1 is picked to be just large enough to satisfy the requirements on the error in the closed loop temperature achieved in steady state. The resulting steady-state heat flux is the necessary heat flux for maintaining a low closed loop temperature error when a disturbance is active.

3.8.2. Example 2:

Consider a bar of unit length, of unit conductivity and unit coefficient of thermal expansion. Both ends of the bar are maintained at zero temperature. We are interested in maintaining the length of the bar uniform, utilizing the least amount of thermal energy.

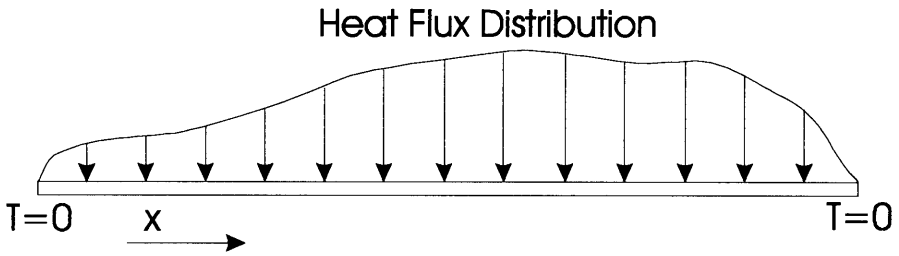

Figure 3.8.1 Example 2, rod of unit length with unit conductivity.

The cost functional in this case trades off the square of the error in the length versus the square of the amount of control effort used.

$$J = \left(\int_0^1 T(x)dx \right)^2 + \frac{1}{\lambda} \int_0^1 \phi^2(x)dx \qquad 3.8.9$$

Equation 3.8.9 can be rewritten as:

$$J = \int_0^1 \frac{1}{\lambda} \phi^2(x)dx + \int_0^1 \int_0^1 T(x)T(\xi)dxd\xi \qquad 3.8.10$$

Comparing the above cost functional with 3.7.1 it can be seen that we have both a first order and a second order term in the cost functional:

$$L_1 = \frac{1}{\lambda} \phi^2(x) \quad and \quad L_2 = T(x)T(\xi) \qquad 3.8.11$$

Substituting these quantities in equation 3.8.11 in the condition of optimality, equation 3.7.10, we obtain:

$$\phi_c(x) = -\lambda \int_0^1 \int_0^1 G(\sigma, x) T(\xi) d\xi d\sigma \qquad 3.8.12$$

This can be rewritten as:

$$\phi_c(x) = -\lambda \int_0^1 G(\sigma, x) d\sigma \int_0^1 T(\xi) d\xi \qquad 3.8.13$$

The Green's function in this case can be analytically calculated as: (see I.Stackgold (1979))

$$\begin{aligned} G(x,\xi) &= x(1-\xi) \quad x < \xi \\ &= \xi(1-x) \quad x > \xi \end{aligned} \qquad 3.8.14$$

Substituting equation 3.8.14 in equation 3.8.13, and integrating we get:

$$\phi_c(x) = -\lambda \frac{x(1-x)}{2} \int_0^1 T(x) dx \qquad 3.8.15$$

Equation 3.8.15., suggests that the optimal distribution for the heat flux with the error in the measured length being fed-back. It should be noticed that the optimal distribution of heat input is parabolic.

3.8.3. Example 3:

In the examples considered so far, the distribution of the disturbance has not been considered. If the disturbance distribution is restricted to specific functions, this information could be incorporated into the design of the controller via the cost functional.

Let $\phi_{rms}^2(x) = E[\phi_D^2(x)]$ be the root mean squared (r.m.s.) value of the disturbance distribution, this implies that more of the controller heat flux should be made available in regions where the disturbance is active. This can be accomplished by incorporating it in the cost functional as shown in equation 3.8.16., i.e. here we are penalizing the availability of the heat flux lesser in regions where the disturbance magnitude is larger. Similarly, if temperatures at certain locations should be better controlled, when compared to other locations, a function *b(x)* could be used to address this need, i.e., *b(x)* is selected to be large in regions where a high temperature error cannot be tolerated. The cost functional can then be modified to:

$$J = \int_0^1 \frac{1}{\lambda \phi_{rms}} \phi_c^{\,2}(x) + b(x)T^2(x)dx \qquad 3.8.16$$

Applying the condition of optimality, equation 3.7.10 the optimal input distribution is:

$$\phi_c(x) = -\lambda \int_0^1 \phi_{rms}(x)G(\xi,x)b(\xi)T(\xi)d\xi \qquad 3.8.17$$

It can be seen from the above that the feed back gain is higher in regions where the disturbance is active and in regions with more stringent temperature error.

3.9. Design procedure for specific processes:

The following indicate the steps involved in designing heating and cooling for the purpose of temperature control in specific processes. (Similar steps can be followed for controlling temperature gradients and dimensions of controlled objects).

1. The starting point for the optimal heating/cooling design problem is the specifications on the amount of temperature error that can be tolerated and the characterization of the disturbances for which the control system is being designed. Once these are established, then the goal of the design process is to design the controller with the least amount of hardware, such as the number and strength of heaters and cooling passages.
2. As a first step, the cost functional in equation 3.8.16 can be used to compute the optimal distribution of heat flux, as shown in 3.8.17. This gives the designer an idea of where heating and cooling is needed in the presence of several disturbances and model errors. This distribution can be used as a guideline for narrowing down the regions where heating or cooling is permitted. This can be accomplished by modifying the cost functional as shown:

$$J = \int_0^1 \frac{p(x)}{\lambda \phi_{rms}} \phi_c^{\,2}(x) + b(x) T^2(x) dx \qquad 3.9.4.$$

3. The function $p(x)$ is chosen to be unity in regions where heating and cooling is permitted and a very large number elsewhere. This restricts the input to lie within selected regions within the object. The optimal input heat flux will again have a linear feed back form and the performance can be studied with the restriction on the input locations.
4. This process is continued until the input is constrained to lie within an acceptable number of locations and the performance is satisfactory.
5. After getting reasonably close to the required temperature distribution, with a reasonable number of heating and cooling elements, a parametric search can be

performed in a close neighborhood of this solution, using steps 1 and 2, to fine tune the selection.

At the end of this design procedure, the locations and the steady-state strengths of heating and cooling can be established. The next step is to design the controller so that the transient performance is satisfactory. Several MIMO design techniques for designing the controller have been investigated for addressing this problem. Design techniques that are useful in specific applications can be found on a case by case basis and Chapter 4. illustrates one such technique. The problem of finding a general method of compensator design, that can be applied in any application, is still an open question and should be investigated in future research work.

3.10. Chapter conclusions:

In the context of manufacturing processes, temperature distributions, temperature gradients and dimensions of objects are the quantities that we most often need to control. An approach for calculating the optimal distribution of heat-flux to control the above mentioned quantities is presented in this chapter. A steady-state Green's function description for the steady state heat conduction problem is used in the analysis. If the Green's functions can be computed, analytically, experimentally or numerically, such Green's functions could be used for designing the controller. A cost functional defined over the space variables associated with the problem is constructed and variational calculus is used to derive the condition of optimality for this problem which results in a feed-back form for the optimal heat flux input. The cost-functional should be carefully chosen to truly represent the constraints on the process. This involves a thorough

understanding of the requirements on the process and the costs associated with using inputs at different locations and the cost of temperature errors.

The next chapter presents an example of using this spatial optimization technique to design the optimal heating and cooling locations in a mold. The compensator design for satisfactory transient performance is done after the selection of the heater and cooler locations.

Chapter 4

OPTIMAL DESIGN OF HEATING AND COOLING: AN EXAMPLE

4.1 Introduction:

This chapter presents detailed simulations that have been performed to illustrate the optimal input location technique developed in Chapter 3. The example problem presented in this chapter deals with controlling the steady-state temperature distribution across one face of a rectangular solid. The example problem has been selected to illustrate a technique that could be used to design heating and cooling in molding operations.

This work was motivated in part by the recent work performed in the area of rapid tooling. Walczyk (1996) and Wylonis (1995) have demonstrated the use of rapid tooling technology for the purpose of designing conformal cooling/heating passages in molds. These new techniques have created a way of incorporating complicated cooling and heating passages within molds. These techniques are especially powerful in situations where incorporating heating passages is extremely difficult due to the curvature of the mold and other geometric constraints. See figure 4.1.1 for an example of the upper half of a mold with curvature. Figure 4.1.2 shows how the rapid tooling technique developed by Walczyk (1996) called Profiled Edge Laminate (PEL) technology could be used for incorporating arbitrary passages in molds. There are presently, no guidelines or tools available to design the distribution of heating and cooling passages.

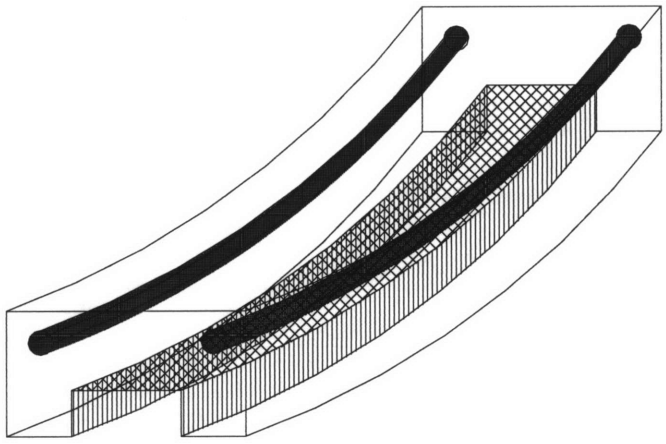

Figure 4.1.1. The upper half of an RTM mold with curvature an heating passages

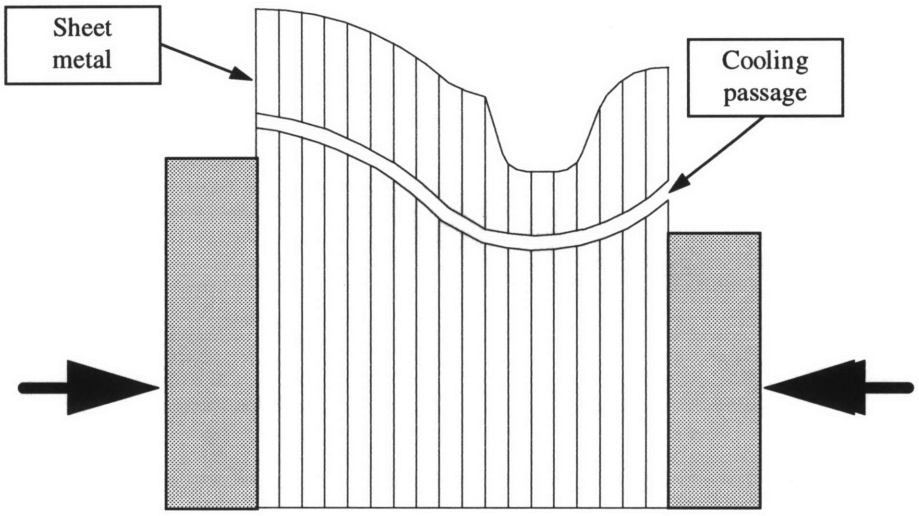

Figure 4.1.2. Conformal passage in a Profiled Edge Laminate mold.

The optimal heating and cooling design technique developed in the previous chapter can now be used to answer the question of where to locate the heating and cooling in a mold. If conformal cooling passages can be incorporated, the technique can be used for determining the shape of such passages.

4.1.1. Resin Transfer Mold (RTM) example problem:

The simulations presented in this chapter demonstrate a technique that could be used to design heating and cooling in an RTM mold. In an RTM mold maintaining a uniform temperature on the mold surface is key to ensuring the uniformity of cure in the component being produced. Curing of composites is an exothermic reaction. This means that thicker parts of the component have a higher amount of heat production within them. If no attempt is made to control the distribution of temperature, this heat generation causes the temperature to be higher closer to the thicker sections of the component. Additionally, there might be some uncertainty present in the amount of heat being released during curing and the ambient temperature could change altering the heat fluxes on the mold. These effects manifest themselves as disturbances on the process. Therefore, a good scheme for active control is needed to maintain a uniform mold surface temperature in the presence of the disturbances.

Although this technique has been developed for RTM, this approach could be used for many other processes where steady-state temperature distributions need to be controlled. For example: in an injection mold, the temperatures of the mold need to be accurately controlled so that the residual stresses in the components being produced do not change from run to run. The disturbances on the process could involve changes in the properties

of the plastic, variations in the ambient temperature etc. The mold temperatures need to be kept constant in the presence of such disturbances.

4.2 Simulation Set-up:

The simulations have been performed for a mold that is rectangular in shape. The mold dimensions are taken to be 0.5m x 1.0m, with the mold material being steel. Three sides of the mold are exposed to the surrounding atmosphere and the fourth side is in contact with the curing plastic.

The temperature that we are interested in controlling is the temperature along the side of mold that is in contact with the part being manufactured. The heat input could be applied anywhere within the mold. Hence, the region over which the temperature is being controlled is a sub-set of the region over which the heat input can be applied. This means that any Green's/influence function that is computed is in general non-symmetric. The Green's function used in Chapter 3, assumes that the region of temperature measurement is the same as the region of heat input. This is because, the Green's function calculation (See Figure 3.5.1) assumes that we could apply a heat input everywhere and the resulting temperature is measured everywhere in the object being considered. This results in a symmetric Green's function. Here however, the input can occur anywhere in the mold but the temperature of interest is only on one face of the mold. The results of Chapter 3 can be easily generalized to the case of non-symmetric Green's functions. Never the less, the conditions of optimality will be re-derived for the special case considered in this chapter.

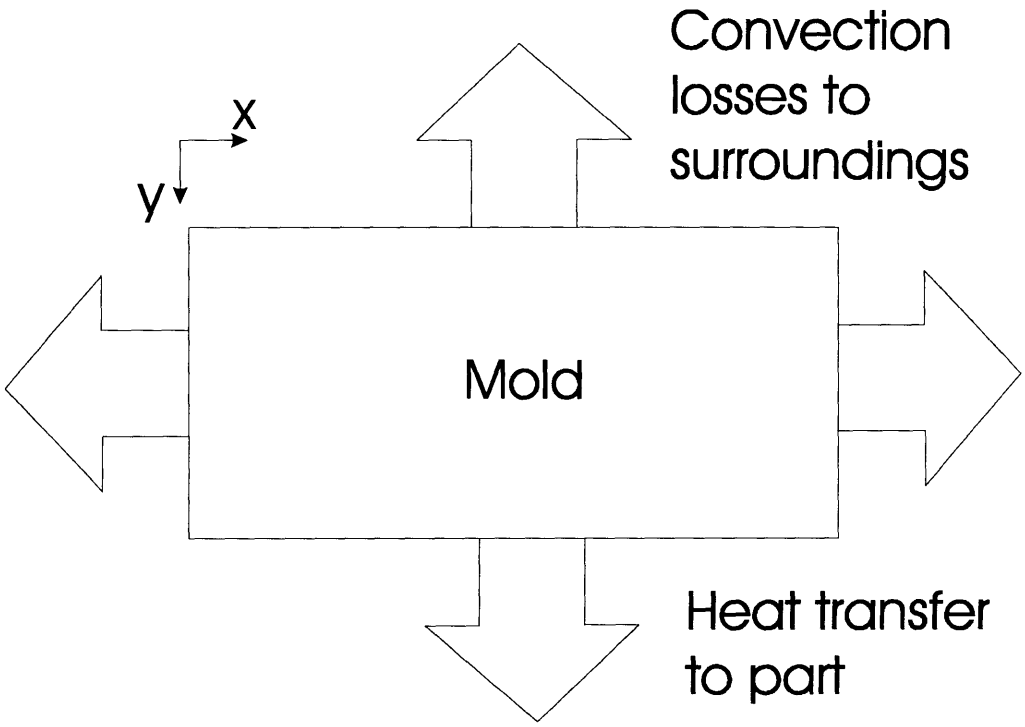

Figure 4.2.1. Schematic of the mold with convection on three sides

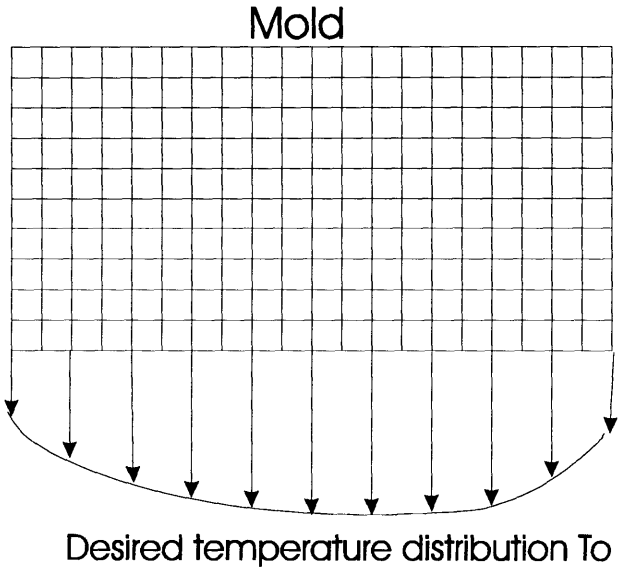

Figure 4.2.2. Reference temperature needed on the bottom surface.

In the RTM mold, if the resin is injected at the center, it flows outward to fill up the mold. This means that if the temperature of the mold is constant across the surface, the resin closer to the outer edges has a higher degree of cure. One of the ways of compensating for this is to maintain the edges cooler than the center while the curing is occurring. Figure 4.2.2 shows one such situation, where the desired temperature drops from the center of the mold to the edge of the mold.

Section 4.3 shows the details of deriving the influence function (non-symmetric Green's function) similar to equation 3.5.5. using a finite difference based model.

4.3 Finite Difference Model for Deriving Influence Functions:

A finite difference (FDE) model for the mold is set up by spatially discretizing the region of the mold. In this example, the finite differences are generated for the steady state problem. The governing equation for the temperature at any node is written by performing energy-balance at that particular node. Figures 4.3.1 , 4.3.2 and 4.3.3 show the FDE scheme for nodes at the corner, on the surface and in the interior of the mold, respectively. The finite difference mesh for this problem has been created with the discretization being equal in both the x and the y directions. (See figure 4.2.1 for x and y directions) i.e., $\Delta x = \Delta y$.

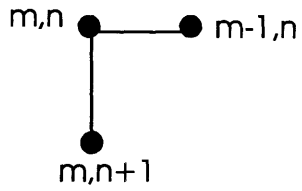

Figure 4.3.1 Finite difference node connectivity for nodes in the top left corner

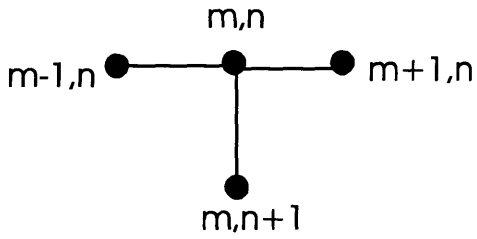

Figure 4.3.2. The finite difference node connectivity for nodes on the top boundary.

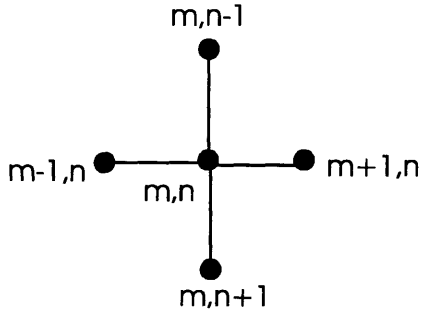

Figure 4.3.3 The finite difference node connectivity for a node in the interior.

Equations 4.3.1, 4.3.2. and 4.4.3 show the steady state governing equations for the temperature of a corner node, a surface node and a node on the interior respectively.

$T_{i,j}$ is the temperature at the 'ij th' node and T_∞ is the ambient temperature. and $\dot{q}_{i,j}$ is the heat flux at a given node. See Incropera and De Witt (1985) for details of the derivation of the equations for the finite difference scheme.

$$\frac{K}{2}\left[T_{m,n+1}-T_{m,n}\right]+\frac{K}{2}\left[T_{m+1,n}-T_{m,n}\right]+h\left[T_\infty-T_{m,n}\right]\Delta x+\dot{q}_{m,n}=0 \qquad 4.3.1$$

$$\frac{K}{2}\left[T_{m-1,n}-T_{m,n}\right]+\frac{K}{2}\left[T_{m+1,n}-T_{m,n}\right]+K\left[T_{m+1,n}-T_{m,n}\right]+h\left[T_\infty-T_{m,n}\right]\Delta x+\dot{q}_{m,n}=0 \qquad 4.3.2$$

$$K\left[T_{m-1,n}-T_{m,n}\right]+K\left[T_{m+1,n}-T_{m,n}\right]+K\left[T_{m+1,n}-T_{m,n}\right]+K\left[T_{m+1,n}-T_{m,n}\right]+\dot{q}_{m,n}=0 \qquad 4.3.3$$

The above equations can be written for nodes everywhere in the object. The resulting set of equations can then be rearranged into the form of equation 4.3.4:

$$M\overline{\mathbf{X}}+N\overline{u}+WT_\infty=0 \qquad 4.3.4$$

Where $\overline{\mathbf{X}}$ is the vector of all the nodal temperatures stacked together. The vector $\overline{u}$ contains the heat input at each node. The elements of W are non zero only for nodes on the surface convecting to the ambient.

Knowing the input heat flux at each of the nodes and the ambient temperature, the temperature vector can be found from equation 4.3.5:

$$\overline{\mathbf{X}}=M^{-1}(-N\overline{u}-WT_\infty) \qquad 4.3.5$$

By picking the vector $\bar{u}$ such that only one element is non zero (in simulations it is assumed to be unity), i.e. we are applying a unit pulse (which is the steady-state counterpart of an impulse in the time domain) at that location, we can compute the temperature at all nodes due to the pulse at the chosen node. By doing this for all the nodes in the finite difference scheme, we can tabulate the Green's function. Figure 4.3.4 shows this procedure. For our purpose we only need the temperatures of the bottom row of nodes. Hence, only the temperatures of the bottom nodes due to the impulse are picked out. These temperatures are stacked up to give us an influence matrix. As was described earlier, this matrix is going to be non-symmetric. This stacking will give the model shown in equation 4.3.6. G will be a rectangular matrix of size m by n, where m is the total number of nodes used and n is the number of outputs considered.

$$T = Gu \tag{4.3.6}$$

This is equivalent to equation 3.5.5 with the integration over the spatial domain performed approximately, by discretizing the spatial domain. The input u has two components, the controller heat flux and the disturbance heat flux, as shown in equation 4.3.7.

$$u = u_C + u_D \tag{4.3.7}$$

After the influence function has been computed, a suitable cost functional that addresses the needs of the process has to be developed. Section 4.4 details the cost functional and the application of the optimality conditions to obtain the optimal distribution.

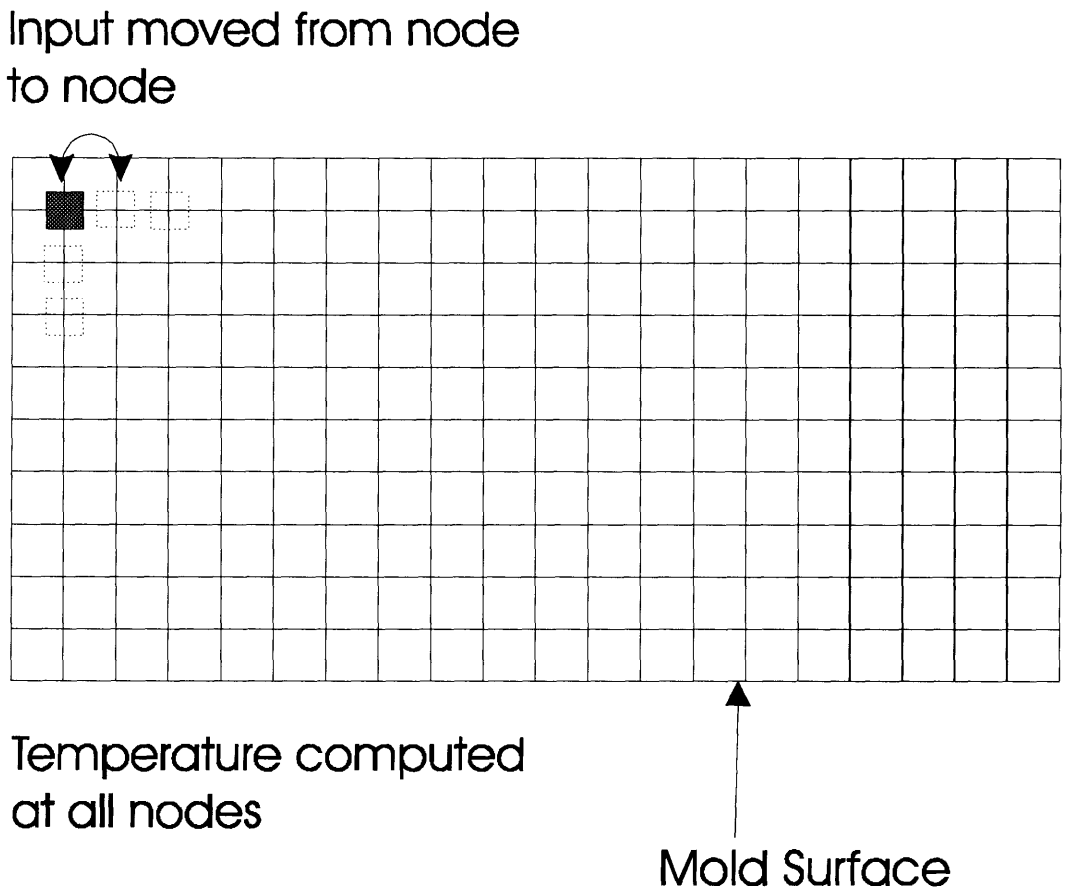

Figure 4.3.4. Procedure for calculating the Green's function (Influence Matrix) *G*.

4.4 The optimization over space:

The cost functional in equation 4.4.1. trades off the error between the achieved temperature and the desired temperature T_0 and the amount of heating or cooling used.

$$J = \frac{1}{2}(T - T_0)^T P(T - T_0) + \frac{1}{2L} u^t Q u \qquad 4.4.1$$

The matrices P and Q are picked to reflect the importance of inputs or temperature error at each of the nodes. L is a scalar gain that will be adjusted at the end of the optimization to satisfy the specifications on the process. The cost functional in equation 4.4.1 is the discretized version of equation 3.7.1. We do not have any second order functionals in this case.

To perform the optimization, the equation 4.3.6 is adjoined to equation 4.4.1 to form the Hamiltonian shown in equation 4.4.2. λ is a Lagrange multiplier.

$$H = \frac{1}{2}(T - T_0)^T P(T - T_0) + \frac{1}{2L} u^T Q u + \lambda^T (T - Gu) \qquad 4.4.2$$

For achieving an optimum, the minimum principle is applied to equation 4.4.2. The expressions shown in equation 4.4.3 have to be satisfied for the minimum principle to hold.

$$\begin{aligned} \frac{\partial H}{\partial T} &= 0 \\ \frac{\partial H}{\partial u} &= 0 \\ \frac{\partial H}{\partial \lambda} &= 0 \end{aligned} \qquad 4.4.3$$

The last condition of equation 4.4.3 gives back the governing equation 4.3.6. The other two conditions of optimality give:

$$\frac{\partial H}{\partial T} = PT - PT_0 + \lambda = 0$$
$$\frac{\partial H}{\partial u} = \frac{Qu}{L} - G^T\lambda = 0 \qquad 4.4.4$$

Eliminating the Lagrange multiplier λ from the equations above we obtain the optimal input to be:

$$u_{CL}^{*} = -LQ^{-1}G^T P(T - T_0) \qquad 4.4.5$$

We need to note here that it seems that if $T=T_0$ then the control input is zero. This is, of course, the nature of any proportional controller. Equation 4.4.5 is a proportional controller, where K_{eq} is the proportional feed-back matrix.

$$u_{CL}^{*} = -K_{eq}(T - T_0)$$
$$Where\ K_{eq} = LQ^{-1}G^T P \qquad 4.4.6$$

The closed loop temperature due to the optimal input given in equation 4.4.6 is obtained by substituting equation 4.4.6 in to equation 4.3.6.

$$T_{CL} = G\left[- LQ^{-1}G^T P(T_{CL} - T_0) + u_D\right] \qquad 4.4.7$$

Adding and subtracting T_0 from both sides and rearranging terms we have:

$$T_{CL} - T_0 = \left[I + LGQ^{-1}G^T P\right]^{-1} Gu_D - \left[I + LGQ^{-1}G^T P\right]^{-1} T_0 \qquad 4.4.8$$

The left hand side of the equation is the error temperature that results due to the controller heat flux and the disturbance heat flux. It can be seen that as the scalar gain L is progressively increased, the error temperature becomes progressively smaller. Therefore

the design procedure consists of increasing the scalar gain until the error becomes satisfactory.

Rearranging the terms in equation 4.4.8, we obtain:

$$T_{CL} = \left[I + LGQ^{-1}G^T P\right]^{-1} LGQ^{-1}G^T PT_0 + \left[I + LGQ^{-1}G^T P\right]^{-1} Gu_D \qquad 4.4.9$$

So the optimal closed loop input in terms of T_0 and u_D is given by:

$$u_{CL}^{*} = -LQ^{-1}G^T P\left\{\left[I + LGQ^{-1}G^T P\right]^{-1} LGQ^{-1}G^T PT_0 - IT_0 + \left[I + LGQ^{-1}G^T P\right]^{-1} Gu_D\right\}$$

4.4.10

Equation 4.4.10 gives the closed loop heat flux that results in the presence of a disturbance, for a given set point of temperature. This gives the designer a tool for evaluating the amount of heating and cooling needed at the different locations in the mold, under the requirements of achieving a certain temperature while rejecting the effect of the disturbance. Hence for a given set of worst case disturbances and set points that one may need, the locations and intensity of heat flux can be computed.

4.4.1. Effects of model errors:

The effects of modeling errors can also, similarly, be studied. Assume for example, that the optimal control has been designed based on equation 4.4.5. If the structure and magnitude of worst case modeling errors can be estimated, the effects of such errors on the controller can be studied. In addition, the influence function can be re-computed experimentally after the heating/cooling has been designed in. In what follows, a technique for compensating for the effects of modeling errors is presented:

If model errors are present, the true Green's function could be represented as:

$$\tilde{G} = G + \Delta G \qquad 4.4.11$$

Where ΔG is the error in the model (we have assumed an additive form for the uncertainty, however this method works even for uncertainty that is multiplicative). So the governing equation for the system will be:

$$T = \tilde{G}(u_C + u_D) \qquad 4.4.12$$

Hence, the closed loop temperature with the true Green's function is given by:

$$T_{CL} = \left[I + L\tilde{G}Q^{-1}G^T P\right]^{-1} L\tilde{G}Q^{-1}G^T PT_0 + \left[I + L\tilde{G}Q^{-1}G^T P\right]^{-1} \tilde{G}u_D \qquad 4.4.13$$

The closed loop heat input with the uncertain Green's function is then given by

$$u_{CL}^{*} = -LQ^{-1}G^T P\left\{\left[I + L\tilde{G}Q^{-1}G^T P\right]^{-1} L\tilde{G}Q^{-1}G^T PT_0 - IT_0 + \left[I + L\tilde{G}Q^{-1}G^T P\right]^{-1} \tilde{G}u_D\right\}$$

4.4.14

This optimal closed loop heat flux captures the effects of model uncertainties, set-points and the disturbances. Equation 4.4.14. can be used to study the effect of worst case disturbances and the worst case model errors. A good picture of where heating and cooling are needed in the mold under different situations could be found using this equation.

4.4.2. Design procedure for narrowing down the locations of input:

1. Equation 4.4.14. can be used to study the required heat flux disturbance for the different combinations of possible model uncertainties, worst case disturbances and set points.

2. After studying these required heat fluxes, the designer can restrict the set of inputs to fewer regions within the mold. The idea behind doing this is to narrow down the specific regions where the input is needed.
3. The optimal required heat flux at these restricted regions is then computed using the same procedure by suitably manipulating the entries in the Q matrix. This gives the exact amount of heating and cooling needed at these restricted locations.

Section 4.5 shows steps involved in selecting input locations using simulations that were performed using Matlab. The finite difference model and the optimization were implemented using Matlab routines.

4.5 Simulation results:

The mold dimensions used for simulation were 0.5m by 1.0m. There are 20 nodes along the x axis and 10 nodes along the y axis. This implies that the size of the finite differences is given by $\Delta x = \Delta y = 0.05$m. The reference temperature T_0 is taken to be a half sinusoid added to a flat temperature distribution. The reference temperature is plotted in figure 4.5.1. The nodes are numbered from 1 to 20 on the bottom surface and the corresponding desired temperature is plotted for the nodes on the bottom surface.

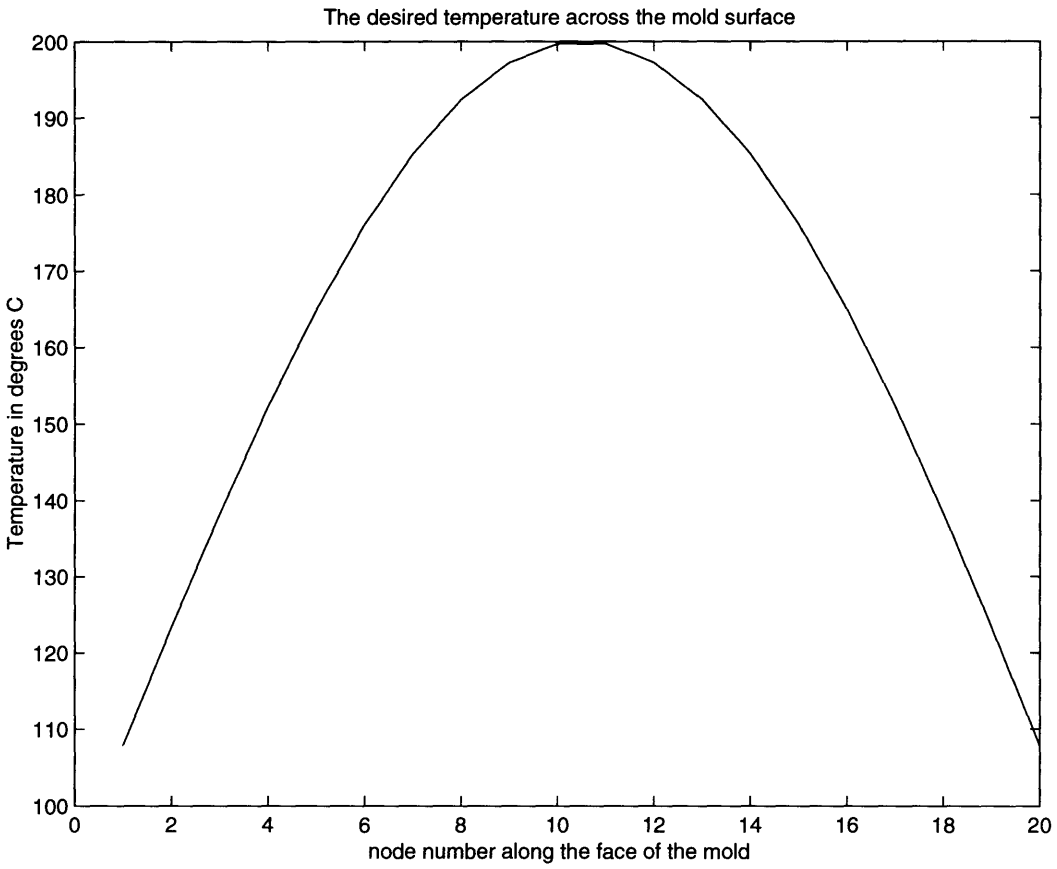

Figure 4.5.1. The desired temperature on the bottom surface of the mold.

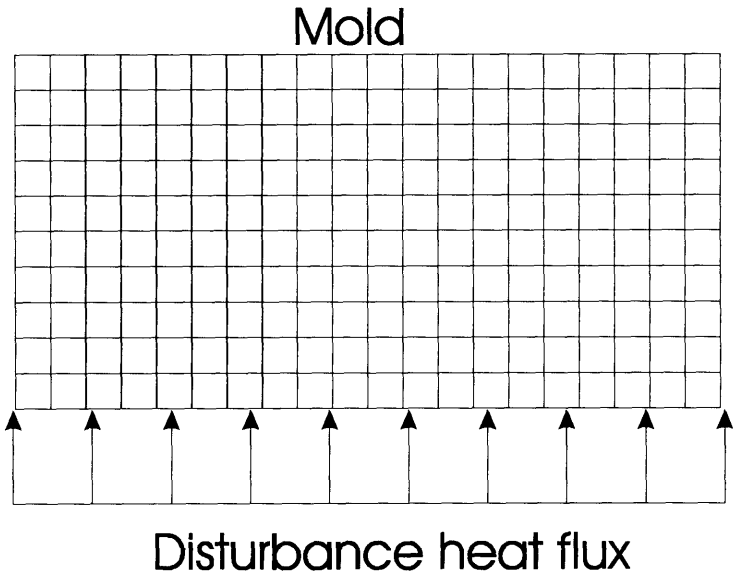

Figure 4.5.2. A disturbance that is constant across the surface.

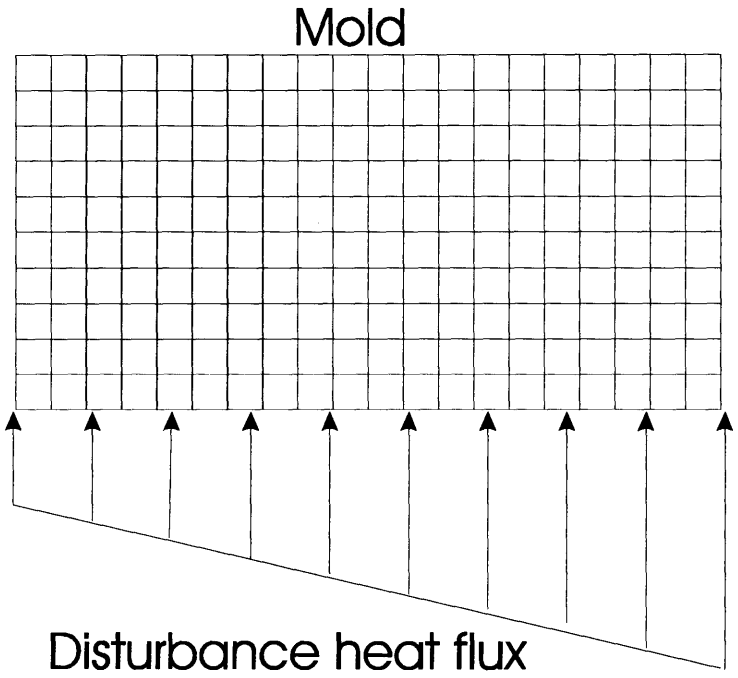

Figure 4.5.3. A disturbance that is linearly varying across the surface.

As was mentioned ahead, curing of the composite is an exothermic reaction. Uncertainties in this reaction manifests itself as a heat flux disturbance on the mold surface in contact with the component. Two particular disturbances have been considered for the simulations performed. The first disturbance is shown in Figure 4.5.2. This is a disturbance whose intensity is constant across the face of the mold. Such a disturbance could be caused by a part of constant thickness. The second disturbance that has been considered is shown in Figure 4.5.3. This is a disturbance whose intensity varies a linearly across the face of the mold. This could be the exothermic reaction caused by a part whose thickness varies linearly across the mold.

Figures 4.5.4 and 4.5.5 show plots of the value of the disturbances at each of the nodes, selected for the simulations. Since the disturbance acts only on the bottom surface of the mold, in figures 4.5.4 and 4.5.5, disturbance has a non-zero value only on the nodes at the bottom surface.

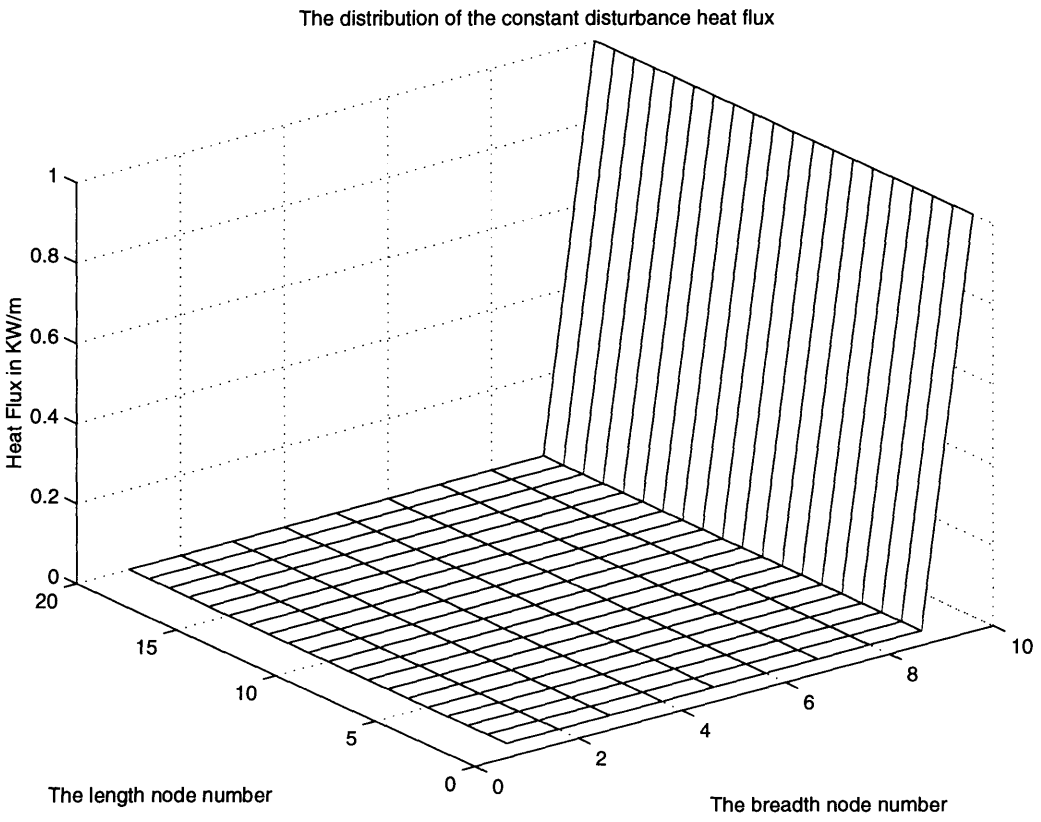

Figure 4.5.4. Distribution of disturbance whose intensity is constant magnitude across the face of the mold.

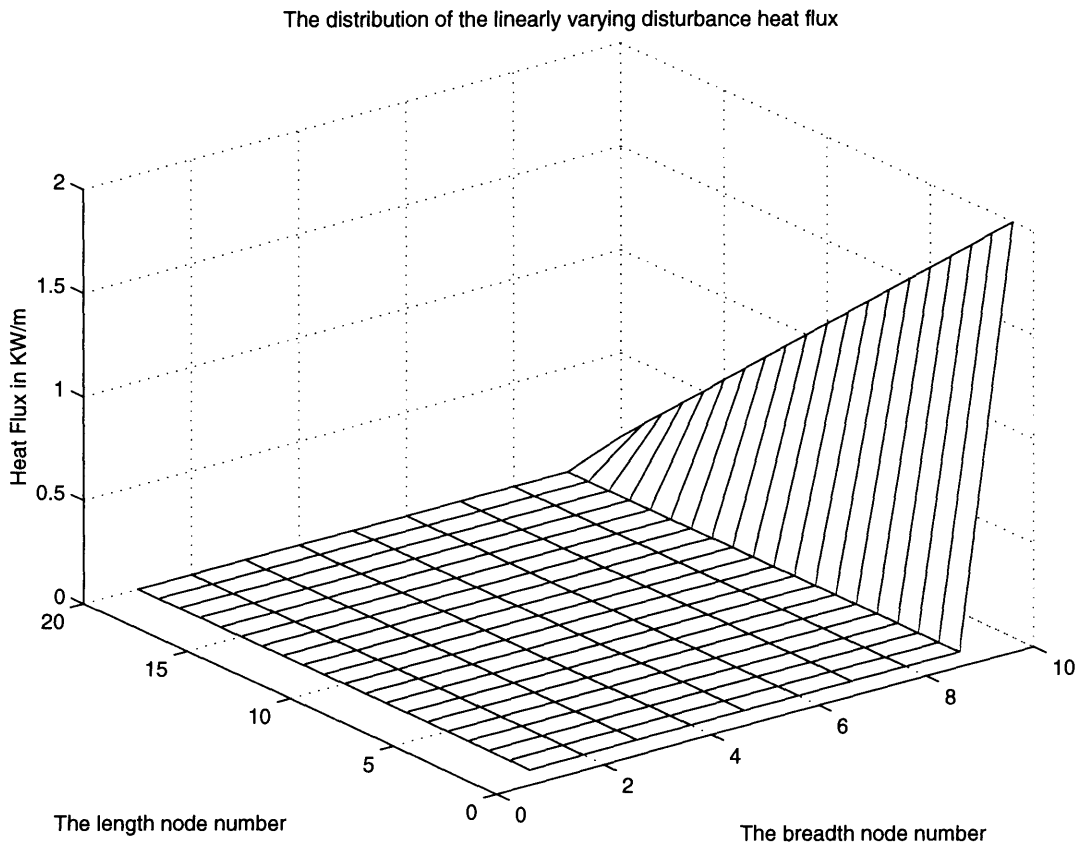

Figure 4.5.5. Distribution of disturbance whose intensity varies linearly across the face of the mold.

4.6 Design process for selecting locations for heat flux:

In any typical mold, the input is constrained to lie within specific regions of the mold. These restrictions could be caused by geometric constraints, or are a result of structural constraints on the mold. Alternately, if a large amount of heating or cooling is needed in the mold, it may not be possible to design such heating and cooling very close to the surface. Also, it is easier to extract a large amount of heat with a passage that can wind through a larger volume than with a passage that winds through a smaller volume. The example presented here illustrates how such considerations can be incorporated into the analysis.

In the example discussed in this chapter, the design for maintaining a desired temperature profile on a mold surface is split up into two parts. In the first part, input is restricted to the half of the mold away from the surface so that large heaters or coolers that reside close to the center of the mold, can be designed. In the second part, smaller heaters will later be placed close to the surface so that the transient response of the system can be improved.

4.6.1. Input restriction to half of the mold:

If no input is permitted on specific nodes in the simulation, this restriction can be implemented in by placing a very large penalty on having input on those nodes. This is accomplished in the matrix Q in equation 4.4.1., by picking high values for the corresponding elements of Q where no input is allowed. If heaters/coolers are not permitted in the bottom half of the mold, large values are picked for the elements in Q corresponding to the bottom half of the mold. The closed loop heat flux and the resulting

closed loop temperatures are then computed using equations 4.4.5 and 4.4.7. The parameter L is picked high enough that the temperature distribution is within acceptable limits. This results in the heat flux distribution shown in figure 4.6.1. Figure 4.6.2 shows the corresponding closed loop temperature plotted along with the desired temperature. It can be seen that the achieved temperature is very close to the desired temperature. The corresponding error temperature is shown in figure 4.6.2a.

It should be noted here that, so far, the effects of disturbances and model uncertainties have not been studied. In the following section, the effects of disturbances on the closed loop heat flux are studied.

4.6.2. Effect of disturbances on closed loop behavior:

The disturbances described in figures 4.5.2 and 4.5.4 are applied to the face of the mold and the resulting heat flux and temperatures are recalculated using equations 4.4.5 and 4.4.7. The parameter L is again adjusted so that the specifications on the temperature error are met. The first disturbance which is a constant disturbance is applied to the surface of the mold in contact with the part. The resulting heat-flux distribution and temperature distribution can be seen in figures 4.6.3 and 4.6.4., respectively. It can be seen that the closed loop heat flux changes from figure 4.6.1. to compensate for the applied disturbance. The resulting error temperature is plotted in figure 4.6.4a.

The second disturbance shown in figures 4.5.3 and 4.5.5., is applied to the face of the mold and the same procedure is carried out for the second disturbance. The resulting heat flux distribution is shown in figure 4.6.5. The corresponding closed loop temperature is

plotted along with the desired temperature in figure 4.6.6. The error temperature in this case is indicated in figure 4.6.6a. Again it can be seen that the disturbance was efficiently rejected.

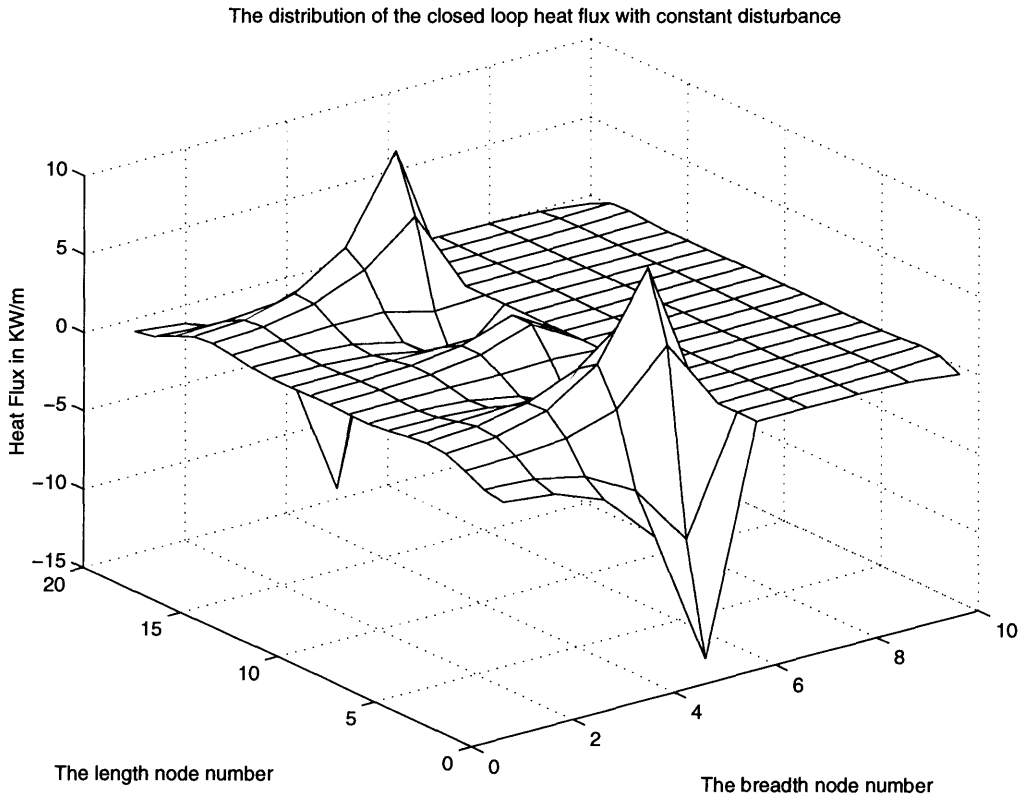

Figure 4.6.1. The heat flux distribution in the upper half of the mold with no disturbances present.

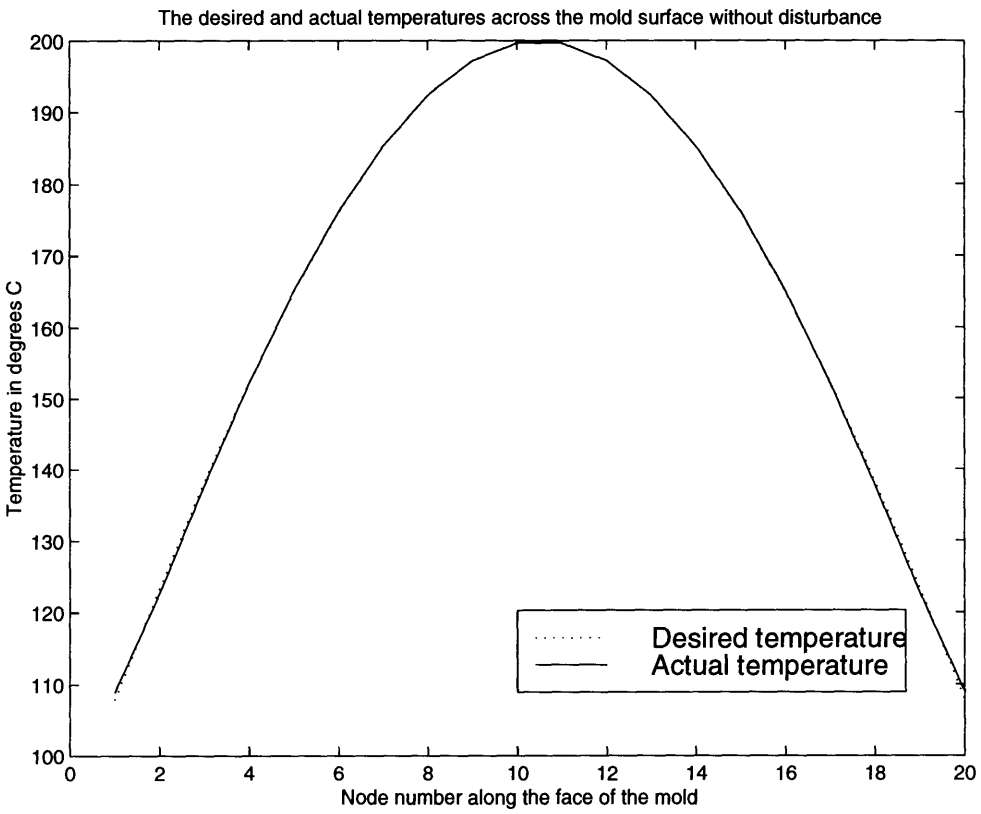

Figure 4.6.2. The Actual vs. Desired temperatures without any disturbance.

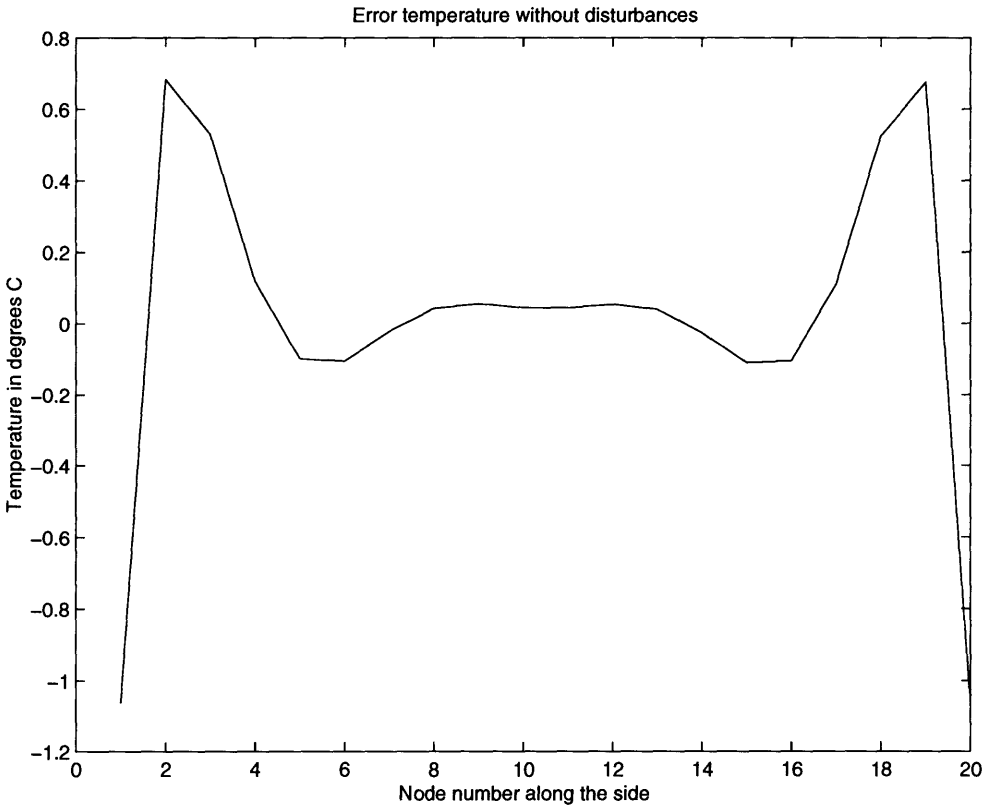

Figure 4.6.2a. The error temperature when no disturbances are present.

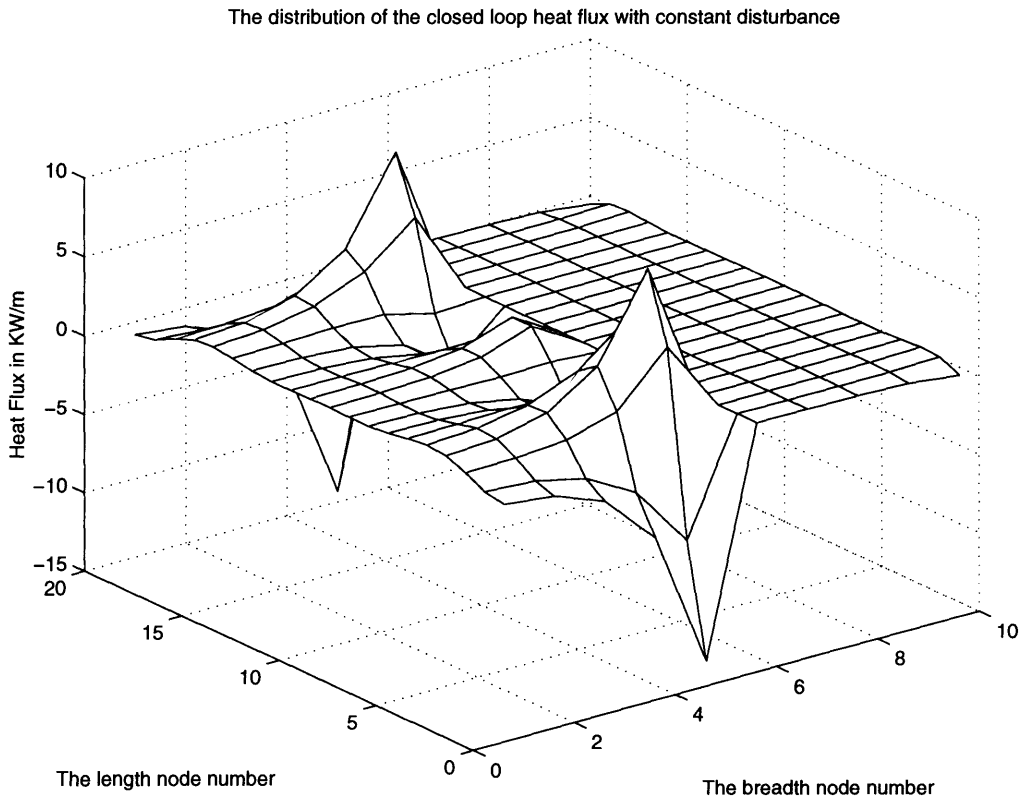

Figure 4.6.3. Heat flux distribution due to the constant disturbance.

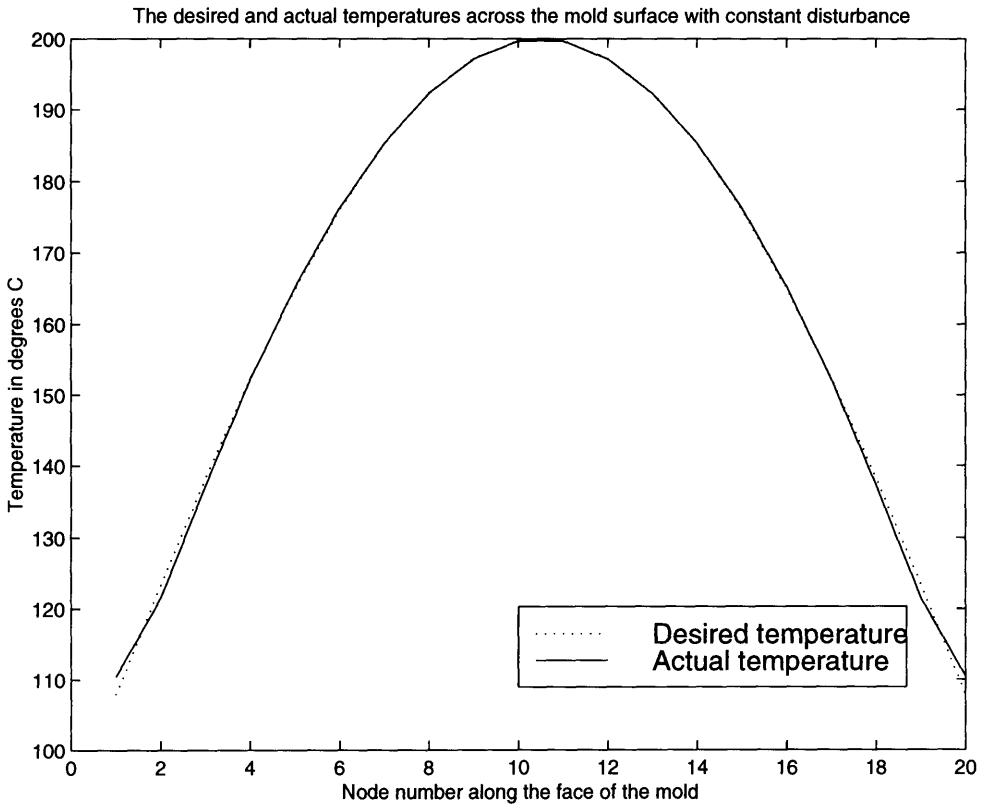

Figure 4.6.4. The desired and the actual temperature with constant disturbance.

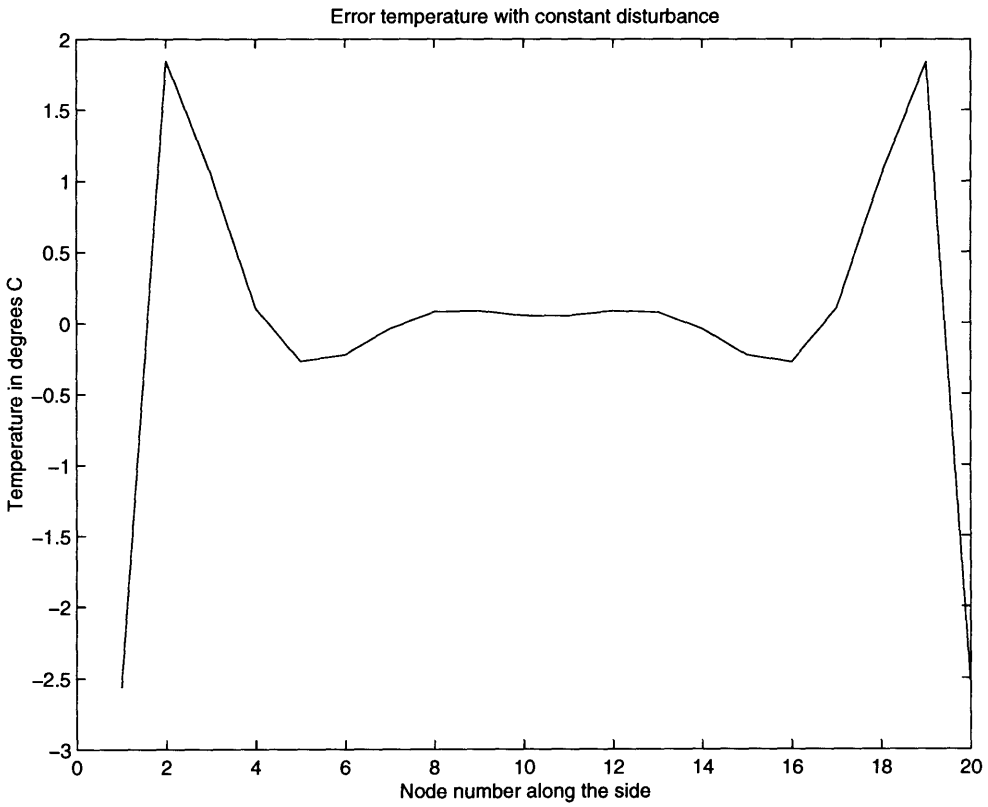

Figure 4.6.4a. The closed loop error temperature when a constant disturbance is present.

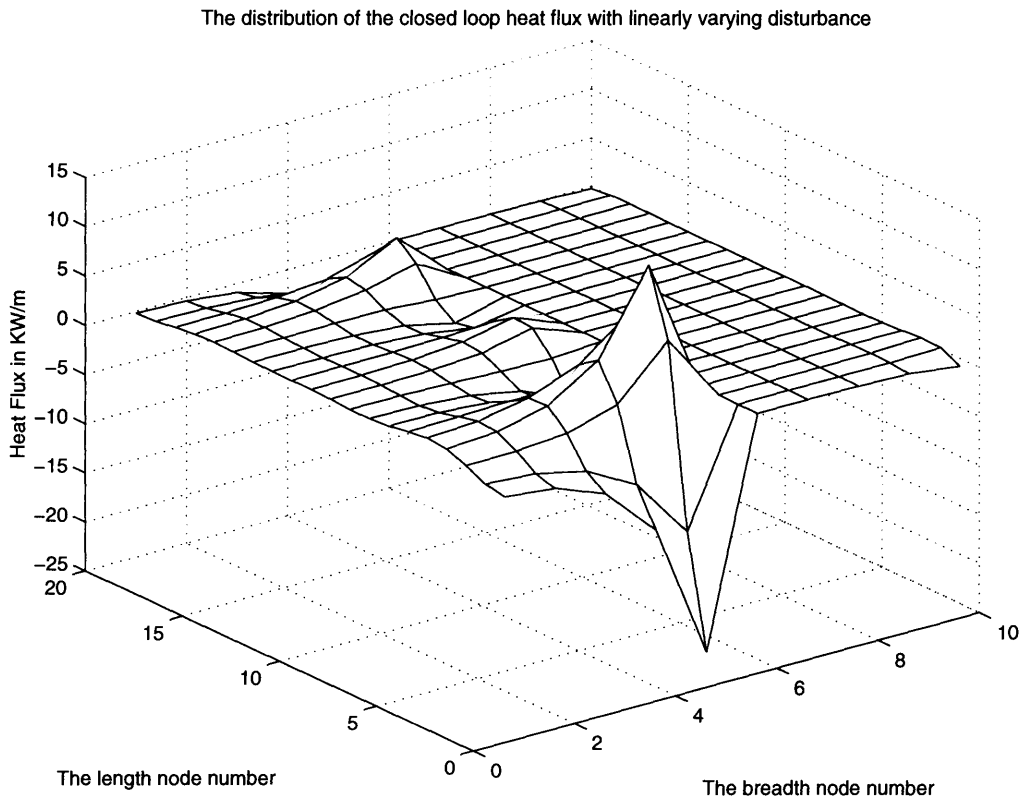

Figure 4.6.5. The closed loop heat flux when the linearly varying disturbance is present.

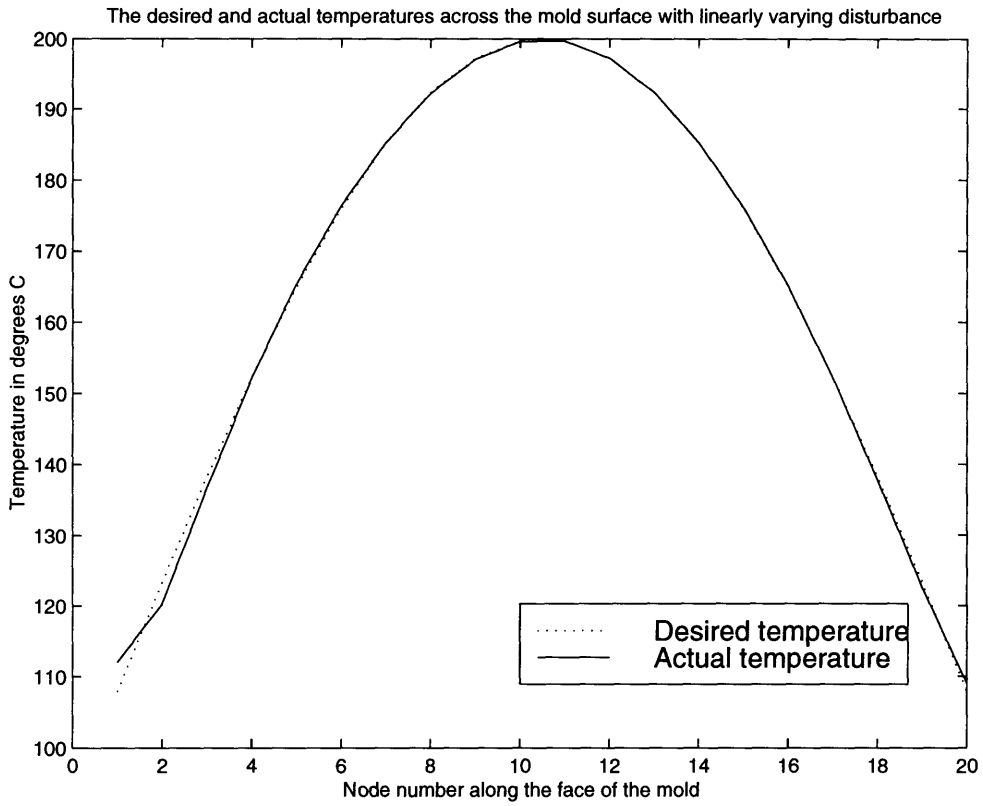

Figure 4.6.6. The closed loop temperature distribution when a linearly varying disturbance is present.

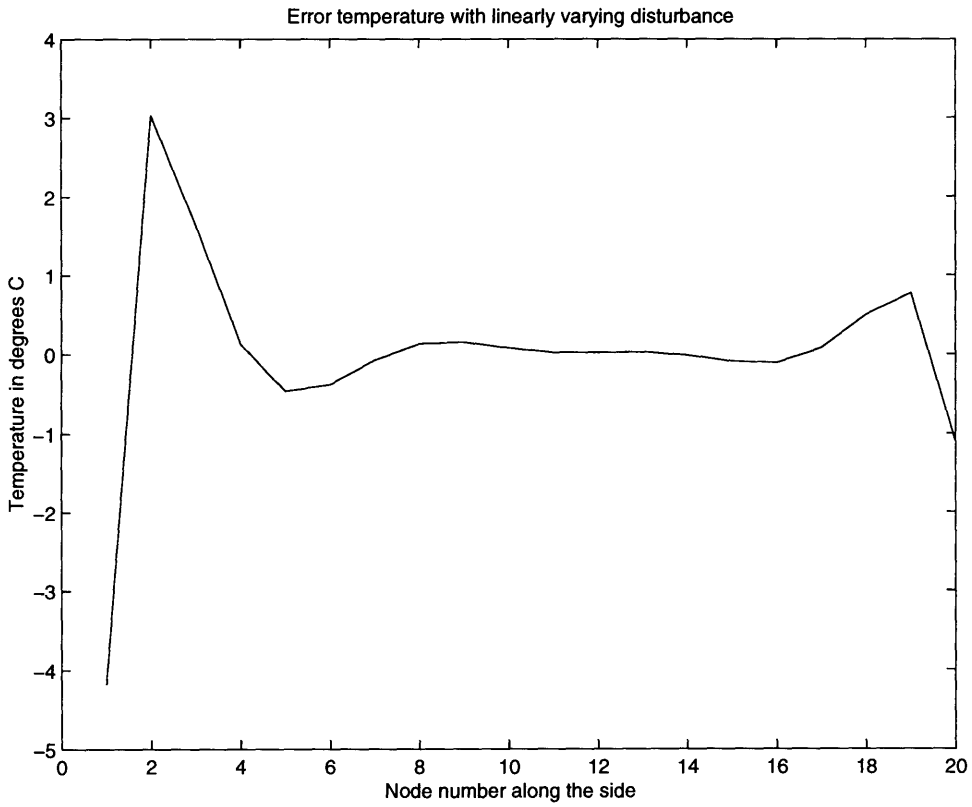

Figure 4.6.6a. The temperature error when a linearly varying disturbance is present.

4.6.3. Input restriction to fewer locations:

After observing the heat flux plots for the different worst case scenarios, i.e. figures 4.6.1., 4.6.3., and 4.6.5., the design engineer can get a good idea of which regions need heating and which need cooling under different scenarios. This is used as a guide line to narrow down these regions so that a smaller number of heaters/coolers can be used to get the same performance. In the present case, ten nodes with the highest magnitude of heating/cooling input have been picked to be the final locations of the inputs. In practice, this could be the starting point for a parametric search within a small neighborhood of these ten nodes. Figure 4.6.7., shows the ten nodes in the finite difference grid where the inputs are going to lie.

Now, the performance of the closed loop system, with the inputs constrained to these specific nodes can be studied using a similar procedure as was used earlier in this section. In the matrix Q, the elements corresponding to the ten nodes are picked to be small and the rest of the elements are picked to be very large. Equations 4.4.5 and 4.4.7 are then recalculated for the new Q matrix and the scalar gain L is adjusted again to lower temperature error. Figures 4.6.8. and 4.6.9. show the closed loop heat flux needed at each of the ten nodes and the corresponding closed loop temperature. Figure 4.6.9a shows the corresponding error temperature. It should be noted that the error temperature did not worsen even though the input has been constrained to fewer locations.

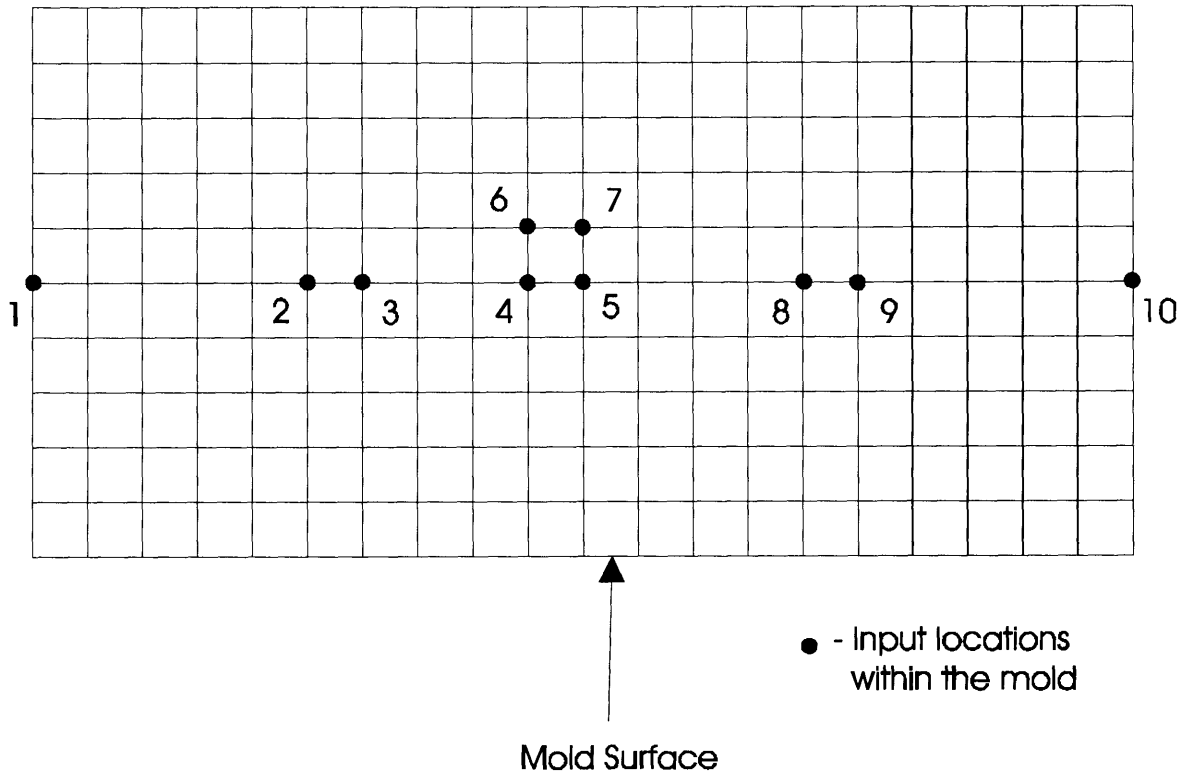

Figure 4.6.7. The restricted set of input locations..

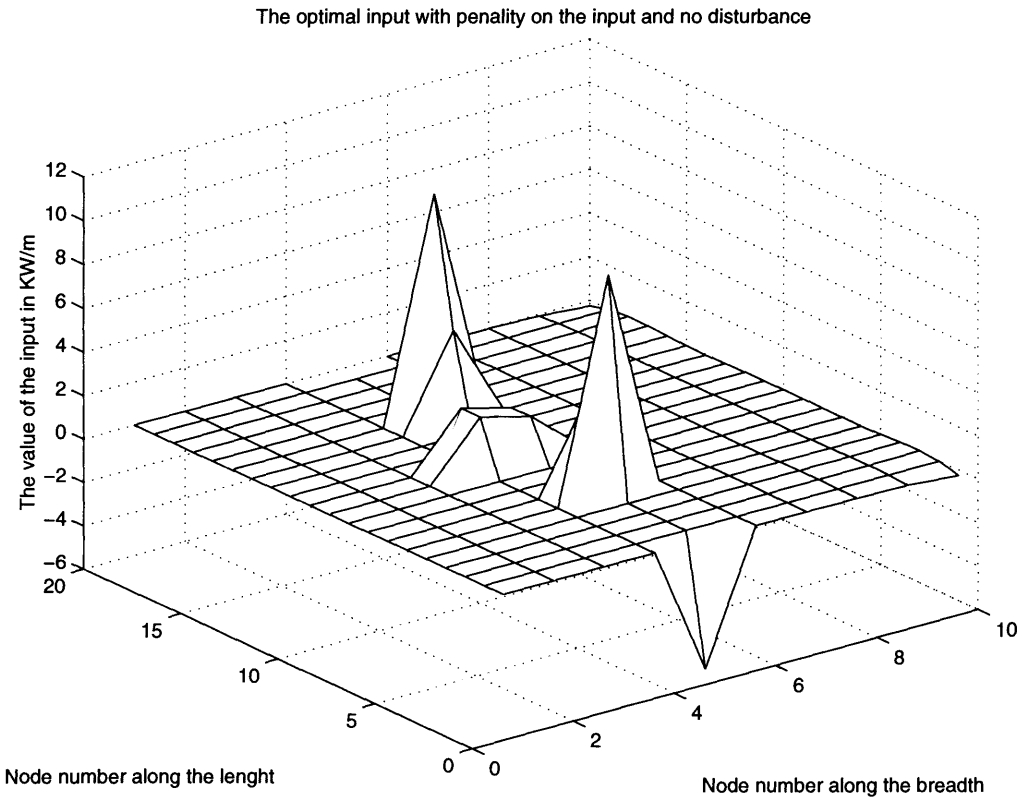

Figure 4.6.8. The heat-fluxes needed at each of the nodes when no disturbance is present.

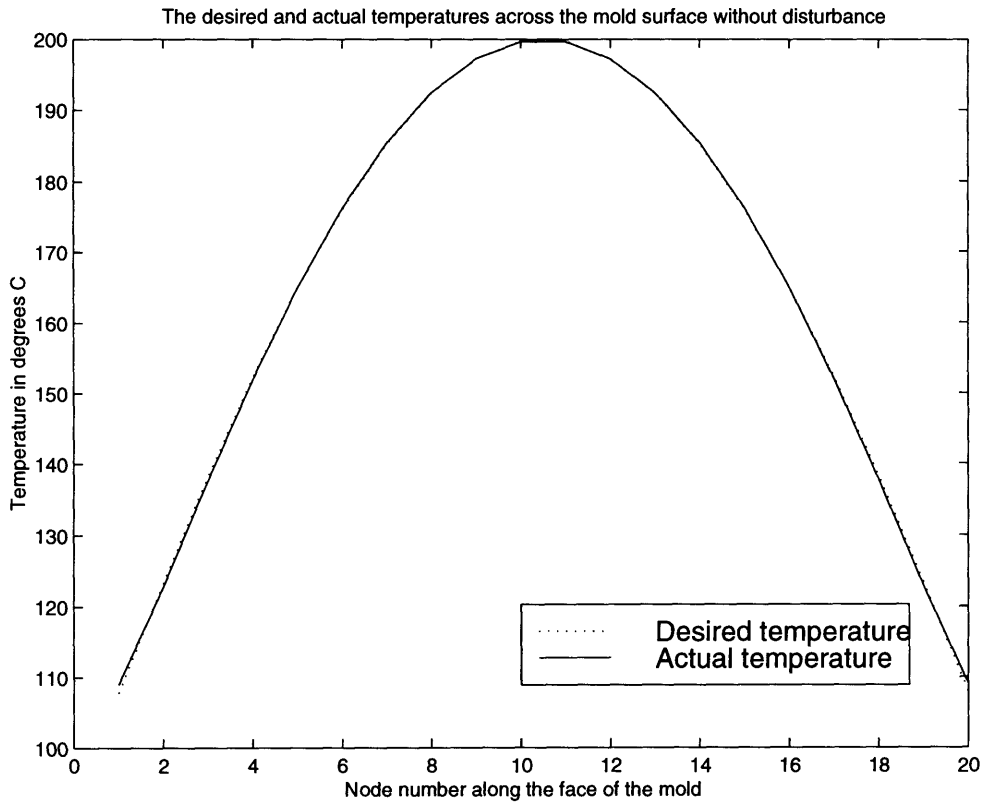

Figure 4.6.9. The temperatures at each of the nodes with input restricted to ten nodes and no disturbance present.

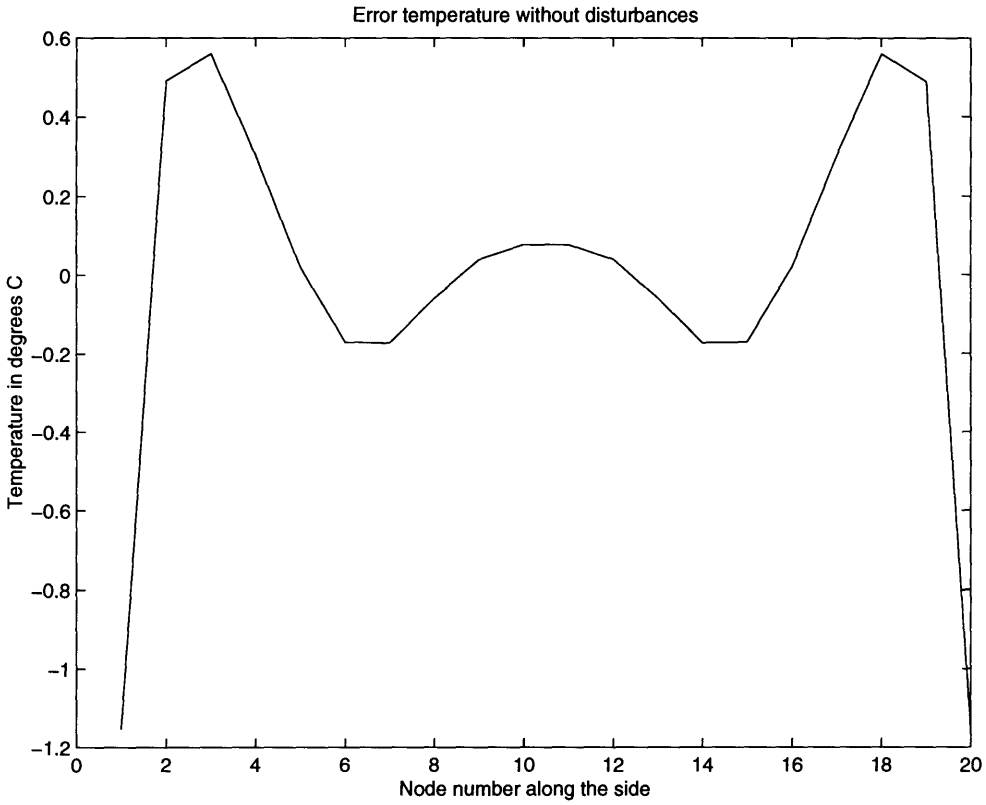

Figure 4.6.9a. The error temperature when inputs are constrained to ten nodes and no disturbance is present.

The effects of the two types of disturbances can be studied in a similar way as before. Figures 4.6.10 and 4.6.11. show the closed loop heat flux the closed loop temperatures with the constant disturbance shown in figure 4.5.2. Figure 4.6.11a shows the corresponding closed loop error temperature.

Figures 4.6.12 and 4.6.13.show the closed loop heat flux and the corresponding temperatures for the linearly varying disturbance shown in figure 4.5.3. Figure 4.6.13. shows the corresponding closed loop error temperature. Figure 4.6.13a shows the corresponding error temperature. It should be observed that restricting the input to fewer nodes did not significantly degrade the performance of the controller in the presence of disturbances.

This completes all the steps in the design process for achieving a desired temperature distribution with the input restricted to very few nodes.

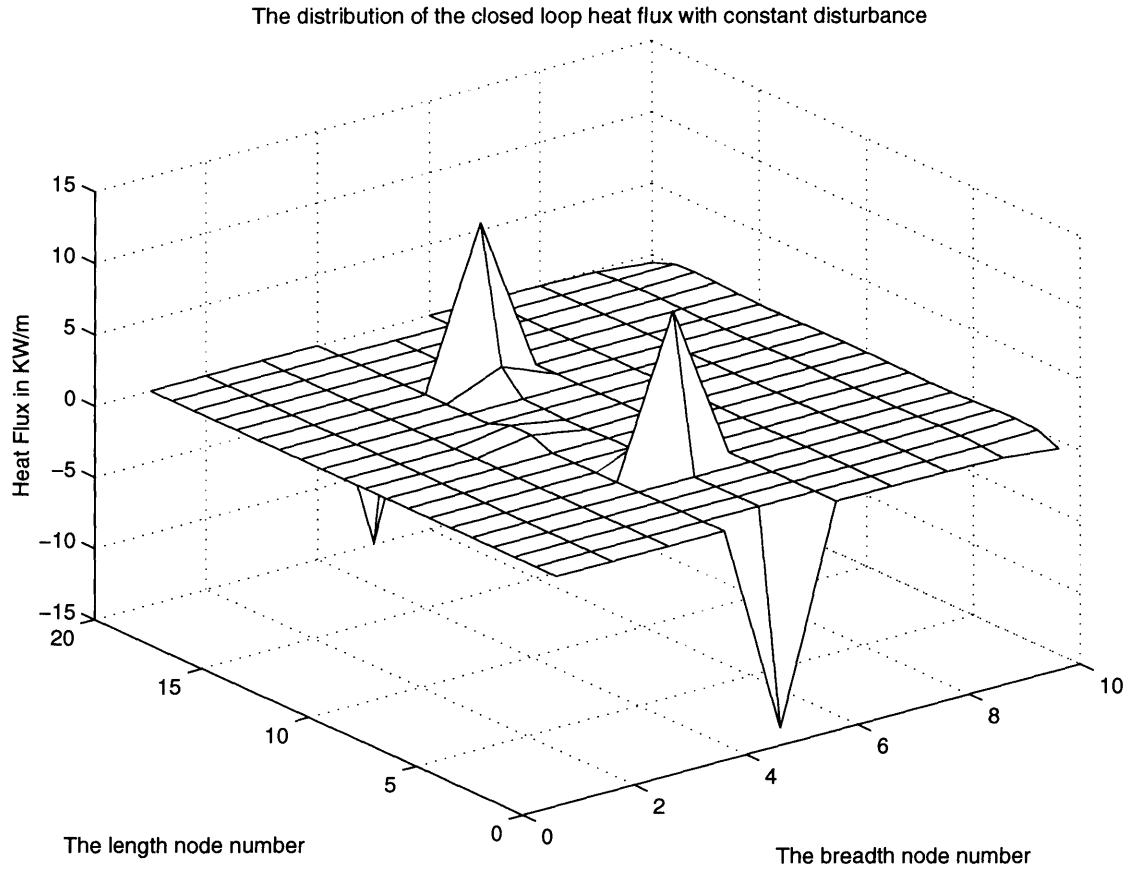

Figure 4.6.10. The closed loop heat flux with constant disturbance when input restricted to ten nodes.

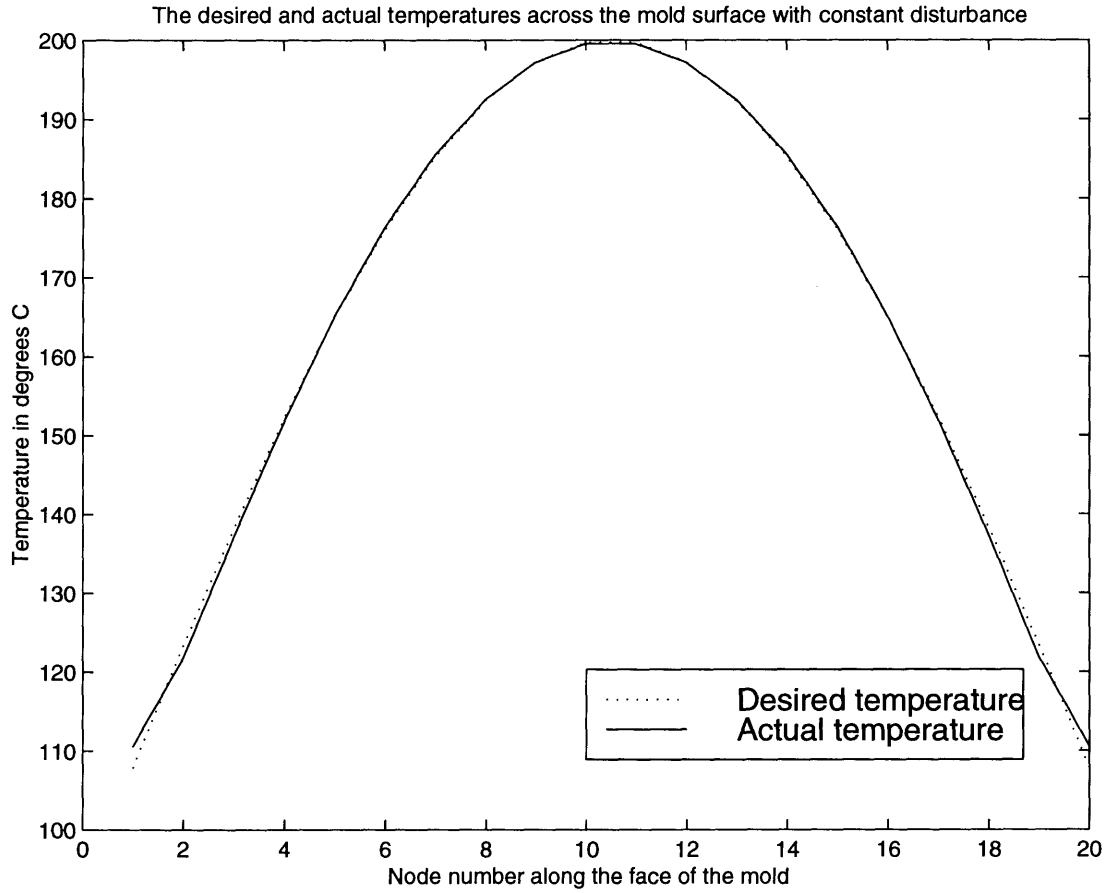

Figure 4.6.11. The closed loop temperature with constant disturbance when input restricted to ten nodes.

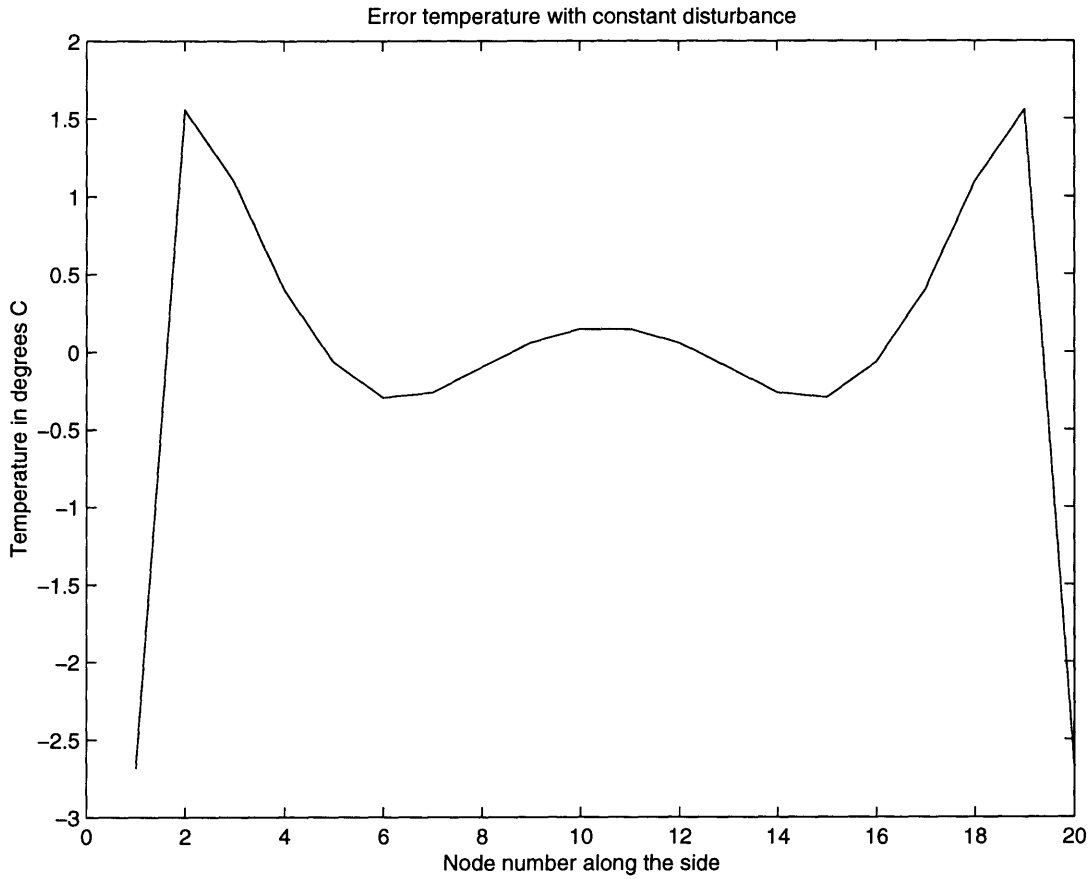

Figure 4.6.11a. The error temperature due to a constant disturbance when input restricted to ten nodes.

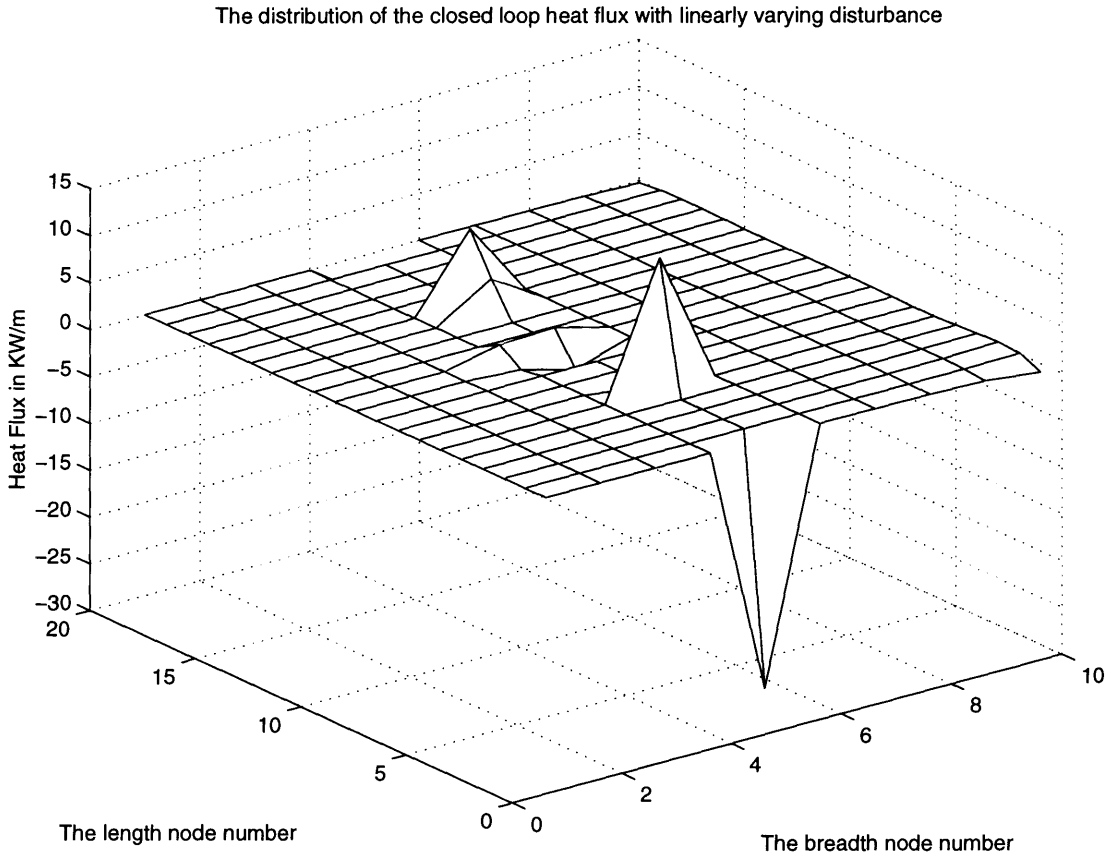

Figure 4.6.12. The closed loop heat flux for the linearly varying disturbance when input restricted to ten nodes.

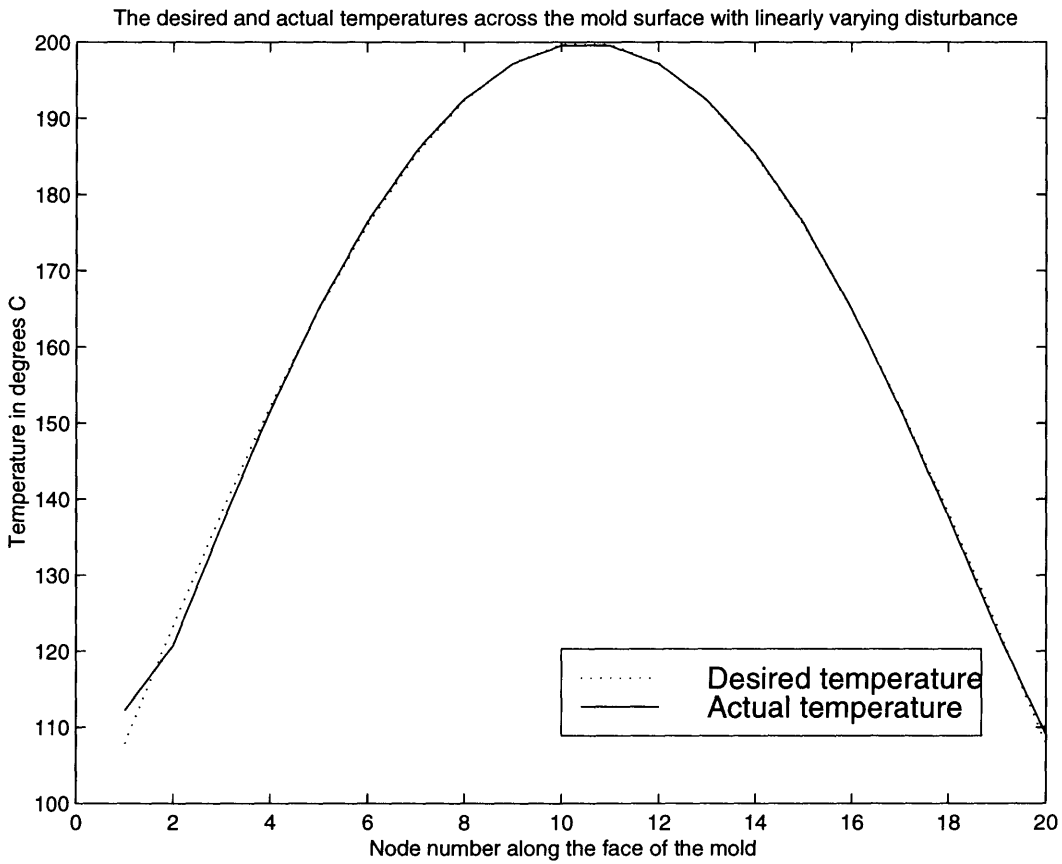

Figure 4.6.13. The closed loop temperature for the linearly varying disturbance when input restricted to ten nodes.

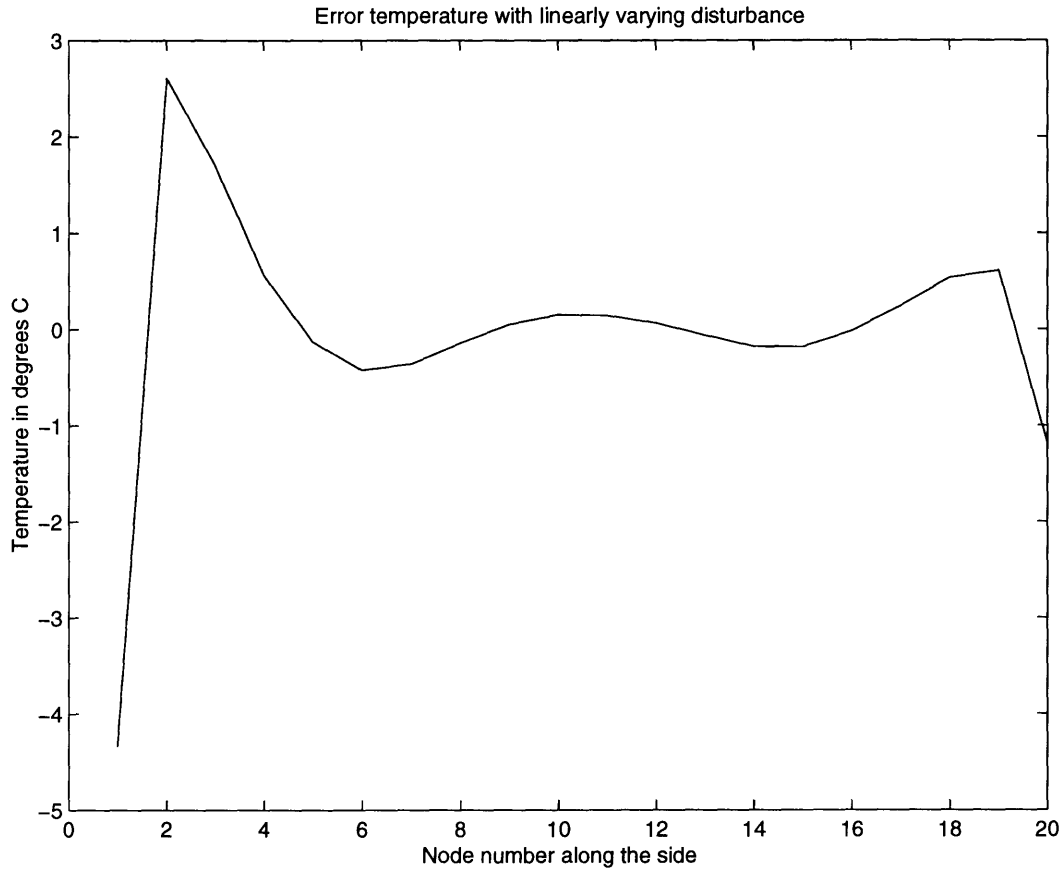

Figure 4.6.13a. The closed loop error temperature distribution with a linearly varying disturbance when input restricted to ten nodes..

4.7 Conclusions from steady-state design:

The following conclusions can be drawn from the steady-state design method developed in the prior section:

1. A technique for locating heating and cooling for achieving a desired steady state temperature distribution has been developed.
2. The method yields a closed loop form for the heat flux in terms of the temperature error.
3. Constraints on the distribution of inputs can be easily incorporated into the analysis.
4. Effects of disturbances can be easily studied due to the feed-back structure for the solution.
5. A sub-optimal method for obtaining the fewest number of heaters and coolers to achieve the desired steady-state performance can be obtained by using this method.

The next step is to add the dynamics back into the heat equation and design the transient part of the controller so that stable operation can be guaranteed while ensuring desirable performance at higher frequencies. These two objectives should be achieved while maintaining the steady state performance obtained by the steady state design performed so far.

4.8 Transient Design:

In the previous sections of this chapter, a technique for determining the locations and strengths of heaters needed for good steady-state performance has been developed. The feed back gain selected in equations 4.4.5. and 4.4.6. is very large in order to satisfy, as

best as possible, the requirements on the temperature error. Equations 4.4.5 and 4.4.6 are rewritten here in equation 4.8.1.:

$$\begin{aligned} u_{CL}^{\ *} &= -LQ^{-1}G^{T}P(T-T_0) \\ u_{CL}^{*} &= -K_{eq}(\Delta T) \end{aligned} \qquad 4.8.1.$$

Introducing the dynamics into the system, the output temperatures on the bottom surface of the mold can be related to the input heat-flux at the ten selected nodes. This input-output relationship can be represented by a multi-input multi-output (MIMO) matrix transfer function. Equation 4.8.2 shows the matrix transfer function where $\mathbf{T}(s)$ and $\mathbf{U}(s)$ are the temperature vector and the input vector respectively.

$$\begin{bmatrix} T_1(s) \\ T_2(s) \\ \vdots \\ T_{20}(s) \end{bmatrix} = \begin{bmatrix} G_{11}(s) & G_{12}(s) & \cdots & G_{110}(s) \\ G_{21}(s) & \ddots & & \\ \vdots & & \ddots & \\ G_{201}(s) & & & G_{2010}(s) \end{bmatrix} \begin{bmatrix} U_1(s) \\ U_2(s) \\ \vdots \\ U_{10}(s) \end{bmatrix}$$

i.e., $\mathbf{T}(s) = \mathbf{G}(s)\mathbf{U}(s);$ 4.8.2.

Then equation 4.3.6. is the steady state portion of the above MIMO transfer function and can also be written (by setting *s=0* in equation 4.8.2.) as:

$$\mathbf{T}(0) = \mathbf{G}(0)\mathbf{U}(0); \qquad 4.8.3.$$

The steady-state design preformed so far has evaluated the structure of the compensation at *s=0*. We need to determine a compensation that yields a stable operation for the closed loop system while retaining the same structure for the closed loop system in steady state.

The following section details the procedure for computing the transfer-function in equation 4.8.2.

4.8.1. The Dynamic model:

To compute the transfer function matrix shown in equation 4.8.2., dynamics need to be added to the static model developed in section 4.3. This can be done by discretizing the PDE in equation 3.3.1., with respect to the space domain while retaining the continuity in the time domain. Equation 4.8.4. shows the governing equation for an interior node, obtained by discretizing with respect to the space domain while retaining continuity in the time domain. Similar equations can be written for the other nodes in the solid. (See Incropera and DeWitt (1985)). Stacking up the differential equations obtained for all the nodes in the solid, a state-space description for the system can be obtained as shown in equation 4.8.5. The output matrix (**C** matrix) is then selected so that the outputs are the temperatures at the nodes on the bottom surface of the mold.

$$\rho C_p \frac{dT_{i,j}}{dt} = k\left\{\frac{1}{(\Delta x)^2}\left[T_{i+1,j} + T_{i-1,j} - 2T_{i,j}\right]\right\} + k\left\{\frac{1}{(\Delta y)^2}\left[T_{i,j+1} + T_{i,j-1} - 2T_{i,j}\right]\right\} + q_{i,j} \qquad 4.8.4.$$

$$\begin{aligned} \dot{\mathbf{X}} &= \mathbf{AX} + \mathbf{BU}; \\ \mathbf{Y} &= \mathbf{CX}; \\ \mathbf{X} &= [T_1, T_2, \cdots, T_{200}]^T; \\ \mathbf{U} &= [q_1, q_2, \cdots q_{10}]^T; \\ \mathbf{Y} &= [T_{181}, \cdots T_{200}]^T; \end{aligned} \qquad 4.8.5$$

The transfer functions corresponding to the state-space description in equation 4.8.5. is the same as the MIMO transfer function discussed in equation 4.8.2. This state-space model has been used to compute the Bode-plots shown in figure 4.8.2.

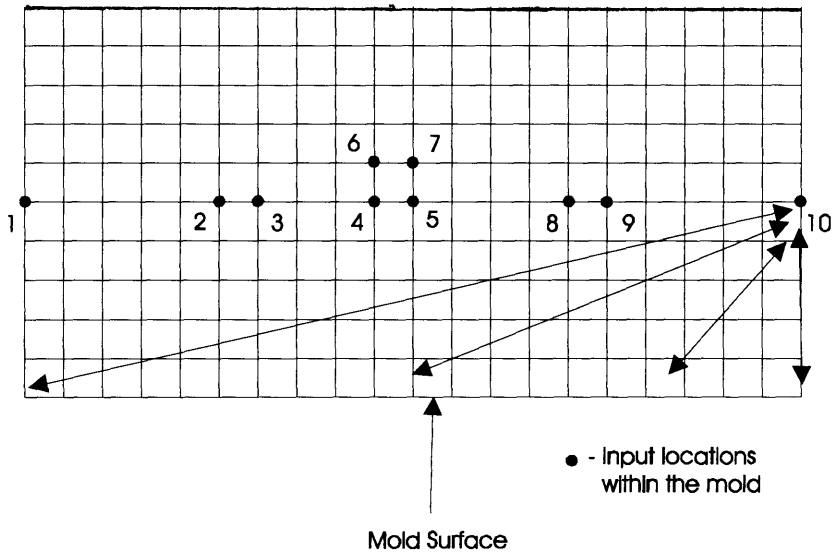

Figure 4.8.1. Transfer function between the 10^{th} heater and the temperatures at the bottom nodes.

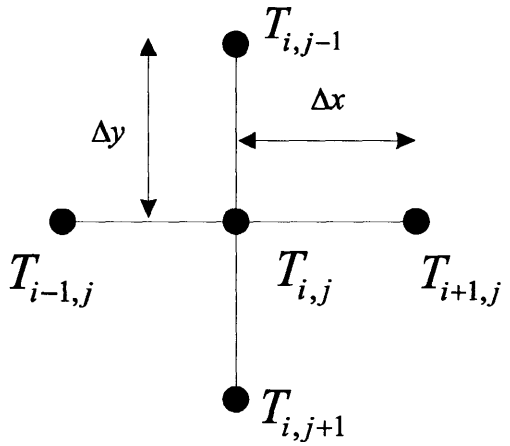

Figure 4.8.2. The notation for temperatures in the finite difference scheme.

Before the compensation scheme is presented, a few observations can be made from the Bode plots. Firstly, the transfer-functions between the heat inputs and the temperature measurements are characterized by exponential phase loss and exponential gain attenuation with increasing frequency. Further, the phase loss and gain attenuation worsens with increase in the physical distance between the inputs and the measurements. For example, consider the transfer functions between the 10^{th} heater situated at node number 70 and the twenty nodes on the mold surface in contact with the part. These Bode plots correspond to the transfer functions of the last column in the transfer function matrix shown in equation 4.8.2. Figure 4.8.1. shows the heater and the sensors between which the transfer functions are being computed. The Bode plots corresponding to these transfer functions are plotted in figure 4.8.3. The phase loss and the gain attenuation can be noticed to decrease with frequency. Also, the curves with the higher phase loss and gain attenuation correspond to the transfer functions between the 10^{th} heater and the nodes that are farther from the heater.

As a part of the steady state design a large proportional gain has been selected to best satisfy the requirements on the steady-state error. If this gain were applied over all frequencies, it is easy to drive the closed loop system unstable. Therefore a suitable scheme must be devised to stabilize the system while maintaining the same steady-state gain. The next section details a technique to design a compensator to ensure stability while achieving the same steady-state performance discussed in the earlier sections. The approach consists of rolling off the high steady state gain with frequency using a first order roll off.

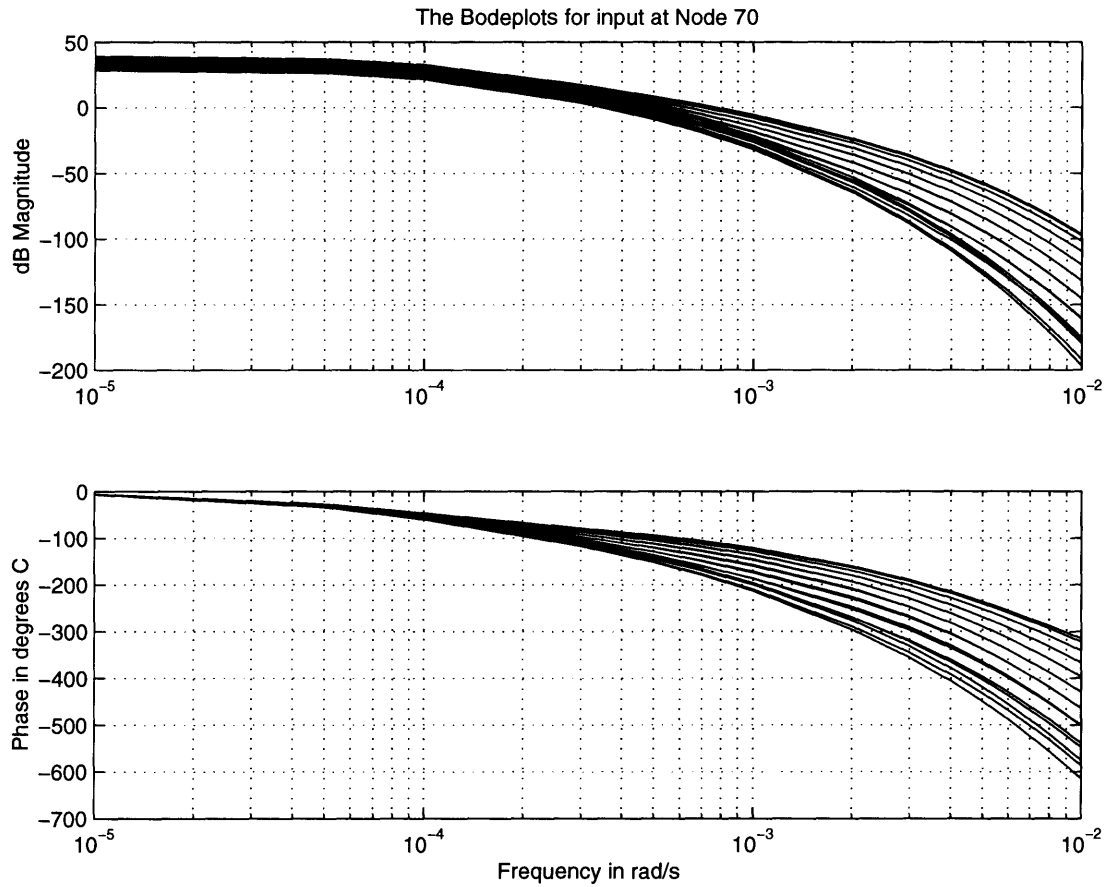

Figure 4.8.3. The Bode plots between input no: 10 and the output temperatures at the bottom nodes..

4.9. Rolling off the gain to stabilize the system.

Designing a compensator so that the steady-state gain is as calculated in the prior section, while guaranteeing stability of the closed loop system is the goal in this section. Many multi-input multi-output (MIMO) compensation schemes can be envisaged to accomplish this task. However, the technique that is presented here is appealing for its ease of implementation and for the ease with which additional inputs can be incorporated to improve the transient performance.

It can be observed from the Bode plots that the lag increases exponentially with frequency. This implies that using the high feed-back gain of equation 4.8.1. across all frequencies, will cause instability. The technique used here to stabilize the system is: roll off the steady state gain with a first order frequency interpolation function as shown in figure 4.9.1.

That is, the compensator transfer function matrix can be represented as:

$$K(s) = \frac{1}{1+\tau s} K_{eq} \qquad 4.9.1$$

The MIMO loop transfer function is then given by:

$$G(s)K(s) \qquad 4.9.2$$

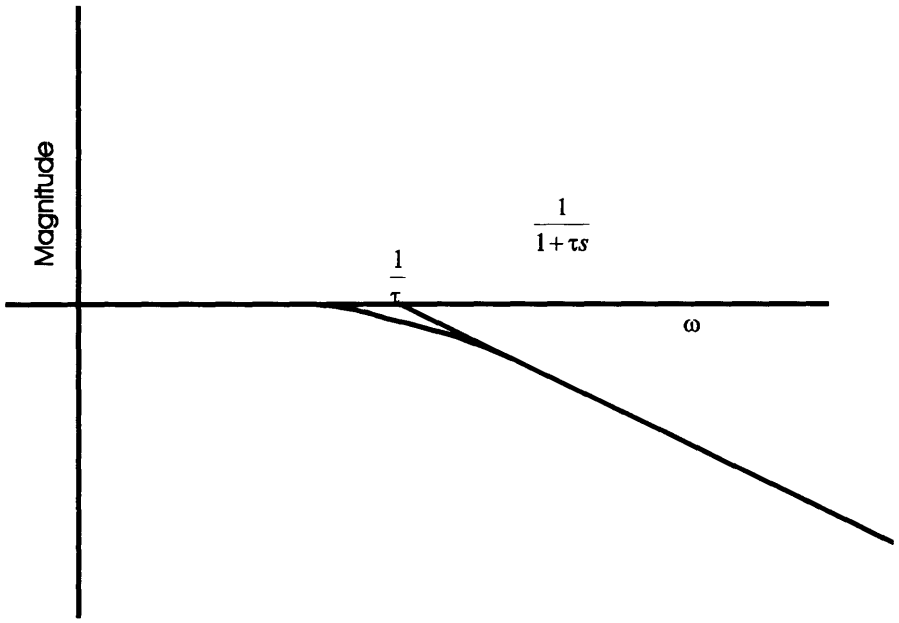

Figure 4.9.1. First order transfer function used as a frequency blending function for rolling-off K_{eq}

The compensator design problem is then to determine the break frequency $1/\tau$ so that the closed loop system is stable. Thus the MIMO controller design problem is reduced to finding a suitable break frequency $1/\tau$.

First an intuitive argument is presented on how to identify this break frequency and then the MIMO Nyquist criterion is used to determine the exact value of this break frequency.

It was seen that the phase loss in the transfer function between a given heater and a given sensor increases with the distance between the heater and the sensor. This implies that in the transfer function between the heater and sensor farthest from each other has the highest phase loss. Instability will be introduced if the phase loss between this heater sensor combination has increased beyond 180^{o} at gain cross-over. The time constant between this heater and sensor can be selected as a first estimate for the desired the break frequency in the first order roll off shown in figure 4.9.1. Figure 4.9.2. shows this largest distance for the mold being considered here. Hence if τ is large enough, we can "slow down" the response of the heaters enough, so that instability does not occur. However, we need to quantify this reasoning to get estimates of the margins of stability that can be obtained using this technique.

For this purpose, MIMO Nyquist criterion can be used. (See Maciejowski (1989)). The MIMO Nyquist criterion requires that if $\det(I + G(s)K(s))$ has P_c zeros and P_0 poles in the closed right half plane, then just as in case of SISO systems, the principle of the argument shown in equation 4.9.3. can be used to determine stability.

$$\Delta \arg\{\det(I + G(s)K(s))\} = -2\pi(P_c - P_0) \qquad 4.9.3$$

Here, $\Delta \arg$ denotes the change in the argument as *'s'* traverses the Nyquist contour once-up the imaginary axis, then along a semi-circular arc in the right half-plane and then up the negative imaginary axis to the origin. In our case, $P_0 = 0$, since $G(s)K(s)$ does not have any unstable poles. Nyquist criterion then requires that for closed loop stability, the number of clock wise encirclements of the origin should be zero. Hence if the Nyquist contour of $\det(I + G(s)K(s))$ does not encircle the origin in the counter-clockwise direction, the closed loop system can be guaranteed to be stable.

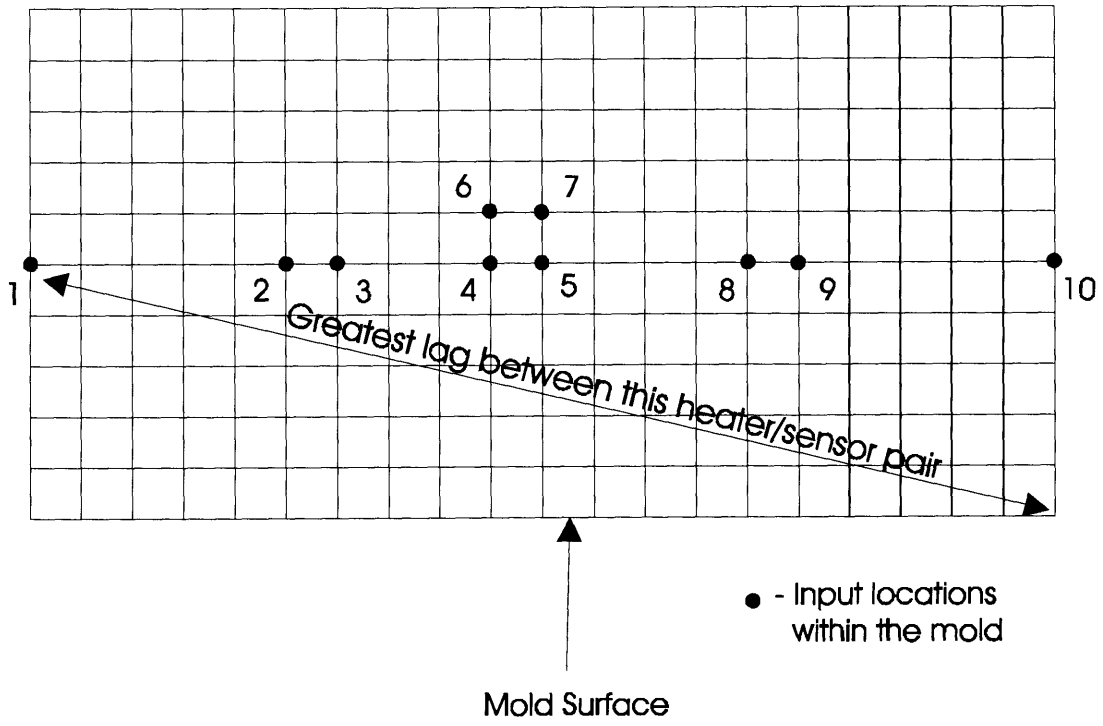

Figure 4.9.2. The greatest lag occurs between the pair of heater and sensor farthest from each other.

The intuitive argument, presented earlier, could now be used to determine if increasing the value of τ has the effect of making the system stable. The MIMO Nyquist plot can be used for this purpose. The following is a numerical procedure for plotting the MIMO Nyquist plot:

1. The $\det(I + G(i\omega)K(i\omega))$ can be computed at a selected frequency "ω", for any given value of the break frequency τ. This calculation yields a single complex number, which is a point on the MIMO Nyquist contour.
2. By performing this calculation at a given set of frequencies, a set of points on the Nyquist contour could be obtained. Joining these points in the complex plane, we can obtain the Nyquist plot for a given τ.
3. The break frequency is then changed by changing τ. The calculations in 1 and 2 are repeated for the same set of frequencies and Nyquist plots are plotted.

The above procedure was performed for different τ's and the corresponding Nyquist plots are shown in Figure 4.9.3. The different values of τ corresponding to each of the Nyquist contours are indicated on the contours. It can be noticed that the Nyquist plots predict that the closed loop system goes unstable in between the break frequencies of $1/(7\times10^6)$ and $1/(5\times10^6)$ Hz.

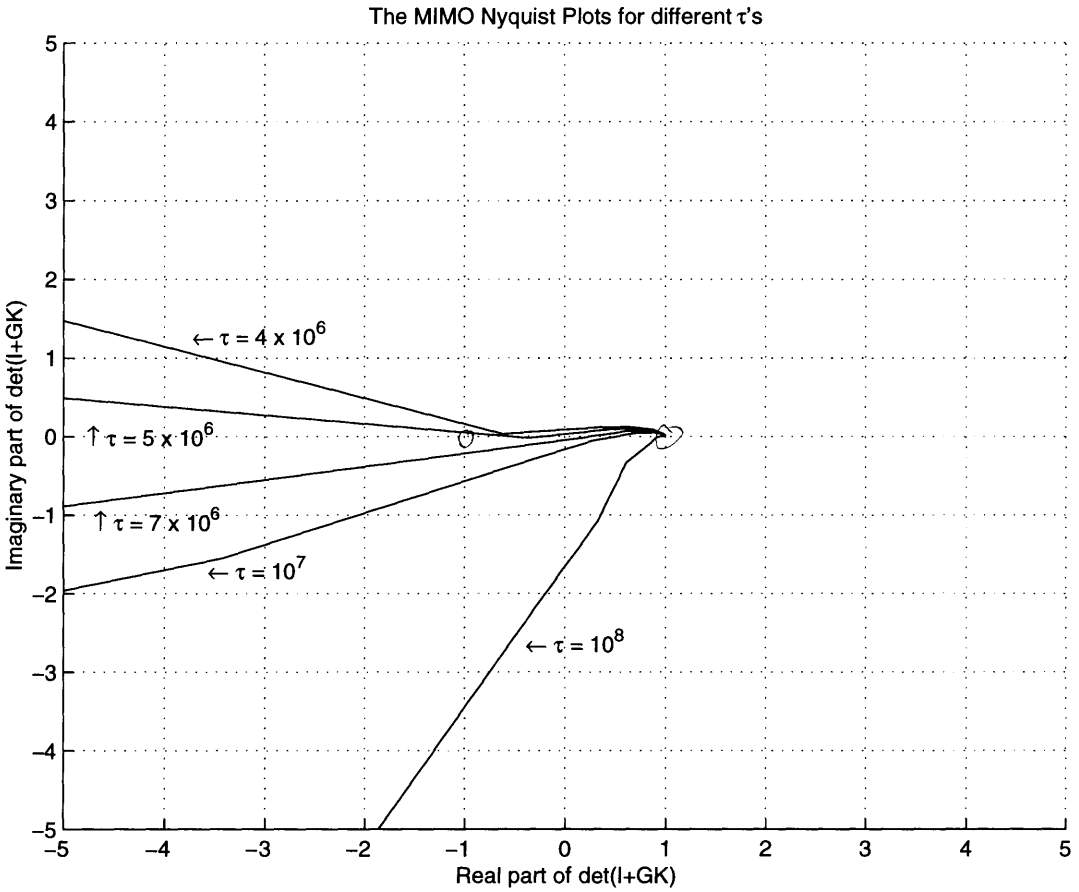

Figure 4.9.3. The MIMO Nyquist plot for the closed loop system for different τ's.

4.10. Verification of the MIMO Nyquist prediction:

Simulations were set up in Simulink to test the predictions obtained from the Nyquist plots. The finite difference state space model of 4.8.5 was used for the simulations. Before the closed loop system is considered, the open loop transient response is studied. Figure 4.10.1., shows the step response of the system. The value of the step-input is the steady-state optimal input derived in section 4.6., and the step input is given at time t=0. The initial condition is assumed to be a zero temperature distribution everywhere. Figure 4.10.1 shows the temperature response at each of the bottom nodes. The figure 4.10.2., compares the final value obtained from the step response with the value of the reference temperature used in section 4.6.

The response in figure 4.10.1., seems to have a non-minimum phase behavior. This is however, not the right conclusion. The dip in the response of some of the temperatures is because the optimal input, which is applied as a step, has negative elements in it.

Figures 4.10.3-4.10.6. show the temperature response for the closed loop system for different τ's. It can be seen that, just as predicted by the MIMO Nyquist criterion, instability occurs just when the value of τ decreases below $7x10^6$.

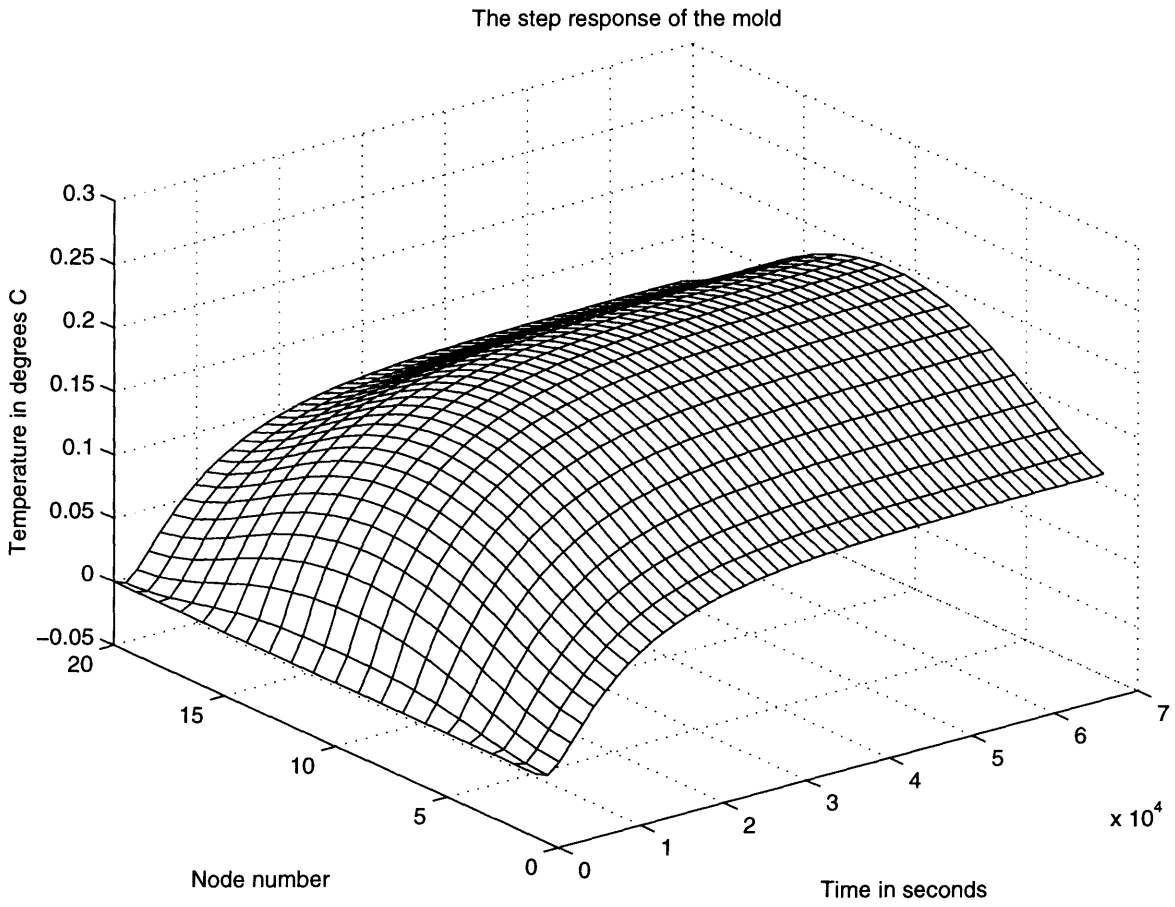

Figure 4.10.1. The step response for the temperature distribution on the bottom surface.

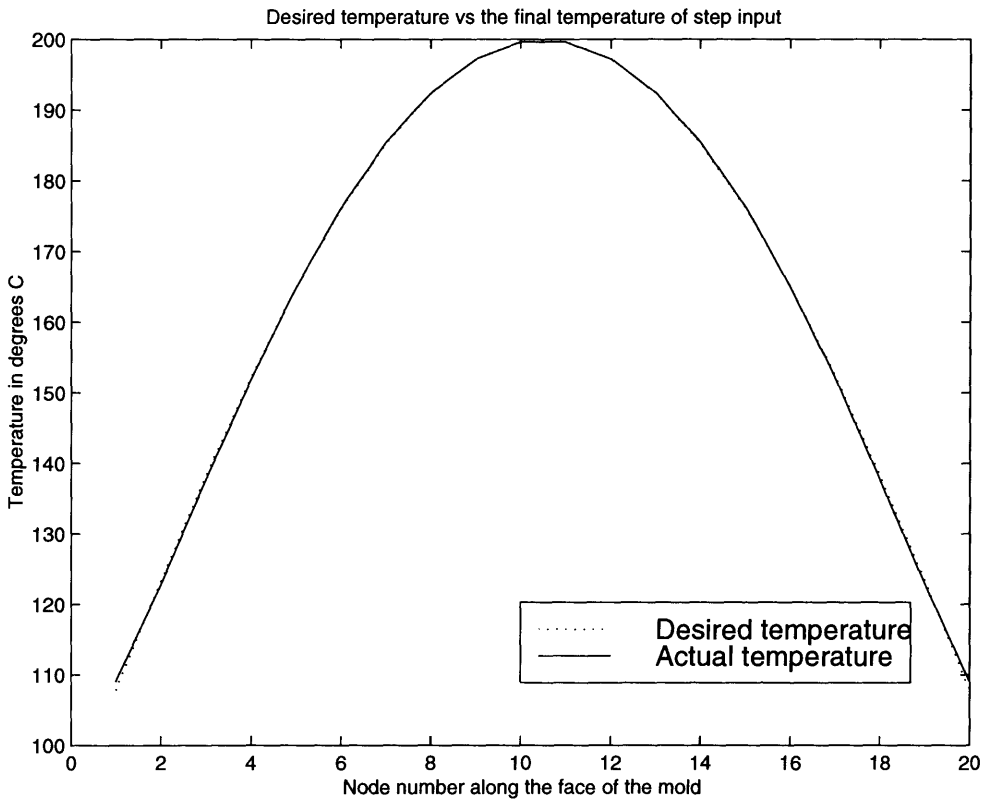

Figure 4.10.2. The value of the final temperature obtained from the step response along with the desired temperature.

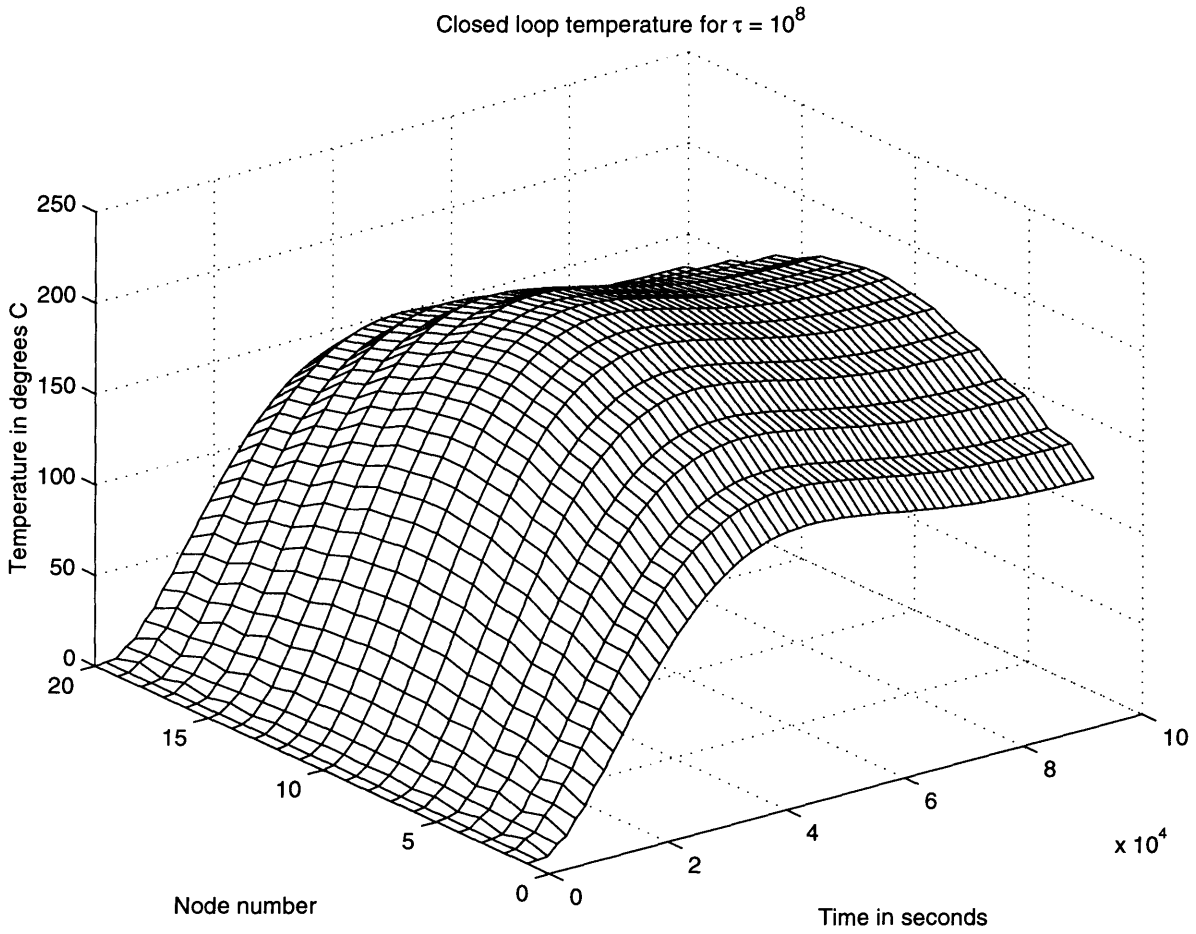

Figure 4.10.3. Closed loop temperature response for $\tau = 10^8$.

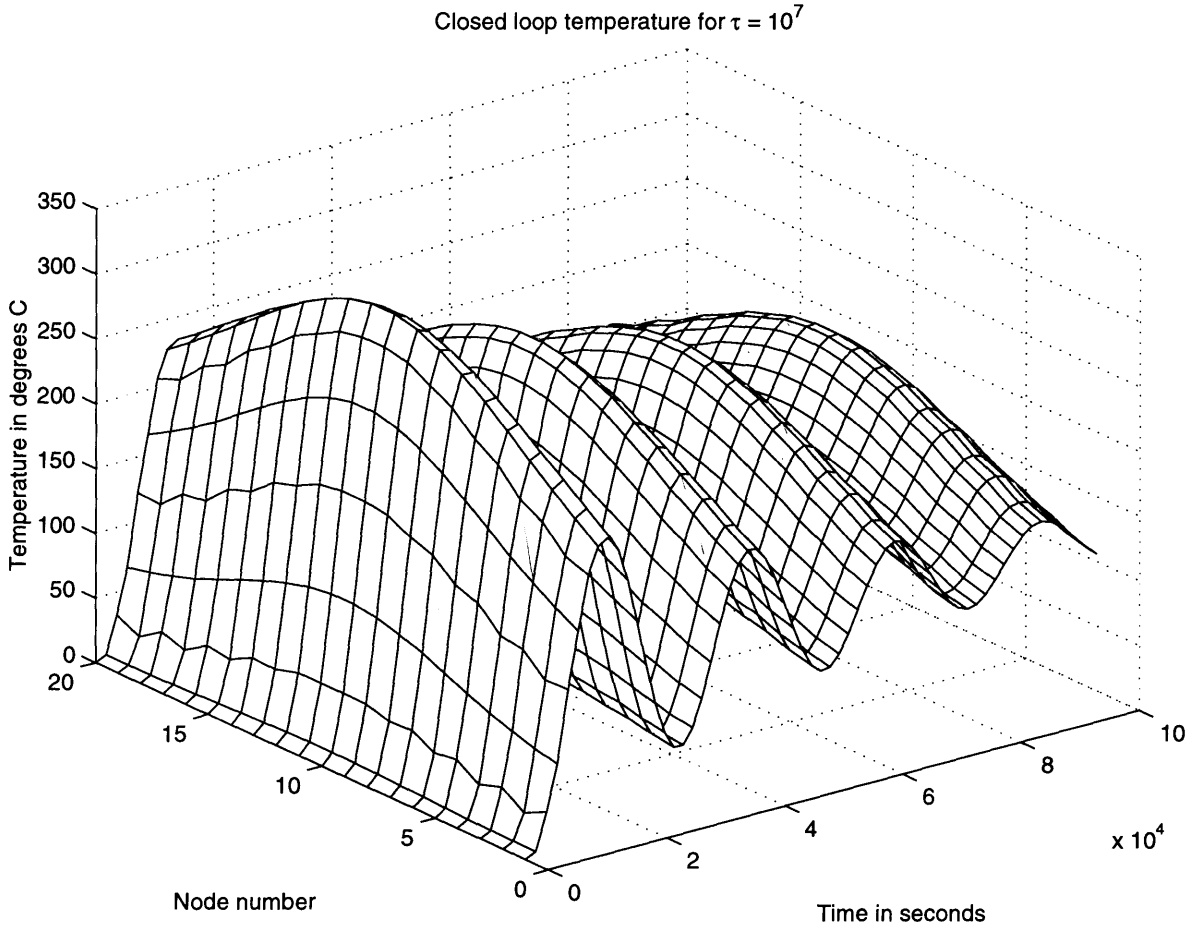

Figure 4.10.4. Closed loop temperature response for $\tau = 10^7$.

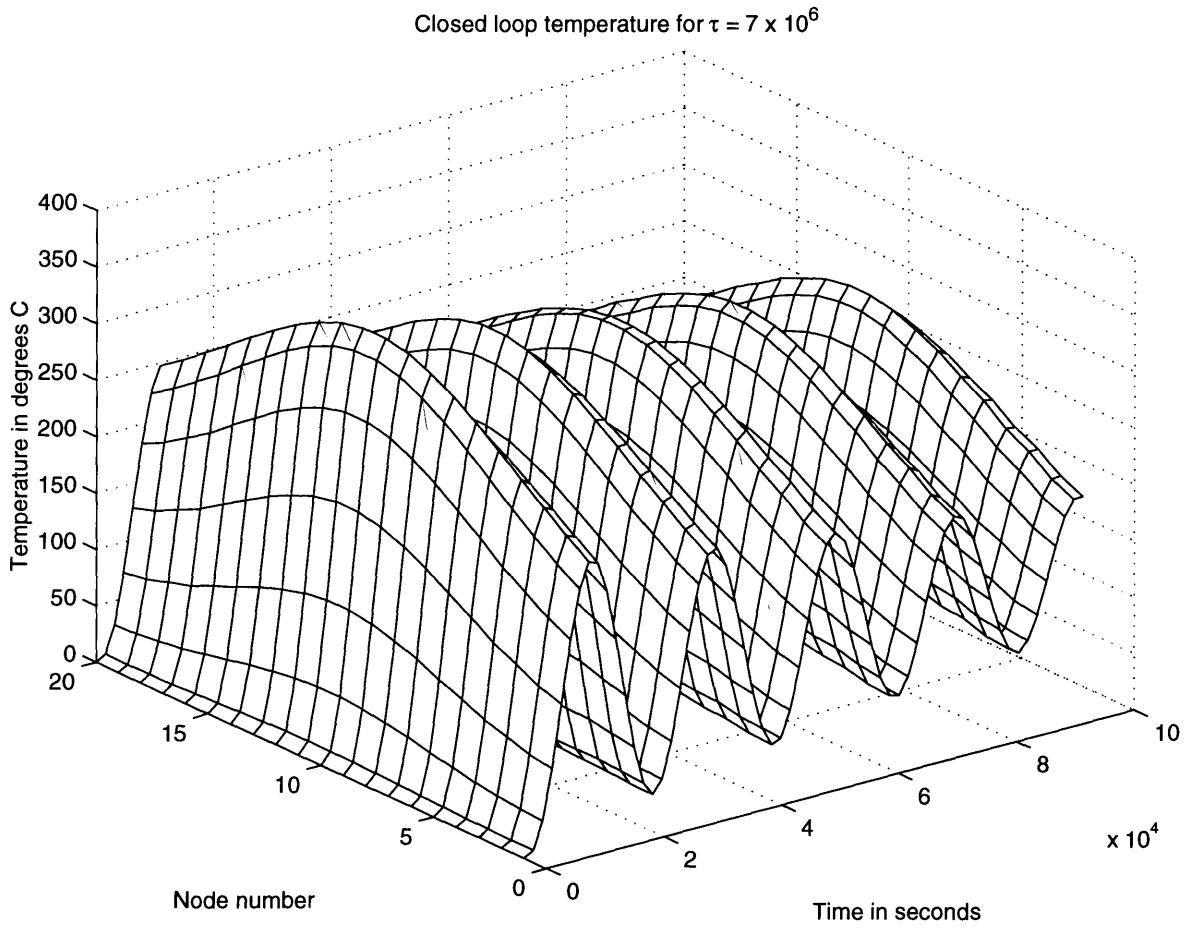

Figure 4.10.5. Closed loop temperature response for $\tau = 7 \times 10^6$.

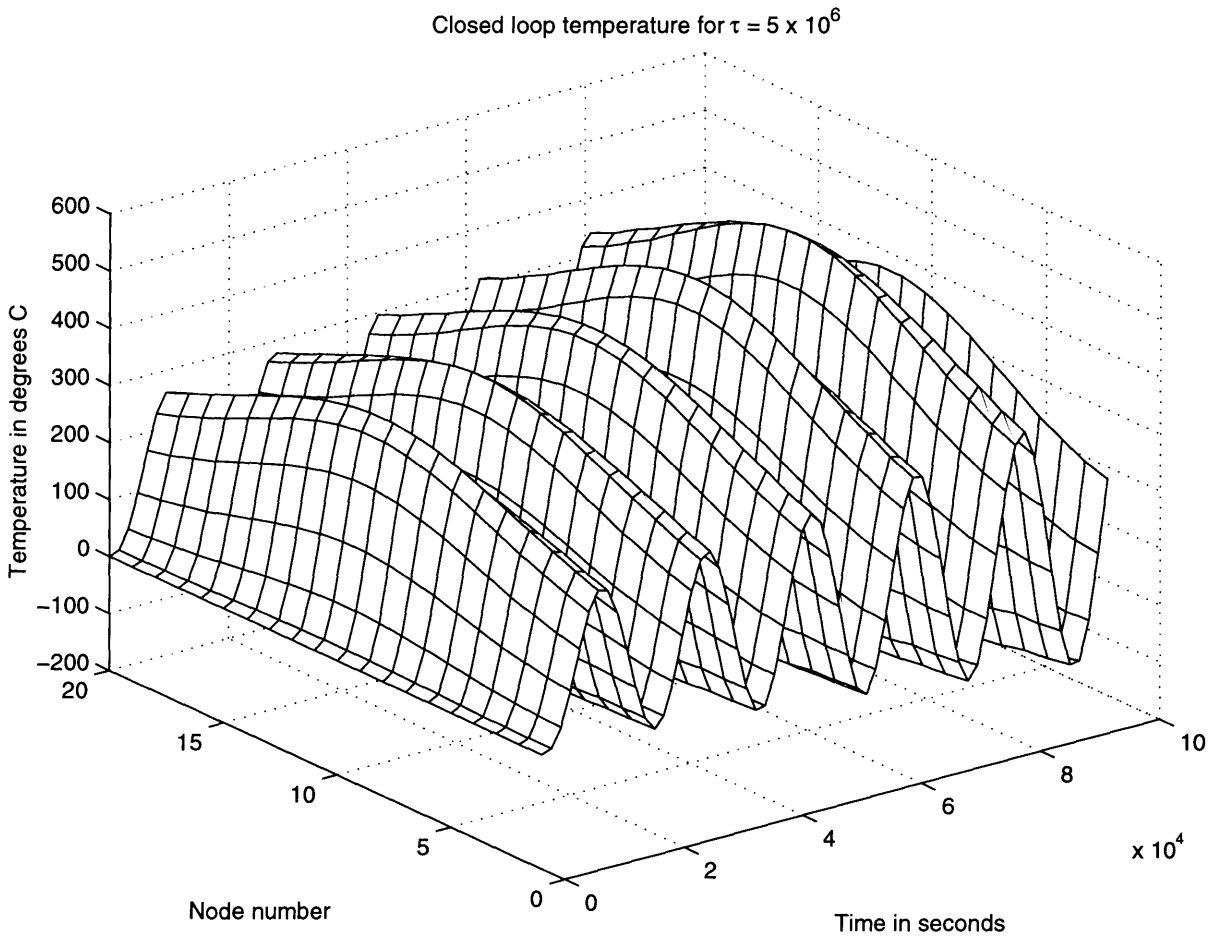

Figure 4.10.6. Closed loop temperature response for $\tau = 5\text{x}10^6$

Comparing figures 4.10.1. and 4.10.4, we can see that the speed of response of the closed loop system is limited by the time constant between the heaters and the sensors. This is the feature of any conduction system where the lag between the heater and sensor determines the speed of the response.

Sometimes, there is a need to improve this response time. The only way of achieving this is by decreasing the distance between the heaters and the sensors. There are two ways of approaching this problem. One involves the addition of heaters, which are much smaller in strength compared to the main heaters, closer to the sensors. In a molding example, this can be achieved by installing ribbon heaters on the surface of the mold.

The second approach is to embed thermocouples closer to the heaters there by decreasing the effective distance between the heaters and sensors. In both the cases, the closed loop system can be properly designed so that in steady sate, the additional heaters and sensors do not play a part. These details are discussed in what follows.

4.11. Improving the response of the system with additional heaters:

The heating developed in the earlier sections is designed for attaining the desired steady-state while keeping the closed loop system stable. If we desire to improve the transient response of the system, smaller heaters could be installed closer to the surface of the mold. This cuts down the physical lag between the heaters and the sensors. In practice, ribbon heaters could be placed on the mold surface. (See Jansen 1993).

The design of the controller is now split up into two parts. The structure of the low frequency part of the design is left the same. The new heaters are installed closer to the surface of the mold and the compensator for actuating these smaller heaters is made so that these heaters are actuated only by high frequency components of the temperature error and have no effect at low frequencies. A cross-over network type design can be used to separate the two parts of the design.

To complete the design, a high frequency gain between the "high frequency" heaters and the sensors needs to be evaluated. Figure 4.11.1. shows a set of 10 high-frequency heaters along with the low-frequency heaters.

A helpful feature of a heat conduction system is that the influence of the heaters at high frequencies tends to be localized. That is, $G(i\omega)$ appears to be more and more sparse at high frequencies. This is a direct result of the fact that the higher frequencies tend to be attenuated to a larger degree when moving away from the heater. Figure 4.11.2. illustrates this fact. Hence, the feedback matrix at high frequencies could be easily designed to be a matrix with zeros everywhere except in the elements corresponding to the nearest nodes on the bottom of the mold. The actual magnitudes of the non-zero elements in the high-frequency feed-back matrix K_{hf} (see equation 4.11.1) will be selected later.

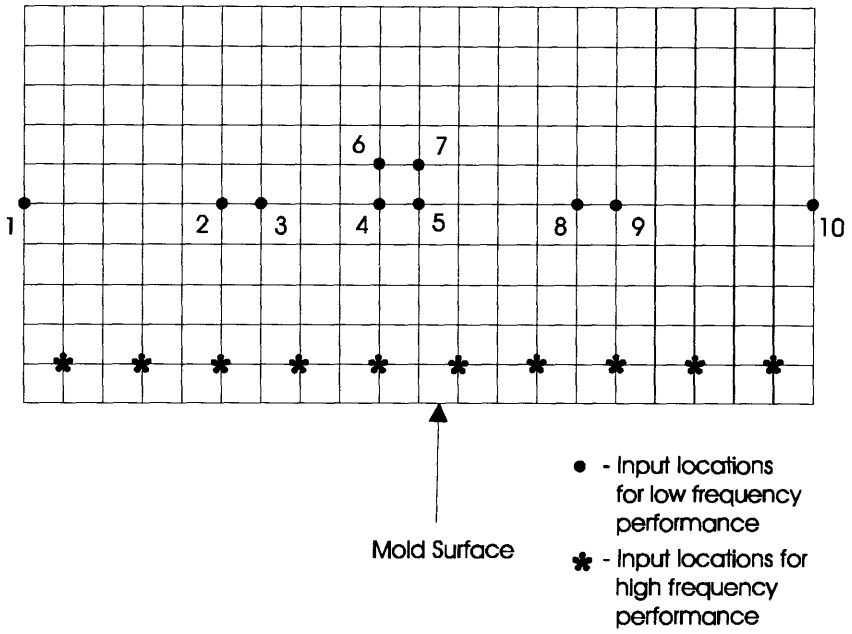

Figure 4.11.1. The high frequency heaters located closer to mold surface.

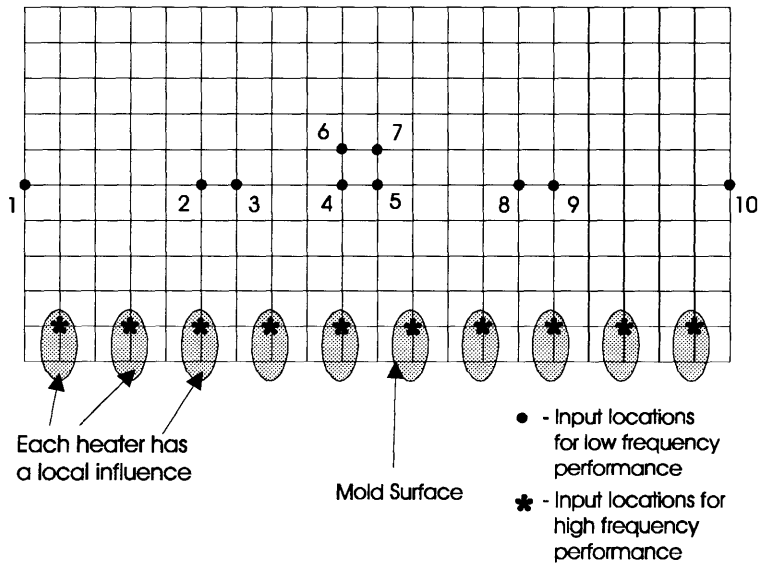

Figure 4.11.2. High frequency heaters have localized action at high frequencies.

Hence a compensator structure is chosen so that the high frequency (K_{hf}) and low frequency gains (K_{eq}) are active in the appropriate frequency ranges. Equation 4.11.1. shows the structure of such a feed-back compensator. Here again τ and τ_1 should be selected to guarantee satisfactory and stable operation of the closed loop system.

$$K(s) = \frac{1}{1+\tau s} K_{eq} + \frac{\tau_1 s}{1+\tau_1 s} K_{hf} \qquad 4.11.1$$

The two frequency blending functions are:

$$\begin{aligned} &\frac{1}{1+\tau s} \ : \textit{For the low frequencies} \\ &\frac{\tau_1 s}{1+\tau_1 s} \ : \textit{For the high frequencies} \end{aligned} \qquad 4.11.2$$

τ_1 *and* τ should be appropriately selected to guarantee stability.

A new simulation is now set up as shown in figure 4.11.3. We now have three design parameters that we need to evaluate: K_{hf} , τ_1 *and* τ . This is more complicated than the simple design procedure with only the low-frequency heaters. Figure 4.11.4. shows the closed loop performance of this system.

Several values of K_{hf} , τ_1 *and* τ have been tried. Figure 4.11.4. shows the Nyquist plot for one specific set of values. It can be seen that this gives stable operation

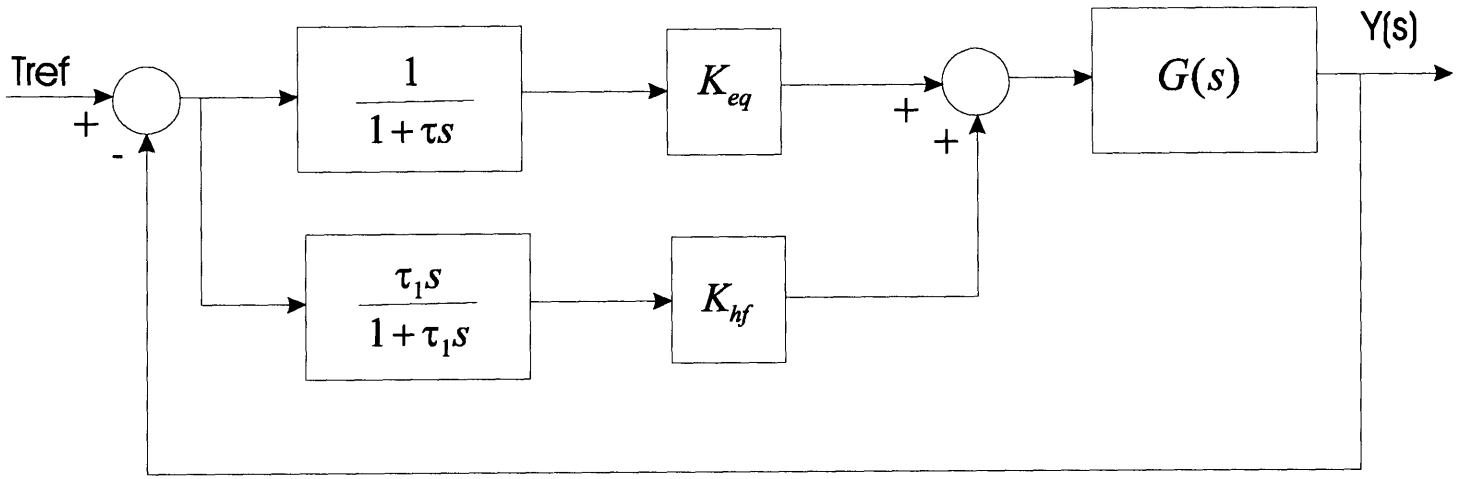

Figure 4.11.3. Closed loop system with both high frequency and low frequency heaters present.

Figure 4.11.5. shows the response of the closed loop system at one particular node on the bottom of the mold, for values of $\tau = 5x10^6$ and $\tau_1 = 10^3$ and different values for the magnitude of the non-zero entries in K_{hf}. It can be seen that increasing the value of the K_{hf} improves the response of the system. However, this comes at the cost of having to use larger ribbon heaters, which are expensive. An engineering judgment should be made to decide on the size of the ribbon heaters needed.

4.12. Conclusions:

This chapter has presented a design technique for designing heating and cooling in molding applications. The steps involved in this design are as follows:

1. The steady state heat equation and a corresponding quadratic cost functional which weighs the amount of heating/cooling used (in steady-state) with the temperature error (in steady-state) are formulated.
2. The input is restricted to only those locations where heating/cooling can be applied. This is achieved by selecting weights in the quadratic cost functional.
3. The optimization is performed and a proportional feed-back form for the steady-state input is obtained, in terms of the temperature error.
4. The effects of several steady-state disturbances and model errors are studied using the formulation developed and the cost function is adjusted to obtain a satisfactory temperature error in the presence of these model errors and disturbances.
5. By observing the results steps 1-4, input is further restricted to fewer locations by modifying the weighting matrices and the steps 1-4 are performed again.
6. This results in identifying the amount of heat needed in steady state at the various locations and the structure of the compensator at zero frequency.

7. The transient heat conduction is now introduced and the transfer-function matrices are evaluated.
8. A first order roll off is applied to the steady-state proportional gain obtained in step 4.
9. Multi-input multi-output (MIMO) Nyquist criterion is used to evaluate the break frequency for the first order roll off.
10. Additional smaller heaters are then incorporated into the design and a frequency cross-over scheme is used to ensure that the smaller heaters are active only at high frequencies. The break frequency for the smaller heaters along with the high-frequency proportional gain are used as additional design parameters.

The above approach has been presented for a molding application. However such a design technique can be effectively used for other steady-state temperature control applications.

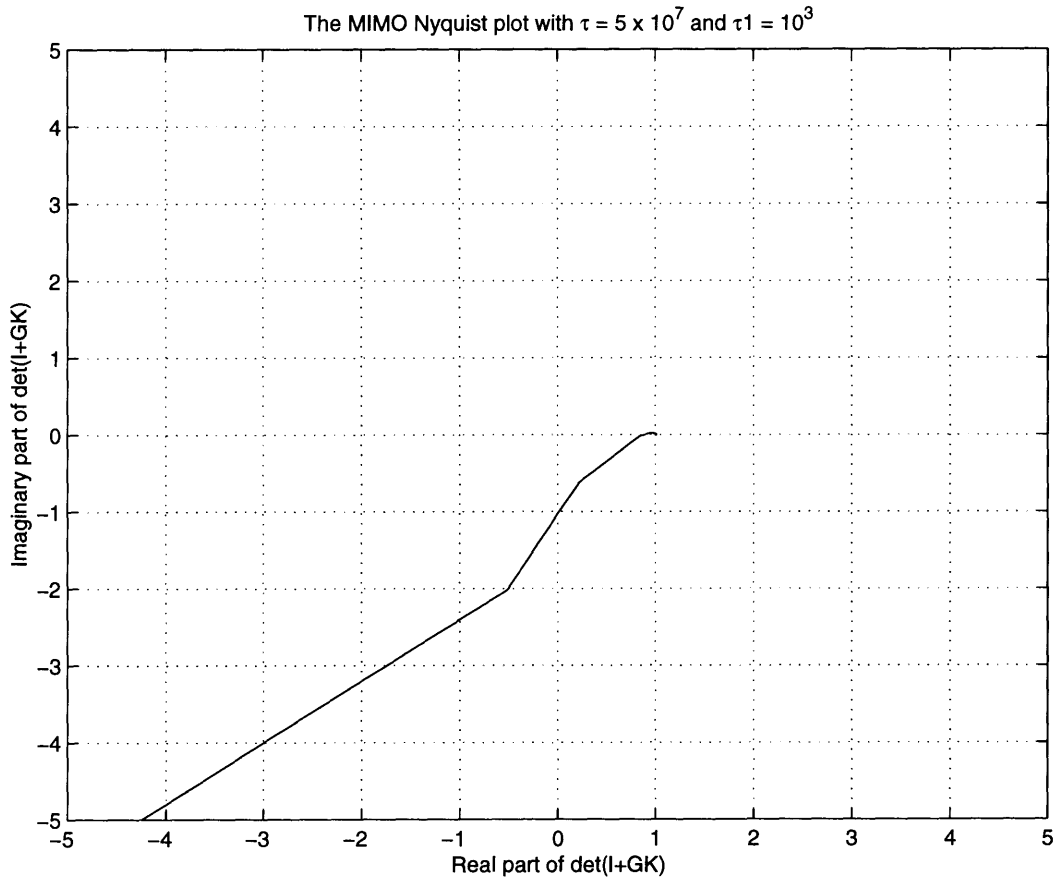

Figure 4.11.4. The Nyquist plot for the case with both high frequency and low frequency heaters.

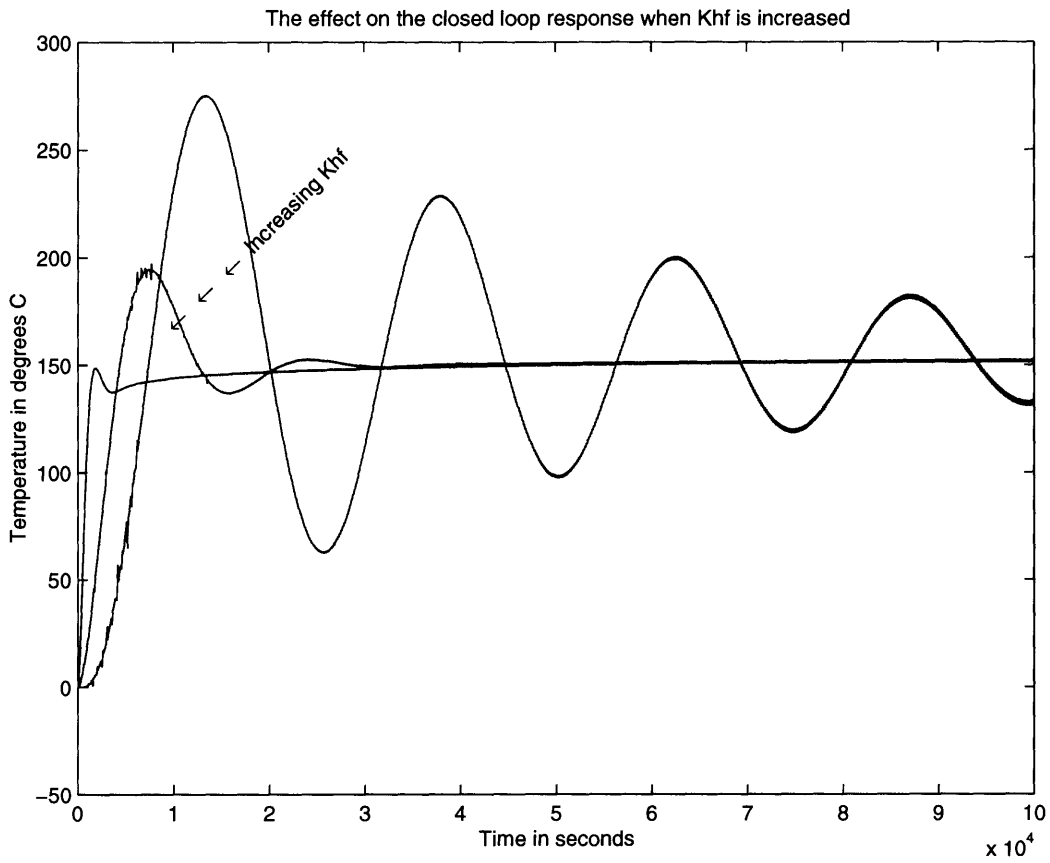

Figure 4.11.5. The response of the closed loop system for different values of K_{hf}, when both high frequency and low frequency are heaters present

Chapter 5

OPTIMAL CONTROL OF TRANSIENT TEMPERATURES: EXAMPLE

5.1. Introduction

The examples studied in the previous chapters involved applications that could be addressed as a steady state temperature distribution control problem. There are applications where this simplification is not possible. These are problems in which the temperature transient of the entire object is to be controlled and no steady temperature distribution needs to be controlled. The examples of these types of processes can be seen in heat treatment operations.

In heat treatment operations, temperature transients determine the material properties of the object being manufactured. In the steel industry, several products such as steel strips, slabs etc. are manufactured for different applications where, each application stipulates the material properties and strength properties for the steel. The different alloying elements added and the nature of heat treatment rendered influences these properties.

The example presented here is one of heat treating a steel slab that is manufactured by hot rolling of a larger billet. Hot rolling is one of the primary manufacturing processes used in the steel industry producing products ranging from strips of steel to I-beams to plates and slabs used in a wide variety of applications. In most of these applications maintaining uniform and consistent material properties of the steel is extremely important. The material properties determine the mechanical properties of the rolled steel

like strength, hardness, weldability, formability etc. These properties critically depend on the temperature history of the finished product. Hence, it is imperative that one control the temperature history of the slab in order to achieve uniform and consistent material properties. This should be done not only across each slab or strip but also from run to run.

It is typical to have many process disturbances such as: varying initial temperatures of slabs coming out of the furnace, variation in the temperature of the cooling water with the time of the day and with the season. These disturbances vary with both space and time. Hence a distributed parameter systems approach, such as the approach in this thesis is a natural one resulting in a superior control algorithm. This chapter presents an application of a distributed parameter optimal tracker to the manufacture of plates used for making bridges, ships, pressure vessels etc. It should be noted that the techniques discussed in this chapter are applicable to several other processes such as: hot-strip rolling and continuous casting, involving the control of temperature transients.

Figure 5.1.1. shows a schematic of a typical slab mill. The billets (thick slabs) are brought in to the mill from the continuous casting unit. The production process starts with the steel billets (slabs) being heated in the furnace. The billets are then reheated to above the recrystalization temperature and passed through a rough rolling step where the thickness is reduced. An intermediate cooling is then applied to the hot slab by spraying cool water on the slab. The temperature at the end of the intermediate cooling is brought close to the recrystalization temperature and a finish rolling operation is performed where

the size of the slab is brought down to the desired thickness. A second cooling unit is then used to cool the slab down through a desired temperature trajectory. It should be noted here that the water jets and sprays in the two cooling units are present both above and below the slabs. (The schematic only shows sprays above the slab). The term Accelerated Cooling is used to describe the two cooling units described above. Accelerated Cooling is typically employed in the cooling of the hot rolled slabs ranging form 1/4" to 4" in thickness.

There are several benefits to using accelerated cooling units. The cooling in between the two stages, which is the first cooling unit, serves to reduce the cycle time thereby increasing the productivity. Since the temperature during the first stage of cooling is still above the recrystallization temperature, the material properties of the finished product are not dependent on the nature of cooling at this stage. However, care has to be taken to not impart excessive thermal stresses to the slab so that distortions are prevented. At the end of the first stage of cooling, the temperature of the slab is still above the recrystallization temperature. However, one needs to ensure a uniform temperature across the slab, in order to achieve uniform properties during the finish rolling. The uniformity of temperature is important also to ensure the uniformity of cooling at the second stage of cooling. This will be explained in detail in the section dealing with the description of the cooling process.

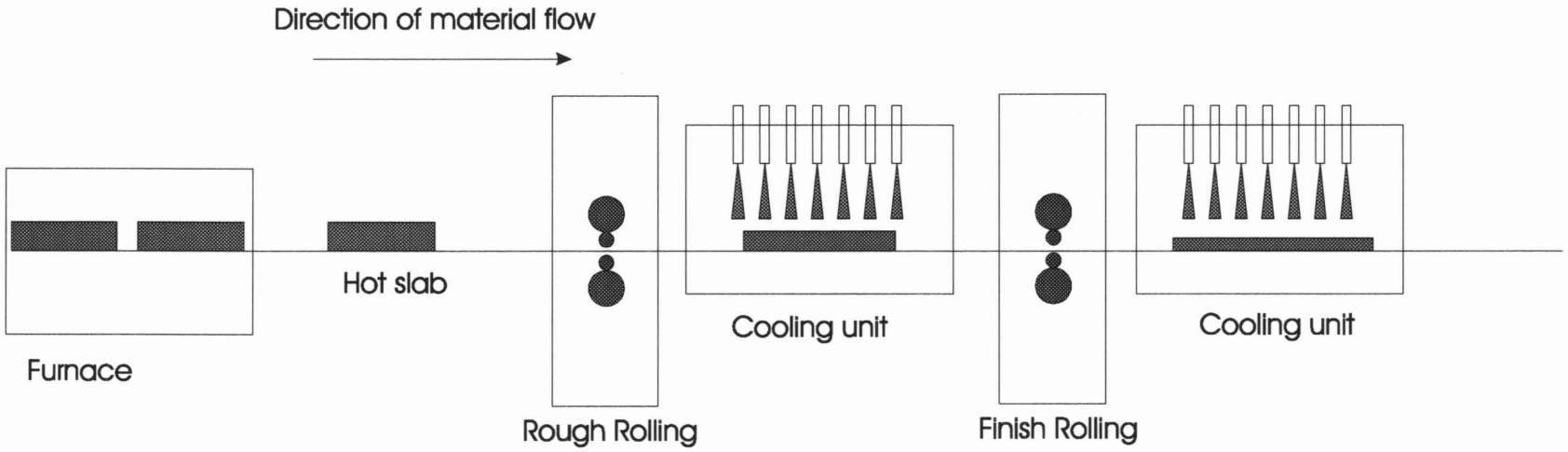

Figure 5.1.1. Schematic of a slab mill.

The cooling after finish rolling is used to impart the desired material properties. This step is the primary driving factor for implementing accelerated cooling in slab mills. There are considerable savings in alloying costs, in using accelerated cooling here. This cost saving is obtained by using the cooling system to heat treat the steel in order to impart the same desired mechanical properties that one would obtain by alloying. An added benefit is that the productivity increases due to decreased cooling time.

In order to maintain the uniformity of cooling rates on the upper and lower sides of the slab, several sprays are used on either side of the slab. The water sprayed at the center of the slab has to flow over the edges of the slab. This causes a higher cooling rate for the edges compared to the center of the slab. This can be avoided if the sprays are designed so that the heat fluxes are more evenly distributed. Some times, induction heaters are installed after the cooling unit is designed, to compensate for this effect. Figure 5.1.2. shows a typical cross section of a cooling unit.

5.2. Requirements on this process:

The accelerated cooling problem considered here has several requirements. Firstly, the EPA regulates the total amount of water consumed by the plant. Hence, the amount of water consumed by the plant should be minimized. This will help in reducing the total water consumption of the whole steel plant. Additionally, the water saved by effective control can be used elsewhere in the steel plant. Not having excessive cooling where it is not needed, can eliminate the use of induction heaters. This will have the benefit of reduced hardware as well as energy costs.

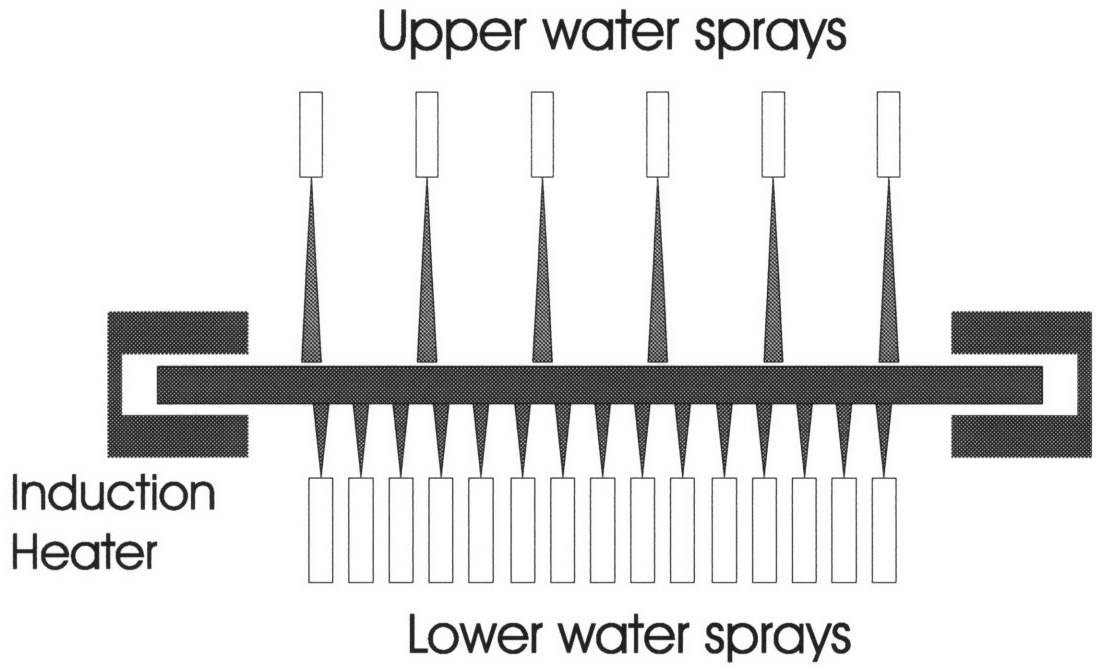

Figure 5.1.2. Cross Section of the accelerated cooling unit.

Secondly, the cooling rates should be very accurately controlled. The material properties and the mechanical properties depend very critically on the cooling trajectory. Any variations in the temperatures from run to run and from point to point in the object being heat-treated results in non-uniform properties. These are not desirable for the consumers of the steel, such as, the automobile and construction companies. Changes in material properties change the formability, mechanical strength and weldability etc. of the steel being produced. At the same time, excessive and non-uniform cooling rates may cause residual stresses which may warp the slab or have a negative effect on the quality of the surface of the steel produced. Thirdly, the terminal temperature of the process should be accurately controlled. This again has direct bearing on the material properties of the steel.

To address these issues a suitable controls approach along with a suitable model should be selected. As has been the approach throughout this thesis, we will address this problem as an optimal control problem.

5.3. Sources of disturbances:

There are several sources of disturbances on the process:

1. The heating in the furnace could be uneven, this causes a build up of thermal gradients in the slab prior to cooling.
2. When the slab is brought out of the furnace, it is guided to the rolling mill on skids which are cooler and this produces cold spots on the slab. (See figure 5.3.1.)

3. Cooling water temperature could change effecting the HTC. (See. Wolf et. al. (1993))
4. Surface distortions before cooling can cause puddling of water during cooling and can cause variation in the amount of cooling
5. During cooling, a few nozzles could develop lower flow-rates, thereby altering the cooling heat flux , locally.
6. There can be measurement errors due to the emmissivity changes.

5.4. Anomalous nature of the cooling water jets:

The disturbances in temperature discussed in the previous section pose a severe problem, because the cooling is performed using water jets. The heat fluxes that the jets can extract from the hot slab has an inverse relationship with the surface temperature of the slab. This means that if we start with a cold spot on the surface of the slab, that location experiences a higher heat flux and becomes even colder (see figure 5.4.1.). Thus there is a compounding of the temperature difference between the different parts of the slab. This results in a greater variation in properties of the steel within each specimen.

The reason for the inverse relationship for the heat fluxes with the slab temperature can be explained by the film boiling phenomenon. When a cooling jet is sprayed on to a hot slab, there are different regimes of boiling that result. There is a central region where there is no boiling taking place. This is immediately followed by a region where there is nucleate boiling taking place. See figure 5.4.2., which shows the different regimes of boiling heat transfer. (Also see Southwick (1986)).

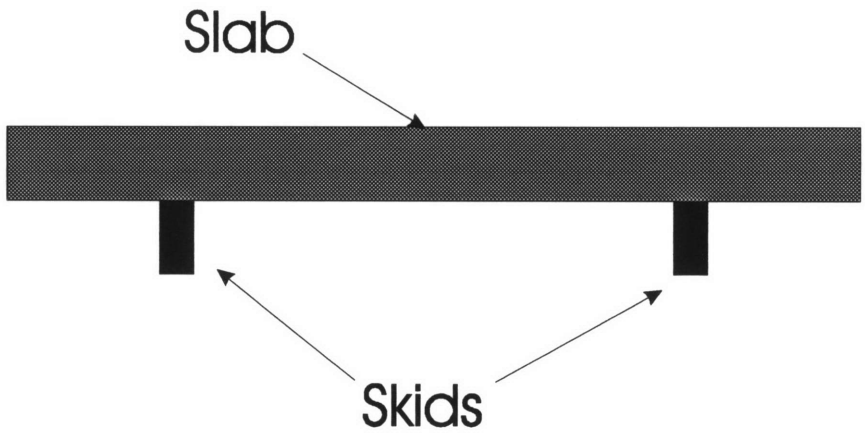

Figure 5.3.1. The slab is brought out on skids which can cause cold spots.

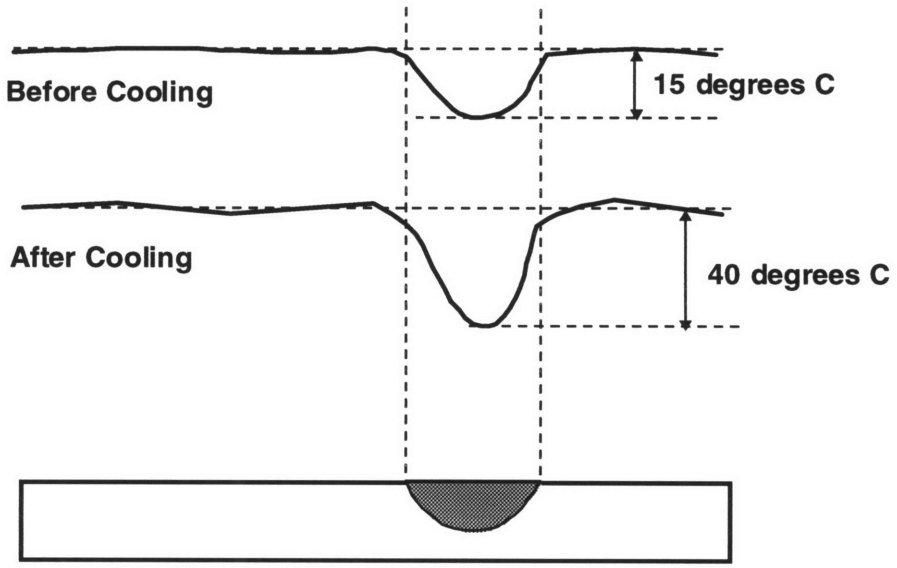

Figure 5.4.1. Amplification of the temperature difference when cold spots are present.

These two regions are characterized by a high values of heat fluxes. Immediately after the nucleate boiling regime there is a brief period of transition boiling followed by a fully developed film. The region of film boiling is characterized by lower heat fluxes. (See Incropera and DeWitt (1985) & Wolf et. al. (1993)).

The effective average heat flux extracted this jet can then be computed by by taking a weighted average over the area of the slab. Figure 5.4.3. shows the top view of the jet impinging on the hot slab. The three concentric circles show the different regions of boiling heat transfer. The heat-transfer in region 3 is considerably less efficient when compared to regions 1 and 2.

When the slab becomes hotter, the region 3 moves inward. This causes the effective heat flux to diminish, due to the reduced area of more efficient heat transfer (see figure 5.4.4). Alternatively, let us consider two situations, in which the temperature is the same but the jet velocities are different. The case with a higher jet velocity, has the effect of pushing the region 3 farther out. This increases the area of more effective heat transfer. Thus increased jet velocity has the effect of increased average heat flux. (see figure 5.4.5.)

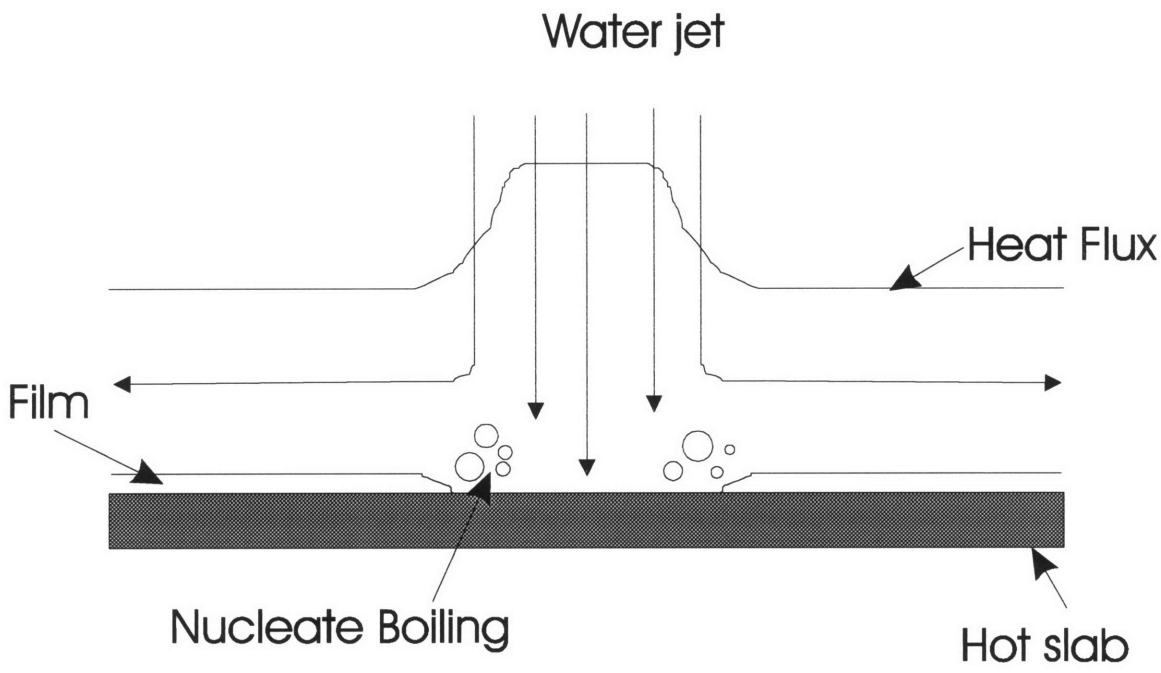

Figure 5.4.2. The different regimes of boiling heat transfer in a cooling jet.

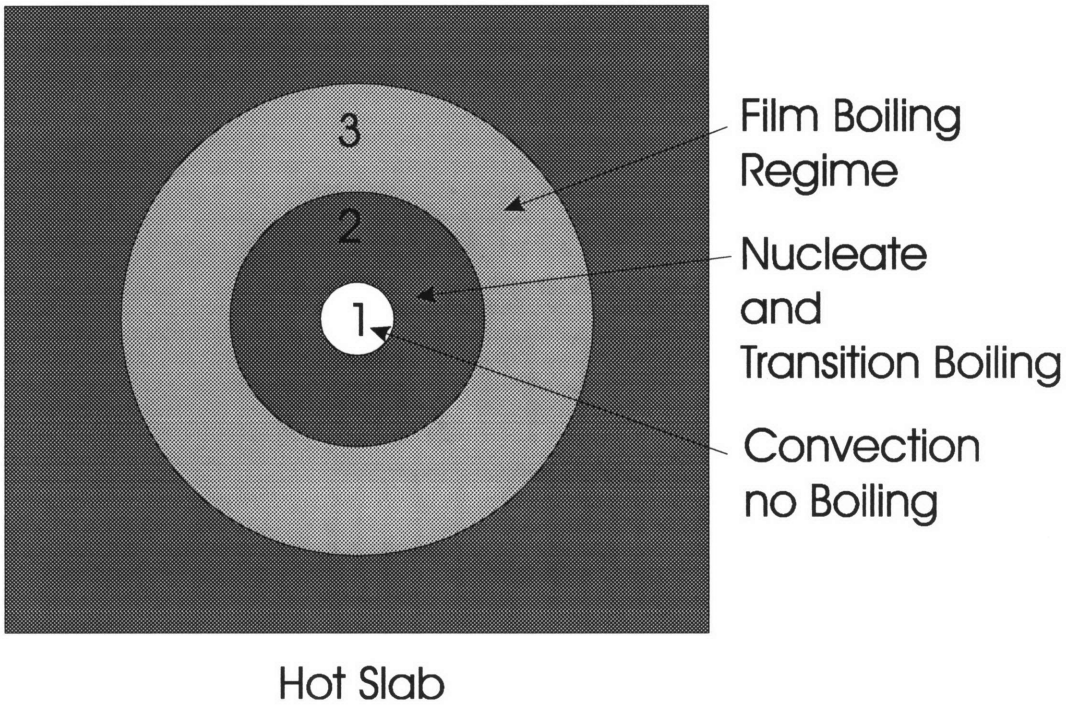

Figure 5.4.3. Top view of the jet with different boiling regimes.

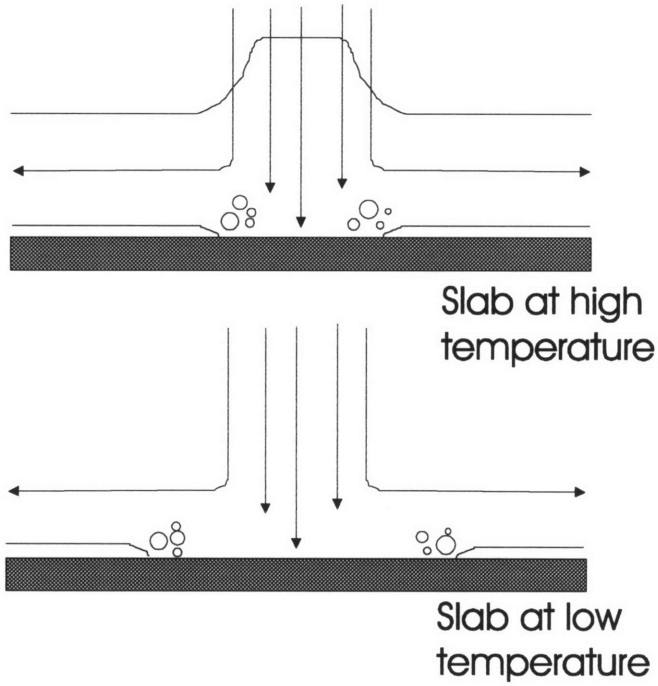

Figure 5.4.4. Film boiling regime moves inwards when temperature is higher.

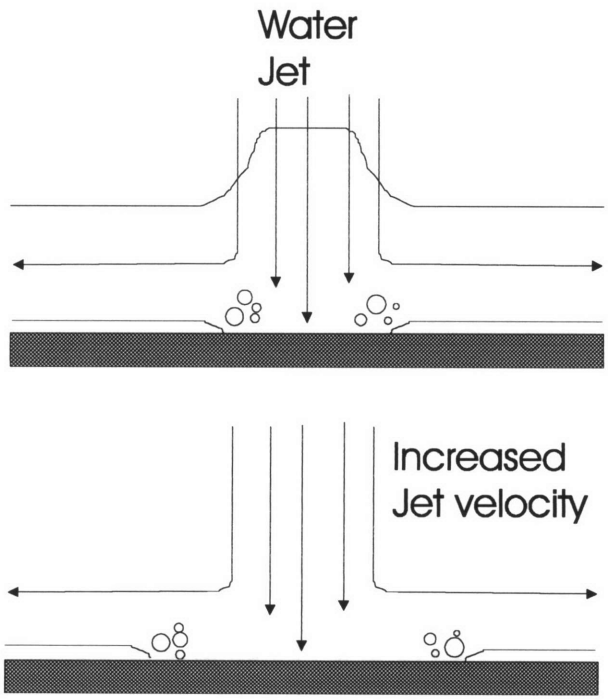

Figure 5.4.5. Film boiling region moves outward when jet velocity is increased.

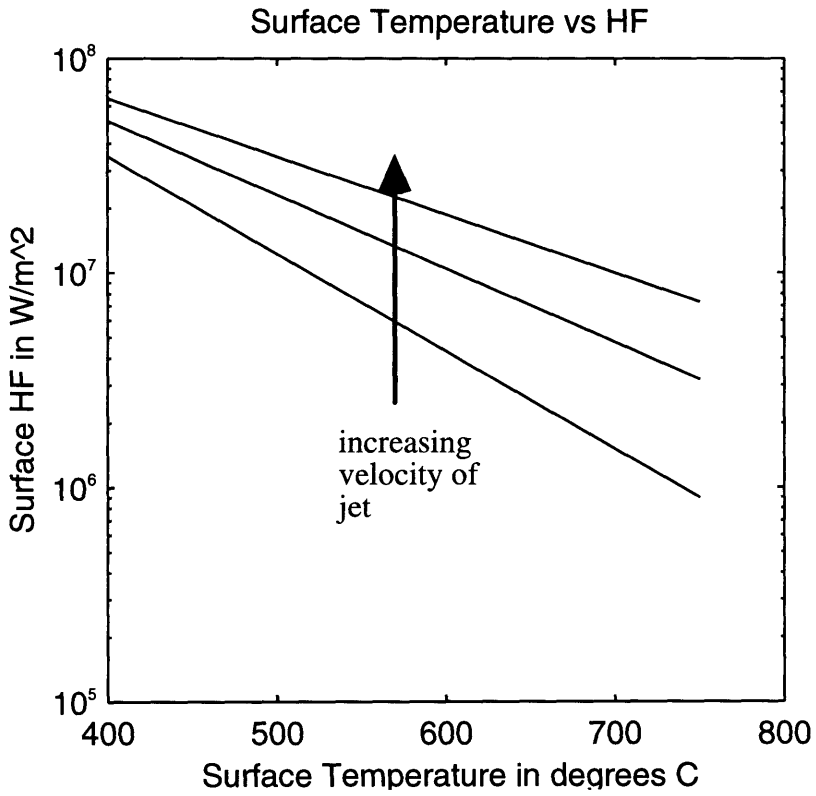

Figure 5.4.6. The relationship between the surface temperature,jet velocity and the surface heat flux.

Figures 5.4.4. and 5.4.5. illustrate this effect of the changes in the film initiation location.

Figure 5.4.6. shows a plot of the Jet velocity vs. Surface Heat Flux and Surface Temperature vs. Surface Heat Flux.

5.5. Model for process:

The temperatures inside the slab are governed by the heat conduction equation:

$$\begin{aligned}
&\rho C_p \frac{\partial}{\partial t} T(x,y,z,t) = \nabla(k(\bar{x})\nabla)\, T(x,y,z,t) + q(x,y,z,t); \\
&\qquad (x,y,z) \in D; \quad D\text{:}\{the\ domain\} \\
&\mathrm{B}_o T(x,y,z,t) = q_b(x,y,z,t); \ \ (x,y,z) \in \partial D; \ \{boundary\} \\
&T(x,y,z,0) = T_o(x,y,z);. \\
&q(x,y,z,t)\ is\ the\ heat\ input\ within\ the\ domain. \\
&q_b(x,y,z,t)\ is\ the\ heat\ input\ on\ the\ boundary.
\end{aligned} \qquad 5.5.1.$$

Where the material properties listed in Equation 5.5.1. can have a temperature dependence:

$$\begin{aligned}
&\rho \ : is\ the\ density \\
&C_p : is\ the\ specific\ heat \\
&k(\bar{x}) : is\ the\ conductivity\ of\ the\ material
\end{aligned} \qquad 5.5.2.$$

And the other entries in Equation 5.5.1. are

$$\begin{aligned}
&\nabla = \frac{\partial}{\partial x} + \frac{\partial}{\partial y} + \frac{\partial}{\partial z} \\
&Bo\text{: } Boundary\ conditions \\
&T(\bar{x},t) : temperature\ distribution
\end{aligned} \qquad 5.5.3$$

In the simulations presented here, the slab is modeled as a two dimensional rectangular object, so the above equation only has x and y as the space variables. This simplification of the problem into only a two dimensional problem is only for the ease of performing

simulations. The general technique presented here can just as easily be applied to a three dimensional case.

5.5.1. Finite difference based model for the heat conduction in the slab:

The heat conduction equation (Equation 5.5.1.) should be approximated with a set of ordinary differential equations, which may then be used for control purposes. There are many ways of achieving this transformation including using truncated Eigen function expansions, finite difference models and finite element models. In this case, a finite difference scheme is used to model the transient temperature variations. The discretization is performed only with respect to the space variables, leaving the time as a continuous variable. This type of an approach is used to generate differential equations which could be used for controller design. This section details the development of such a model.

In the present case the slab is rectangular in shape and the inputs occur on the upper and the lower surfaces of the slab. The discretization is performed along the length and across the thickness as shown. The inputs are assumed to be present at each of the boundary nodes on the top and the bottom. The sides are assumed to be insulated by assuming negligible heat transfer due to free convection on the boundary. Figure 5.5.1. shows the schematic of the finite difference scheme.

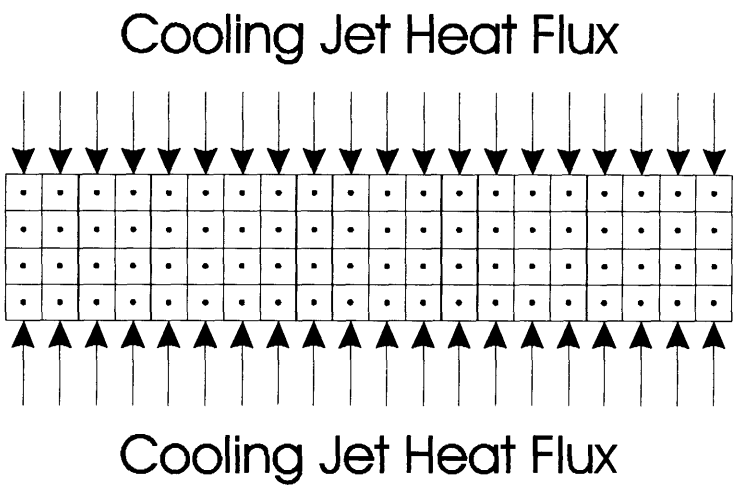

Figure 5.5.1. Finite Difference Scheme for Accelerated Cooling Simulation.

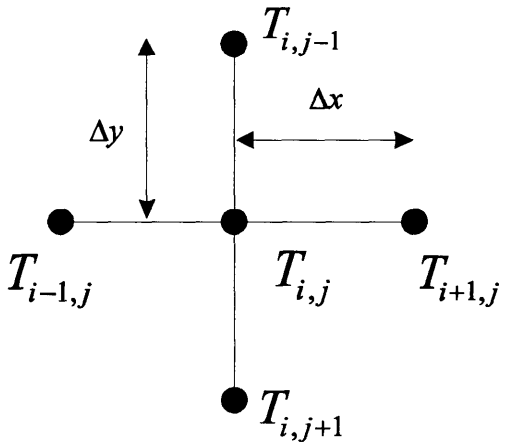

Figure 5.5.2. Notation for the nodes in a finite difference scheme.

To derive the finite difference based model, we need to perform an energy balance between adjacent nodes. Figure 5.5.2. shows the notation used for different nodes. Δx *and* Δy are the distances between the nodes along the x and y axis respectively. Writing the energy balance for each node gives the following equation for the temperature at the node *i,j*:

$$\rho C_p \frac{dT_{i,j}}{dt} = k\left\{\frac{1}{(\Delta x)^2}\left[T_{i+1,j} + T_{i-1,j} - 2T_{i,j}\right]\right\} + k\left\{\frac{1}{(\Delta y)^2}\left[T_{i,j+1} + T_{i,j-1} - 2T_{i,j}\right]\right\} + q_{i,j} \qquad 5.5.4.$$

The left hand side of equation 5.5.4. is the rate of change of heat content at node *i,j* and this equals the rate of heat flow from each of the neighboring nodes plus the rate of heat generation at node *i,j*.

The equation 5.5.4., can be written for each of the nodes. The nodes at the top and bottom of the slab have a cooling heat flux term. The rest of the nodes do not have the heat input term because there is no heat source or sink present there. By suitably numbering the nodes and stacking the equations up we arrive at a set of coupled differential equations which form the state-space model shown below.

$$\begin{aligned} &\dot{\mathbf{X}} = \mathbf{AX} + \mathbf{BU}; \\ &\mathbf{X} = [T_1, T_2, \cdots, T_{mn}]^T; \\ &\mathbf{U} = [q_1, q_2, \cdots q_{2n}]^T; \\ &m : number of nodes along thickness \\ &n : number of nodes along width \end{aligned} \qquad 5.5.5.$$

5.6. Control Approach:

In the section 5.4. we have seen the anomalous nature of cooling with water jets. Compensating for the variations in the initial conditions is extremely important. By far the largest source of product property variation results due to the variation in the initial conditions. An effective way of approaching this problem is to estimate the heat-fluxes that need to be extracted at different locations at different times. Knowing the jet characteristics, we can then calculate the jet velocities that are needed to achieve the desired heat fluxes.

5.6.1. Process requirements

There are competing process performance requirements and these are listed below:

1. EPA regulates the amount of water that could be consumed while cooling. Hence, conserving "control energy" will result in savings in the cooling water. Therefore the control scheme used should try to conserve the amount of "control energy" used.
2. Cooling rates determine the grain structure and certain other material properties. Hence, deviations from the desired cooling rates should be penalized by the control algorithm.
3. The terminal temperature is important, as this determines, what phases exist in the steel at the end of the cooling.

5.6.2. Optimal closed loop solution:

We should construct a cost functional that incorporates the above process requirements into it. This cost functional can be used for deriving an optimal control solution to the problem. A quadratic cost functional shown in equation 5.6.1. is used for this

application. The first term on the right hand side corresponds to the weighting of the final temperature attained, on the cost function *J*. This weight can be increased or decreased by increasing or decreasing the elements of the matrix **P**. The second term in *J* is the weighting on the temperature profile during cooling which can be modulated by varying **Q**. The last term of *J* is the weight on the input which can be modulated by changing **R**.

$$J(\mathbf{U}) = \left(\mathbf{X}(T_f) - \mathbf{X}_D(T_f)\right)^T \mathbf{P}\left(\mathbf{X}(T_f) - \mathbf{X}_D(T_f)\right) + \int_0^{T_f} \left\{\left(\mathbf{X}(t) - \mathbf{X}_D(t)\right)^T \mathbf{Q}\left(\mathbf{X}(t) - \mathbf{X}_D(t)\right) + \mathbf{U}^T \mathbf{R}\mathbf{U}\right\} dt \qquad 5.6.1.$$

Where:

t : *time during cooling*
T_f : *The final time at the end of cooling*
$\mathbf{X}(t)$: *Vector of temperatures at all nodes*
$\mathbf{X}_D(t)$: *Vector of desired temperature trajectories*
$\mathbf{U}(t)$: *input vector*
$\mathbf{P} \geq 0; \mathbf{Q} \geq 0; \mathbf{R} > 0$; *weighting matrices*

The optimal control problem is then to evaluate the optimal input **U**(t) that minimizes the cost-functional in 5.6.1. for the system with the state space description shown in equation 5.5.5. with a specific initial temperature distribution. The initial condition varies due to process variations.

$$\dot{\mathbf{X}} = \mathbf{A}\mathbf{X} + \mathbf{B}\mathbf{U}; \qquad \mathbf{X(0)} = \mathbf{X_0} \text{ : } \textit{The measured initial temperature} \qquad 5.6.2.$$

The above problem is the classical finite horizon linear quadratic optimal tracking problem. By suitably choosing the matrices **P, Q** and **R** one could weigh the different control objectives suitably. One of the advantages of posing the problem this way is that we obtain a feedback solution which could help us investigate the advantage of being able

to measure temperatures during cooling. This could motivate research work in the development of suitable sensors. However, in the present situation, we only need an open-loop solution. The solution to the optimal control problem is via the time varying matrix Riccati differential equation and the loop adjoint equation, shown here in the set of equations 5.6.3. A detailed derivation and a discussion of several theoretical issues can be seen in Lewis F.L., (1986).

$$
\begin{aligned}
&-\dot{\mathbf{S}}(\mathbf{t}) = \mathbf{A}^T\mathbf{S} + \mathbf{SA} - \mathbf{SBR}^{-1}\mathbf{B}^T\mathbf{S} + \mathbf{Q}; : \textit{Riccati Differential} \\
&\mathbf{S}(T_f) = \mathbf{P}; \qquad\qquad\qquad\qquad\qquad \textit{Equation} \\
&\\
&-\dot{\mathbf{V}}(t) = (\mathbf{A} - \mathbf{BK})^T\,\mathbf{V}(t) + \mathbf{QX}_D(t); \; :\textit{Adjoint Equation} \\
&\mathbf{V}(T_f) = \mathbf{PX}_{\mathbf{D}}(T_f); \\
&\\
&\textit{Feedback Matrix}: \\
&\mathbf{K}(t) = \mathbf{R}^{-1}\mathbf{B}^T\mathbf{S}(t); \\
&\\
&\textit{The optimal closed loop input is}: \\
&\\
&\mathbf{U}^*(t) = -\mathbf{K}(t)\mathbf{X}(t) + \mathbf{R}^{-1}\mathbf{B}^T\mathbf{V}(t);
\end{aligned}
\qquad 5.6.3.
$$

The solution found in equation 5.6.3. is a closed loop solution. However, the temperature measurements on the slab are possible only before the slab is placed in the cooling chamber. Once the slab enters the cooling chamber, no pyrometric measurements are possible. (See figure 5.6.1.). However, the usefulness of the above solution lies in the fact that, if some temperature data could be collected during the cooling process, one could evaluate the potential benefits of this. This is because the solution is in a feed-back form and if in process measurements are available, this could be better used to calculate the required cooling heat flux.

This could help evaluate the benefits from the development of new types of temperature measurement devices that could measure temperatures, in process, during cooling. For example, electrical resistance of the slab could be measured at selected locations on the slab. Electrical resistance is a function of temperature and therefore if the electrical resistance measurements are taken at different locations in the slab, these can be used to estimate the temperature distributions during cooling. This estimate can then be used to compute the optimal input shown in equation 5.6.3. Figure 5.6.2. shows a schematic of such an in-process temperature measurement method.

In the present case, such an in-process temperature measurement is not available. The only temperature measurement that is available is obtained by pyrometric measurement just prior to the cooling. The following section details an approach for using the optimal feed-back solution to derive an equivalent open-loop solution that can be used in this process.

5.6.3. Optimal open-loop solution:

We could make use of the closed loop solution of equation 5.6.3. to derive an optimal open loop solution. We know that the optimal input is given by:

$$\mathbf{U}^*(t) = -\mathbf{K}(t)\mathbf{X}(t) + \mathbf{R}^{-1}\mathbf{B}^T\mathbf{V}(t); \qquad 5.6.4.$$

Substituting this for **U**(t) in equation 5.6.4. we obtain:

$$\begin{aligned} \dot{\mathbf{X}}(t) &= \mathbf{A}\mathbf{X}(t) - \mathbf{B}\mathbf{K}(t)\mathbf{X}(t) + \mathbf{B}\mathbf{R}^{-1}\mathbf{B}^T\mathbf{V}(t); \\ \mathbf{X}(0) &= \mathbf{X}_0; \end{aligned} \qquad 5.6.5.$$

If we know the initial condition in the above equation 5.6.5., we can compute the state trajectory. The initial condition can be estimated with the measurement as shown in

figure 5.6.1. Let us call this state trajectory $\tilde{\mathbf{X}}(t)$. We can then compute the optimal open loop input by substituting $\tilde{\mathbf{X}}(t)$ in equation 5.6.4.:

$$\mathbf{U}_{OL}{}^{*}(t) = -\mathbf{K}(t)\tilde{\mathbf{X}}(t) + \mathbf{R}^{-1}\mathbf{B}^{T}\mathbf{V}(t); \qquad 5.6.6.$$

This is the expression for the time trajectory for the heat-flux distribution across the top and bottom of the slab that compensates for variations in the initial condition. It is clear that such a scheme can only compensate for variations in initial conditions and cannot compensate for other in-process variations. This drawback can be overcome if in-process temperature measurements are available during cooling, using the closed lop solution derived in the prior section.

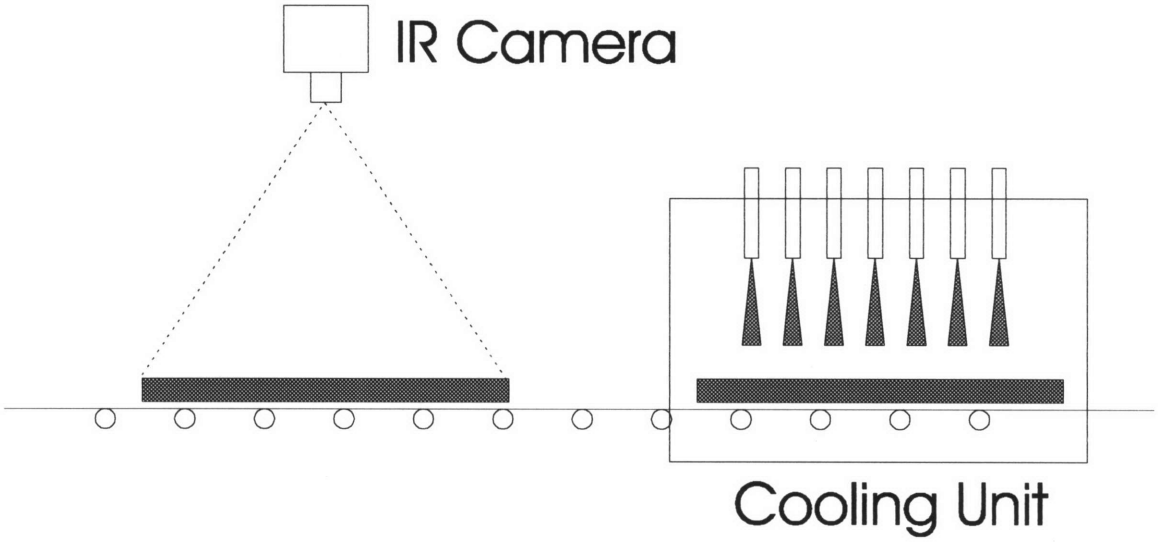

Figure 5.6.1. Temperature Measurements available only before cooling.

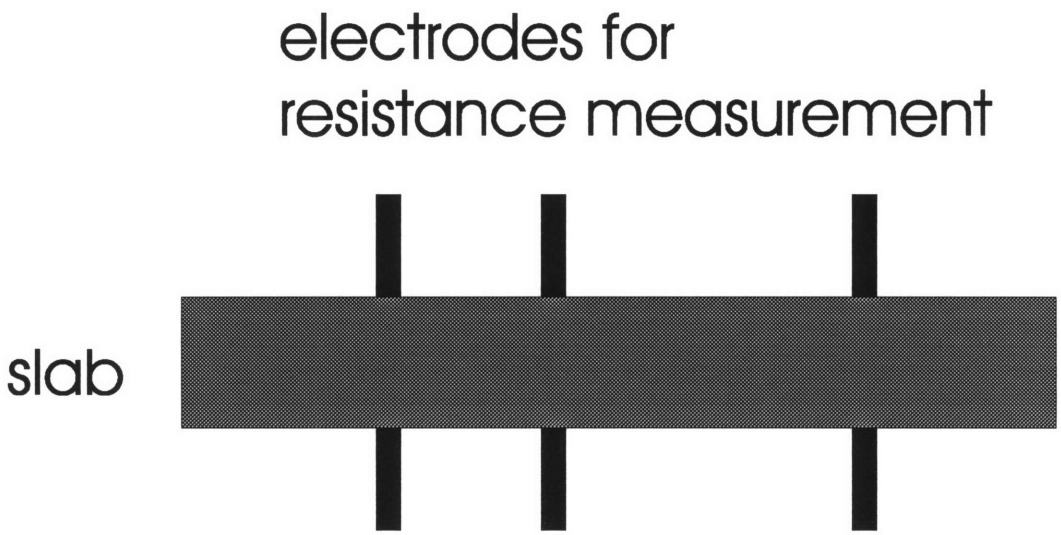

Figure 5.6.2. Possible temperature measurement scheme for in-process measurement.

5.7. Numerical simulation of the cooling process

5.7.1. Details of simulation set up:

To illustrate the performance of the controller, the following simulations were performed. A steel slab of dimensions 2cm x 50cm was considered with cooling on the upper and the lower surfaces. The simulations were performed with 30 nodes along the length and 3 nodes along the thickness. So we have a total of 90 nodes which give us a state-space of size 90. Hence the model used here is:

$$\begin{aligned} &\dot{\mathbf{X}} = \mathbf{AX} + \mathbf{BU}; \\ &\mathbf{X} = [T_1, T_2, \cdots, T_{90}]^T; \\ &\mathbf{U} = [q_1, q_2, \cdots q_{60}]^T; \end{aligned} \qquad 5.7.1.$$

The initial temperature of the slab is assumed to be as shown in figure 5.7.1. There is a hot spot in the center of 750C. The rest of the slab has a uniform temperature of 700C, which is the ideal initial condition. In this case the hot spot is the disturbance in the initial condition. Figure 5.7.1. shows a schematic of the slab with the initial temperature distribution.

An arbitrary desired cooling temperature trajectory is generated by adding a sinusoid to a linear cooling profile. The cooling profile was generated primarily to illustrate the effect of the controller and is not based on a requirement on the cooling rates in the process. We can see the desired temperature trajectory in both figure 5.7.2. and figure 5.7.3. as the solid line and this is the value for the desired state trajectory, $\mathbf{X}_D(t)$, that will be used in the simulations.

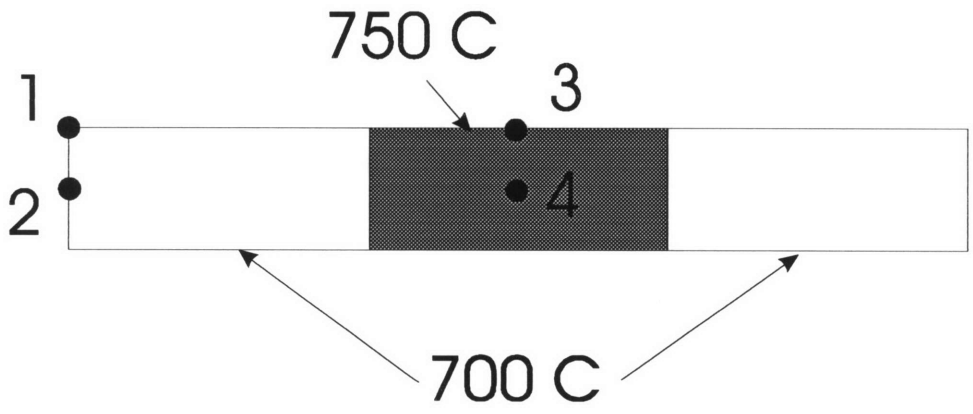

Figure 5.7.1. Slab initial conditions used in simulation.

5.7.2. Numerical techniques for computing optimal solution:

Before we proceed to study the effect of this arbitrary initial condition, we need to compute the values of the Riccati matrices and the adjoint states for different time instants. We need these to compute the optimal input in equation 5.6.6. That is, we need to solve equations 5.7.2. and 5.7.3 backwards in time.

$$\begin{aligned} -\dot{\mathbf{S}}(t) &= \mathbf{A}^T\mathbf{S} + \mathbf{S}\mathbf{A} - \mathbf{S}\mathbf{B}\mathbf{R}^{-1}\mathbf{B}^T\mathbf{S} + \mathbf{Q}; : \textit{Riccati Differential} \\ \mathbf{S}(T_f) &= \mathbf{P}; \qquad\qquad\qquad\qquad\qquad \textit{Equation} \end{aligned} \tag{5.7.2.}$$

$$\begin{aligned} -\dot{\mathbf{V}}(t) &= (\mathbf{A} - \mathbf{B}\mathbf{K})^T\,\mathbf{V}(t) + \mathbf{Q}\mathbf{X}_D(t); \; :\textit{Adjoint Equation} \\ \mathbf{V}(T_f) &= \mathbf{P}\mathbf{X}_D(T_f); \end{aligned} \tag{5.7.3.}$$

Equations 5.7.2., and 5.7.3., are nonlinear matrix differential equations. These equations have been solved using the 4th order Matrix Runge-Kutta algorithm.

The following gives the details of the Matrix Runge-Kutta method used here. If the right hand side of equation 5.7.2. is denoted as:

$$f(\mathbf{S},t) = \mathbf{A}^T\mathbf{S}(t) + \mathbf{S}(t)\mathbf{A} - \mathbf{S}(t)\mathbf{B}\mathbf{R}^{-1}\mathbf{B}^T\mathbf{S} + \mathbf{Q} \tag{5.7.4.}$$

The Riccati equation (eqn. 5.7.2.) can then be written as:

$$\begin{aligned} \frac{d\mathbf{S}}{dt} &= -f(\mathbf{S},t) \\ \mathbf{S}(T_f) &= \mathbf{P} \end{aligned} \tag{5.7.5.}$$

The above equation 5.7.5. should be solved backwards in time. Let h denote the time step used for the purpose of numerical integration. If we denote the value of $f(\mathbf{S},t)$ evaluated at the n^{th} and $(n\text{-}1)^{th}$ time step as:

$$
\begin{aligned}
& f(\mathbf{S}_n, t_n) = f(\mathbf{S}(t_n), t_n) \\
& \textit{and} \\
& f(\mathbf{S}_{n-1}, t_{n-1}) = f(\mathbf{S}(t_n - h), t_n - h)
\end{aligned}
\qquad 5.7.6.
$$

Using the 4th order Runge-Kutta rule we can compute $\mathbf{S}_{n-1}$ as:

$$
\begin{aligned}
k_1 &= hf(\mathbf{S}_n, t_n) \\
k_2 &= hf(\mathbf{S}_n - \frac{k_1}{2}, t_n - \frac{h}{2}) \\
k_3 &= hf(\mathbf{S}_n - \frac{k_2}{2}, t_n - \frac{h}{2}) \\
k_4 &= hf(\mathbf{S}_n - k_3, t_n - h) \\
\mathbf{S}_{n-1} &= \mathbf{S}_n - \frac{k_1}{6} - \frac{k_2}{3} - \frac{k_3}{3} - \frac{k_4}{6} - O(h^5)
\end{aligned}
\qquad 5.7.7.
$$

By picking the integration time h suitably, we can compute the Riccati matrix at different time instants. Similarly we can solve the adjoint equation 5.7.3. using 4th order Matrix Runge-Kutta method.

5.7.3. Selection of parameters in cost functional:

The weighting matrices **P**, **Q** and **R** in the cost function (equation 5.6.1.), were taken to be diagonal matrices of the form $p\mathbf{I}$, $q\mathbf{I}$ and $r\mathbf{I}$. Where, **I** is the identity matrix and p, q and r are scalars. By selecting the scalar weights p, q, and r we can weigh the different factors in the cost functional as per our requirement. This structure for the weighting matrices, implies that the temperature errors across the slab are penalized exactly the same. Similarly the penalty on the control input has been selected to be the same for all regions of the slab. This structure could be changed by changing the structure of **P**,**Q** and **R**, if one wishes to penalize temperatures and control inputs in certain regions more than the temperatures and control inputs in other regions.

The values of p, q, and r can be selected, using Bryson's method and equation 5.7.8., shows the guidelines for selecting these different scalar parameters. This is the finite horizon counterpart of the expressions in equation 2.4.13.

$$\begin{aligned} \frac{1}{p} &\approx \left\|\Delta X(t_f)\right\|^2 \\ \frac{1}{q} &\approx t_f \times \left\|\Delta X(t)\right\|^2 \\ \frac{1}{r} &\approx t_f \times \left\|U_m\right\|^2 \end{aligned} \qquad 5.7.8.$$

Where t_f is the final time at the end of cooling and $\left\|\Delta X(t_f)\right\|$ is the norm of the maximum allowable deviation in the final temperature and this deviation was selected to be 5°C for each node. Similarly $\left\|\Delta X(t)\right\|$ is the maximum allowable deviation in the norm of the state at any given instant of time which was selected to be 10°C at each node. The norm of U_m is the maximum allowable input that is possible and this was selected to be 10^7 W/m^2. This depends on the saturation characteristics of the jets. The scalar parameters p,q and r are selected this way and they are "tweaked" around values selected in equation 5.7.8. until satisfactory performance is obtained.

5.7.4. Simulation results

With the initial condition shown in figure 5.7.1., equations 5.7.2. and 5.7.3. are solved numerically, to compute the optimal input $\mathbf{U}^*(t)$ and the optimal temperature trajectory $\tilde{\mathbf{X}}(t)$. The elements of $\mathbf{U}^*(t)$ give the different desired heat fluxes at different locations of the surface of the slab. Figures 5.7.2 and 5.7.3. show the resulting temperature trajectories plotted for locations numbered from 1-4 in figure 5.7.1. These temperatures

are plotted along with the desired temperature trajectory. Figures 5.7.4 and 5.7.5. show the corresponding cooling heat flux trajectories at nodes numbered 1 and 3 respectively.

As was mentioned ahead, the weighting matrices were selected so as to penalize the temperature errors everywhere in the slab the same. However, we can influence the temperature of the surface much more easily than the temperature at the center of the slab (since cooling is available only on the surface). The consequence of this is that, by putting the same severe restriction the center temperature as the boundary temperature, the control input will be higher (in magnitude) than necessary and will result in cooler surface temperature and a hotter interior. By noting the temperatures in figures 5.7.2 and 5.7.3., we can see that the temperature at node 1 on the surface, more or less, follows the shape of the desired temperature trajectory but is a little lower. The temperature at the center lags a bit and is higher than the desired temperature profile. This has occurred because temperatures at all the nodes are weighed the same. The optimization algorithm then gives us a temperature trajectory which when averaged over all the nodes is close to the desired trajectory.

Comparing the temperature trajectories in figures 5.7.4 and 5.7.5., it can be noticed that the plot of the inputs at the corner and the center differ significantly at the beginning, by a factor of about seven. However, once the disturbance was rejected, the input values were very similar. The temperature profiles in figures 5.7.2., and 5.7.3., show that in the center of the slab with the higher initial condition, the cooling curves are initially far steeper

than at the corner steep temperature profiles. However, once the disturbance is rejected the cooling profiles look identical.

The next step is to translate the heat fluxes that we have generated into variables concerning the cooling process such as the temperature of the coolant, velocity of the jet/spray etc. This involves a thorough understanding of the cooling process which involves several boiling regimes in addition to forced convection. This problem is very well studied and analyzed by the engineers at the steel plants. In addition, there are many publications that deal with modeling and characterizing cooling jets. A survey and discussion of this problem can be found in Wolf, et. al., (1993). Several publications on using jets to cool steel can be seen in this survey paper. e.g. Ochi et. al., (1983) and Ishigai et. al. (1978). Using the models available from these sources, a look up table can be constructed to translate the required heat fluxes into parameters of the cooling jet that can be controlled (e.g. Jet velocity, volume flow rate etc.). The look up table can be used in real-time to determine the cooling jet parameters for a given desired heat flux at different time instants.

5.7.5. Control method when material properties have temperature dependence:

The technique presented in this chapter could be easily adapted to the situation where the properties of the steel vary with temperature. Equations 5.6.1-5.6.6. hold good even if the matrices **A**,**B**, **C** are time dependent. If the temperature trajectory is known, the time dependence of the material properties can be found (since material properties depend on temperature). This information could be used to capture the effects of parameter

variations with temperature in a time varying linear model. An approach for performing this could be:

1. Compute the temperature trajectory assuming no parameter variations.
2. With this temperature trajectory, compute the time variations for the different parameters such as density, heat capacity and conductivity etc.
3. Using the finite difference model, represent the matrices **A**(t), **B**(t) and **C**(t) as time varying matrices.
4. Perform the same optimization procedure and obtain the temperature trajectory.
5. Repeat steps 1-4 until convergence is obtained.

5.8. Conclusions:

The nature of the physics of the cooling process during accelerated cooling results in an amplification effect of the initial temperature error. This has an adverse effect on the quality of the steel produced. We have presented a distributed parameter control algorithm that efficiently compensates for the variations in the initial condition. The approach is based on evaluating the optimal feed-back solution and calculating the optimal open loop solution by simulating the closed loop solution on a model of the system. However, the approach presented here gives a feed back solution to the controlled cooling problem. This enables one to study the benefits of developing sensors for temperature measurements during cooling by sprays. The method developed here could be easily applied to several other controlled cooling problems encountered in the steel industry as well as in other industries where time trajectories of temperature distributions need to be controlled.

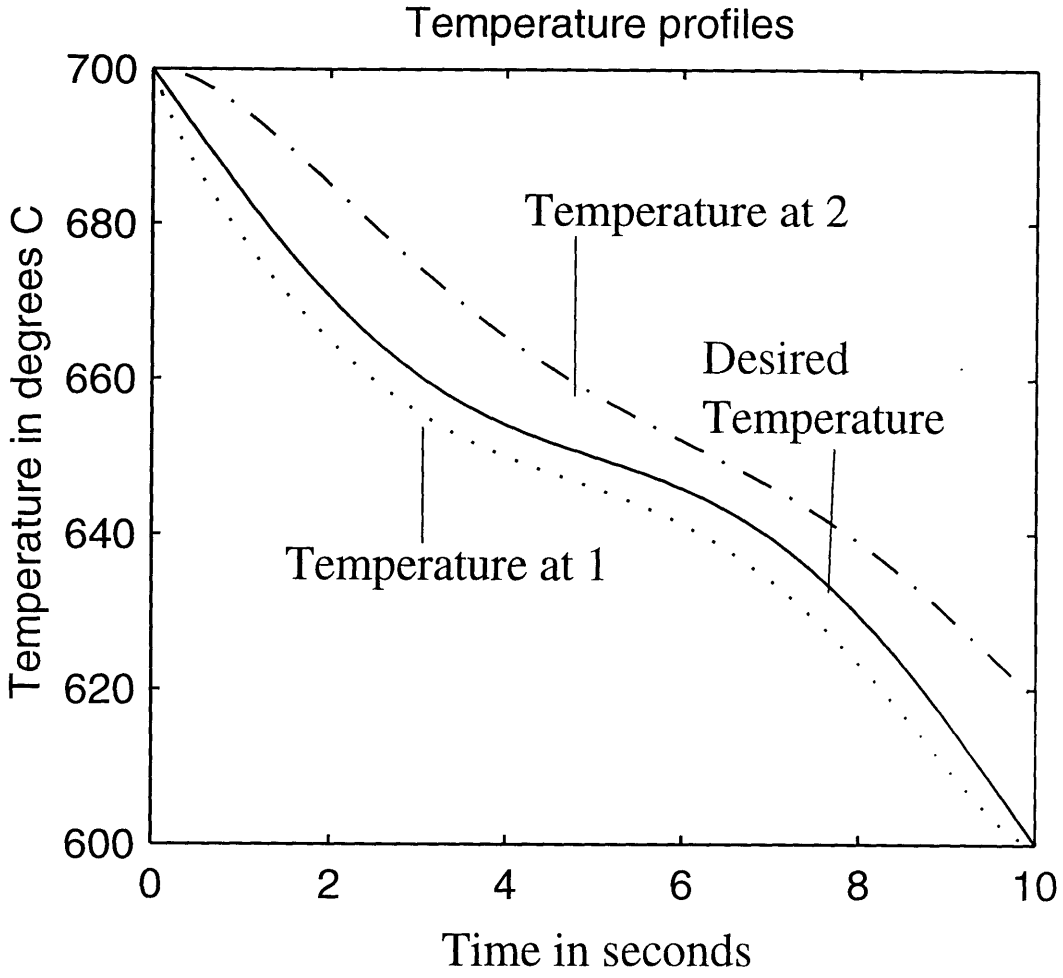

Figure 5.7.2. Cooling trajectories for the nodes at the corner.

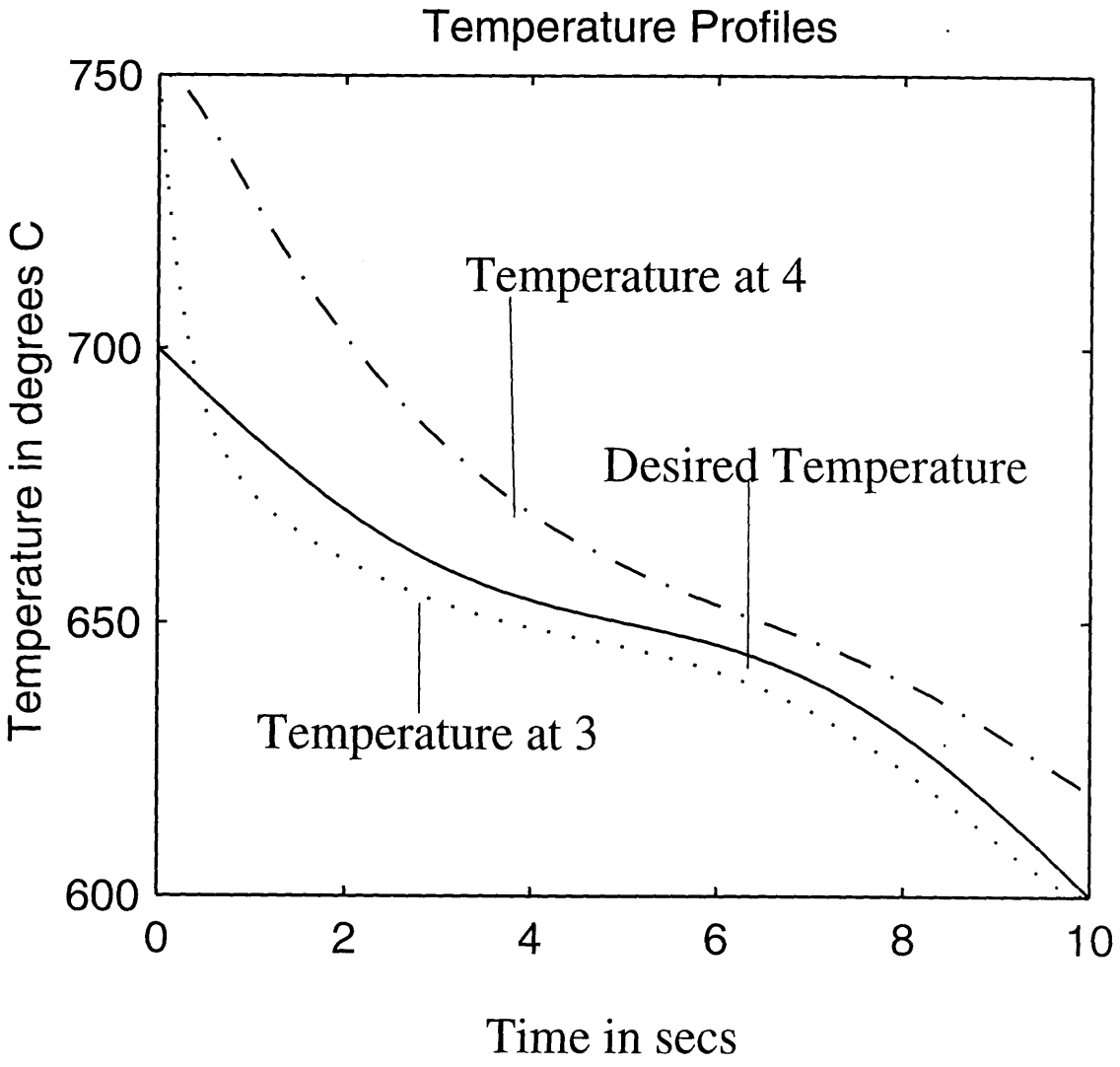

5.7.3. Cooling trajectory for the nodes in the center.

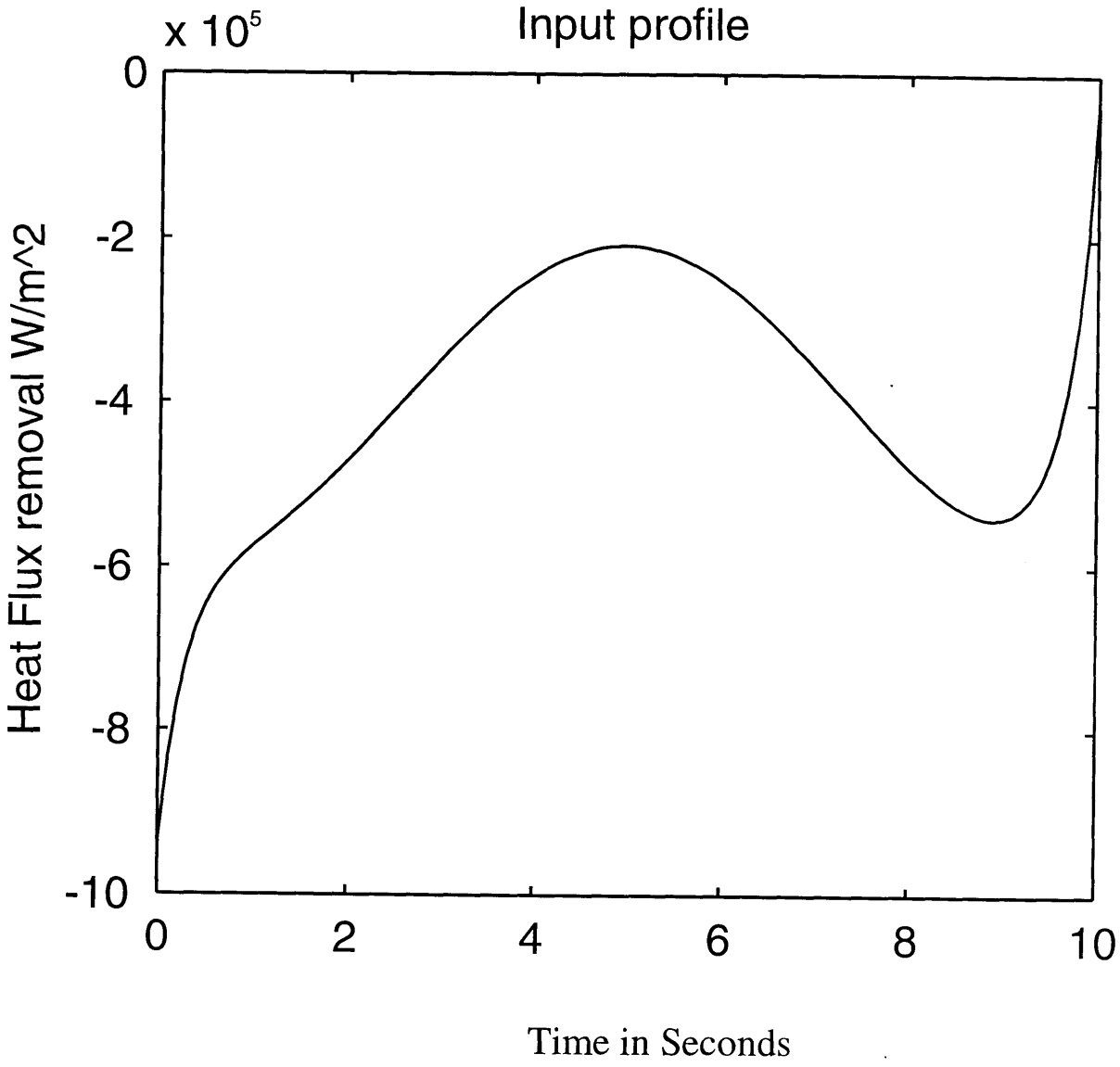

5.7.4. Trajectory of heat flux over the corner node.

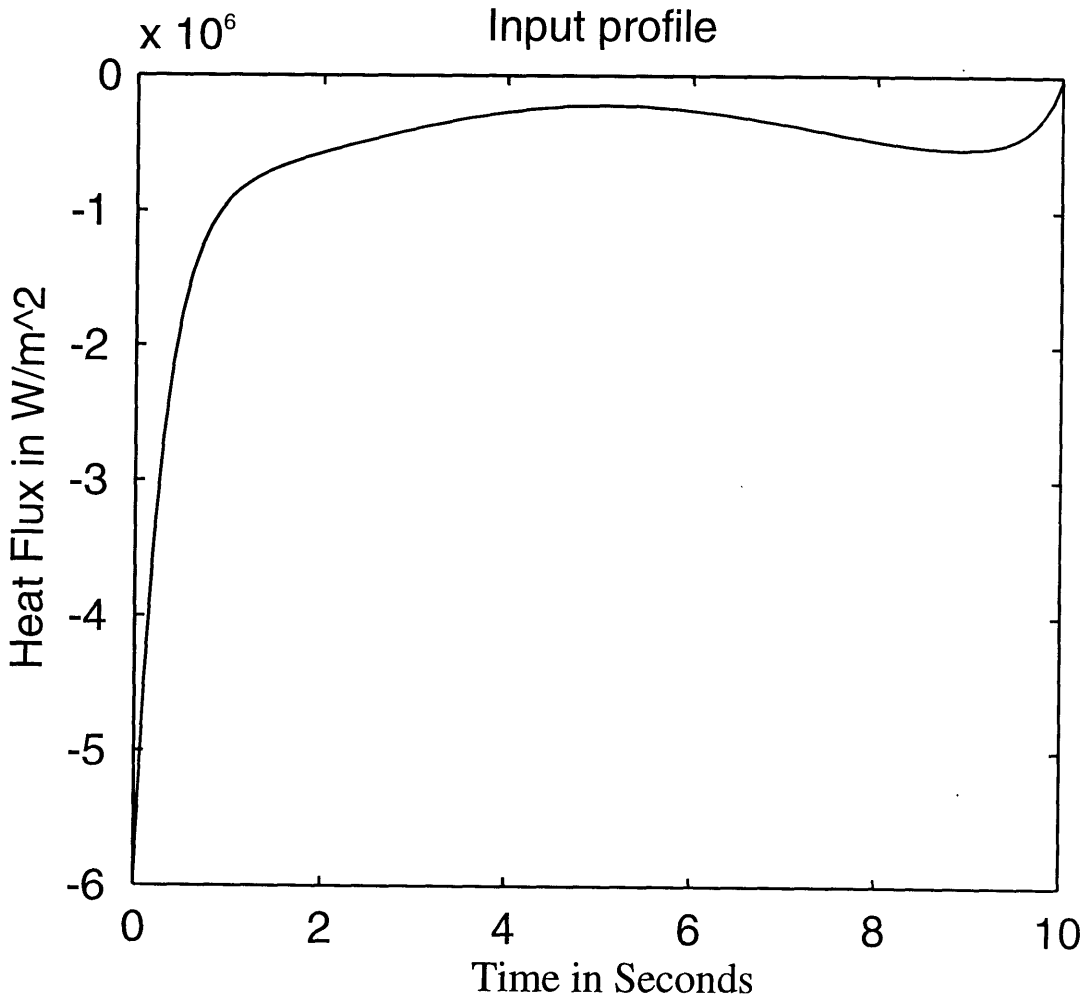

Figure 5.7.5. Trajectory of heat flux over the center node.

Chapter 6

CONCLUSIONS AND FUTURE WORK

6.1 Conclusions from thesis:

This thesis has explored the problem of controlling temperature distributions in a variety of manufacturing processes. The several issues pertaining to the implementation of temperature distribution control in these manufacturing processes have been identified. In addition, a few implementations of temperature distribution control have been demonstrated in this thesis. The following specific claims are made as contributions of this thesis:

1. Different processes such as heat treatment, molding operations, welding, flame-bending etc., have been studied and the corresponding differences in temperature control requirements have been identified. Examples: Heat treatment requires controlling transient temperature distributions vs. resin transfer molding which requires controlling steady-state temperature distributions. Injection molding requires temperature distribution control vs. Flame bending requires temperature gradient control.
2. The vast amount of literature in the theory of distributed parameter systems control has been evaluated for its applicability to controlling heat conduction in manufacturing processes. Existing techniques that are applicable to controlling some process have been identified. For example: use of finite horizon linear quadratic optimal control for problems in heat treatment. However, several shortcomings in the state-of-the-art have been identified. These are:

- Lack of techniques for determining the optimal distribution of heat flux for desired steady-state performance.
- Need for MIMO control approaches for control of heat conduction that do not utilize full-state estimation.
- Non-availability of techniques for sensor and actuator location for disturbance rejection
- Lack of techniques for selecting heat flux distribution and creating a closed loop system robust to model uncertainties.

3. A novel technique for optimal input distribution has been developed in Chapters 3., and 4. These chapters form the central contributions to this thesis and answer some of the issues identified as deficiencies in the current state of the art. A generalized optimization problem defined in chapter 3., can be used to derive steady-state optimal heat flux distributions in a variety of problems requiring either temperature distribution control or temperature gradient control or length control. This technique yields a useful method for determining the distribution of inputs to guarantee adequate steady-state performance in the presence of model uncertainties and external disturbances. Additionally, this technique can also be used in situations where full state estimates are unavailable.
4. Chapter 4., illustrates a complete compensator design method for steady-state temperature distribution control. The steps included in this design procedure are:
   a) determining the optimal locations for the minimum number of heaters and coolers that provide the required steady-state performance
   b) evaluating the effects of process disturbances and model uncertainties

c) designing stable compensation while guaranteeing steady-state performance

d) incorporating additional actuators to improve transient performance.

5. The application of two techniques from linear optimal control to specific temperature control problems has been illustrated in Chapters 2., and 5. Chapter 2., shows the implementation of a Linear Quadratic Gaussian (LQG) type compensator to steady-state temperature control and Chapter 5., illustrates the application of a finite horizon linear quadratic tracker to the problem of controlling transient temperatures in an accelerated cooling application.

We have also identified several areas of possible future research. The following section highlights some of these possible research avenues.

6.2 Future work:

This section details work that has been performed as a part of this research work in the context of optimal sensor location. A description of an experimental set up for studying optimal sensor locations is presented.

6.2.1. Optimal sensor location in heat conduction systems:

There are two specific types of problems that are of interest in the context of optimal sensor location:

1. The first problem deals with obtaining a full state estimate of the state (temperature) which is then used for control. This is similar to the situation in Chapter 2, where the optimal controller utilized an optimal estimator (Kalman Filter).

2. The second problem deals with optimally locating sensors when the temperature distribution is estimated by interpolating between a set of temperature measurements using interpolating functions.

The first situation is well studied in the DPS literature and section 1.3. lists some of the publications on this topic. The general approach is based on choosing locations for sensors so that the error covariance in the temperature distribution estimate is minimized. The goal of the control problem is to minimize the cost function in equation 6.2.1.

$$J = \lim_{T\to\infty} E\left\{\int_0^T (\mathbf{x}^T\mathbf{Q}\mathbf{x} + \mathbf{u}^T\mathbf{R}\mathbf{u})dt\right\} \qquad 6.2.1.$$

Where **x** is the state, which in the present case corresponds to the temperature distribution depending on the type of state-space description for the heat conduction system. **Q** is the matrix weighting on the error in the state and **R** is the matrix weighting on the input **u.** Using the stochastic separation principle this can be separated into an optimal estimation problem and a deterministic optimal control problem, as seen in section 2.4. The sensor location problem is then defined using the optimal estimation problem. If the state equations in the case where the measurements and the state are corrupted by noise are given by:

$$\begin{aligned}\dot{\mathbf{X}} &= \mathbf{A}\mathbf{X} + \mathbf{B}\mathbf{U} + \Gamma w \\ \mathbf{Y} &= \mathbf{C}\mathbf{X} + v\end{aligned} \qquad 6.2.2.$$

Where "w" and "v" are assumed to be zero mean Gaussian stochastic processes, with covariances:

$$E\{ww^T\} = \mathbf{W} \geq 0, \qquad E\{vv^T\} = \mathbf{V} > 0 \qquad 6.2.3.$$

The matrix **C** in equation 6.2.2., depends on the location of the sensors. Therefore, the steady state estimation error covariance $\mathbf{P}_f$ is given by the positive semi-definite solution to the Algebraic Riccati Equation:

$$\mathbf{A}^T\mathbf{P}_f + \mathbf{P}_f\mathbf{A} - \mathbf{P}_f\mathbf{C}^T\mathbf{V}^{-1}\mathbf{C}\mathbf{P}_f + \Gamma\mathbf{W}\Gamma = 0 \qquad 6.2.4.$$

A measure for the goodness of the steady state estimation process can then be defined as:

$$\mathbf{M} = Trace(\mathbf{P}_f) \qquad 6.2.5.$$

Clearly, **M** is a function of the output matrix **C** and the sensor error covariance **V**. Both **C** and **V** are dependent on the sensor locations. Therefore, **M** depends on the locations of sensing points. Therefore the optimal sensor location problem is one of determinig the locations of the sensors so that **M** is minimized.

6.2.2. The optimization method:

The optimization method will consist of numerically searching for local minima for **M**. The coordinates of the measurement locations span the parameter space. A method such as the conjugate gradient method could be used for this purpose. However, this is numerically intensive and a few trials performed as a part of this thesis did not yield proper convergence. One alternative that could be considered to circumvent such numerical difficulties involves a sequential optimization method where the measurement locations are chosen for one sensor at a time, minimizing **M** for each sensor. At each step of the optimization, a single sensor is located at the best location leaving the sensors located by prior steps at the same locations. This however is a sub-optimal configuration of sensor locations, since a better optimum would be expected by simultaneously locating all the sensors.

The second approach for optimal sensor location is useful in situations where full-state estimates are not used in the distribution control problem. This is similar to the mold temperature control problem in Chapter 4. The temperature distribution can be found by interpolating the temperature measurements. For this purpose a suitable interpolation function needs to be used. Kaiser (1968) uses Lagrange polynomials for interpolating the measured temperatures. The interpolated temperature can then be used for the closed loop temperature controller. The error in the resulting closed loop temperature distribution can be minimized under different "worst-case" scenarios, similar to Chapter 4. A parametric optimization problem, similar to the one described in the prior paragraph can then be used to select the measurement locations to minimize the error in the closed loop temperature distribution.

An experiment has been set up to study the optimal sensor location problem and the following section details this experiment.

6.2.3. Experimental setup for studying optimal sensor location:

The experiment is intended to study the effect of the number and location of measurements on the error in the temperature distribution estimate. Figures 6.3.1., and 6.3.2. show a schematic and a photograph of the experimental set up. The experiment consists of heating a rectangular specimen on the surface using a plasma torch. The bottom of the specimen is in contact with a water cooled block. An infrared camera is used to measure the surface temperature of the steel slab.

The infrared camera provides temperature distribution for the entire surface and thus the temperature estimate obtained from this measurement will be the best achievable temperature estimate using surface temperature measurements. This estimate can be used as a basis for evaluating the performance of temperature distribution estimators using temperature measurements at fewer locations. One can select temperature measurements at a few distinct locations from the measured temperature distribution obtained from the infrared camera. The temperature estimation can be performed using these few locations and the error in the temperature estimate can be compared to the one obtained by using the entire temperature field measured by the camera. This can be used to evaluate the performance of an estimator that utilizes a limited number of temperature measurement locations. Thus this experiment can be used to experimentally verify the predictions from any optimal sensor location strategy.

6.2.4. Other Future work:

The first topic that needs to be researched is the problem of optimal sensor location strategies, both for situations involving state estimation and for situations involving interpolating temperature measurements. The experiment described above, or a similar experimental set up can be used for this purpose.

The heating/cooling technique developed in Chapters 3 and 4 needs to be tested in a variety of manufacturing processes discussed in the thesis. Experimental investigations utilizing the method presented in these chapters should be set up so as to facilitate the transfer of this technology into industrial applications.

The steady-state design methodology presented in Chapters 3., and 4., has general applicability to a variety of situations, however the transient part of the design has been developed for applications similar to molding operations. An approach for a generalized transient design could be pursued as a topic of research. One particular technique for designing stable controllers has been presented in this thesis, involving frequency blending functions to roll off a high steady-state gain. Other techniques for transient design with more general applicability, without too much additional complexity should be developed.

Application of the techniques of Chapters 3 and 4 to processes such as wear control, structural distortion control etc. should be investigated. These processes can also be characterized by Green's functions and therefore can be addressed by the formulation presented in Chapters 3 and 4.

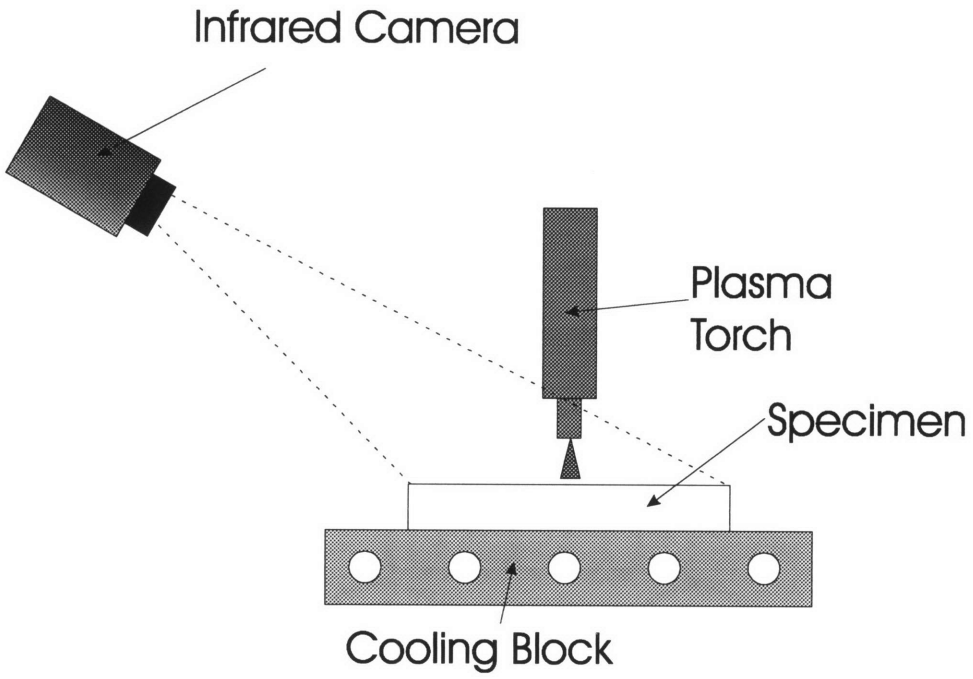

Figure 6.2.1. The schematic of the sensor-location experiment.

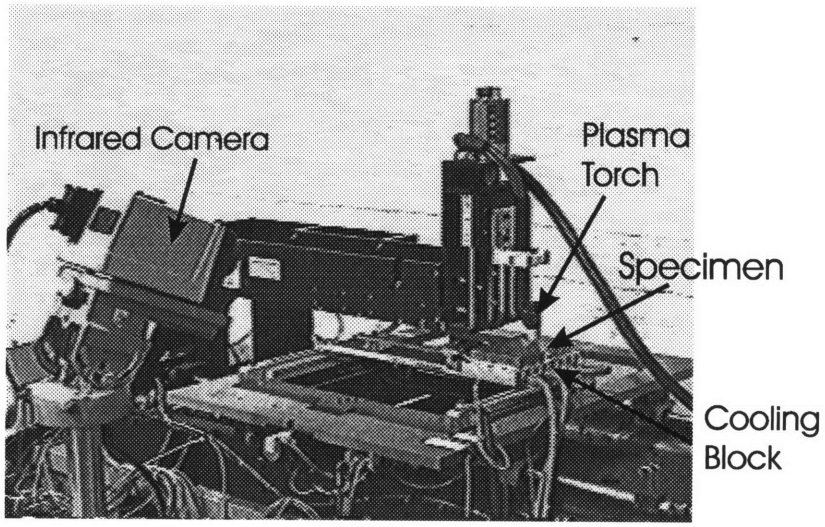

Figure 6.3.2. The layout of the experimental setup to study sensor location problem.

REFERENCES:

Amouroux, M., and Babary, J.P., (1975) Optimal point wise control for a class of distributed parameter systems. Proc. 6th Int. IFAC Congr., Boston Massachusetts, 24-30 August 1975.

Amouroux, M., and Babary, J.P., (1978) On the optimal point wise control and parametric optimization of distributed parameter systems, Int. J. of Control, 28, No. 5, pp. 789-807.

Amouroux, M., and Babary, J.P., (1979) On optimization of zones of action for an optimal control problem for distributed parameter systems, Int. J. of Control, 29, No. 5, pp. 861-869.

Anderson, B.D., and Moore, J.B., (1985) Linear optimal control, Prentice Hall, Englewood Cliffs, N.J., 1985.

Athans, M., (1969) Some remarks on the control of distributed parameter systems. 1969 JACC, Boulder, Colorado (1969), pp. 1-12.

Aziz, A.K., Wingate, J.W., and Balas, M.J (1977) Control theory of systems governed by partial differential equations. Academic Press, New York (1977).

Balakrishnan, A.V., (1965) Optimal control in Banach spaces. SIAM J. Control. vol. 3, 109-127 (1965).

Balakrishnan, A.V., (1976) Applied functional analysis, Springer, Berlin.

Ball, D.J., and Hewitt, J.R., (1974) The optimal control of the temperature profile within a heat conduction system. Journal of Mech.Eng. Sci., 16, 79 (1974).

Bensoussan, A. (1972) Optimization of sensor location in a distributed parameter system. Lect. Notes Math., 1972, pp. 294.

Bryson,A.E., and Ho, Y.C., (1975) Applied optimal control. Halstead Press, 1975.

Burger, J. (1976) Emplacement optimal des actionneurs ponctuels ou par zones dans un systeme gouverne par une equation lineaire d'evolution du premier ordre. RAIRO J-5.

Butkovshii, A.G., and Pustylnikov, L.M., (1987) Mobile control of distributed parameter systems. Ellis Horwood,Chichester.

Butkovskii, A.G., (1969) Theory of optimal control of distributed parameter systems. Elsevier, Amsterdam.

Cannon J.R., and Klien , R.E., (1970) Optimal selection of measurement loctions in a conductor for approximate determination of temperature distributions. JACC, 28-C, (1970)

Caravani, P., Dipillo G., and Grippo, L., (1975) Optimal location of a measurement point in a diffusion process. Proc. 6th Int. IFAC Congress, Boston, Massachusetts, 1985.

Carslwaw, H.S., and Jaeger, J.C., (1959) Conduction of heat in solids., Oxford Press.

Courant, R., and Hilbert, D., (1962) Methods in mathematical physics, Vol. I and II, Interscience, New York.

Delfour, M., Payre, G., and Zolesio, J.P., (1982) Optimal design of a minimum weight thermal diffuser with constraint on the output thermal flow. Appl. Math. Optim., 9, pp. 225-262.

Delfour, M.C., and Mitter, S.K., (1972) Controllability and observability for infinite-dimensional systems. SIAM J. of Control, vol. 10, pp. 329-333.

Doumanidis, (1996) Control of the scan welding process. Japan-USA Symposium on Flexible Automation, Boston, MA (1996)

Doumanidis, C. (1988). Modeling and control of thermal phenomena in welding. Ph.D. Thesis, Department of Mechanical Engineering, MIT (1988)

El Jai A., and Pritchard A.J., (1988) Sensors and controls in the analysis of distributed systems. Ellis Horwood Limited, Chichester, United Kingdom.

El Jai, A., and Najem, A., (1984) Optimal actuator location in a diffusion process. Lect. Notes Control Inf. Sci., 62, Part I.

Fattorini, H.O., (1967) Controllability of higher order linear systems. Mathematical Theory of Control, (eds. A.V. Balakrishnan and L.W. Neustadt), Academic Press, New York.

Fattorini, H.O., (1975) Boundary control of temperature distributions in a parallelopipedon. SIAM J. Control, 13, pp. 1-13.

Goodson, R.E., and Klein, R.E., (1970) A definition and some results of distributed systems observability. IEEE Trans. Autom. Control, 15.

Goodson, R.E., and Klien, R.E., (1970) A definition and some results for distributed system controllability and observability. IEEE Trans. on Auto. Control, AC-15, 165-174 (1970)

Gould, L.A., and Murray-Lasso, M.A., (1966) On the modal control of distributed systems with distributed feedback. IEEE Trans. on Automatic Control, Vol. AC-11, No.4, Oct. 1966.

Ichikawa, A., and Ryan, E.P., (1979) Sensor and controller location problems for distributed parameter systems. Automatica, 15.

Incropera, F.P., and DeWitt, D.P., (1985), Fundamentals of heat and mass transfer. John Wiley, New York.

Ishigai, S., Nakanishi, S., and Ochi, T., (1978) Boiling heat transfer for a plane water jet impinging on a hot surface. Proc. 6th Int. Heat Transfer Conf., v.1., FB-30,pp.445-450.

Jansen, (1993) Control of residual stresses in injection molding. PhD Thesis, University of Delft, The Netherlands.

Kaiser, K.W., (1968) Optimal control of steady-state surface temperature distributions. Ph.D. Thesis, Department of Aero-Astro., MIT.

Kaiser, K.W., (1971) A method of determining the heater-sensor configuration in temperature distribution control. IFAC Symposium on the Control of Distributed Parameter Systems, Banff, !971.

Kaiser, K.W., (1981) Design methodology for a coolable deformable mirror. Rept. No. CSDL-C-5438, The Charles Stark Draper Laboratory, Inc., Cambridge, Massachusetts.

Kalpakjian, (1995) Manufacturing engineering and technology, Addison-Wesley, (1995).

Kamen, E.W., (1976) Module structure of infinite-dimensional systems with applications to controllability, SIAM J. of Control and Optimization, Vol. 14, pp. 389-408.

Kubrusly, C.S., (1977) Distributed parameter system identification: a survey. Int. J. of Control, 26.

Kubrusly, C.S., and Malebranche, H., (1985) Sensors and controllers location in distributed systems: a survey. Automatica, 21, No. 2, pp. 117-128.

Kumar, S., and Seinfeld, J.H. (1978). Optimal location of measurements in tubular reactors. Chem. Eng. Sci., 33.

Kwakernaak, H., and Sivan, R., (1972) Linear Optimal Control Systems, Wiley, New York.

Lausterer, G.K., (1977) State estimation and optimal control of distributed parameter systems. Ph.D. thesis, SUNY, Buffalo, New York.

Lausterer, G.K., Ray, W.H., and Martens, H.R., (1977) The real time application of distributed parameter state estimation theory to a two dimensional heated ingot. 2nd., IFAC symposium on Distributed Parameter Control Theory, Coventry, 1977.

Lewis, F.L., (1986) Optimal Control, John Wiley, New York.

Lions, J.L., (1971) Optimal control of systems governed by partial differential equations. Springer-Verlag, N.Y., 1971.

Lions, J.L., (1980) On the foundation of the optimal control of distributed systems. Lect. Notes Control Inf. Sci., 22.

Maciejowski, J.M., (1989) Multivariable feedback design. Addison-Wesley, (1989)

Mader, H.F., (1976) Modell und modale regelung eines technishch reealisierten Warmeleitsystems. Regelungstechnik 24, pp 347. (1976)

Martin, J. Cl. E., (1976). On the controllability of parabolic systems by scanning controls. IEEE Trans. Autom. Control., 21, No. 4.

Masmoudi, R.A. (1993) Modeling and control of geometric and thermal properties in arc welding. Ph.D. Thesis, Department of Mechanical Engineering, MIT (1993)

Miho, T., Katoh, N., and Yamamoto, S., (1992) A new zone melting process based on control of distributed parameter system. Kagaku Kogaku Ronbunshu, vol. 18, no. 6, (1992)

Mitter S.K., (1969) Optimal control of distributed parameter systems, JACC, Boulder, Colorado. pp. 13-48.

Morari, M., and O'Dowd, J., (1980) Optimal sensor location in the presence of nonstationary noise. Automatica, vol. 16, pp. 463-480.

Mudawar, I., and Deiters, T.A., (1994) A universal approach to predicting temperature response of metallic parts to spray quenching. Int. HJ. Heat Mass Transfer, vo. 37, no. 3, pp. 347-362.

Ochi, T., Nkaninshi, S., and Kaji, M., (1983) Cooling of a hot plate with an impinging circular water jet. Multi-phase flow and heat transfer III, Part A: Fundamentals., Eds., Veziriglu and Bergles. Elseveir.

Omatu and Seinfeld, (1989) Distributed parameter systems: theory and applications. Oxford University Press (1989).

Omatu, S., and Seinfeld, J.H., (1983) Optimization of sensor and actuator location in a distributed parameter system. J. Franklin Inst., 315.

Omatu, S., Koide, S., and Soeda, T., (1978) Optimal sensor location problem for linear distributed parameter systems. IEEE Trans. Autom. Control. 23.

Ray, W. H., (1978) Some recent applications of distributed parameter systems theory. A survey. Automatica, 14.

Ray, W.H., and Lainiotis, D.G. (1978). Distributed parameter systems: Identification, Estimation and Control, Dekker, New York.

Russell, D.L., (1973) A unified boundary controllability theory for hyperbolic and parabolic partial differential equations, Studies in Appl. Math., vol 52, 189-211 (1973)

Sakawa, Y. (1974) Controllability for partial differential equation of parabolic type, SIAM J. of Control, vol. 12, pp. 389-400.

Seidman, T.I., (1973) Problems of boundary control and observation for diffusion processes., Math. Res. Rep., No. 73-10.

Sha, D., (1995) Effect of dynamic thermal boundaries on residual stresses in injection molding. M.S., Thesis in Mechanical Engineering, MIT.

Southwich, P.D., (1986) Accelerated Cooling of steel, The metallurgical society, Inc., Pittsburgh, PA (1986).

Stakgold, I., (1979). Green's Functions and Boundary Value Problems. John Wiley, New York.

Takeda, T., and Hosokawa, Y., 1986, Development of dynamic accelerated cooling process., Proc. symp. on accelerated cooling, The metallurgical society of AIME, Pittsburgh, PA, Aug., 1985.

Triggiani, R., (1975) Controllability and observability in Banach spaces with bounded operators. SIAM J. Control, vol. 13.

Tzafestas, S.G., (1982) Control of distributed parameter systems, Theory and applications, Pergamon Press, Oxford.

Ummethala, U.V., and Hardt, D.E., (1994) Distributed parameter systems control of manufacturing processes. USA-Japan Symposium on Flexible Automation, Kobe (Japan).

Ummethala, U.V., and Hardt, D.E., (1996) Control of accelerated cooling of steel: A distributed parameter systems approach. USA-Japan Symposium on Flexible Automation, Boston (USA)

Upadhyay, R., (1988) Compression molding of composites: Mold heating system design. Advances in polymer technology, Vol 8, No 3, 243-264 (1988)

Vidyasagar, M., and Higgins, T.J., (1973) A basic theorem on distributed control and point stabilization. ASME, Journal of Dyn. Syst. Meas. Control, vol. 67.

Walczyk, D.W., (1996) Rapid fabrication methods for sheet metal dies. Ph.D. Thesis, Department of Mechanical Engineering, MIT (1996)

Wang, P.K.C., (1964) Control of distributed parameter systems. Advances in control systems, 1964, V.1., pp. 75-172.

Wang, P.K.C., (1964b) On the stability of equilibrium of a diffusion system with feedback control. IEEE Trans. on Auto. Control, Oct. 1964, pp. 585-586.

Wang, P.K.C., (1964c) Optimum control of distributed parameter systems with time delays. IEEE Trans., on Automatic Control.

Wang, P.K.C., (1971) Feedback stabilization of distributed systems with application to plasma stabilization. Instability of continuous systems, (ed. H. Leipholz), Springer, Berlin.

Wilkinson, R.H., (1965) Study of surface thermal gradients on instrument structural elements, MIT Sc.D. Thesis T-416, May 1965.

Wolf., D.H., Incropera, F.P., and Viskanta, R., (1993) Jet impingement Boiling. Advances in Heat Transfer.,Vol. 23, pp.1-132.

Wylonis, E.M., (1995) Production of injection molding tooling with conformal cooling channels using the three dimensional printing process. M.S. Thesis in Mechanical Engineering, Department of Mechanical Engineering, MIT (1995).

Yu, T.K., and Seinfeld, J.H., (1973) Observability and optimal measurement location in linear distributed parameter systems. Int. J. Control, vol. 18.